Doctoral   Engineering

2013-1

Power Quality Improvement of Distributed Generation Integrated Network with Unified Power Quality Conditioner.

Shafiuzzaman Khan Khadem
Technological University Dublin, skkhadem@gmail.com

Follow this and additional works at: https://arrow.tudublin.ie/engdoc

Part of the Electrical and Electronics Commons

Power Quality Improvement of Distributed Generation Integrated Network with Unified Power Quality Conditioner

MD. SHAFIUZZAMAN KHAN KHADEM, *BSc*, *MSc*

A thesis submitted for the Degree of Doctor of Philosophy
to the Dublin Institute of Technology

Under the supervision of
Dr Malabika Basu and Dr Michael Conlon

School of Electrical Engineering Systems,
Dublin Institute of Technology,
Republic of Ireland

January 2013

Dedicated to my Late Parents
Wife and Children

Abstract

With the increased penetration of small scale renewable energy sources in the electrical distribution network, maintenance or improvement of power quality has become more critical than ever where the level of voltage and current harmonics or disturbances can vary widely. For this reason, Custom Power Devices (CPDs) such as the Unified Power Quality Conditioner (UPQC) can be the most appropriate solution for enhancing the dynamic performance of the distribution network, where accurate prior knowledge may not be available. Therefore, the main objective of the present research is to investigate the (i) placement (ii) integration (iii) capacity enhancement and (iv) real time control of the Unified Power Quality Conditioner (UPQC) to improve the power quality (PQ) of a distributed generation (DG) network connected to the grid or microgrid. The following developments have been achieved through this PhD research;

(i) **Placement of UPQC in DG network**

A proper placement of a UPQC has been identified in a DG integrated grid connected microgrid network, together with the feedback sensors to cope with the bidirectional power flow without compromising the power quality controlling features. In the presence of DG sources and a UPQC in an active distribution network, the following issues have been analysed;

(a) the placement of a UPQC and its sensors in the network,

(b) impact of the sensor placement on the UPQC control to perform the specified task,

(c) performance of UPQC with bi-directional power flow in the network and

(d) the advantages of DG inverter in the presence of UPQC

Depending on the location and integration technique of DG sources as well as locating of the UPQC sensors which is based on its control technique, a new placement arrangement and integration method of the UPQC at the point of common coupling (PCC) have been identified.

(ii) UPQC$_{\mu G}$ - a new integration method

A new integration method of the UPQC has been developed: that can help the DGs to deliver quality power in the case of islanding and help to reintegrate with the grid seamlessly postfault. Islanding detection and reconnection techniques, together with associated control schemes, have featured in the conventional UPQC system. Hence, it is termed UPQC$_{\mu G}$. The advantages of the proposed UPQC$_{\mu G}$ configuration and integration system are to compensate voltage interruptions in addition to voltage sags/swells, and harmonic and reactive power compensation in the interconnected mode. The DG Inverter with storage supplies the active fundamental power only and the shunt part of the UPQC compensates the reactive and harmonic power of the load during both interconnected and islanding mode. Therefore, the system can work both in interconnected and islanded mode. The advantage of the DG Inverter is that it does not require to be disconnected during the islanded mode and hence the islanding detection and reconnection technique need no longer be a part of the inverter. In all conditions, the DG Inverter only provides the active power to the load and grid. Thus it reduces the control complexity of the DG inverter as well as improves the PQ of the microgrid.

(iii) Capacity enhancement

A novel method of capacity enhancement and operational flexibility of the UPQC at a distribution network level has been proposed, providing modularity and redundancy for better efficiency and reliability. For high current compensation at a low voltage distribution level, multiple Shunt APF units in modular and distributed mode, connected with a common dc linked capacitor, can be a solution to develop a Distributed UPQC (D-UPQC). This novel method is proposed here for the D-UPQC system where the multiple shunt APF units are based on hysteresis current control and operated in a power sharing mode. The related design and control issues are also discussed.

(iv) **Design and control**

Implementation of the proposed integration and capacity enhancement methods, and the modification in design with an advanced and real time control strategy have been developed. As a part of design and integration, issues including capacity enhancement and operational flexibility, the detailed switching dynamics with a parameter selection procedure for the APF_{sh} unit has been studied. Active power loss associated with the design parameters has also been analyzed as a rating requirement of the shunt APF unit. Control methods for parallel operation of multiple APF units are also discussed. Due to the common DC link, a circulating current could flow within the APF units. In the case of hysteresis control with multiple APF units, the design issues have been discussed for the proper selection of design parameters to reduce the circulating current flow.

The required active distribution network has been designed in MATLAB using SimPowerSystems and RT-LAB tools. A real-time simulation environment in a SIL (software-in-loop) configuration with a hardware synchronization mode, has been developed using the real-time simulator from OPAL-RT. The performance of the proposed $UPQC_{\mu G}$ and D-UPQC method have been tested in real-time.

I certify that this thesis which I now submit for examination for the award of the Degree of Doctor of Philosophy, is entirely my own work and has not been taken from the work of others save and to the extent that such work has been cited and acknowledged within the text of my work.

This thesis was prepared according to the regulations for postgraduate study by research of the Dublin Institute of Technology and has not been submitted in whole or in part for an award in any other Institute or University.

The work reported on in this thesis conforms to the principles and requirements of the Institute's guidelines for ethics in research.

The Institute has permission to keep, to lend or to copy this thesis in whole or in part, on condition that any such use of the material of the thesis be duly acknowledged.

Signature_____ Date _____

Candidate

Acknowledgements

All praise to almighty Allah who has given me the opportunity to carry out the research work successfully for the award of the Degree of Doctor of Philosophy. I express my sincere gratitude also to all of those people who directly and indirectly helped me for the completion of this task. This PhD thesis constitutes the work that I have carried out at the School of Electrical Engineering Systems, Dublin Institute of Technology, Ireland.

I take this opportunity to express my deep sense of gratitude to my research supervisors Dr Malabika Basu and Dr Michael Conlon for their inspiring and stimulating guidance, invaluable thought provoking suggestions, constant encouragement and unceasing enthusiasm at every stage of this research work.

I thank all of the members of Dublin Institute of Technology, and in particular Dr Eugene Coyle, Dr Jayanti N Ganesh, Mr Michael Farrell and Mr Kevin Gaughan, for their permanent support during my stay in Ireland.

Many thanks to my colleagues Nasif Shams, Dr Moin Hanif, Dr Umakant Dwivedi, Lubna Mariam, Benish K Paelly for their valuable suggestions, excellent cooperation and encouragement during the course of my PhD work.

I also wish to thank Mr Terence Kelly, Mr Michael Feeney and Mr Finbarr O'Meara for their help in carrying out experimental work.

Finally, I would like to extend my deepest gratitude and personal thanks to those closest to me. In particular, I am extremely grateful to my wife Lubna Mariam for tolerating my long hours of absence from home, for her sacrifice, patience and excellent cooperation during the entire period of this research work. Her loving, caring and sacrificing attitude has been the driving force in this endeavour and, no words of thanks are enough.

Abbreviations

APF	_	Active Power Filter
CPD	–	Custom Power Device
CSI	_	Current Source Inverter
DAFS	_	Distributed Active Filter System
DG	_	Distributed Generation
DFIG	_	Double-Fed Induction Generator
DSP	–	Digital Signal Processor
DSTATCOM	–	Distribution Static Compensator
D-UPQC	_	Distributed Unified Power Quality Conditioner
DVR	–	Dynamic Voltage Restorer
EMC	_	Electromagnetic Compatibility
EPS	–	Electric Power System
EU	_	European Union
FLL	_	Frequency Locked Loop
GTO	_	Gate Turn Off Thyristor
HIL	–	Hardware-in-Loop
HPF	–	High Pass Filter
HDS	_	Harmonic Detection Sensors
IGBT	–	Insulated Gate Bipolar Transistor
IEEE	–	Institute of Electrical Engineers
IEC	–	International Electrotechnical Commission
LPF	–	Low Pass Filter
PCC	–	Point of Common Coupling
PI	–	Proportional Integral
PLL	–	Phase Lock Loop
PQ	_	Power Quality
PWM	–	Pulse Width Modulation
RCP	–	Rapid Control Prototype
SIL	–	Software-in-Loop
SPWM	–	Sinusoidal Pulse Width Modulation
SSB	–	Solid-state Breaker
STATCOM	–	Static Compensator
THD	–	Total Harmonic Distortion

TDD	–	Total Demand Distortion
UPQC	–	Unified Power Quality Conditioner
UPS	–	Uninterruptible Power Supply
VSI	–	Voltage Source Inverter

Table of Content

List of Figures

List of Tables

List of Symbols

v_s, v_g	Instantaneous Source / supply Voltage
i_s	Instantaneous Source / supply Current
p, P, q, Q	Instantaneous active and reactive powers
$\bar{p}$, $\bar{q}$	Average active and reactive powers (dc values)
$\tilde{p}$, $\tilde{q}$	Ripple active and reactive powers (ac values)
v_α , v_β	Voltages in the α-β frame
i_α , i_β	Currents in the α-β frame
i_d , i_q	Currents in synchronous reference frame
$\bar{V}_t$	Voltage at the point of common coupling (PCC) in vector form
v_l	Instantaneous load voltage
v_{sh}	Instantaneous voltage injected by the series active filter
v_t	Instantaneous voltage at the PCC
$i_{s,ref}$	Supply reference current
$i_{sh,ref}$	Shunt active filter reference current
C_{dc}	DC link capacitor
m_a	Amplitude modulation ratio
V_{dc}	dc link voltage
$V_{dc,ref}$	Reference dc link voltage
Q_{sh}	Single-phase Reactive Power
L_{sh}	Shunt Interfacing Inductor
H	Hysteresis band
E_1	Inverter Output Voltage
f	Grid frequency [Hz]
Z_g	Magnitude of the grid impedance [Ω]
θ_g	Grid impedance angle [deg]
ω	Angular frequency of the output voltage [rad/s]
ω*	Reference angular frequency [rad/s]
ωc	Cut-off angular frequency [rad/s]

ω_o	Resonant frequency [rad/s]
m	Phase droop coefficient
n	Amplitude droop coefficient

Chapter 1

Introduction

1.1 **Background**

Centralized power generation systems are facing the twin constraints of shortage of fossil fuel and the need to reduce emissions. Therefore, emphasis has increased on distributed generation (DG) networks with integration of renewable energy systems into the grid or on isolated microgrids (µGrid). This leads to energy efficiency and reduction in emissions. This can also reduce the long transmission line electrical power losses. With the increase of renewable energy penetration in the grid, power quality (PQ) challenges of the medium to low voltage power distribution system is becoming a major area of interest. Most of the integration of renewable energy systems to the grid takes place with the aid of power electronics converters. The main purpose of the power electronic converters is to integrate the DG to the grid in compliance with PQ standards. However, high frequency switching of inverters can inject additional harmonics to the systems, creating major PQ problems if not implemented properly. On the other hand, Custom Power Devices (CPD) such as STATCOM (Static compensator), DVR (Dynamic Voltage Restorer) and UPQC (Unified Power Quality Conditioner) are the latest development of interfacing devices between the distribution supply (grid) and consumer appliances. This class of equipment is designed to overcome voltage/current disturbances and improve the power quality by compensating the reactive and harmonic power generated or absorbed by the load. Therefore, the aim of the present research to

explore the power quality improvement of distributed generation integrated networks with a unified power quality conditioner.

The rest of this section describes briefly the related issues of this research includes DG and microgrids, power quality problems, mitigation techniques, CPDs and real-time simulation. The remainder of this chapter is outlined as follow: Research objectives are described in section 1.2 which is followed by the research contribution in section 1.3. Section 1.4 is the details of the structure and content of the remaining chapters.

1.1.1 Distributed Generation (DG) and Microgrid (µGrid)

Distributed generation (DG) is the term often used to describe small-scale electricity generation, but there is no consensus on how DG should be defined. In some cases, DG is defined on the basis of the voltage level, whereas elsewhere the definition is based on the principle that DG is connected to circuits from which consumer loads are supplied directly. Usually DG is classified according to its different types and operating technologies. A detailed description of the types, technologies, applications, advantages and disadvantages of every available resource and technology is given in [1].

Fig 1.1 shows a typical DG connected µGrid system. Some of the benefits of this system are pointed out in [1, 2]. Although the benefits of DG includes voltage support, diversification of power sources, reduction in transmission and distribution losses and improved reliability, PQ problems are also of growing concern. Solar and wind energy are the most promising DG sources and their penetration level in the grid is also on the rise. Therefore, the study here is limited to the PQ disturbances due to solar and wind energy systems connected to the grid or µGrid system.
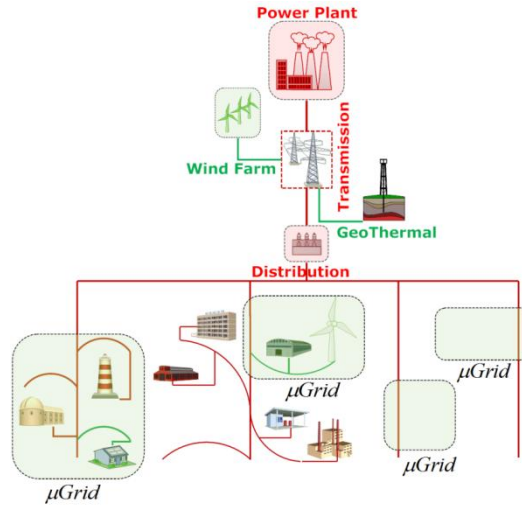
Fig 1.1 A Typical DG connected distribution system with μGrid

1.1.2 Power Quality (PQ) issues in DG or Microgrid (μGrid) system

Approximately 70 to 80% of all PQ related problems can be attributed to faulty connections and/or wiring [2]. Power frequency disturbances, electromagnetic interference, transients, harmonics and low power factor are the other categories of PQ problems (shown in Table 1.1) that are related to the source of supply and types of load [3]. Among these events, harmonics are the most dominant. The effects of harmonics on PQ are specially described in [2, 5]. According to the IEEE, harmonics in the power system should be limited in two ways; limit the harmonic current that a user can inject into the utility system at the point of common coupling (PCC) or limit the harmonic voltage that the utility can supply to any customer at the PCC. Details of these limits can be found in [5]. The IEC (International Electro-technical Commission) and the EU uses the term EMC (Electromagnetic Compatibility) which is "the ability of an equipment or system to function satisfactorily in its electromagnetic environment without introducing intolerable electromagnetic disturbances to anything in that environment" [6,7]. Again, the DG interconnection standards are to be followed when considering PQ, protection and stability issues [8]. Among the DG sources, PQ issues

related to solar and wind energy systems are the major concerns here. Therefore, a brief discussion has been introduced here.

Power Freq Disturbance	Electro-Magnetic Interference	Transient	Harmonics	Electrostatic Discharge	Power Factor (PF)
i. Low Freq phenomena	i. High freq phenomena	i. Fast, short-duration event	i. Low freq phenomena	i. Current flow with different potentials	i. Low PF causes equipment damage
ii. Produce Voltage sag / swell	ii. Interaction between electric and magnetic field	ii. Produce distortion like notch, impulse	ii. Produce waveform distortion	ii. Caused by direct current or induced electrostatic field	

1.1.2.1 Solar photovoltaic (PV) system

Though the output of a PV panel depends on solar intensity and cloud cover, the PQ problems depend not only on irradiation but also on the overall performance of the solar photovoltaic system. This includes the PV modules, the filtering and the inverter controlling mechanism. Studies presented in [9], show that the short fluctuation of irradiance and cloud cover play an important role for low-voltage distribution grids with high penetration of PV. Concerning DG, voltage disturbances can cause the disconnection of inverters from the grid and therefore result in loss of energy supplied. Also, consideration of the long term performance of grid-connected PV systems shows a remarkable degradation of efficiency due to the variation of the source and performance of the inverter [10].

The general block diagram of a grid connected PV system is shown in Fig 1.2. Centralized or decentralized operation of PV systems can also be used and the overview of these PV-Inverter-Grid connection topologies along with their advantages and disadvantages are discussed in [10].

These power electronics converters, together with the operation of non-linear appliances, inject harmonics to the grid. In addition to the voltage fluctuation due to irradiation changes, cloud cover or shading effects can make the PV system unstable in

terms of grid connection. Therefore, this needs to be considered in the controller design for the inverter [11-14].
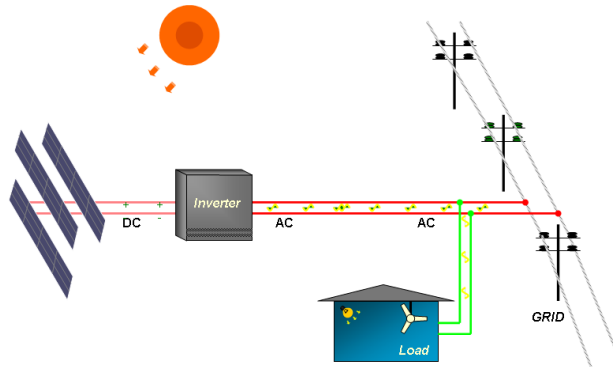
Fig 1.2 General structure of grid-connected PV system

1.1.2.2 Wind energy system

Fig 1.3 shows a simplified representation of some of the common types of wind energy systems. From the design perspective, some configurations involve the generators being directly connected to the grid through a dedicated transformer while others incorporate power electronic interfaces. Recent analysis and study [15] shows that the impact of the yaw error and horizontal wind shear on the power (torque) and voltage oscillations is more severe than the effects due to the tower shadow and vertical wind shear.
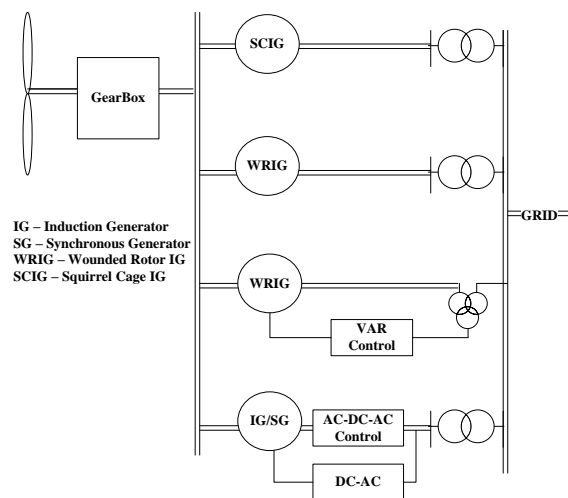
Fig 1.3 Different types of wind energy system

A literature survey [16] of the new grid codes adopted for wind power integration has identified the problems of integrating large amounts of wind energy to the electric grid. It suggests that new wind farms must be able to provide voltage and reactive power control, frequency control and fault ride-through capability in order to maintain system stability. An overview of the developed controllers for the converter of grid connected system has also been discussed in [17] and showed that the DFIG has now the most efficient design for the regulation of reactive power and the adjustment of angular velocity to maximize the output power efficiency. However, the drawbacks of converter-based systems are harmonic distortions injected into the system.

1.1.2.3 Anti-islanding

Anti-islanding is one of the important issues for grid-connected DG systems. A major challenge for the islanding operation and control schemes is the protection coordination of distribution systems with bidirectional flows of fault current. This is unlike the conventional over-current protection for radial systems with unidirectional flow of fault current. Therefore extensive research has been carried out and an overview of the existing protection techniques with islanding operation and control, for preventing disconnection of DGs during loss of grid, has been discussed in [18].

In terms of DG connected grid or μGrid systems, however, DG integration includes some level of power electronics to improve controllability and operating range. Whatever connection configuration is used, each DG system itself has an effect on the PQ of the distribution or transmission system. These PQ problems related to the most commonly used DG systems (solar, wind, hydro and diesel) are given in Table 1.2 [19]. Here it shows that wind energy systems can potentially introduce higher PQ problems than the other forms of generation level. Diesel generator goes a superior perform but has highest green house gas emissions.

Table 1.2 PQ problems related to DG systems

PQ Problems	Wind Energy	Solar Energy	Micro/ Small Hydro	Diesel
Voltage Sag/Swell	●		●	●
Over/Under Voltage	●			●
Voltage Unbalance		●		
Voltage Transient	●			
Voltage Harmonics	●	●	●	
Flicker	●	●		●
Current Harmonics	●	●	●	
Interruption	●	●		

1.1.3 Cost of PQ and mitigation techniques

The impacts of power quality are usually divided into three broad categories: direct, indirect and social. The detail of these impacts has been described in [20]. A recent survey [21] reported PQ costs for EU-25 countries exceeds €150bn where industry accounts for over 90% of this wastage. Dips and short interruptions account for almost 60% of the overall cost to industry and 57% for the total sample. Fig 1.4 shows the PQ costs for the EU-25 countries by sector. At the same time it is necessary to consider the impact of DG in terms of the cost of power quality. In [22], a method to evaluate the dip and interruption costs due to DG into the grid has been proposed.

There are two ways to mitigate the effects of power quality problems - either from the customer side or from the utility side. The first approach is called load conditioning, which ensures that the equipment is less sensitive to power disturbances, allowing operation even under significant voltage distortion. The other solution is to install line conditioning systems that suppress or counteract the power system disturbances. Several devices including flywheels, super-capacitors and other energy storage systems, constant voltage transformers, noise filters, isolation transformers, transient voltage surge suppressors, harmonic filters are used for the mitigation of specific PQ problems. Custom power devices (CPD) such as STATCOM, DVR and UPQC are capable of

mitigating multiple PQ problems associated with utility distribution and end user appliances.
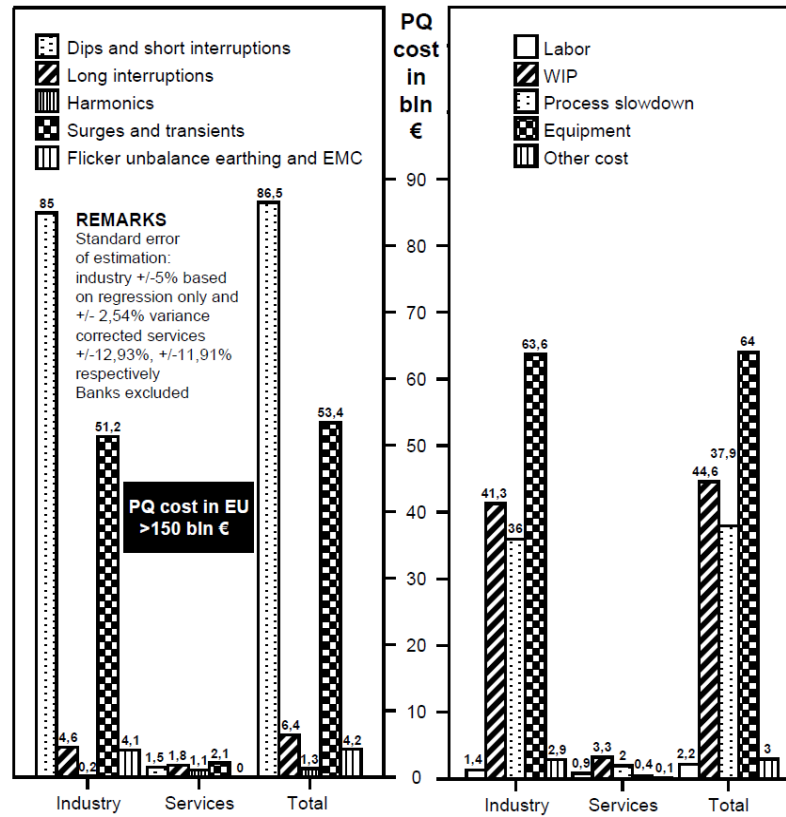
Fig 1.4 Extrapolation of PQ cost to EU economy in LPQI surveyed sectors [21]

1.1.4 Custom Power Devices (CPDs)

The Custom Power (CP) concept was first introduced by N.G. Hingorani in 1995 [23]. Custom Power embraces a family of power electronic devices, or a toolbox, which is applicable to distribution systems to provide power quality solutions. This technology has been made possible due to the widespread availability of cost effective high power semiconductor devices such as GTO (gate turn-off thyristor) and IGBT (insulated-gate bipolar transistor), low cost microprocessors or microcontrollers and techniques developed in the area of power electronics.

DSTATCOM (Distribution STATCOM) is a shunt-connected custom power device specially designed for power factor correction, current harmonics filtering, and

load balancing. It can also be used for voltage regulation at a distribution bus level [24]. It is often referred to as a shunt or parallel active power filter (APF_{sh}) and it consists of a voltage or a current source PWM converter, as shown in Fig 1.5(a). It operates as a current controlled, voltage source and compensates current harmonics by injecting the harmonic components generated by the load but phase shifted by 180 degrees.

The DVR is a series-connected custom power device to protect sensitive loads from supply side disturbances (except outages). It can also act as a series active power filter (APF_{se}), isolating the source from harmonics generated on the load side. It consists of a voltage-source PWM converter equipped with a dc capacitor and connected in series with the utility supply voltage through a low pass filter (LPF) and a coupling transformer [25] as shown in Fig 1.5(b). This device injects a set of controllable ac voltages in series and in synchronism with the distribution feeder voltages such that the load-side voltage is restored to the desired amplitude and waveform, even when the source voltage is unbalanced or distorted.

(a)   (b)
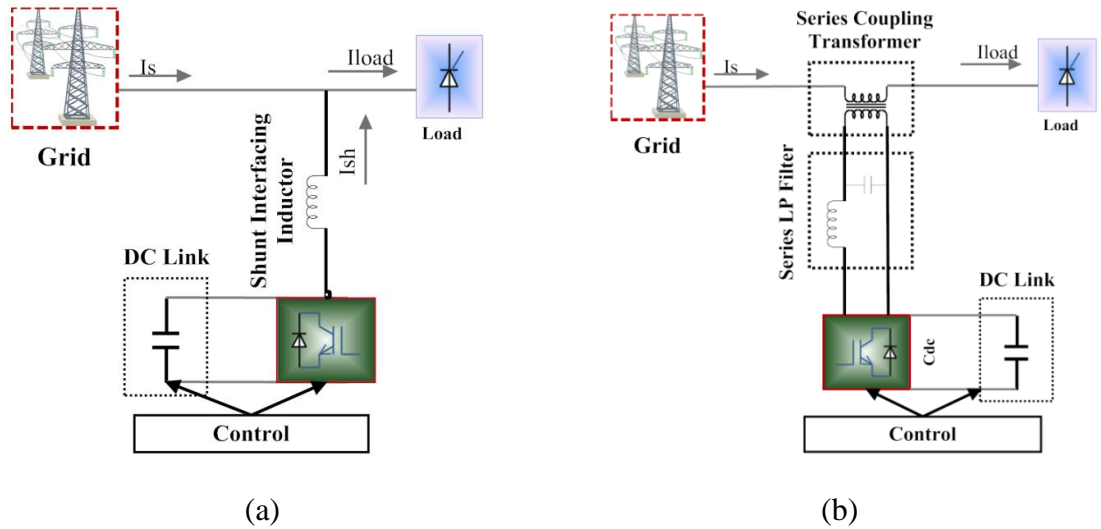
Fig 1.5 System configuration of (a) DSTATCOM and (b) DVR

UPQC is the integration of series and shunt active filters, connected back-to-back on the dc side and sharing a common DC capacitor [26] as shown in Fig 1.6. The

series component of the UPQC is responsible for mitigation of the supply side disturbances: voltage sags/swells, flicker, voltage unbalance and harmonics. It inserts voltages so as to maintain the load voltages at a desired level; balanced and distortion free. The shunt component is responsible for mitigating the current quality problems caused by the consumer: poor power factor, load harmonic currents, load unbalance etc. It injects currents in the ac system such that the source currents become balanced sinusoids and in phase with the source voltages.
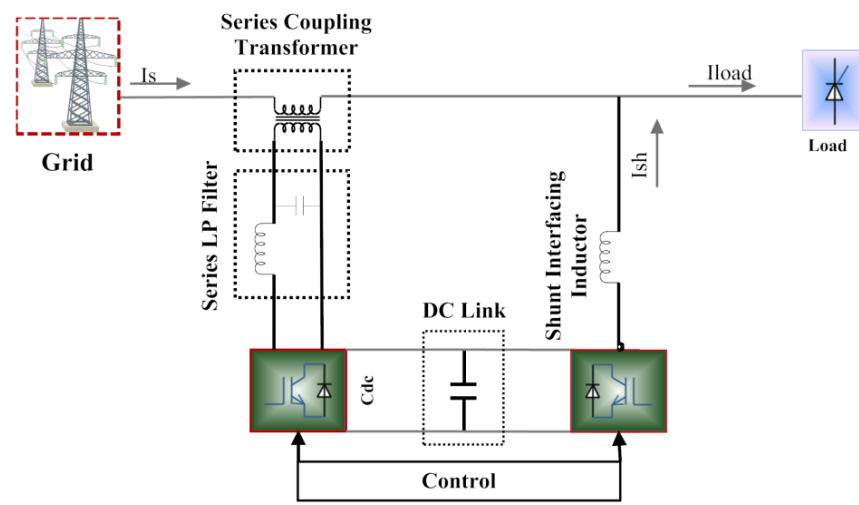
Fig 1.6 System configuration of UPQC

Recent trends in the power generation and distribution system shows that the penetration level of DG into the grid has increased considerably. End user appliances are becoming more sensitive to power quality conditions. Extensive research on CPDs for the mitigation of PQ problems is also being carried out. CPDs can find significant application in integrating solar and wind energy sources to the grid. They play an important role in the concept of the custom power park in delivering quality power at various levels.

1.1.5 Real-time performance study

With the advancement of technology, real-time performance of any system can be observed using a real-time simulator. Instead of developing the complete actual system at full capacity, either the controller/system can be modelled in software or can be built in hardware or can be a combination of both. In real-time simulation, the accuracy of the computations depends upon the precise dynamic representation of the system and the processing time to produce the results. In fact, the processing time at a given time-step must be shorter than the real clock time duration. Real-time simulators are typically used in three different application categories [27]:

(i) Rapid Control Prototype (RCP): Here the controller is implemented using a real-time simulator and is connected to the physical plant.

(ii) Hardware-in-Loop (HIL): In that case, a physical controller is connected to a virtual plant executed on a real-time simulator, instead of to a physical plant.

(iii) Software-in-loop (SIL): Here, both the controller and the plant can be simulated in real-time in the same simulator. In that case, the simulator must be more powerful. SIL can also be a combination of RCP and HIL.

Fig 1.7 shows the real-time simulation structure in a SIL configuration used to develop the real-time environment by OPAL-RT. With the combination of MATLAB SPS (Sim Power System) from MATHWORKS and the RT-LAB toolbox from OPAL-RT, the real-time model of the power system and controller is developed for the real-time simulator. The developed model is then re-arranged to Master (SM_) and Slave (SS_) subsystems to obtain the real performance virtually in Console (SC_), as shown in Fig 1.7(a), or through the real scope, as shown in Fig 1.7(b). The hardware synchronization mode can also be used for RCP/HIL or a combination with SIL.
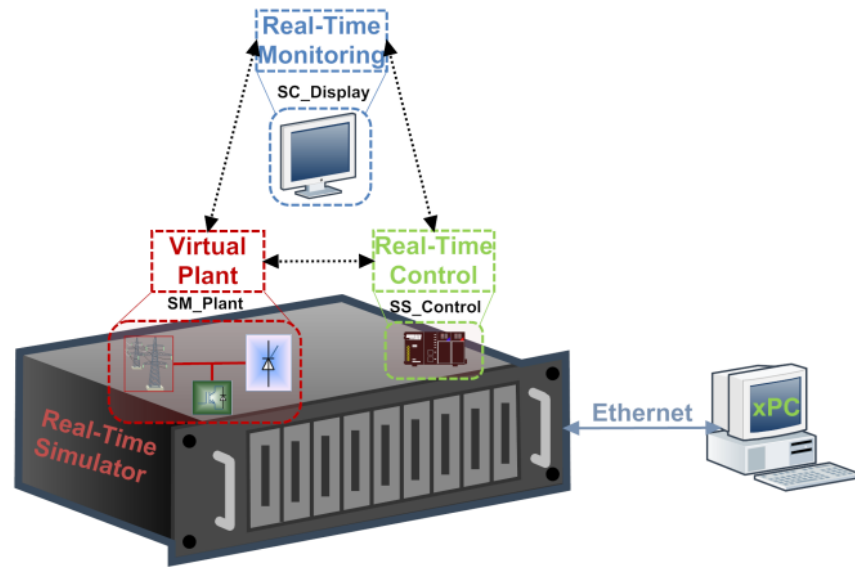
(a)
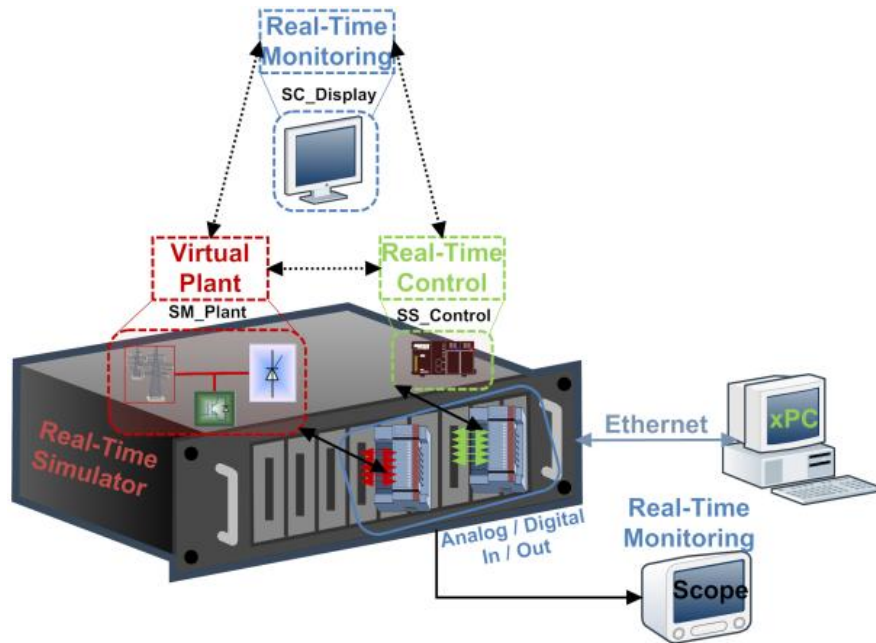
(b)

Fig 1.7 Real-time simulation structure in SIL configuration (a) software synchronization and (b) hardware synchronization mode

1.2 **Research Objectives**

With the increased penetration of small scale renewables in the electrical distribution network, maintaining or improving power quality has become more critical than ever where the level of voltage and current harmonics or disturbances can vary

widely. For this reason, Custom Power Devices (CPDs) such as the Unified Power Quality Conditioner (UPQC) can be the most appropriate solution for the dynamic performances of the distribution network, where prior knowledge of disturbances may not be accurately known.

Therefore, the main objective of the present research is to investigate

(i) the placement

(ii) integration

(iii) capacity enhancement and

(iv) real time control

of the Unified Power Quality Conditioner (UPQC) to improve the power quality (PQ) of a distributed generation (DG) network connected to the grid or microgrid (µGrid).

1.3 **Research Contribution**

The research work described here to achieve the objectives mentioned in the previous section has led to the following contribution and developments;

(i) Literature review dealing with the following

- Power quality issues related to DG integrated network

- Design and control of Custom Power Devices (CPDs)

- Application of CPDs in a DG network

- Parallel operation of Inverter and APF

- Placement and Integration of UPQC in the DG network

- Capacity extension of UPQC

(ii) Design of D-STATCOM / Shunt APF

The switching dynamics of a 3-phase, 3-wire (3-leg) D-STATCOM / Shunt Active Power Filter (APF) with hysteresis band, current controller has been studied.

The interdependence among the design parameters and their effects on the loss calculation has also been studied. Extensive calculation and simulation work have been performed for a 3-phase, 3-wire STATCOM. To demonstrate the performance, this analysis has been applied to a $400V_{L-L}$ distribution system, to study the effects of design parameter selection and their role on power loss calculation. Simulated and calculated results are presented in graphical mode to facilitate the display and selection of the important design parameters for different switching frequencies, together with their associated losses and kVA ratings. The procedure can be followed to design the parameters for other topologies, like 3-phase, 4-wire or single phase systems.

(iii) Placement and Control of UPQC in DG integrated network

In a DG integrated electrical distribution system, DG sources can be connected to the electric power system as micro-generation (μGen) or in a μGrid arrangement to supply the active power to the grid and/or load. A DG converter should also be capable of detecting the unintentional islanding or grid voltage disturbances to be islanded/disconnected. UPQC as a Custom Power Device is introduced at the PCC to (i) prevent propagation the current harmonics generated by the non-linear loads towards the grid, (ii) maintain the voltage and current THD at PCC within the IEEE limits and (iii) compensate the grid voltage sag / swell to provide a balance and stable voltage at the PCC. In the presence of DG sources and a UPQC in an active distribution network, the following issues have been analysed;

(a) the placement of UPQC and its feedback sensors in the network,

(b) impact on the control method of UPQC,

(c) performance of the UPQC with bi-directional power flow in the network and

(d) the privilege of DG system in the presence of UPQC

Depending on the location and integration technique of DG sources, as well as the location of the UPQC sensors which is based on its control technique, a new placement

arrangement at the point of common coupling (PCC) and integration method of UPQC has been identified.

(iv) UPQC$_{\mu G}$ - a new integration method

To extend the operational flexibility of DG inverter and to improve the power quality in grid connected DG based μGrid/μGen system, a new hierarchical control method and integration technique of UPQC have been proposed here. μGrid / μGen system (with or without storage), the load and the shunt part of the UPQC (shunt APF) are placed at or after the PCC. The series part of the UPQC (series APF) is placed before the PCC and in series with the grid. The UPQC current sensor, for reactive and harmonic power compensation, measure only the load current. Islanding detection and reconnection techniques are introduced in the normal UPQC and hence it is termed as UPQCμ$_G$. Depending upon the control strategy and integration technique, the operation of UPQC$_{\mu G}$ can be of two types;

A. UPQCμ$_{G-I}$

- UPQC compensates voltage interruptions in addition to voltage sags/swells, harmonic and reactive power compensation in the interconnected mode. Therefore, the DG inverter can still be connected to the system during the voltage sag/interrupt condition. Thus it extends the operational flexibility of DG inverter in μGrid/μGen system (referred to as μG).

- The shunt part of the UPQC compensates the reactive and harmonic (QH) power of the load in islanding mode. Therefore, primary control is based on the functionality of the series and shunt part of UPQC.

- Islanding detection technique is introduced in the UPQC as a secondary control. Therefore, DG inverter can remove the islanding detection technique from its control system.

- Both in current and voltage control mode, μG system is required to provide only the active power to the load. Therefore, it can reduce the control complexity of the inverter.

- Only the grid resynchronization/reconnection method needs to be the part of control of μG.

B. UPQCμG-IR

- In addition to the previous method and technique, the reconnection method is also the part of UPQC and hence the UPQCμG-IR has the total control of islanding operation and reconnection for a smooth operation of μG with a high quality power service.

- The system can even work in the presence of a phase difference (within limit) between the grid and μG.

For both cases, a communication between the UPQC and μG is required for secondary control.

(v) D-UPQC: A way to enhance capacity and achieve flexibility

In high power applications, the filtering task cannot be performed for the whole spectrum of harmonics by using a single converter due to the limitations on switching frequency and power rating of the semiconductor devices. The relative power loss of the APF unit is also high. Therefore, compensating the reactive harmonic components to improve the power quality of the DG integrated system as well as avoiding the large capacity centralised APF, multiple Shunt APF units in distributed (parallel) modular mode and connected with a common dc linked capacitor can be a solution (termed the Distributed UPQC or D-UPQC). Due to the common DC link between the parallel APF units, a zero sequence circulating current (ZSCC) could flow. Reduction of ZSCC by selecting the appropriate design parameters for hysteresis based current controller is one of the key issue to the development of D-UPQC and this issue has been discussed here.

(vi) Real-time control

An active distribution network has been designed in MATLAB using SimPowerSystems. A real-time simulation environment, in SIL configuration with hardware synchronization mode, has been developed using RT-LAB from OPAL-RT which is powered by Intel Core 2 Quad, 2.66 GHz speed with a total of 8 Core system. The performance of the proposed UPQC$_{\mu G}$ and D-UPQC in the distribution network have then been analyzed in the real-time environment.

1.4 Outline of the Thesis

This research report is divided into seven chapters.

Chapter One

The first chapter contains a brief introduction on DG and Microgrid, including the PQ issues related to DG/microgrid and the PQ cost and mitigation technique using CPDs.

Chapter Two

As the design and control are important parts of the present research, the second chapter deals with these issues of CPDs. Switching dynamics of shunt APF, selection of design parameters and associated power loss have been analyzed. The control methods of the UPQC have been reviewed.

Chapter Three

Placement issues of presently available UPQC in DG integrated networks and integration techniques with capacity enhancement are reviewed in chapter three. Simulation has been performed to analyze the placement issues.

Chapter Four

Parallel operation of shunt the APF and Inverter is very important for the proposed capacity enhancement of D-UPQC in an active distribution network. Therefore, the

fourth chapter reviews the parallel operation strategies of DG Inverters as well as APFs in active load sharing or distributed conditions.

Chapter Five

The fifth chapter describes the integration method and control of the proposed UPQC$_{\mu G}$. Simulation results show the details of the performance study. Real-time performance is also observed in SIL configuration using real-time simulator from OPAL-RT.

Chapter Six

The design and control strategy of the proposed D-UPQC for capacity enhancement and operational flexibility has been introduced in chapter six. The proposal has been verified through some simulation studies. Real-time performance is also observed in SIL configuration using real-time simulator from OPAL-RT.

Chapter Seven

The conclusions of this research work are presented in the final chapter. Future work is also proposed.

Chapter 2

Design and Control Strategies of Custom Power Devices

2.1 Introduction

As the UPQC is a back-to-back combination of series and shunt APF and is directly connected to a dc link capacitor, both the design and controlling mechanism of the APF in terms of the series and parallel connection are very important. Therefore, to achieve a better solution for the design of UPQC and the controlling method, an extensive review of previous research papers has been conducted. The design procedure and the control mechanism for both the series and shunt APF are described briefly. The selected control method of the UPQC has then been discussed.

This chapter is organized as follow: Section 2.2 deals with the design issues of shunt APF part of a UPQC where the emphasis has been given on (i) derivation of equations for harmonic and reactive power calculation based on working principle and tetrahedron phasor diagram, (ii) study of switching dynamics and (iii) calculation of design parameters. Design part of the series APF is discussed in section 2.3 which is followed by the design of UPQC in section 2.4. Control strategies have been discussed in section 2.5. Finally an example procedure has been described for the selection of design parameters of APF_{sh} associating with the active power loss in section 2.6.

2.2 Design of Shunt Active Power Filter (APF$_{sh}$)

To date, more than hundred research papers on APF and UPQC have been published in international journals and presented at conferences. Most of the papers surveyed are based on a specific control mechanism. Some of them deal with the basic design configuration for single/three phase, three or four wire power distribution system. The design configuration of these filters depends on the type of converter, topology, number of phases, interfacing inductor, DC link capacitor and switching frequency. Further details of these classifications can be found in [28-30]. Detailed discussion on classification is beyond the scope of this study. The aim of this chapter is to organize the overall design procedure for the most commonly used hysteresis current control based shunt APF (APF$_{sh}$) system and to discuss the critical issues that should be taken into design consideration while choosing the specific controlling method.

The basic configuration of the Shunt APF has already been given in Section 1.1.4 of the previous Chapter. Generally its compensating functionality consists of two main blocks: Converter (power processing) and Active Filter Controller (signal processing) [29-31].

As there are two types of passive energy storage devices (capacitor and inductor), converters are also classified as two types. For the current source APF$_{sh}$ (CAPF$_{sh}$), the inductor acts as the energy storage device whereas the capacitor is the storage device in the voltage source APF$_{sh}$ (VAPF$_{sh}$). Compared to the CAPF$_{sh}$, the VAPF$_{sh}$ (hereafter, referred as APF$_{sh}$) is less expensive, lighter, with higher efficiency of operation, low cost and easier to control [32-34]. Moreover, the IGBT modules that are now available are more suitable for the voltage-source converter (VSC) because of the connected free-wheeling diode in anti-parallel with each IGBT. This means that the IGBT does not need to provide the capability of reverse-blocking in itself, thus bringing more flexibility to device design in a compromise between conducting and switching losses

and short-circuit capability than the reverse-blocking IGBT. On the other hand, the current-source converter (CSC) requires either series connection of a traditional IGBT and a reverse-blocking diode as shown in Figure 2.1(b), or the reverse-blocking IGBT that leads to more complicated device design and fabrication, and slightly worse device characteristics than the traditional IGBT without reverse-blocking capability [26]. In fact, almost all active filters that have been put into practical applications have adopted the voltage-source PWM converter equipped with the DC capacitor as the power circuit. More details of the comparison can also be found in [26, 32].
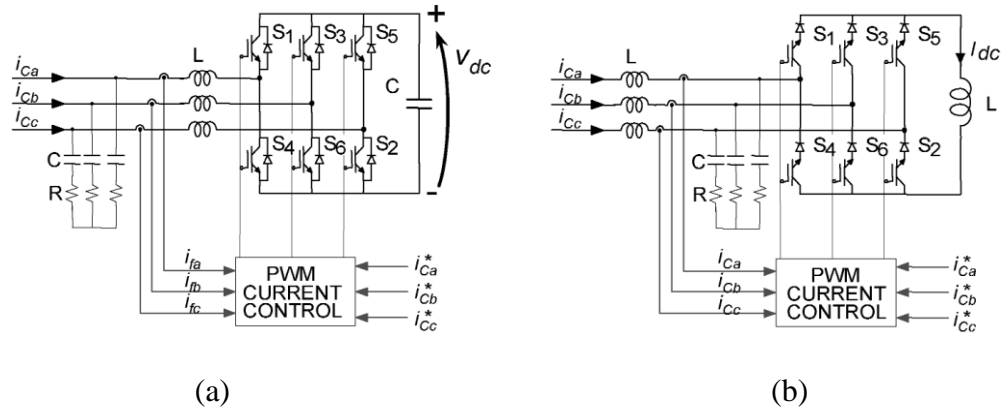
Fig 2.1 a) Voltage source and b) Current source Shunt Active Power Filter [26]

Whatever the converter types, topologies or number of phases, there are some basic and most important components/parameters that are needed to be properly designed to compensate unbalanced and non-linear loads. These are;

    i.   DC link voltage

    ii.   DC storage capacitor

    iii.   Interfacing inductor

    iv.   Hysteresis band

    v.   Switching frequency of the PWM inverter

    An isolation transformer is also used in the H-bridge VSI topology for load compensation [35] to provide the isolation between the inverter legs and for short circuit

protection of the DC storage capacitor due to the switching in different inverter legs. It prevents the compensator from supplying DC load current. In addition of these, another capacitor is sometimes used as a passive filter to minimize the ripple effect due to PWM switching. The value of this capacitor depends on the order of the required cancellation of harmonic frequency component [36, 37]. Digital filtering in the controlling mechanism is one of the processes to overcome this problem [37]. Passive filters can also be combined with active power filters to improve the power quality of the supply by reducing the THD below 1% [38]. The basic algorithm for determining the passive filter components for harmonic power compensation has been described in [39].

2.2.1 Working principle

Fig 2.2(a) shows a simple 3-phase 3-wire power system with APF$_{sh}$. The purpose of a APF$_{sh}$ is to compensate the reactive and harmonic power of non-linear loads so that harmonics from the load current are not injected into the grid. Thus the *THD$_{Is}$* is minimized and the grid current is kept in phase with the grid voltage. To achieve this, the power transfer from the APF$_{sh}$ to the PCC, as shown in Fig 2.2(b), is performed in a controlled manner so that $\theta_{pcci} = \theta_{pccv} = 0$.
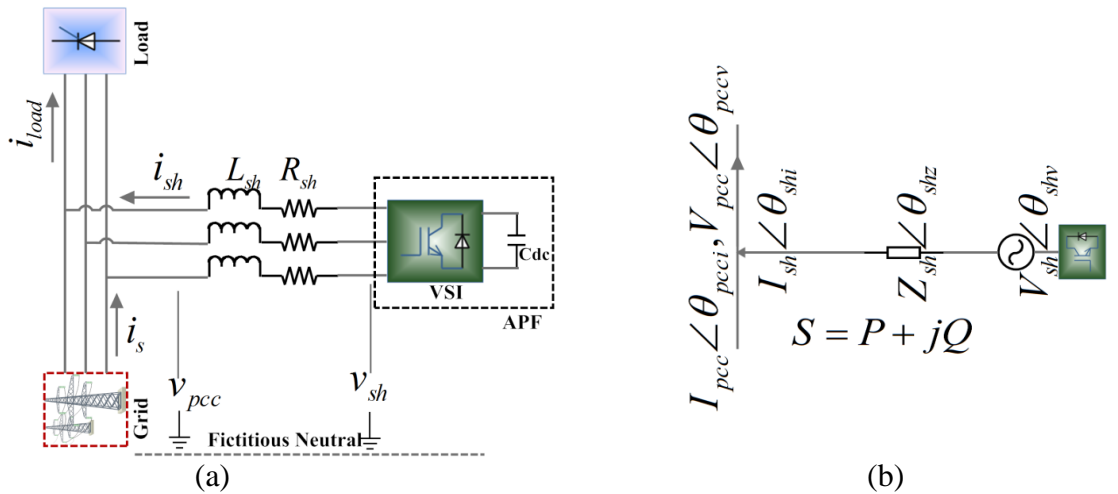
Fig 2.2 (a) A 3-phase 3-wire power system with APF$_{sh}$; (b) Power transfer from APF$_{sh}$ to the PCC

Therefore, the injected current of the APF$_{sh}$ can be written as;

$$\overline{I_{sh}} = \frac{V_{sh}\angle\theta_{shv} - V_{pcc}}{Z_{sh}\angle\theta_{shz}} \tag{2.1}$$

The voltage will be;

$$\overline{V_{sh}} = V_{pcc} + Z_{sh}I_{sh}\angle(\theta_{shz} + \theta_{shi}) \tag{2.2}$$

Injected power at the PCC can be obtained as;

$$S_{sh} = V_{pcc}\overline{I_{sh}^*} = \frac{V_{pcc}(V_{sh}\angle-\theta_{shv} - V_{pcc})}{Z_{sh}\angle-\theta_{shz}} = \frac{V_{pcc}V_{sh}}{Z_{sh}}\angle(\theta_{shz}-\theta_{shv}) - \frac{V_{pcc}^2}{Z_{sh}}(\angle\theta_{shz})$$

$$= \left\{\left(\frac{V_{pcc}V_{sh}}{Z_{sh}}\cos(\theta_{shz}-\theta_{shv})\right) - \frac{V_{pcc}^2}{Z_{sh}}\cos(\theta_{shz})\right\}$$

$$+ j\left\{\left(\frac{V_{pcc}V_{sh}}{Z_{sh}}\sin(\theta_{shz}-\theta_{shv})\right) - \frac{V_{pcc}^2}{Z_{sh}}\sin(\theta_{shz})\right\}$$

$$= \left\{\left(\frac{V_{pcc}V_{sh}}{Z_{sh}}\cos\theta_{shv} - \frac{V_{pcc}^2}{Z_{sh}}\right)\cos\theta_{shz} + \frac{V_{pcc}V_{sh}}{Z_{sh}}\sin\theta_{shv}\sin\theta_{shz}\right\}$$

$$+ j\left\{\left(\frac{V_{pcc}V_{sh}}{Z_{sh}}\cos\theta_{shv} - \frac{V_{pcc}^2}{Z_{sh}}\right)\sin\theta_{shz} - \frac{V_{pcc}V_{sh}}{Z_{sh}}\sin\theta_{shv}\cos\theta_{shz}\right\}$$

$$S_{sh} = \{A\cos\theta_{shz} + B\sin\theta_{shz}\} + j\{A\sin\theta_{shz} - B\cos\theta_{shz}\} \tag{2.3}$$

where, $\frac{V_{pcc}V_{sh}}{Z_{sh}}\cos\theta_{shv} - \frac{V_{pcc}^2}{Z_{sh}} = A$ and $\frac{V_{pcc}V_{sh}}{Z_{sh}}\sin\theta_{shv} = B$

Subsequently, this transferred power can be divided into its fundamental and harmonic components. The components can be given as;

$$S_{sh} = P_{sh} + jQ_{sh} = (P_{shf} + P_{shH}) + j(Q_{shf} + Q_{shH}) = \sqrt{P_{shf}^2 + Q_{shf}^2 + H_{sh}^2} \tag{2.4}$$

where, $H_{sh} = \sqrt{P_{shH}^2 + Q_{shH}^2}$

This can be reflected in the power tetrahedron diagram [26], as shown in Fig 2.3. Therefore, from (2.3 and 2.4), putting the values of A and B, it can be written as;

$$\begin{cases} P_{shf} = \left(\frac{V_{pcc}V_{sh}}{Z_{sh}}\cos\theta_{shv} - \frac{V_{pcc}^2}{Z_{sh}}\right)\cos\theta_{shz} \\ Q_{shf} = \left(\frac{V_{pcc}V_{sh}}{Z_{sh}}\cos\theta_{shv} - \frac{V_{pcc}^2}{Z_{sh}}\right)\sin\theta_{shz} \\ H_{sh} = \frac{V_{pcc}V_{sh}}{Z_{sh}}\sin\theta_{shv} \end{cases} \tag{2.5}$$
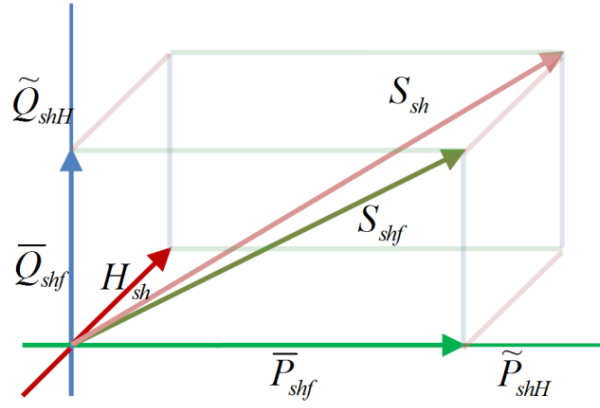
Fig 2.3 Power tetrahedron diagram for APF$_{sh}$

Now, as $\angle\theta_{shv}$ is very small $(sin\theta_{shv} = \theta_{shv}; cos\theta_{shv} = 1)$, then $\angle\theta_{shi}$ is approximately depends on $\angle\theta_{shz}$, i.e. the injecting/compensating current depends on the type of impedance. If Z_{sh} is inductive, then $\angle\theta_{shz} = 90^0$, therefore,

$$\begin{cases} P_{shf} = 0 \\ Q_{shf} = \frac{V_{pcc}V_{sh}}{Z_{sh}} - \frac{V_{pcc}^2}{Z_{sh}} = V_{pcc}I_{sh} \\ H_{sh} = \frac{V_{pcc}V_{sh}}{Z_{sh}}\theta_{shv} = V_{pcc}I_{sh} \end{cases} \tag{2.6}$$

It indicates that the active fundamental power (P_{shf}) transfer from the APF$_{sh}$ to the PCC is zero. The compensating reactive and harmonic power can be controlled by varying the amplitude of V_{sh} and θ_{shv} (the phase difference between the voltage at VSI and PCC). From (2.6) it is also found that the APF$_{sh}$ can compensate the reactive power only when $V_{sh} > V_{pcc}$. The maximum compensating capacity of the filter can also be found by solving $\frac{dQ_{shf}}{dV_{pcc}} = 0$. Therefore, the maximum reactive power compensation capacity of the 3-phase APF$_{sh}$ will be;

$$Q_{shf-max} = 3\frac{V_{pcc-max}^2}{Z_{sh}} \tag{2.7}$$

and it occurs when $V_{sh} = 2V_{pcc}$ $\hspace{2cm}$ (2.8)

Similarly, the maximum harmonic compensation capacity of a 3-phase APF$_{sh}$ can be obtained as;

$$H_{sh-max} = 3\frac{V_{pcc-max}V_{sh-max}}{Z_{sh}} \text{ ; while } sin\theta_{shv} = 1 \tag{2.9}$$

24

Therefore, (2.7) or (2.9) can be used to calculate the maximum reactive or harmonic compensation capacity of a 3-phase APF_{sh}.

The main VSI rating for the reactive and harmonic power compensation of the APF_{sh} can be written as;

$$\begin{cases} VSI_{rating-q} = S_{vsi-q} = \sqrt{Q_{shf}{}^2 + P_{loss}{}^2} \\ VSI_{rating-h} = S_{vsi-h} = \sqrt{H_{sh}{}^2 + P_{loss}{}^2} \end{cases} \tag{2.10}$$

where P_{loss} is the total active power loss of the APF_{sh} during its compensation task which includes conduction loss of interfacing inductor, transformer (if any), VSI and switching loss of VSI. The value of conduction and switching losses of VSI mainly depends on the DC voltage source of the switches, current flow and energy transfer during the on-off condition and the switching frequency [43]. If the overall impedance of the APF system is considered as $(j\omega L_{sh} + R_{sh})$, then the P_{loss} will be;

$$P_{loss} = 3I_{sh}^2 R_{sh} \tag{2.11}$$

where I_{sh} is the rms value of the compensating current, R_{sh} represents the conduction and switching losses per phase of the VSI and the isolation transformer (if any) [34].

For circuit simplicity and to describe the compensating power exchange mechanism between the APF and grid PCC, a working diagram of phase A is shown in Fig 2.4, where S_w represents the switch of the switching devices. When $v_{sh} > v_{pcc}$, switch S1 conducts and a leading current flows from the APF to the PCC. In this case, the APF operates in capacitive mode and reactive power Q is generated by the APF. Similarly, $v_{sh} < v_{pcc}$ results in a lagging current in the conducting switch S4. In that case, the APF operates in inductive mode and hence reactive power is absorbed by the APF. Both of the conditions can be represented as an Inverter and Rectifier mode of operation respectively if the VSI of the APF deals with active power exchange [40]. When $v_{sh} = v_{pcc}$, the reactive power becomes zero. The vector diagrams in Fig 2.5 also

clarify the basic working principle and power exchange between the grid and shunt APF. According to Kirchhoff's voltage law, the basic equations for the capacitive mode can be derived as;

$$\begin{cases} v_{sh} - v_{pcc} - L_{sh}\frac{di_{sh}}{dt} - R_{sh}i_{sh} = 0 \; for \; capacitive \\ -v_{sh} - v_{pcc} - L_{sh}\frac{di_{sh}}{dt} - R_{sh}i_{sh} = 0 \; for \; inductive \end{cases} \tag{2.12}$$
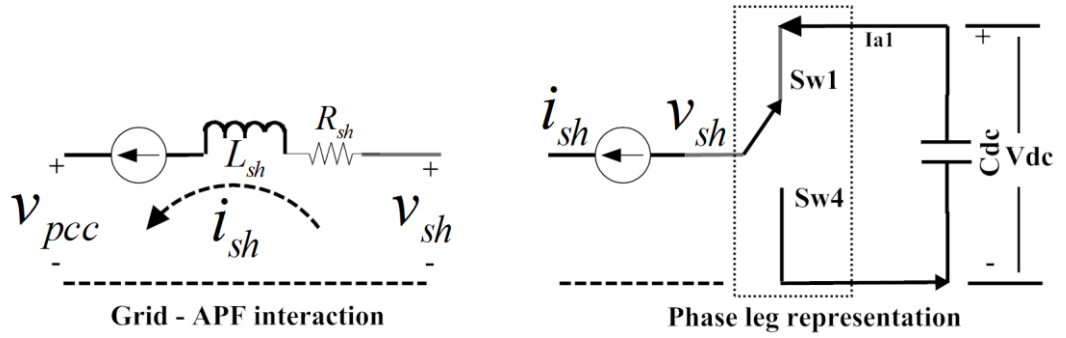
Fig 2.4 Compensating power exchange between the Grid and shunt APF and the phase leg representation for Phase A.
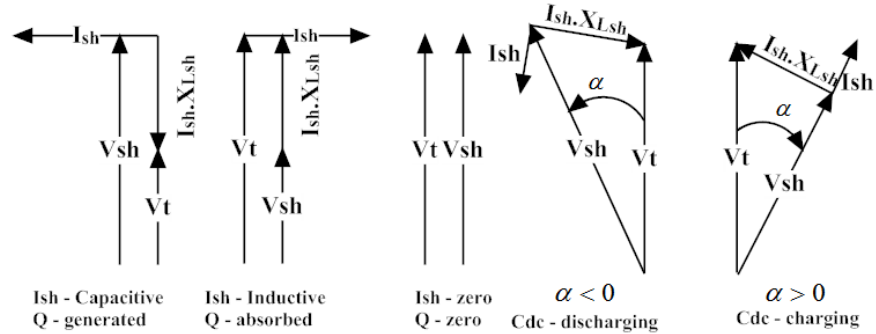
Fig 2.5 Vector diagrams clarifying the working principle of shunt APF system

2.2.2 Switching dynamics

Because of its simplicity of implementation, fast response, enhanced system stability and increased reliability [39, 41], a hysteresis band current controller is generally used to control the actual compensating current (i_{sh}) at the PCC by tracking the desired reference current. Fig 2.6 represents the switching dynamics for one phase of the APF$_{sh}$. It also shows how the compensating current (i_{sh}) tracks the reference

current (i_{shref}) within the hysteresis band limit (h). For H-bridge single phase system, the detailed switching dynamics has been studied in [34]. Similar approach can be implemented here for single / three phase system and can be generalized with respect to V_{sh}.
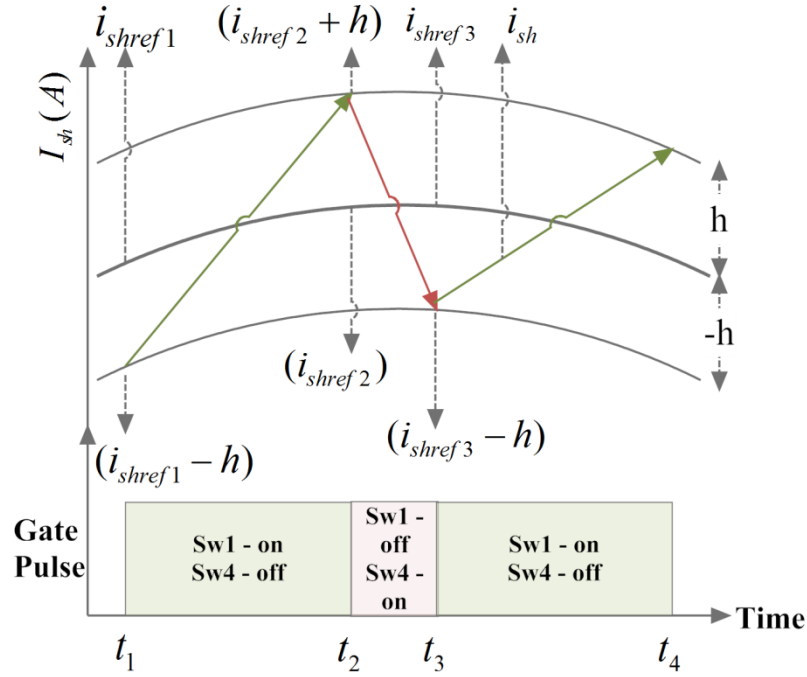
Fig 2.6 Switching dynamics of a hysteresis based current controller

The switching on and off time for Sw1 or Sw4 can be found as [34];

$$\begin{cases} Sw1_{on} = \frac{(2h+h_{on})L_{sh}}{v_{sh}-v_{pcc}-i_{sh}.R_{sh}} \\ Sw1_{off} = \frac{(2h-h_{off})L_{sh}}{v_{sh}+v_{pcc}+i_{sh}.R_{sh}} \end{cases} \tag{2.13}$$

where, $h_{on} = i_{shref2} - i_{shref1}$ and $h_{off} = i_{shref3} - i_{shref2}$

These (h_{on}, h_{off}) values are negligible for a smooth variation of reference current [34] and it occurs when switching frequency is high or close to its maximum. During low/minimum switching frequencies the variation of reference current could be high and then it may be required to consider in case of minimum switching frequency calculation. The general equation for the switching frequency can be written as;

27

$$f_{sw} = \frac{1}{S1_{on} + S1_{off}} = \frac{1}{\left[\frac{(2h+h_{on})L_{sh}}{v_{sh} - v_{pcc} - i_{sh}.R_{sh}}\right] + \left[\frac{(2h-h_{off})L_{sh}}{v_{sh} + v_{pcc} + i_{sh}.R_{sh}}\right]} \tag{2.14}$$

2.2.3 Calculation of design parameters

For simplicity, the following section will discuss the procedure for harmonic current compensation. A similar procedure can be followed for reactive current compensation. As the $VSI_{rating-h}$ value is calculated from H_{sh} and P_{loss} of the APF$_{sh}$, (which depends on the V_{sh}, I_{sh}, L_{sh} and f_{sw}) to compensate specific harmonics, the maximum limit of these values should be considered to determine the maximum acceptable P_{loss} as well as $VSI_{rating-h}$. Again, from the study of switching dynamics it is found that the switching frequency is very much dependent on the V_{pcc}, V_{sh} and I_{sh}, L_{sh} and h. Therefore, the proper value and selection procedure of these parameters are very important to determine the capacity of the APF$_{sh}$ to perform its required tasks. Based on the working principle and on the power flow and switching dynamics study, the following steps describe the procedure and criteria for the selection of design parameters.

2.2.3.1 Switching frequencies (f$_{sw}$)

Considering that h_{on} and h_{off} are negligible for smooth varying reference current and high frequency conditions, the switching frequency (2.14) can be simplified as;

$$f_{sw} = \frac{v_{sh}^2 - \left(v_{pcc} + i_{sh}.R_{sh}\right)^2}{4hL_{sh}.v_{sh}}$$

$$= \frac{v_{sh}}{4hL_{sh}}\left[1 - \left\{\frac{V_{pcc-max}}{v_{sh}}\left(\sin wt + \frac{i_{sh}R_{sh}}{V_{pcc-max}}\right)\right\}^2\right] \tag{2.15}$$

where, $v_{pcc} = V_{pcc-max} \sin wt$. The solution of this equation to derive the maximum (f_{swmax}), minimum (f_{swmin}) and zero-crossing (f_{swzero}) switching frequency has been explained in [34] and can be found as;

$$f_{swmax} = \frac{v_{sh}}{4hL_{sh}} \tag{2.16}$$

28

$$f_{swzero} = f_{sw,max}\left[1 - \left(\frac{i_{sh}R_{sh}}{v_{sh}}\right)^2\right] \tag{2.17}$$

$$f_{swmin1} = f_{sw,max}\left[1 - \left\{\frac{V_{pcc-max}}{v_{sh}}\left(1 + \frac{i_{sh}R_{sh}}{V_{pcc-max}}\right)\right\}^2\right] \tag{2.18}$$

$$f_{swmin2} = f_{sw,max}\left[1 - \left\{\frac{V_{pcc-max}}{v_{sh}}\left(1 - \frac{i_{sh}R_{sh}}{V_{pcc-max}}\right)\right\}^2\right] \tag{2.19}$$

Over a complete cycle, the switching frequency and compensating current (i_{sh}) also vary. The maximum compensating current can be found where ($v_{sh} - v_{pcc}$) is maximum and this can be explained from (2.1) and Fig 2.4. That is, when v_{pcc} is near to 0 (zero), I_{sh} should be maximum. Therefore, it is clear that the maximum switching frequency, f_{swmax} should occur at or near the zero crossing condition (depending on the reactive and harmonic components of the load current). Also, at this point, h_{on} and h_{off} both are negligible compared to *2h*. Equation (2.16) should then be modified as;

$$f_{swmax} = \frac{v_{sh}(0)}{4hL_{sh}} \tag{2.20}$$

where $v_{sh}(0)$ represents the value of v_{sh} at or near the zero crossing condition. Similarly i_{sh} should be minimum where ($v_{sh} - v_t$) is minimum. Here, the switching frequency will also be minimum. At that condition, the values h_{on} and h_{off} should be comparable to *2h* and will have an effect on calculating the minimum switching frequency, f_{swmin}. Therefore, equations (2.18) and (2.19) may not give the accurate result and hence the general equation (2.15) should be used to calculate the other switching frequencies.

The relation between the V_{dc} and v_{sh} for single and three phase VSI can simply be obtained from [39], as shown in Fig 2.7. Therefore, (2.20) can be used to calculate the f_{swmax} for single or three phase system. Thus it can be written as;

$$f_{swmax} = \begin{cases} \frac{V_{dc}}{8hL_{sh}} \ for \ 1 - phase, 1 - leg \ system \\ \frac{V_{dc}}{4hL_{sh}} \ for \ 1 \ or \ 3 - phase, H - bridge \ system \\ \frac{V_{dc}}{12hL_{sh}} \ for \ 3 - phase, 3 - leg \ system \end{cases} \tag{2.21}$$
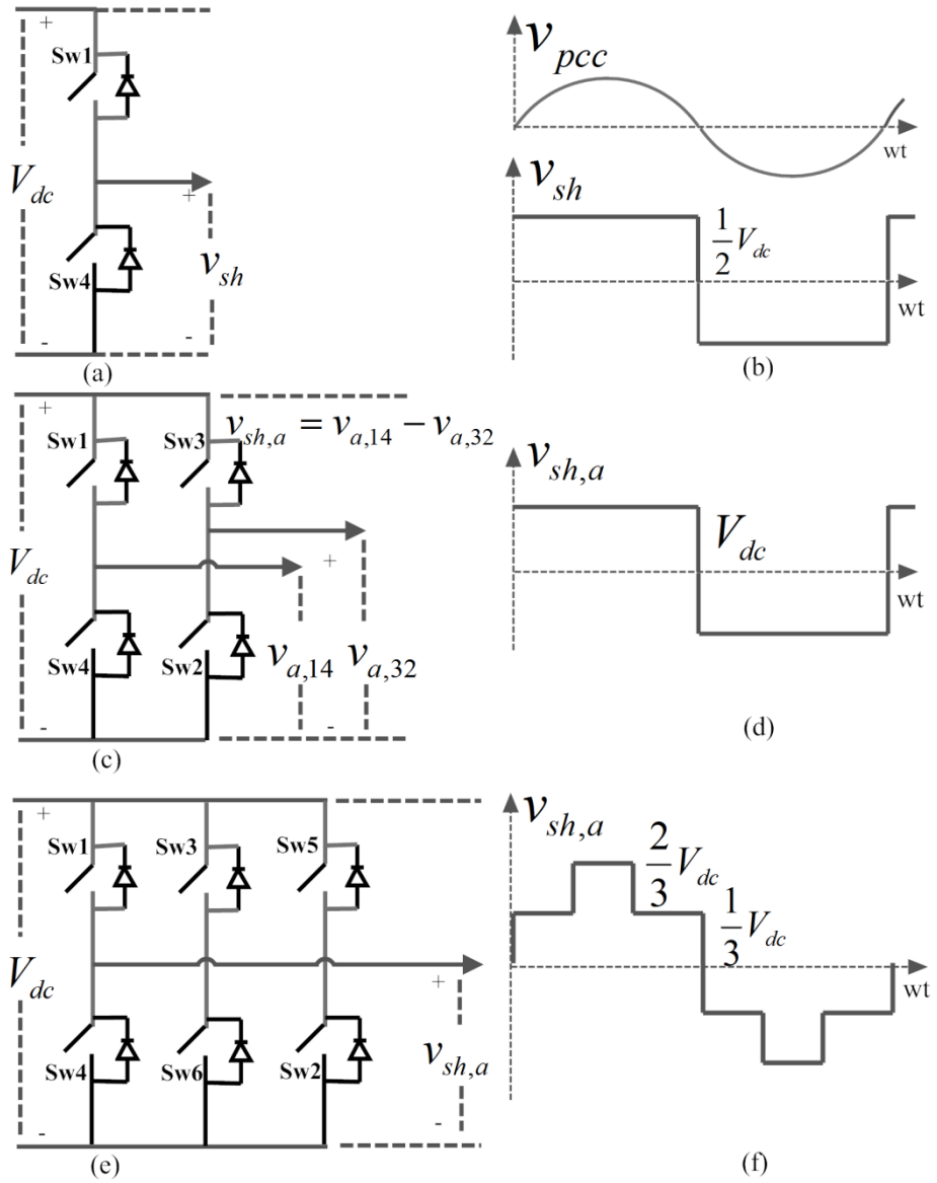
Fig 2.7 a) Switching configuration of VSI and output waveform for (a,b) 1-phase, 1-leg; (c,d) 1-phase, H-bridge and (e,f) 3-phase 3-leg

2.2.3.2 Interfacing inductor (L_{sh})

The derived methods in [35-38] for calculating the value of L_{sh} are mainly based on a fixed frequency PWM converter with an assumption that the ripple current attenuation or peak compensation current and the maximum harmonic voltage also are known. The value of L_{sh} can also be calculated from (2.6) where the value of H_{sh}, V_{sh} and I_{sh} should be pre-determined.

$$L_{sh} = 3\frac{V_{pcc}}{\omega H_{sh}}V_{sh} \tag{2.22}$$

In the case of a hysteresis band current controller, this value of L_{sh} can easily be calculated from (2.20), once the values of f_{swmax} and hysteresis band (h) are set. As the switching devices, typically, have a limit for the maximum switching frequency and therefore the value of L_{sh} also should have a minimum value which is acceptable for the compensating devices. It is found that the f_{swmax} of IGBT is around 20kHz. The minimum value of L then should be;

$$L_{shmin} = \frac{v_{sh}(0)}{4hf_{swmax(IGBT)}} \tag{2.23}$$

Once the value of $v_{sh,}$ and f_{shmax} are fixed, the limit of L_{shmax} for a specified APF$_{sh}$ can be determined by lowering the value of h within the acceptable range.

2.2.3.3 *Hysteresis band (h)*

From (2.16), it is clear that the selection of hysteresis band is very important for selecting the switching frequency and there should be a typical range of h to keep the THD_{Is} within 5% as specified by IEEE [42]. This can be found as;

$$h = k.I_{shmax} \tag{2.24}$$

where, $k = 0.05 \sim 0.15$. Although there are several advantages associated with hysteresis band controllers as mentioned earlier, the only disadvantage is the varying switching frequency with the system voltage. This can be overcome by fixing the switching frequency with a modified or variable hysteresis controller [43, 44] but then the complexity in the system control may increase.

2.2.3.4 *DC link voltage (V_{dc})*

The purposes of the DC link capacitor (C_{dc}) are - i) to maintain the V_{dc} with minimal ripple in steady-state, ii) to serve as an energy storage element to supply the reactive power of the load and iii) to supply the real power difference between the load and source during the transient period. Therefore, the size of the C_{dc} should be selected,

and the controller should be designed in such a way, that the APF can compensate the real power difference for a short transient period (typically a number of msec.) after which the controller should be able to adjust the reference current. Thus the V_{dc} can be maintained at a reference value.

Depending on the topology, different methods or approaches have been presented in [35–38, 43] to develop the relation between V_{pcc}, V_{sh} and V_{dc}. For a 3-ph, 3-leg system, considering the amplitude modulation factor, m_a=1, the minimum value of V_{dc} should be at least equal to $2V_{pcc-max}$ [35], or $2\sqrt{2}.V_{sh}$ [36-38], or greater then $\sqrt{3}.V_{shmax}$ [43]. Based on this information, the minimum value of V_{dc} can be derived as;

$$V_{dc} > \sqrt{3}.V_{pcc-max} \tag{2.25}$$

Although the higher V_{dc} does not have much impact of current THD, it can increase the voltage THD at the PCC and thus degrade the quality of the source voltage [45]. Therefore, lowering the difference between V_{pcc} and V_{sh} will improve the system performance and stability of the voltage at PCC.

2.2.3.5 DC link capacitor (C_{dc})

As an energy storage element, the DC link capacitor should be capable of performing all the functions described in the DC link voltage section. And in general, the energy handling capacity determines the size of the capacitor. The basic equation can be written as;

$$C_{dc} = \frac{2.S.n.T}{V_{dcmax}^2 - V_{dcmin}^2} = \frac{2.S.n.T}{\{(1+z)V_{dc}\}^2 - \{(1-z)V_{dc}\}^2} = \frac{S.n.T}{z.V_{dc}^2} \tag{2.26}$$

where S is the power required to be i) compensated during the steady state condition [46], or ii) supplied to the load during the transient condition [34, 46], or iii) absorbed due to the load change during the transient condition [34], or iv) compensated in DVR mode during voltage sag/swell conditions [47]. T is the required time period for one

complete cycle, n is the number of cycles for energy transfer and z is the percentage of V_{dc} to replace the V_{dcmax} and $V_{dcmin,}$ the maximum and minimum allowable V_{dc} respectively to perform the specific task. For a specific system, it is better to consider the higher value of C_{dc} so that it can handle all of the above conditions. It also helps to get a better transient response and lower the steady-state ripple.

2.3 **Design of Series Active Power Filter (APF$_{se}$)**

The purpose of the Series APF is to compensate the voltage disturbance such as sag/swell, flicker, voltage unbalance. Voltage sag/swell, the most commonly occurring PQ problems, are usually caused by a short-circuit current flowing into a fault and can be illustrated in a simplified model as shown in Fig 2.8. The magnitude and phase of the voltage dip at the Point of Common Coupling (PCC) are determined by the fault and supply impedances, using the following equation [48]:

$$V_{sag} = \frac{Z_P}{Z_S + Z_P} V_S \tag{2.27}$$

$$\angle\emptyset_{sag} = \tan^{-1}\frac{X_P}{R_P} - \tan^{-1}\frac{X_S + X_P}{R_S + R_P} \tag{2.28}$$

Where V_{sag} is the voltage during the sag at the PCC, $Z_P = R_P + jX_P$ is the impedance between the PCC and the fault, and $Z_S = R_S + jX_S$ is the source impedance at PCC and the source voltage V_S.

<div align="center">(a)   (b)</div>
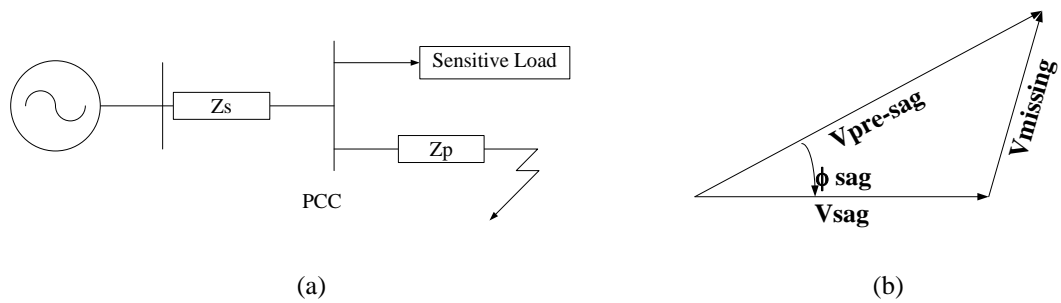
Fig 2.8 a) Distribution system with fault and b) vector diagram of voltage sag with phase jump and the used definition of pre-sag, sag and missing voltage

Though the connection topology differs and mainly depends on the injection transformer and half or H-bridge or multi-level inverter connection, there are some basic parameters that should be calculated/chosen properly for the design of series APF. Details of the topologies and their basic comparison, which is beyond the scope of this study, can be found in [49]. The parameters that are needed to be designed properly to compensate the voltage disturbance are as follow;

i.   Injecting transformer

ii.   Interfacing inductor / low pass filter

iii.   DC link capacitor and storage device

2.3.1 Injection transformer

The basic function of the injection transformer is to increase the voltage supplied by the filtered VSI output to the desired level while isolating the DVR circuit from the distribution network. The transformer winding ratio is pre-determined according to the voltage required in the secondary side of the transformer which is generally kept equal to the supply voltage to allow the DVR to compensate the full supply voltage sag [50]. The turns ratio of the transformer can be determined from the following design concept: If the DVR has the capability of compensating for a voltage-sag depth up to X% in a single-phase sag, then the compensating voltage V_{sag} in each phase can be found as follows [51]:

$$v_{sag} = v_{pcc} \frac{X}{100} \tag{2.29}$$

The maximum output voltage of the PWM inverter is:

$$v_{se-PWM} = \frac{V_{dc}}{\sqrt{2}} \tag{2.30}$$

2.3.2 Interfacing inductor / Low pass filter (LPF)

Low pass passive filters including the interfacing inductor are used to convert the PWM inverted pulse waveform into a sinusoidal waveform. This is achieved by

removing the switching ripples produced by the VSI. These filters can be placed either in the high voltage side or in the low voltage side of the injection transformers as shown in Fig 2.9.
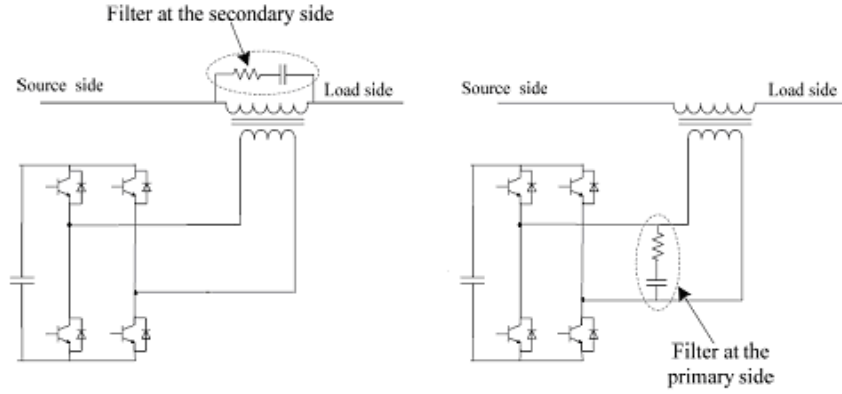
Fig 2.9 Placement of LPF in APFse

When the filters are on the inverter side, higher order harmonics are prevented from passing through the voltage transformer. This will reduce the stress on the injection transformer. In this case, a 50-Hz voltage drop appears across the filter/interfacing inductor when no voltage sag occurs. Therefore, the inductor is designed to reduce the voltage drop to less than 1% of a nominal line-to-neutral of supply voltage [51]. Fig 2.10 shows the equivalent circuit of a single phase series APF$_{se}$ where the output of the VSI can be derived as;

$$v_{se-PWM} = v_{sag} + jZ_{se}i_{se} \tag{2.31}$$

Assumes that the fundamental current flowing through C_{se} is negligible. Then from (2.31) the value of inductor can be determined.

The value of C_{se} can be calculated using the Cut-off frequency (f_c) equation of an LC filter;

$$f_c = \frac{1}{2\pi\sqrt{L_{se}C_{se}}} \tag{2.32}$$

Again, if the filter is placed in the load side, the higher order harmonic currents do penetrate to the secondary side of the transformer, hence, a higher rating of the

transformer is necessary [52]. However the leakage reactance of the transformer can be used as a part of the filter, which will be helpful in tuning the filter.
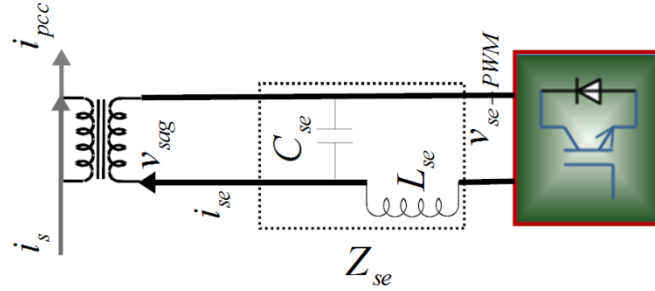
Fig 2.10 Equivalent circuit of single phase series APF

2.3.3 DC link capacitor and energy storage device

An energy storage device is used to supply the real power requirement for compensation during a voltage sag. Flywheels, Lead acid batteries, Superconducting magnetic energy storage (SMES) and Super-Capacitors can be used as energy storage devices.

As the DC link capacitor is between the series and shunt APF for the design of UPQC, the calculation is the same as in the case of shunt APF.

2.4 Design of Unified Power Quality Conditioner (UPQC)

Two possible ways of connecting the UPQC to the point of common coupling (PCC) are discussed in [24]:

- Right-shunt UPQC: The APF_{sh} is connected to the load side and the series to the supply side;

- Left-shunt UPQC: The APF_{sh} is connected to the supply side and the series component to the load side.

Comparing the characteristics of these two configurations, the right-shunt UPQC has the advantages over the left-shunt UPQC in terms of operation (i) in zero power

injection/absorption mode, (ii) to make the power factor unity at the load terminal, (iii) to supply the entire load reactive power requirement. It also has been shown that the dc capacitor control of the right-shunt UPQC structure is simpler. Thus, it can be concluded that the right-shunt UPQC is more advantageous.

Once the design parameters for the series and shunt APF are defined, the complete UPQC system is derived with a combination of these two APF. As the required active power for voltage sag compensation will be provided by the DC link capacitor through the $APF_{sh,}$ a DC link voltage control method then should be derived for this purpose. A 12-kVA DSP controlled laboratory prototype UPQC has been designed and installed at the DIT Lab [41].

2.5 Control Strategies

The control strategy is at the heart of the any compensating device. Generation of appropriate switching patterns or gating signals with reference to command the compensating signals determines the control strategy of any compensating devices. In general, it is implemented in three stages [29];

i.   Signal conditioning - sensing of essential voltage or current signal for referencing and implementation of control algorithm. These voltage or current signals could be on the supply side, the load side or on the compensating side. Voltage signals are sensed using either power transformers or Hall-effect voltage sensors or isolation amplifiers whereas current signals are sensed by current transformer or Hall-effect current sensors. Analog or digital filters are sometimes used to eliminate noise from the sensing parameters.

ii.   Derivation of compensating signals – derivation of compensating or reference voltage/current signals depend on the control method and APF configurations. It is the most important part of the control strategies. It also affects on the rating as

well as the transient and steady-state performance of the device. Two methods are used to generate the compensating command: frequency and time domain.

In the frequency domain, the compensating signal is extracted from the source/load signal by application of the Fourier analysis. The device switching frequency is maintained at a value greater than twice of the highest compensating harmonic frequency for effective compensation.

Compensation in the time domain is based on the instantaneous derivation of compensating commands in the form of voltage or current signals. Control method level on instantaneous p-q theory, synchronous d-q reference frame, synchronous detection, flux-based controller, notch filter, PI controller, sliding-mode controller, genetic algorithm, neural network are the most popular in the time domain.

iii. Generation of gate signal - using PWM, Space Vector Modulation, Hysteresis Band, Sliding-mode, Dead-beat control or Fuzzy or neural based control technique.

The control can be carried out using discrete analog and digital devices or advanced microelectronics such as microcontroller or microprocessors.

2.5.1 Shunt Active Power Filter (APF$_{sh}$)

Removing the fundamental part or extraction of harmonic content from non-linear harmonic current to generate the reference current for harmonic power compensation of APF$_{sh}$ using high pass (HPF) or low pass filters (LPF) are a simple part of the control technique. However both methods have a high error in the phase and magnitude of the harmonics calculation [28]. In addition, HPF is sensitive to high frequency noise.

In synchronous detection method, the three-phase currents are assumed to be balanced after compensation, as shown in Fig 2.11. The method is useful for reactive power compensation, current imbalance and mitigation of harmonic current [53].
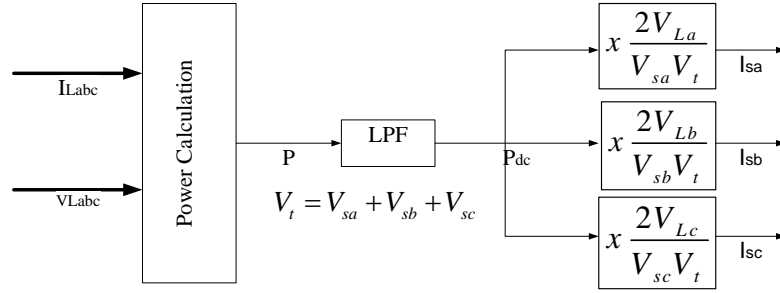
Fig 2.11 Block diagram of Synchronous Detection Method

The synchronous fundamental d-q frame method is derived from the space vector transformation of input signal in a-b-c coordinate to the rotational orthogonal d-q coordinate by means of the Park Transformation. Fig 2.12 shows the block diagram of the synchronous d-q frame method for harmonic current compensation [54]. This method is further improved to detect the desired harmonic frequency for compensation [55].
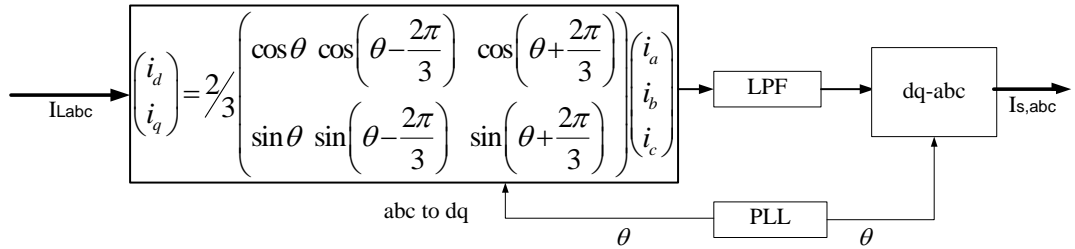
Fig 2.12 Block diagram of d-q synchronous frame method

But the problem associated with these methods is to detect and compensate the per phase harmonic component. Therefore, any disturbance or distortion in the supply side could degrade the performance of the system. The d-q transformation needs also a phase-lock-loop (PLL) circuit to synchronize the transformation with the line frequency and phase.

The *p-q* theory [26] is based on a set of time domain instantaneous powers that can be applied to three phase systems with or without a neutral wire for generic voltage

and current waveforms. Thus, it is valid in the steady state as well as in the transient state. This theory always considers the three phase system as a single unit by transforming voltages and currents from the *abc* to αβ0 coordinates and not a superposition or sum of three single phase circuits. Details of this theory is given in Appendix 1. This p-q theory works properly when the three-phase system is balanced [56]. In [57], a simple modification is proposed by implementing a Phase Lock Loop (PLL) to develop a generalised single-phase p-q theory that can be utilised under the condition of distorted utility voltage.

2.5.2 Series Active Power Filter (APF$_{se}$)

The APF$_{se}$ is controlled to inject the appropriate voltage between the point of common coupling (PCC) and load, such that the load voltages become balanced, distortion free and have the desired magnitude. Theoretically the injected voltages can be of any arbitrary magnitude and angle. However, the power flow and device rating are important issues that have to be considered when determining the magnitude and the angle of the injected voltage [3]. In the case of the UPQC, the implementation of the APF$_{se}$ can be done in two ways [58] depending on the angle of the injected voltage: thus the system is termed as UPQC-Q and UPQC-P. In the first case (UPQC-Q) the injected voltage is maintained 90° in advance with respect to the supply current, so that the series compensator consumes no active power in steady state. In the second case (UPQC-P) the injected voltage is in phase with both the supply voltage and current, so that the series compensator consumes only active power, which is delivered by the shunt compensator through the dc link. A detailed analysis of UPQC rating under different control strategies together with their advantages and disadvantages are presented in [58 - 60]. In the case of UPQC-Q the series compensator requires additional capacity, while the shunt compensator VA rating is reduced as the active power consumption of the series compensator is minimised and it also compensates for

40

a part of the load reactive power demand. In the UPQC-P case the series compensator does not compensate for any part of the reactive power demand of the load, and it has to be entirely compensated by the shunt compensator. Also the shunt compensator must provide the active power injected by the series compensator. Thus, in this case the VA rating of the shunt compensator increases, but that of the series compensator decreases. It can be concluded that the UPQC-Q and UPQC-P are two extreme cases and finding the optimum solution which is located in between is preferable. An analysis for optimisation of the converter rating is presented in [61-63] and an approximate sub-optimal control strategy for UPQC minimum losses operation is proposed.

Comparing the techniques for calculating the reference voltage of the series compensator, it is found that the UPQC-P algorithm has the simplest implementation and involves very little computation [64]. In the UPQC-P case the voltage rating of the series compensator is considerably reduced. Therefore, the UPQC-P control strategy has been used in the UPQC simulation model. For simplicity, only the case of a three-phase, three-wire system has been considered here.

2.5.3 Unified Power Quality Conditioner (UPQC)

The integrated controller of the APF_{se} and APF_{sh} of the UPQC realizes an instantaneous algorithm to provide the compensating voltage reference $v*_C$, as well as the compensating current reference $i*_C$ to be synthesized by the controllers.

The functional block diagram of the UPQC controller is illustrated in Fig 2.13. Generation of compensating voltage and current for Series and Shunt APF is based on the instantaneous p-q theory. In addition, it is shown in Fig 2.13 that the UPQC controller requires a positive-sequence detector, a PWM voltage controller for voltage compensation, a hysteresis current controller for reactive harmonic current compensation and a dc-link voltage regulator.

The phase voltages at the load terminal consists mainly of the positive sequence component (V_{+1}), but can be unbalanced (containing negative- and zero sequence components at fundamental frequency), and can also contain harmonics from any sequence component. The detection of the fundamental positive-sequence component of v_{sa}, v_{sb}, and v_{sc} is necessary in the sinusoidal current control strategy. Fig 2.14 shows the method to detect the fundamental positive sequence of the source voltage [26].

The PWM voltage controller should allow the series active filter to generate compensating voltages according to their references $v*_{Ca}$, $v*_{Cb}$, and $v*_{Cc}$, which can vary widely in frequency and amplitude. Therefore, conventional sine-PWM techniques (SPWM) may not be appropriate due to their inherent amplitude attenuation [65]. Further, the filter (RLC) circuit at the ac output of the PWM converter may cause phase displacements in the compensating voltages v_{ca}, v_{cb}, and v_{cc}. Therefore, feedback control loops are implemented to minimize possible deviations between the reference and actual values generated at the primary sides of the series transformers. The proposed PWM voltage control [26] is given in Fig 2.15.

Different current-control techniques are applied for tracking the reference current: sampled error control, hysteresis band control, sliding mode controller, linear quadratic regulator, deadbeat controller, pole shift controller [24]. From the number of dedicated papers, the hysteresis control appears to be the most preferable for shunt active filter applications. The hysteresis control method has simpler implementation, enhanced system stability, increased reliability and response speed [24, 64, 66]. Therefore, in the UPQC simulation model a hysteresis controller has been used. The advantages of using a hysteresis controller are mentioned below.
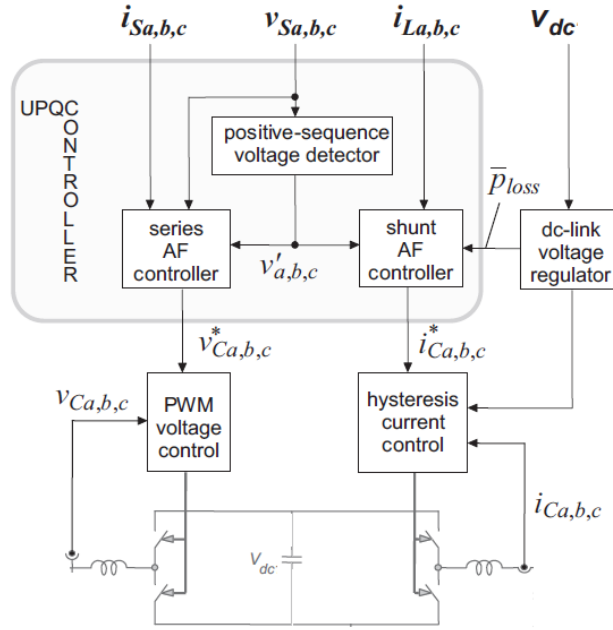
Fig 2.13 Functional block diagram of the UPQC controller
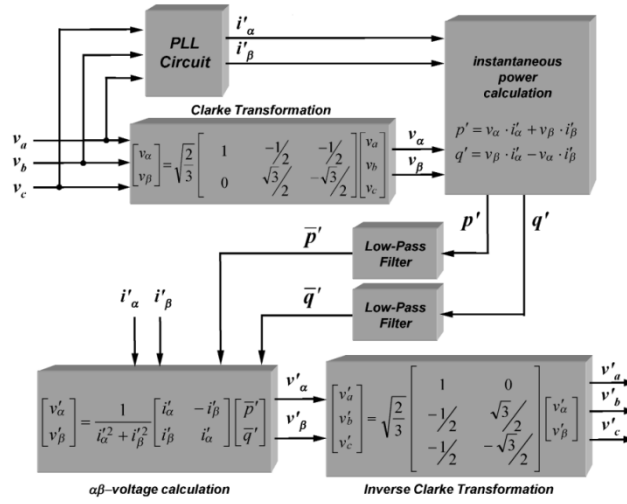
Fig 2.14 Positive sequence detection [26]
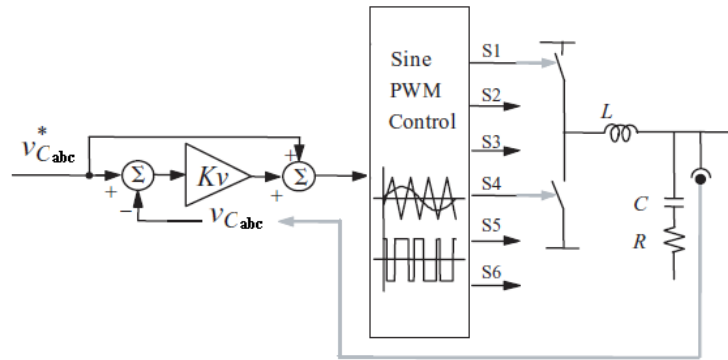
Fig 2.15 PWM voltage control with minor feedback control loops

2.6 **Selection of design parameters for a 3-ph, 3-wire APF$_{sh}$**

This section deals with some simulation study and calculation for the proper selection of design parameters. As an example, the initial target of maximum harmonic compensating current, $I_{shmax,}$ has been set at 100A which requires an APF$_{sh}$ of 48.8 kVA rated capacity (H_{sh}) in a 400V$_{(L-L)}$ distribution system. Again the S_{vsi-h} of the compensator depends on the H_{sh} and P_{loss} which are associated with the V_{sh}, I_{sh} and R_{sh} in (2.6) and (2.11). These are also related to the rating of the switching device and other design parameters including f_{sw}, h and V_{dc}, in (2.17 - 2.26). Therefore a wide range of values of I_{shmax}, h, L_{sh}, R_{sh} and V_{dc} has been chosen to calculate the P_{loss} and S_{vsi-h} and to perform the simulation study to observe the performance of the selected appropriate design components. The connection topology and switching configuration of a 3-ph, 3-wire APF$_{sh}$ together with the chosen parameters range is shown in Fig 2.16.

Fig 2.17(a) shows how the actual VSI_{rating} (S_{vsi-h}) increases with the value of R_{sh} for a specific I_{shmax}. The actual compensating power of the APF, H_{sh} can be calculated from (2.6) and in the Fig 2.17(a) it is represented when R_{sh} is zero. Though R_{sh} is related with the design parameters, in some research articles the value of R_{sh} was considered to be between 0 and 2Ω [67 - 74]. For example, to compensate 48.8 kVA of H_{load}, the required S_{vsi-h} will be 49.0 kVA, if a value of 0.3 Ω for R_{sh} is used as shown in Fig 2.17(a) (point A). The VSI rating will be increased upto 57.7 kVA, if R_{sh} is assumed to be 2Ω. This is shown as point B in Fig. 2.17(a). The corresponding active power loss P_{loss} as a ratio (%) of (P_{loss} / S_{vsi-h}) for the unit is shown in Fig 2.17(b). For $R_{sh} = 0.3$ Ω, the actual P_{loss} is 4.5 kW, calculated from (2.11). In terms of ratio it is around 9.2% of the VSI rating which is reflected as point A in Fig 2.17(b). Point B in Fig 2.17(b) shows the corresponding ratio for the point B in Fig 2.17(a), which is around 52%. Therefore it would be better to lower the R_{sh} value. Considering the ratio of 10% as a loss, it is clear that a value of R_{sh} up to 0.3 Ω would be an acceptable selection for a 49kVA ($I_{shmax} =$

100A) compensator. the shaded part of the Fig 2.17(b) also reflects the possible limits of I_{shmax} for possible R_{sh} values that can be considered between 10% ratio and 1Ω.
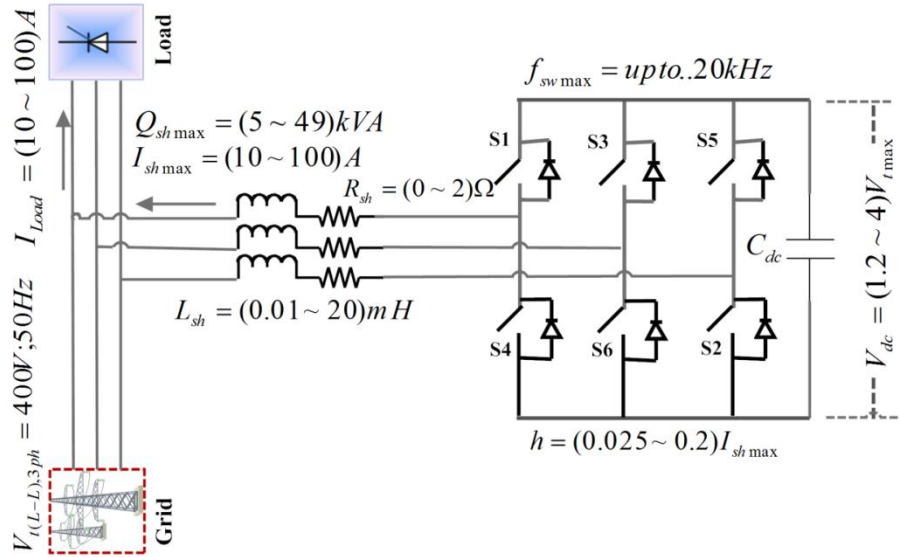
Fig 2.16 A 3-ph, 3-wire D-STATCOM connected to the grid and load at PCC

Again from the switching dynamics study (2.16), it is found that the f_{sw} depends on the system parameters such as V_{dc} or V_{sh}, h, L_{sh}, V_{pcc}, I_{sh} and R_{sh}. Practically, the maximum switching frequency depends on the type of power switching devices. Generally, IGBT switches are preferred in most of the power electronics devices at distribution level due to their fast switching speed, low switching power losses and high power handling capability. With these above stated constraints, the initial limit for some of the parameters was fixed to design a shunt APF which has been given in Table 2.1. The remainder of the component selection has been carried out based on these parameters.

Table 2.1 Initial maximum limit for some of the design parameters

Parameters	Value (Initial Maximum Limit)
Q_{load}	49kVA
$V_{pcc(L-L)}$	400V
I_{shmax}	100A
f_{swmax}	20kHz
R_{sh}	1Ω
P_{loss}	10%
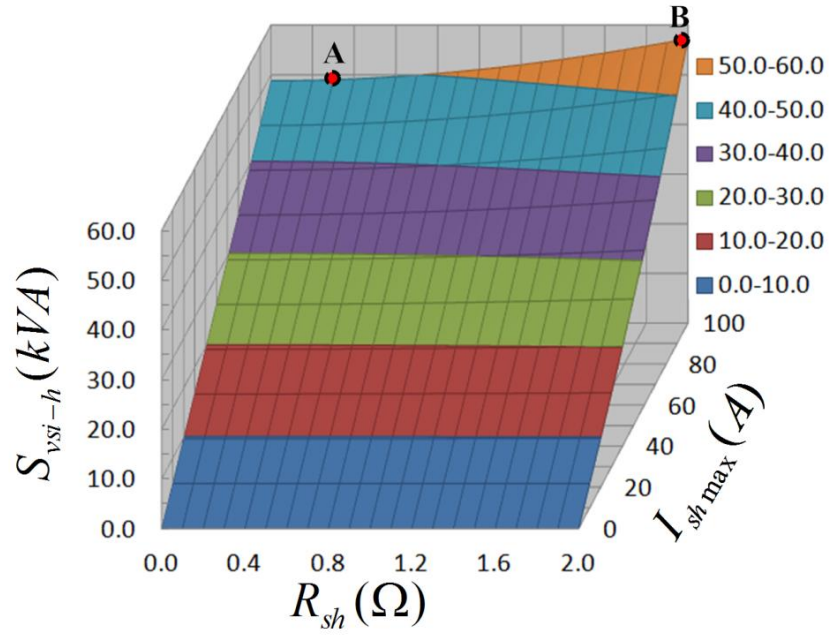
(a)
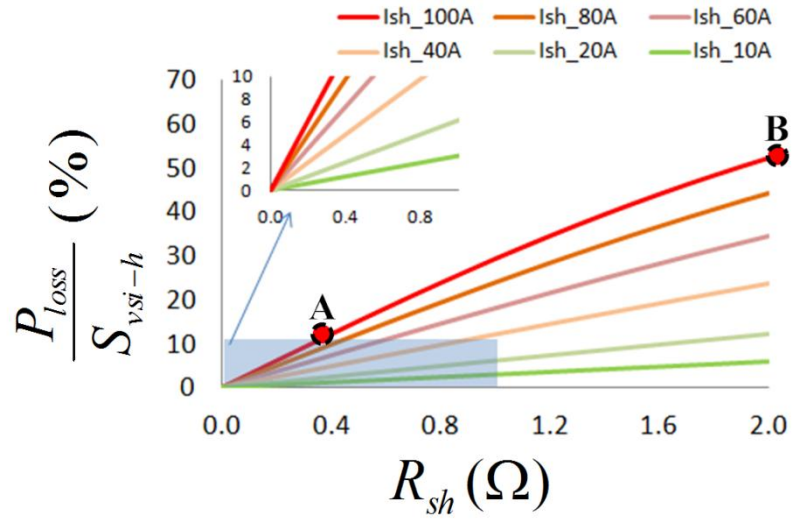
(b)

Fig 2.17 (a) Relation between Actual VSI rating (S_{vsi-h}), R_{sh} and I_{sh}; (b) corresponding loss of inverter

A series of simulation studies and other calculations have been performed based on the design procedure, as shown in Fig 2.18, to select the best values of h and V_{dc} which are further required to set the value of L_{sh} and to determine the limit of I_{sh} and H_{sh} and VSI_{rating} to operate the APF$_{sh}$ within its loss limit or with maximum efficiency. Critical design decisions are then verified against the derived procedure in Section 2.2 and described in the following section.
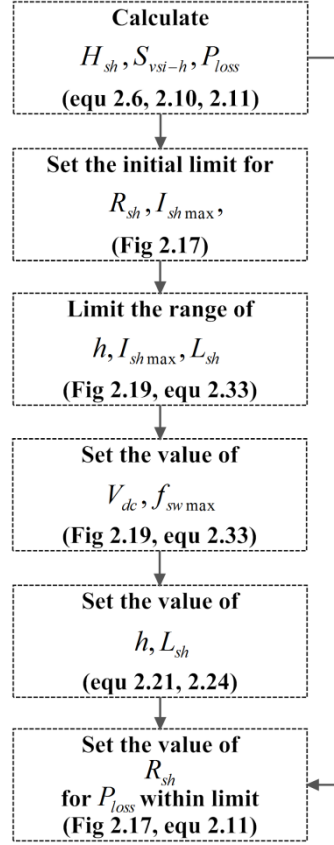
Fig 2.18 Design parameters selection procedure for APF$_{sh}$

2.6.1 Selection of hysteresis band, h

Within the maximum switching frequency and P_{loss} limit, some simulation studies have been performed for different values of compensating current, size of inductor (L_{sh}), ratio of V_{dc}/V_{pccmax} (m) and hysteresis band (h) to select the appropriate band limit and to obtain the best THD_{Is} within the IEEE standard limit. Fig 2.19 shows the result of these simulation studies in terms of THD_{Is} (%) vs h (% of I_{shmax}) which reflects the limits of h that has been considered in (2.24). It is found that for a precise calculation and to obtain the best performance of a D-STATCOM, h should be selected as between 5% to 10 % of I_{shmax}.
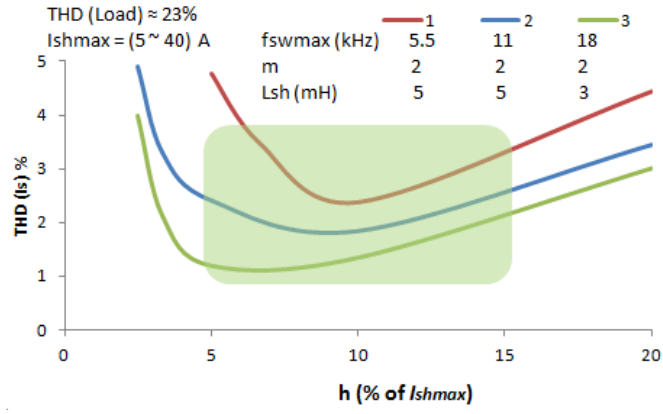
Fig 2.19 Selection of *h* to maintain *THD*_{Is} within IEEE standard.

2.6.2 Limit on the I_{shmax}

The relation between f_{swmax} and I_{shmax} can be derived, from (2.21) and (2.24), as follow;

$$f_{swmax} = \frac{V_{dc}}{12kI_{shmax}L_{sh}} \tag{2.33}$$

It shows that for a constant value of I_{shmax} the maximum switching frequency increases with the decrease of L_{sh}. Again the size limit of L_{sh} can be increased with the increase of m (V_{dc}/V_{pccmax}) and I_{shmax}. For a fixed value of L_{sh} and f_{swmax}, the limit of I_{shmax} can also be increased by reducing h. Fig 2.20(a) shows how the switching frequency increases with the decrease of L_{sh} and increase of m. For $I_{shmax} = 10$A, it is found that a minimum 2mH of L_{sh} should be used with $h = 10\%$ of I_{shmax} and $m = 1.4$ to keep the f_{swmax} within the IGBT switching limit (20kHz), shown in point A. Within this 20kHz, the limit of I_{shmax} can also be increased up to 40A (as shown in the shaded part of Fig 2.20(a) by reducing the L_{sh} to 1mH, at point B) or up to 200A, at point C (as shown in the shaded part of Fig 2.20(b) by reducing the L_{sh} to 0.5mH, $h = 5\%$ and increasing m to 3.6). But in these cases (B and C), there will be a high level of power loss in the VSI unit and the voltage *THD* at PCC will also increase due to the higher V_{dc} (high m) [45]. Therefore, after fixing f_{swmax} (20kHz) and h (10%), the I_{shmax} has been calculated for different L_{sh} and m values which are given in Table 2.2.
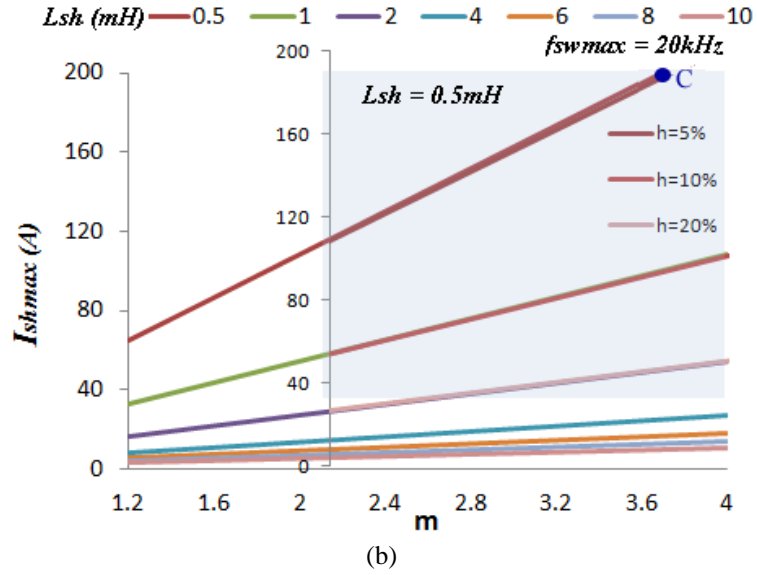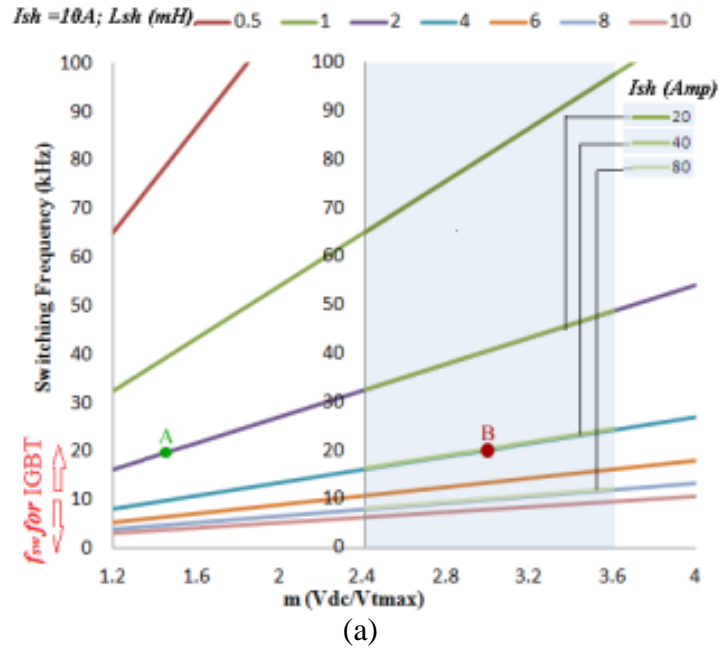
Fig 2.20 (a) Relation between f_{swmax} and L_{sh} for the variation of m and I_{shmax}; (b) Relation between I_{shmax} and L_{sh} for the variation of m and h.

Table 2.2 Values of I_{shmax} and L_{sh} for different V_{dc} condition at $f_{swmax} = 20$kHz

$f_{sw} = 20$K	m									
h =10%	1.2	1.4	1.6	1.8	2	2.4	2.8	3.2	3.6	4
L_{sh} (mH)	I_{shmax} (A)									
0.1	162.6	189.7	216.8	244.0	271.1	325.3	379.5	433.7	487.9	542.1
0.5	32.5	37.9	43.4	48.8	54.2	65.1	75.9	86.7	97.6	108.4
1	16.3	19.0	21.7	24.4	27.1	32.5	37.9	43.4	48.8	54.2
2	8.1	9.5	10.8	12.2	13.6	16.3	19.0	21.7	24.4	27.1
4	4.1	4.7	5.4	6.1	6.8	8.1	9.5	10.8	12.2	13.6
6	2.7	3.2	3.6	4.1	4.5	5.4	6.3	7.2	8.1	9.0
8	2.0	2.4	2.7	3.0	3.4	4.1	4.7	5.4	6.1	6.8
10	1.6	1.9	2.2	2.4	2.7	3.3	3.8	4.3	4.9	5.4
12	1.4	1.6	1.8	2.0	2.3	2.7	3.2	3.6	4.1	4.5

2.6.3 Selection of V_{dc}

A number of simulation studies were performed for various values of I_{shmax}, f_{swmax}, h and L_{sh} to observe the THD_{Is} with respect to V_{dc}. It is found from Fig 2.21 (a and b) that the m value should be at least 1.7 ($V_{dc,min} = 1.7V_{pccmax}$) to obtain a THD_{Is} within the IEEE limit, as shown in the shaded area. This also validates the relation between V_{dc} and V_{pccmax} as given in (2.25). For higher V_{dc}, THD_{Is} is also found to be within the limit, shown in Fig 2.21(c) but it then can degrade the quality of voltage at the PCC. Therefore it is preferable to consider the value of m close to its lower limit. It will also help to reduce the value of R_{sh} by reducing the L_{sh}.
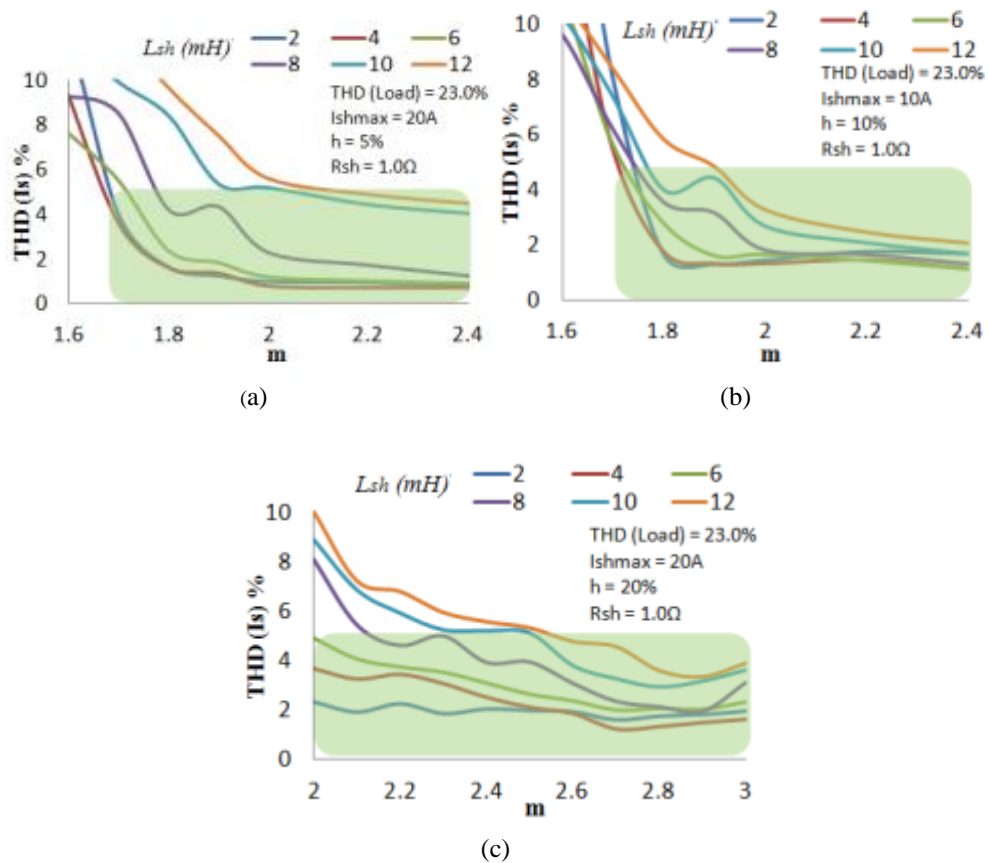
Fig 2.21 THDIs (%) for different values of m, obtained from simulation result for a system to compensate I_{shmax} = 10 to 20A using hysteresis band, h as a) 5%, b) 10% and c) 20%

Fig 2.22 shows how the P_{loss} increases with the decrease of f_{swmax} while other parameters are fixed. This also shows the loss increases with the increase of m. Therefore it is better to chose a lower value of m.

50

Once the values of m, f_{sw} and I_{shmax} are fixed, then the values of h and L_{sh} can be set. Lower the value of L_{sh} will help to reduce the R_{sh}. The value of R_{sh} is set from Fig 2.17 for a fixed value of S_{vsi-h} and P_{loss} within the limit. It is difficult to calculate the switching loss. Therefore, the resistance value (act as a loss emulator) should be low, as it is responsible for conduction loss (transformer + inductor).
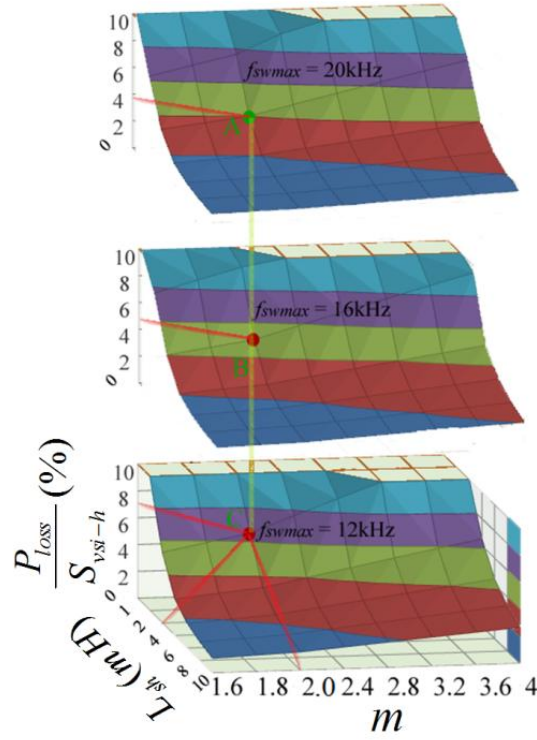
Fig 2.22 Reduction of P_{loss} with the increase of f_{swmax} while the other parameters are constant

2.6.4 Selection of C_{dc}

From the general equation (2.26) it is found that the value of C_{dc} depends on the purposes of the DC link capacitor, as described in section 2.2, the required level of power (S) to be compensated/transferred, the number of cycles (n) and the allowable change of V_{dc} (z). Once the value of V_{dc} (or m) and the number n are fixed, C_{dc} only depends on S and z. Fig 2.23 shows the relation between z and S with respect to C_{dc}. For example, if a compensator is allowed to transfer 20kVA of load power during the transient condition and the task is completed within a half cycle ($n = 0.5$) with an

allowable change in V_{dc} of 10%, then the required capacity of C_{dc} will be around 3000µF for $m = 1.8$, point A, which is further reduced to 2500µF for $m = 2$.
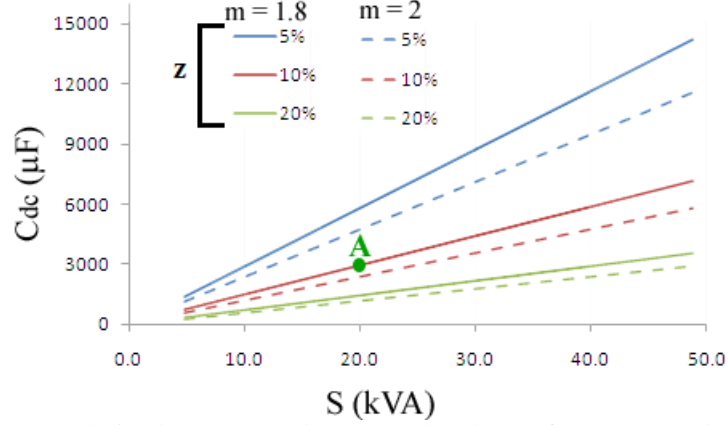
Fig 2.23 Relation between z and S to calculate the C_{dc} for m = 1.8 and 2.0

2.6.5 Verification of switching dynamics and frequencies

As discussed, the design parameters of the APF$_{sh}$ are related to the switching frequency, f_{sw} as well as the hysteresis band, h and V_{dc}. The switching mechanism has been studied and verified with the derived equations in the previous Section 2.2. Table 2.3 shows the design parameters for a specific compensator that has been chosen to investigate the switching dynamics and to determine the switching frequency. Fig 2.24(a) shows the V_{pcc}, V_{sh}, I_s, I_{sh}, I_{load} and Sw$_1$ for phase A when the shunt APF is operating. It is clear that the f_{swmax} occurs near the zero crossing condition where V_{pcc} is close to zero and V_{sh} is 1/3 of V_{dc}. The variation of I_{shref} during one on-and-off time period (h_{on} and h_{off}) of gate Sw$_1$ is also negligible compared to $2h$ (in Fig 2.6). Otherwise, the effect of these values on the calculation of f_{swmax} is negligible. Fig 2.24(b) shows that the system has been designed for $f_{swmax} = 15$kHz which can simply be calculated using (2.13, 2.14) and by neglecting h_{on} and h_{off}. If the values are compared with that in (2.16), f_{swmax} is found to be the same.
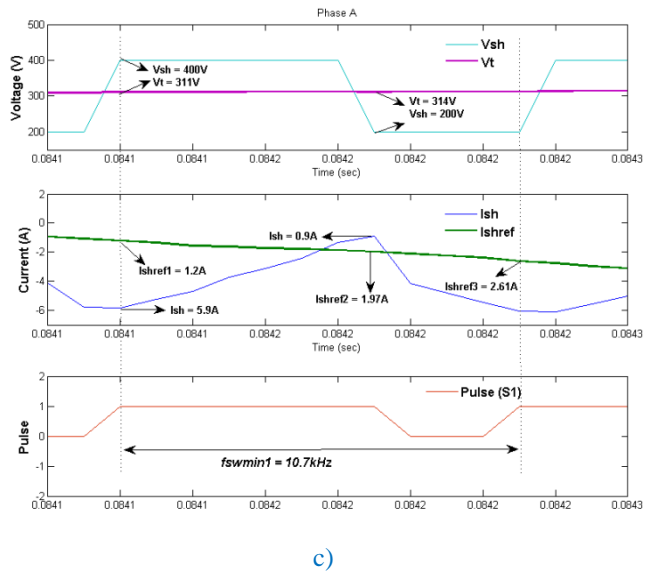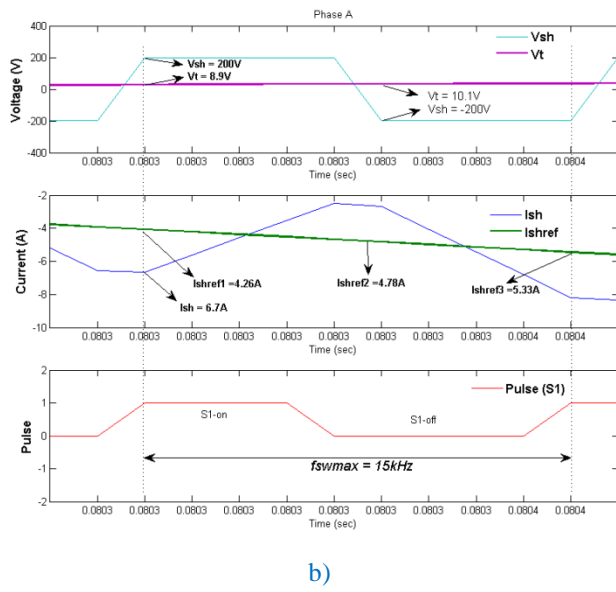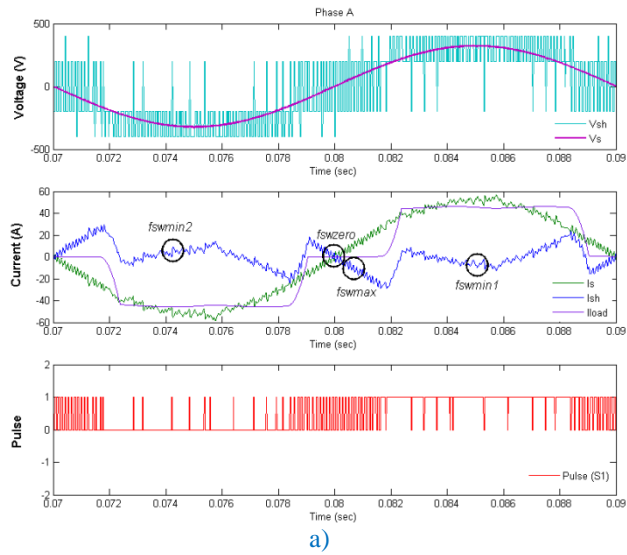
Fig 2.24 (a) One complete cycle of an APF in compensating mode, (b) showing the values of design related parameters to calculate the maximum switching frequencies , f_{swmax} and c) one of the minimum frequency, f_{swmin} at close to 90 deg of supply voltage condition

Table 2.3 Design parameters of a Shunt APF for the verification study of switching frequencies

Component Parameters	Values
Supply Voltage	230 Vrms, 50 Hz
DC link Voltage	600 V
DC storage Capacitor	2200 µF
Interface Inductor	1.666 mH, 1Ω
Hysteresis band (h)	2 Amp
Maximum Compensating Shunt Current	30 Amp

Similarly f_{swmin1} occurs where I_{sh} is close to zero (in Fig 2.24a). At this point, V_{pcc} goes to its positive peak and $V_{sh} = 2/3$ of V_{dc}. h_{on} can be calculated as 0.77A and h_{off} is 0.64 (from 2.13). Putting these values in (2.14), the f_{swmin1} is calculated as 10.7kHz whereas neglecting the values of h_{on} and h_{off} in the calculation gives a value of 12.1kHz. This makes a significant difference in the actual simulated f_{swmin} condition, though it does not have any impact on selection the design parameters.

2.7 Conclusion

Both the design and controlling mechanism for 3-phase 3-wire series and shunt APF system has been reviewed and discussed here as a part of the design and control of a complete UPQC system that can minimize the disturbance of supply voltage as well as cancel the reactive and harmonic part of the load current.

Switching dynamics has been studied to develop the relation between the design parameters and the switching frequencies. This is also verified by simulation. Power losses due to conduction and switching are also co-related with the design parameters and maximum switching frequency. A design parameter selection procedure with an example has been described here by initially setting a maximum switching frequency and loss limit. The best choice of hysteresis band and the minimum value of DC link voltage are set by carrying out extensive simulation to maintain the source current THD within the IEEE limit. Variation of these parameters to design the other components and associated losses are also calculated. A Shunt APF system with a wide range of design parameters has been simulated and the results are shown to compare the design

parameters with their associated power losses and the required kVA rating. This procedure can be generalized to design the parameters for other topologies of APF$_{sh}$ system and would be useful for practical design and development of APF and UPQC.

Chapter 3

Integration and Placement of UPQC in DG Integrated Networks

3.1 **Introduction**

Implementation of Custom Power Devices (CPD) such as UPQC in DG or microgrid systems to improve the power quality is gaining greater importance [75-79]. This chapter deals with the review and analysis of research work that has been completed to date on the integration and placement of UPQC in DG integrated networks. Emphasis has been placed on integration techniques of UPQC in DG or microgrid system together with their advantages and disadvantages. The number of DG systems such as Photovoltaic and Wind Energy Systems are now penetrating more into the grid or microgrid at the same time the number of non-linear loads are also increasing. Therefore, in the presence of DG sources and UPQC in an active distribution network, the following issues have been analysed;

(a) the placement of UPQC and its sensors in the network,

(b) impact of the sensor placement on the UPQC control method,

(c) performance of UPQC with bi-directional power flow in the network and

(d) the advantages of DG inverter in the presence of UPQC

The rest of the chapter discusses the following issues: Section 3.2 deals with the presently available integration techniques of UPQC and DG in a network. The technical standard and other requirements for DG integration in the Electric Power System (EPS) together with the effects of DG integration in terms of Total Harmonic Distortion

(THD) and Total Demand Distortion (TDD) are discussed in section 3.3. This is followed by the placement of UPQC in the network and the related issues are identified and discussed in Section 3.4. Conclusions are made in Section 3.5

3.2 **Integration of UPQC**

Recent reports [75-81] show that significant research and development has been carried out on the application of UPQC to DG integrated networks. As the UPQC can compensate for almost all existing PQ problems in the transmission and distribution grid, integration of a UPQC in the distributed generation network can be multipurpose. As part of the integration of UPQC in DG systems, research has been carried out on the following two techniques: DC-Linked and Separated DG-UPQC systems.

3.2.1 (DG – UPQC)DC-linked

A structure has been proposed in [75-79], as shown in Fig 3.1, where DG sources are connected to a DC link in the UPQC as an energy source. This configuration works both in interconnected and islanded modes (shown in Fig 3.2). In the interconnected mode, DG provides power to the source and loads whereas in the islanded mode, DG (within its power rating) supplies power to the load only. In addition, UPQC has the ability to inject power using DG to sensitive loads during source voltage interruption. The advantage of this system is voltage interruption compensation and active power injection to the grid in addition to the other normal UPQC abilities. The system's functionality may be compromised if the DG resources are not sufficient during the voltage interruption. Economical operation of the system can also be achieved by proper control of the active power transfer between the supply and DG source through a series APF [78]. The proposed system can also reduce the investment cost by nearly one fifth if the UPQC and DG are used separately [79].
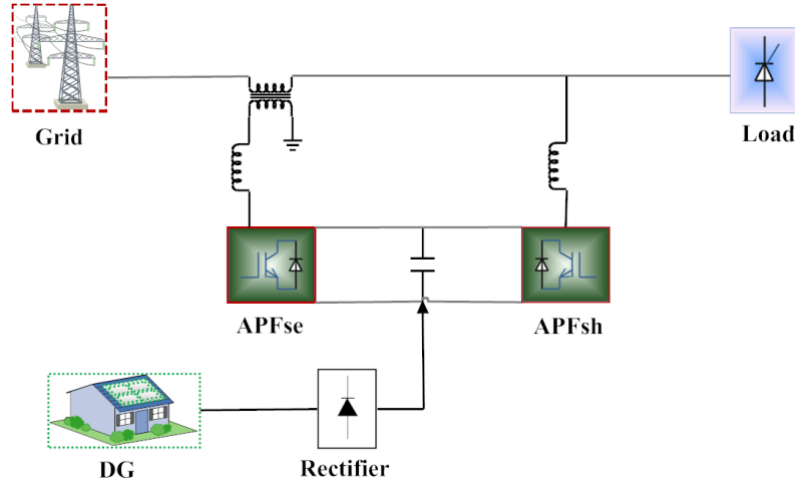
Fig 3.1UPQC with DG connected to the DC link
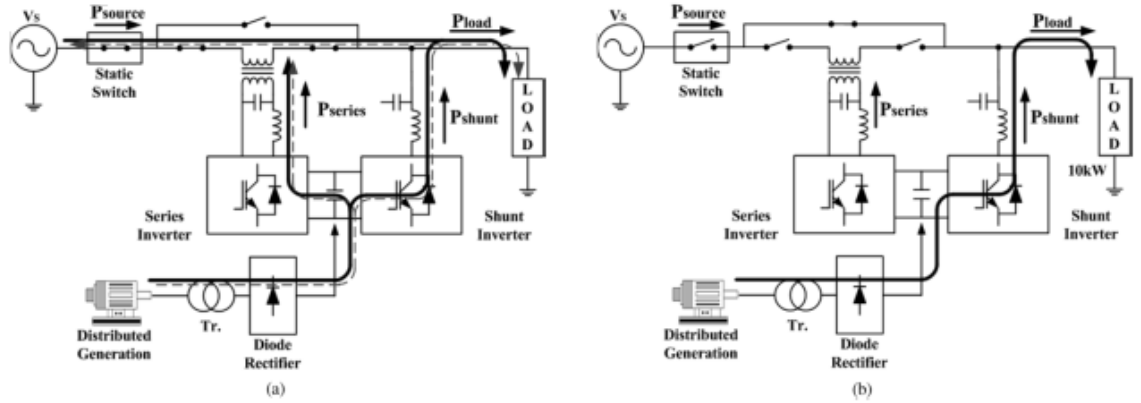
Fig 3.2 (DG-UPQC)$_{DC-linked}$ System operation concept (a) Interconnected mode; (b) Islanding mode [75]

3.2.2 (UPQC – DG)$_{Separated}$

A typical application of a UPQC might be to overcome the grid integration problems of the DG, such as the fixed-speed induction generator (FSIG) as investigated in [80] and shown in Fig 3.3. FSIGs can fail to remain connected to the grid in the event of a grid voltage dip or line fault due to excessive reactive power requirements. The drop in voltage creates over-speeding of the turbine, which causes a protection trip. With the aid of the UPQC, this fault-ride-through capability is achieved, which greatly enhances system stability. Results show that the UPQC is one of the best devices for the integration of wind energy systems to the grid. In the case of a wind farm connected to a weak grid, UPQC can also be placed at the PCC to overcome voltage regulation problems [81]. In these separated systems, the series APF of the UPQC is placed near

the DG side to conduct the voltage regulation by injecting the voltage in phase with PCC voltage. This type of UPQC is referred to as left shunt UPQC [24]. Based on that research study, in addition to the normal functionality of UPQC, some of the other advantages and disadvantages are identified and these are given in Table 3.1 [19].
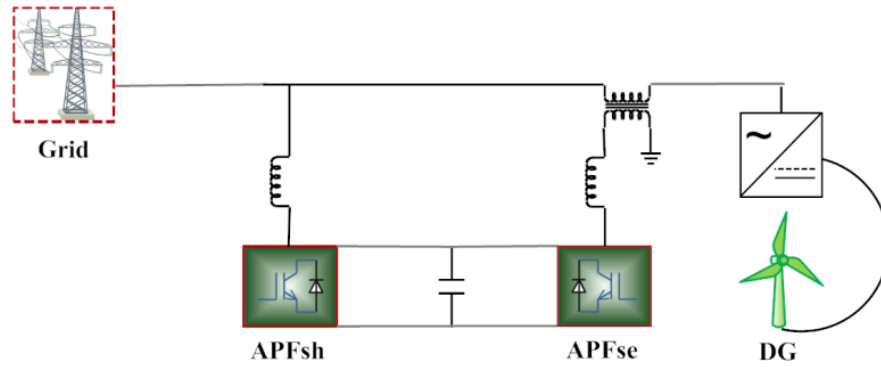
Fig 3.3 Grid connected wind energy system with UPQC

Table 3.1 Comparative analysis of integration techniques of UPQC in DG system

Technique	Advantages	Disadvantages
$(DG\text{-}UPQC)_{DC\text{-linked}}$	i. Compensate voltage interruption ii. Operation in islanding mode – possible iii. Active power transfer during grid connected or microgrid mode – possible iv. System cost for PQ improvement - reduced (remove DG Inverter)	i. Control complexity – high ii. Capacity enhancement in multi-level or multi-module mode – difficult
$(UPQC\text{-}DG)_{Separated}$	i. Capacity enhancement in multi-level or multi-module mode - easy ii. Control – easy iii. Active power transfer during grid connected mode - possible	i. Voltage interruption – may not be possible ii. Operation in islanding mode – may not be possible iii. System cost - high

3.2.3 Cost analysis

In terms of required components, it is clear that the $(DG\text{-}UPQC)_{DC\text{-linked}}$ does not require the grid connecting interfacing converter and thus the cost will be less. The

purpose of the DG inverter / grid-tie inverter is already carried out by the APF_{sh} in the UPQC system. On the other hand in the (DG-UPQC)$_{separated}$ system two complete units of UPQC and DG unit are required along with the interfacing converter. Therefore, the additional grid-tie inverter cost makes it costlier than the previous topology. A comparative analysis of investment cost and economical saving of separated and combined UPQC–DG (Wind Energy System) has been carried out in [79] based on the component cost values in [82]. It is found that, depending on the ratings, the combined (DG-UPQC)$_{DC-linked}$ system can reduce the cost up to one fifth of the separate system.

3.3 Interconnection of DG Source with Electric Power Systems

The nonlinear characteristics of power electronics devices and loads on the power system can be modelled as current sources that inject harmonic currents into the system. Voltage distortion occurs as a result of these currents which cause nonlinear voltage drops across the power system. Due to the increasing application of power electronics equipment such as converters which connect DG sources into the grid or microgrid, this harmonic distortion becomes a growing concern for many customers and for the overall power system. The levels of this distortion can be characterized and quantified by the complete harmonic spectrum magnitude as the total harmonic distortion (THD). But this can often be misleading. For example, many adjustable speed drives exhibit high THD values for the input current when they are operating at very light loads. Though the magnitude of harmonic current is low, its relative distortion is high. A similar problem occurs at the point of common coupling (PCC) when DG sources are connected with the electric power system (EPS) at the distribution level. Here, load harmonics remain constant but the actual supply current from the grid is relatively low and thus the THD at the PCC becomes high. To handle this concern for characterizing harmonic currents in a consistent fashion, IEEE introduced another term, the total demand distortion

(TDD). This term is the same as the THD except that the distortion is expressed as a percent of some rated load current rather than as a percent of the fundamental current magnitude. Guidelines for harmonic current and voltage distortion levels on distribution and transmission circuits are provided in [5].

According to the IEEE Standard 1547 [8], the PCC is defined as; "The Point of Common Coupling (PCC) with the consumer/utility interface is the closest point on the utility side of the customer's service where another utility customer is or could be supplied. The ownership of any apparatus such as a transformer that the utility might provide in the customer's system is immaterial to the definition of the PCC." Fig 3.4 shows the interconnection of DG sources with the EPS and the PCC. The PCC is where harmonic limits are assessed and prevented to propagate from one customer to another. When the DG is connected, harmonic current injection, by the DG unit and the non-linear load, into the Area EPS at the PCC shall not exceed the limits as given in Table 3.2. The harmonic current injections shall be exclusive of any harmonic currents due to harmonic voltage distortion present in the Area EPS without the DG connected.
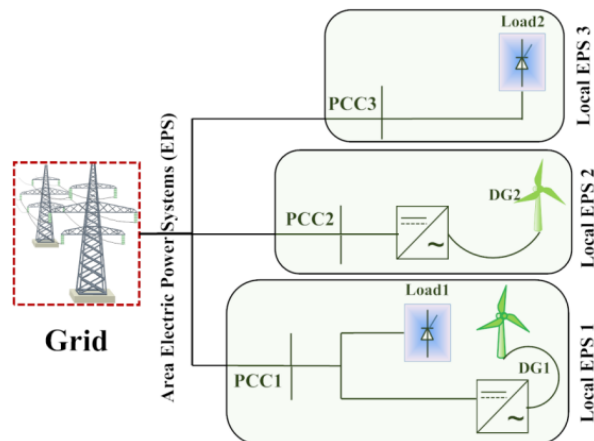
Fig 3.4 Interconnection of DG sources with EPS and PCC

Table 3.2 Maximum harmonic current distortion [IEEE 1547, IEEE 519]

Individual harmonic order, h	$h < 11$	$11 < h < 17$	$17 < h < 23$	$23 < h < 35$	$35 \leq h$	TDD
Percent (%)	4.0	2.0	1.5	0.6	0.3	5.0

61

Mathematically, THD and TDD can be calculated as;

$$THD = \frac{\sqrt{I_2^2 + I_3^2 + I_4^2 \dots \dots + I_h^2}}{I_{pccf}} \qquad (3.1)$$

$$TDD = \frac{\sqrt{I_2^2 + I_3^2 + I_4^2 \dots \dots + I_h^2}}{I_{loadf}} \qquad (3.2)$$

where I is the rms value, f is the fundamental component.

According to [8], DG interconnection system shall detect the unintentional islanding and cease to energize the islanded area within two seconds of the formation of an islanding condition. One of the reasons for this is that the controller of the grid-tie DG inverter is designed to provide only pure active power to the load and grid in the interconnected mode.

Fig 3.5 shows an example of interconnection of DG sources as a micro-generation (μGen) or microgrid (μGrid) with the distribution network. Assuming that the DG source provides the active power to the grid and all the harmonics are injected by the non-linear harmonic load (load1). The position of the current sensors are also shown to measure the THD and TDD for different level of DG injected current (i_{dg1} and i_{dg2}). For the study, two types of DG integration systems (μGrid and μGen) with harmonic (load1) and reactive (load2) load have been considered, where the current fundamentals are $I_{load1max}$ = 207 A and $I_{load2max}$ = 97 A. The relation between the DG supply and load demand is given as;

$$I_{dgmax} = \gamma . I_{loadmax} \qquad (3.3)$$

Measuring points for $i_{load1}, i_{pcc1}, i_{pcc2}$ and i_s in the network are also shown in Fig 3.5. Fig 3.6 shows the initial waveforms at the measuring points and the corresponding THD / TDD values are given in Table 3.3 when both DG sources are not operating. It is to be noted that the THD and TDD are same when DG or any other source is not present in the network. THD at i_{load1} and i_{pcc1} are also same as i_{dg1} is

zero. THD at i_s shows lower than that at i_{pcc1} and it occurs as a resultant effect due to the reactive and harmonic loads with different ratings.
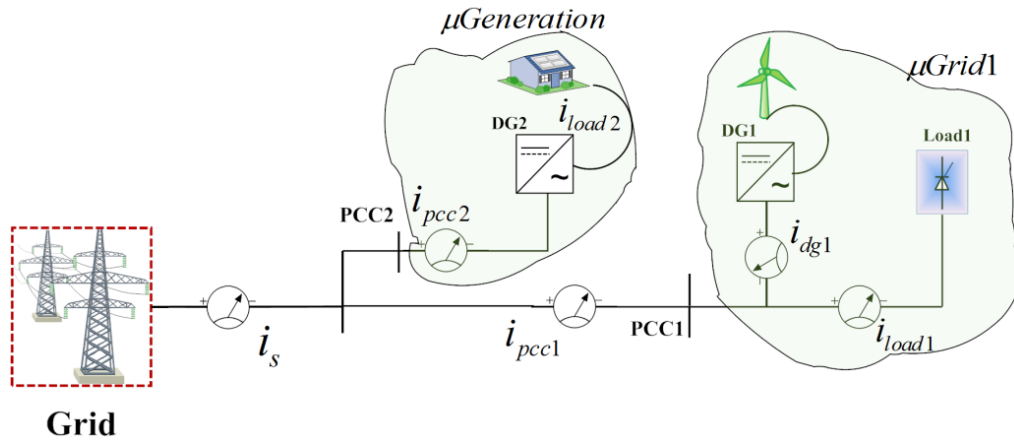
Fig 3.5 Distributed Generation (DG) Integrated Network

Table 3.3 When $i_{dg1} = 0$ and $i_{dg2} = 0$; UPQC is not working

Sensors	i_s	i_{pcc2}	i_{pcc1}	i_{load1}
THD / TDD (%)	17.88	0.20	25.8	25.8
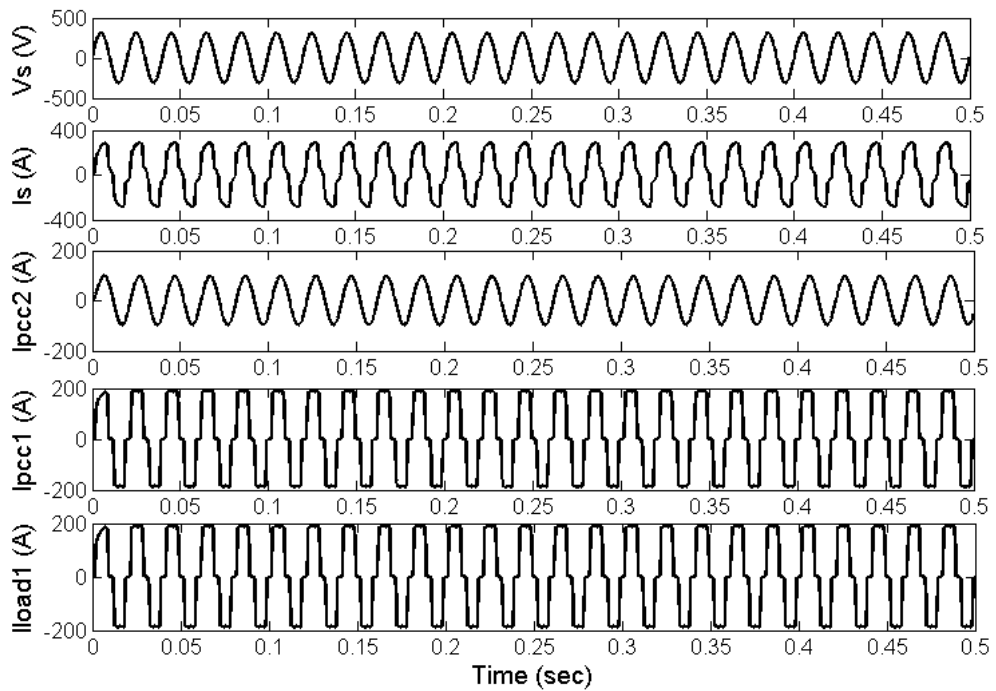
Fig 3.6 Waveforms of the $i_{load1}, i_{pcc1}, i_{pcc2}$ and i_s when $i_{dg1} = 0$ and $i_{dg2} = 0$

Assuming that the DG sources are providing pure fundamental current (i.e. without harmonics), Fig 3.7 shows the effect of the supply current of DG sources on

the measurement of THD values for four conditions at different points in the network. The four conditions are;

(a) Both the DG sources and loads are active

(b) Load2 is inactive

(c) DG1 is inactive

(d) DG2 is inactive.

For all cases, the simulated system has been run for 1 sec. γ is considered to range from 0 to 2, which means the DG units supply from zero up to double of the load fundamental current. It is found that, in Fig 3.7(a), the measured THD at PCC1 becomes maximum when the DG1 supplies the load fundamentals (I_{load1f}). The reason is that at the point the sensor senses only the harmonics of the load current and net fundamental ($I_{pcc1f} = I_{load1f} - I_{dg1f}$) becomes close to zero. But in reality, the DG unit does not supply any harmonics to the PCC and the measured TDD remains unchanged. The peak of the grid (i_s) THD may change the position when the load2 or DG2 (μGen) is inactive, as shown in Fig 3.7(b and d). When DG1 (μGrid) is off, then the grid THD also increases and the peak value depends on the condition of the load (reactive/harmonic) and the supply of DG2, as shown in Fig 3.7(c). Fig 3.8 shows the corresponding waveforms at the measuring points when $i_{dg2} = 0$. It is also found that the DG1 or load1 does not have any impact on the THD at PCC2. Therefore, measuring THD at PCC1 and grid source, when the DG units are running, will provide false information and thus could affect the maintenance of PQ levels for the location.
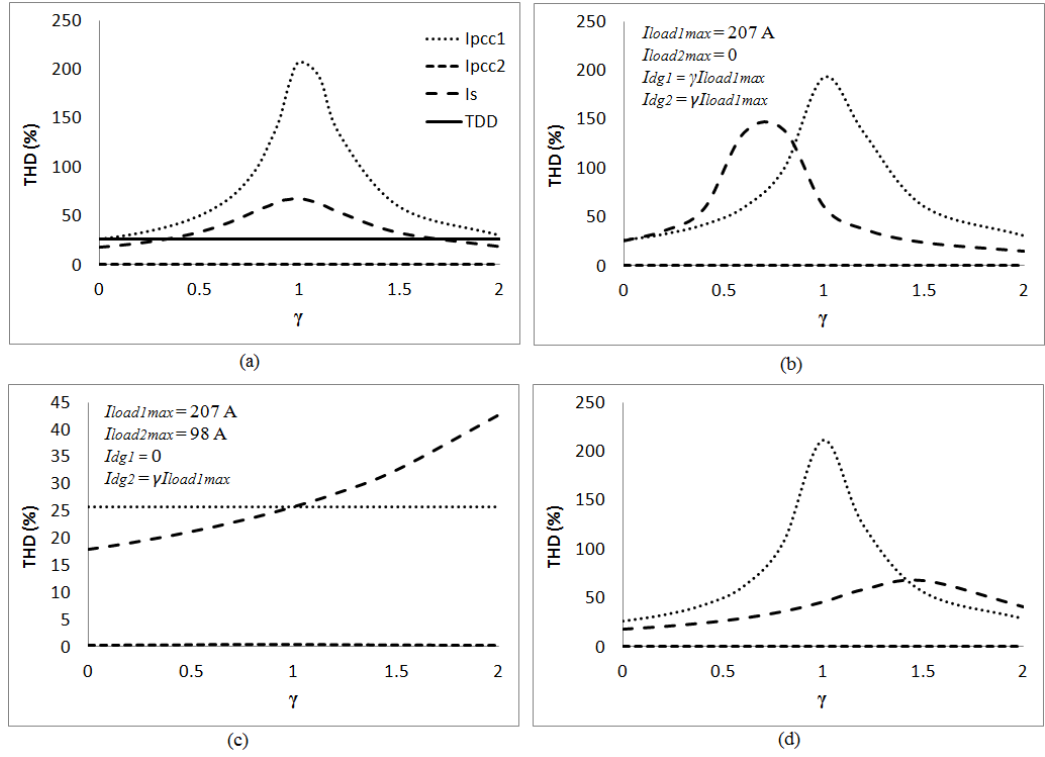
Fig 3.7 Effect of i_{dg} on the calculation of THD at different points.
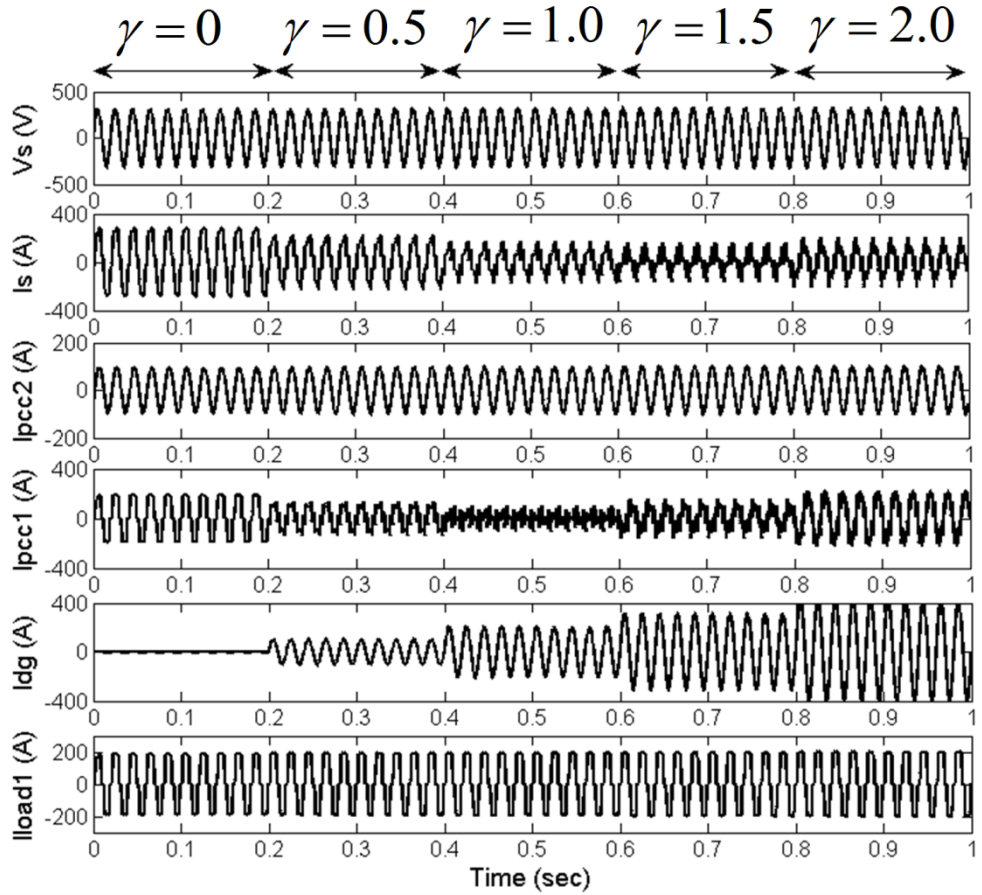
Fig 3.8 Waveforms of the $i_{load1}, i_{pcc1}, i_{pcc2}$ and i_s when I_{dg1} varies from (0 to 2) of $I_{load1fmax}$ and $i_{load2} = 0$

3.4 **Placement of UPQC in DG Network**

In a DG integrated electrical distribution system, DG sources (i) can be connected to the electric power system as a μGen or in a μGrid condition, (ii) have to supply the active power to the grid and/or load and (ii) should be capable of detecting the unintentional islanding or grid voltage disturbances and then be disconnected and (iv) then have to supply the active and reactive power depending on the load demand. The UPQC as a Custom Power Device is introduced at the PCC (i) to prevent the grid and other loads from the current harmonics generated by the non-linear loads, (ii) to maintain the voltage and current THD at PCC within the IEEE limits and (iii) compensate the grid voltage sag / swell to provide a balance and stable voltage at the PCC. In the presence of DG sources the following situations require critical considerations;

(a) the placement of UPQC and its current feedback sensors,

(b) impact of sensor placement on the UPQC control method,

(c) performance of UPQC with the bi-directional power flow in the network and

(d) the privilege/advantage of DG source in presence of UPQC

This will enable the proper placement of UPQC in a DG integrated network. These issues are discussed in the following sections of this Chapter.

For a better understanding, a DG integrated network as shown in Fig 3.5 has been designed and simulated in MATLAB. Design parameters for the UPQC also have been calculated based on the grid and load information which are given in Table 3.4. DG sources are considered to be supplying the fundamental active power. Therefore, harmonics introduced by the DG inverters are not added in the simulation and the analysis. The supplied DG power has been increased in every 0.2 sec interval by putting successive values of $\gamma = 0$, 0.5, 1.0, 1.5 and 2.0 in (3.3).

Table 3.4 Overall DG network parameters for the simulation

Section	Parameter	Value / phase
Grid (3 phase)	Voltage (v_s)	230 Vrms
	Line Frequency (f_s)	50 Hz
Load1 (µGrid)	Load Current (i_{load1})	151 Arms
	Reactive + Harmonic Current	71 Arms
Load2 (µGen)	Load current (i_{load2})	71 Arms
UPQC	DC link Voltage (V_{dc})	600 V
	Series Inductance (L_{se})	0.3 mH
	Series Transformer (T_{se})	1:1
	Switching frequency (f_{se})	10 kHz
	Max Sag Compensation (V_{sag})	50%
	Shunt Inductance (L_{sh})	0.42 mH
	Hysteresis band (h)	7.5 A
	Switching frequency (f_{swmax})	16 kHz
	Max Compensating Current (I_{shmax})	100 Amax
DG	DG current (i_{dg})	Equ (3.3)

3.4.1 Placement of UPQC and its current feedback sensors

In general, a UPQC can be placed before or after the DG unit in an integrated network. The arrangement can be;

(i) PCC-UPQC-DG-Load or

(ii) PCC-DG-UPQC-Load.

The placement of the UPQC feedback voltage and current sensors depend on its control methods and techniques. Therefore, the placement of UPQC can be made in four ways which are given below in Fig 3.9 where i_{fb} and i_{ff} represent the sensing current of the UPQC in feedback and feedforward mode respectively. The actual sensing current of i_{fb} and i_{ff} for all these positions are also shown in Fig 3.9. Without the loss of generality, for the rest of the study, analysis and discussion, i_{pcc2} is assumed to be zero.

3.4.1.1 Position 1

In this position, the UPQC is placed between the PCC and the DG system. Depending on the control mechanism, the placement of sensors is also shown there. In

this case, sensing of load current will be difficult if it is placed in a micro-generation system (μGen). The sensor in the PCC1 (i_{fb}) will also give the current difference between the source (i_s), DG (i_{dg1}) and compensating current (i_{sh}) rather than the actual load current (i_{load1}).

$$i_{fb} = i_{load1} - i_{dg1} - i_{sh};$$
$$i_{ff} = i_{load1}$$

Position 1

$$i_{fb} = i_{load1} - i_{dg1} - i_{sh}$$
$$i_{ff} = i_{load1} - i_{dg1}$$

Position 2

$$i_{fb} = i_{load1} - i_{sh};$$
$$i_{ff} = i_{load1}$$

Position 3

$$i_{fb} = i_{load1} - i_{dg1} - i_{sh};$$
$$i_{ff} = i_{load1}$$
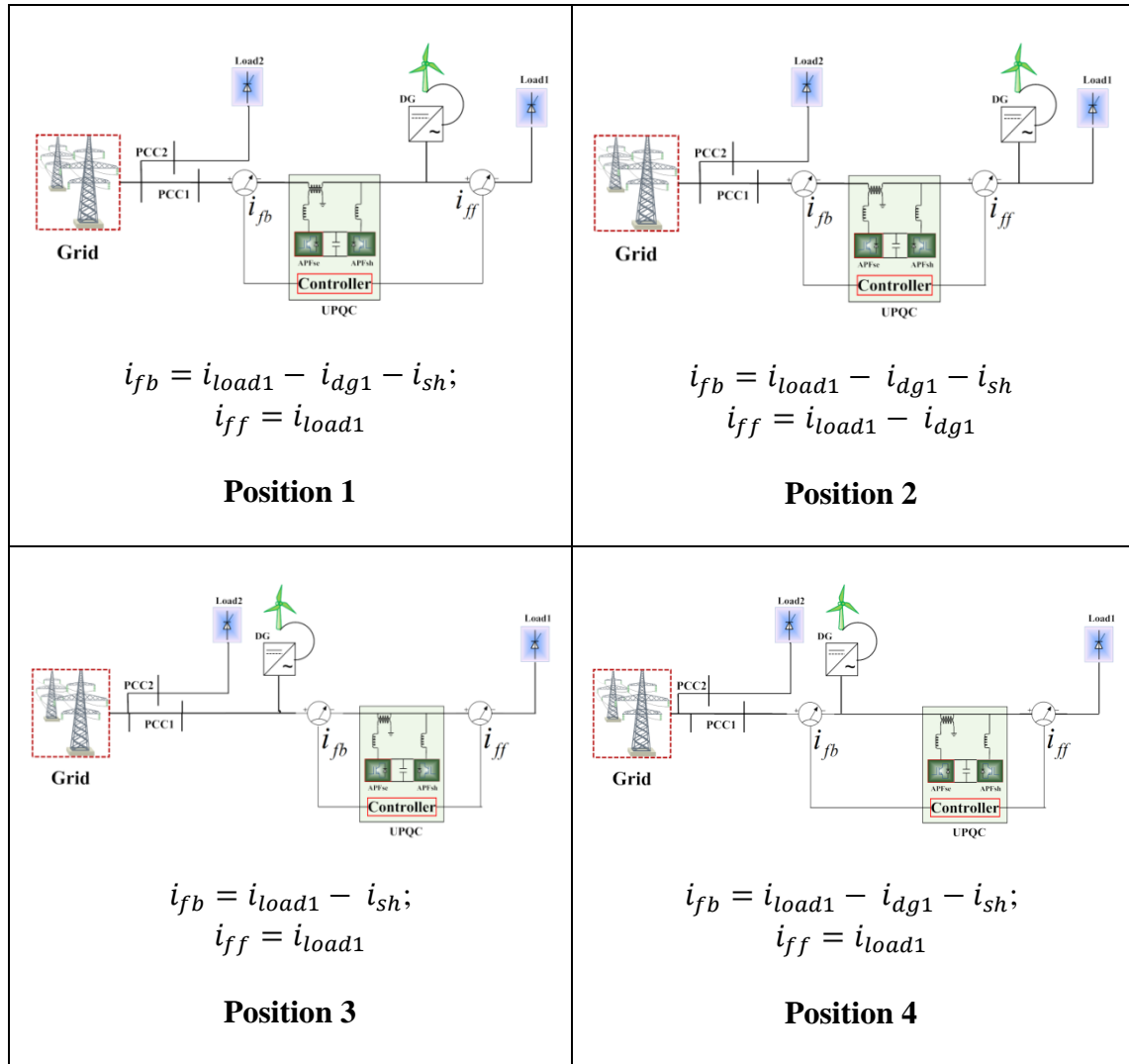
Position 4

Fig 3.9 Placement of UPQC in DG integrated network

3.4.1.2 Position 2

In this position, both the sensors will not sense the real load current. Sensing of load current will be difficult if DG unit is not removed or switched off. Otherwise an additional sensor may be required to measure the i_{dg1} to get the actual load information. In this case UPQC can be placed both in a μGen or μGrid system.

3.4.1.3 Position 3

In this case, the UPQC and the sensors are placed after the DG source. Hence, the sensor i_{ff} will measure the real load current. UPQC will also not sense any disturbance or changes in supply current due to the DG placement. UPQC will not require to measure the i_{dg1} for its own control. This is the most common placement of the UPQC reported in the literature.

3.4.1.4 Position 4

As far as sensing current is concerned, this case is the same as Position 1. The only difference is that the DG source is connected before the UPQC at PCC1.

3.4.2 Impact on UPQC control

It is already mentioned that, in general, the series part of the UPQC is responsible for the compensation of voltage disturbances including sag/swell and to accomplish the task it will sense the voltage waveform at the PCC1. As the DG converter needs to synchronize with the grid for a reliable connection and to transfer the active power to the load and/or grid, the voltage at the PCC and the DG converter should be the same in magnitude. Thus the sensing voltage for UPQC does not have any impact on the generation of the reference signal for voltage compensation. In the case of the active power transfer during sag compensation, APF$_{se}$ of the UPQC will sense only the i_{fb} which is the same for Position 1, 2 and 4. Therefore, the response of the UPQC during sag compensation will be the same for these positions. In Position 3, DG will have no impact on UPQC for sag compensation. Fig 3.10 shows the basic block diagram of the reference voltage generation using positive sequence detection and the control of the series part of the UPQC. Details of this method can be obtained from [26, 74]. Fig 3.11 shows the waveforms at different points for the Position 2 during the supply voltage sag which was applied from 0.04 to 0.4 sec. At the same time, DG current (i_{dg1}) was

increased successively from 0 to 0.75, 1.5 and 2 times of load (i_{load1}) fundamental at 0.1 sec interval. At the time 0.2 sec, i_{pcc1} becomes reverse in flow due to the high current flows from the DG source, as shown by the dot circle in Fig 3.11. The red circle shows the effect of changing DG current in the harmonic compensation current.
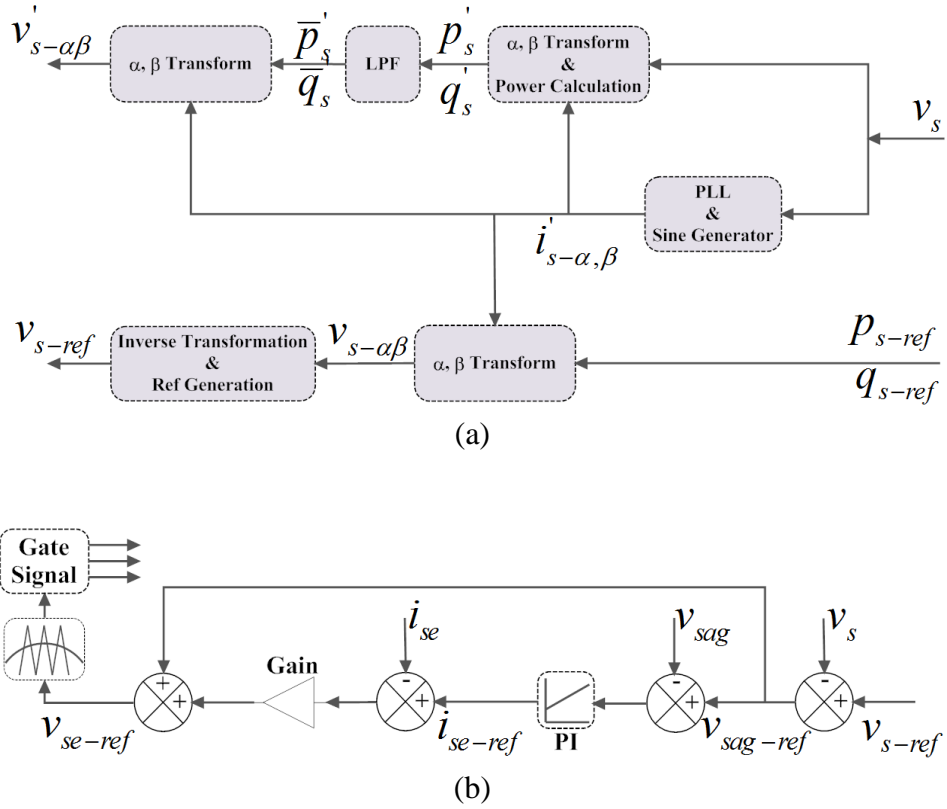
Fig 3.10Generation of (a) source voltage reference and (b) control of series part of UPQC

The shunt part of the UPQC deals with the harmonic and reactive current compensation. Depending on the sensing point of the harmonic sensor to generate the reference current, two types of harmonic compensation mode could be generated, either feedforward (FF) or feedback (FB). In general, feedforward mode is extensively used for its stability and ease of installation where the controller is based on a current-controlled source. On the other hand, the feedback mode is better for stationary conditions but becomes unstable during certain grid conditions [83 - 85].
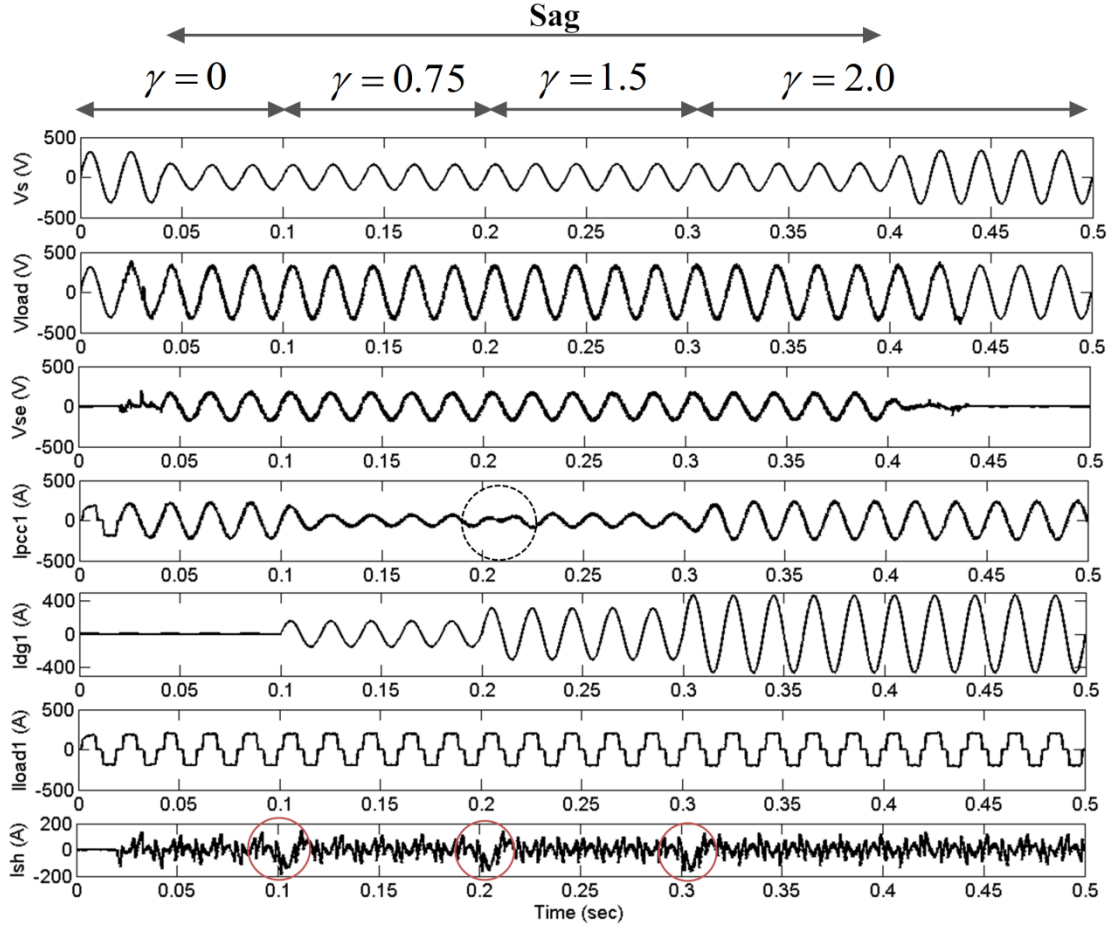
Fig 3.11Performance of UPQC during voltage sag in position 2

In terms of the control method, the shunt part of the UPQC can perform its compensation task directly or indirectly [57, 86]. In the case of direct control, the controller generates the reference current for the harmonic and reactive components based on the sensing point and then controls the shunt current of the UPQC to perform compensation at a desired level. For indirect control, the reference current is generated based on the active or fundamental component at the sensing point and then the UPQC operates or controls its shunt part in such a way that the current at the supply side or at the PCC becomes sinusoidal and in phase with the voltage.

To understand the impact on UPQC control of the placement of UPQC and its sensors for reference current generation, a common reference current generation method and current controller have been chosen here for direct and indirect control using feedback and feedforward compensating modes, which are shown in Fig 3.12 and 3.13.

Because of its simpler implementation, enhanced system stability and increased reliability a hysteresis controller is used. In relation to its response speed for measurement and control action, a faster DSP can avoid the delay problem [41]. In the case of a simulation study, it represents a digital controller. Therefore, the hysteresis control has been chosen here as a current controller. The Instantaneous reactive power theory [26], which is valid in both for steady-state and transient operation and is characterised by the simplicity of its calculations, has been used to generate the reference current.

Table 3.5 shows the required sensors for all types of control methods of the four positions. The waveforms of the reference current have been generated using feedback and feedforward modes and both the direct and indirect control techniques have been applied to observe the overall impact on the UPQC control in terms of (i) reference current generation, (ii) harmonic current compensation, (iii) THD at PCC1 and (iv) TDD, which are discussed in the following section.

Table 3.5 Required Current Sensors

Position	Direct Control		Indirect Control	
	FB mode	FF mode	FB mode	FF mode
1	i_{pcc1}, i_{sh}	i_{load1}, i_{sh}	i_{pcc1}	$i_{pcc1}, i_{load1}, i_{dg1}$
2	i_{pcc1}, i_{sh}	$i_{load1}, i_{dg1}, i_{sh}$	i_{pcc1}	i_{pcc1}, i_{load1}
3	i_{pcc1}, i_{sh}	i_{load1}, i_{sh}	i_{pcc1}, i_{dg1}	i_{pcc1}, i_{load1}
4	i_{pcc1}, i_{sh}	i_{load1}, i_{sh}	i_{pcc1}	$i_{pcc1}, i_{load1}, i_{dg1}$

3.4.2.1 Generation of reference current

Fig 3.14 shows the waveforms of the reference current in FB and FF mode for all the positions. Based on the generated reference signals for all positions and control methods, Table 3.6 is prepared and it shows that Position 1 and 4 with FF mode in direct control do not have any impact on the generation of reference signal. Position 3 is most commonly used but in that case DG has no impact at all on the overall performance of the UPQC. By its nature, the output from a RET (Renewable Energy

72

Technology) based μGrid / μGen system is uncontrollable and therefore generation of a reference current and control will be affected for the other positions (1 and 4 in FB mode and 2 in FB and FF mode) and control methods. Thus it will have an impact on the performance of UPQC.
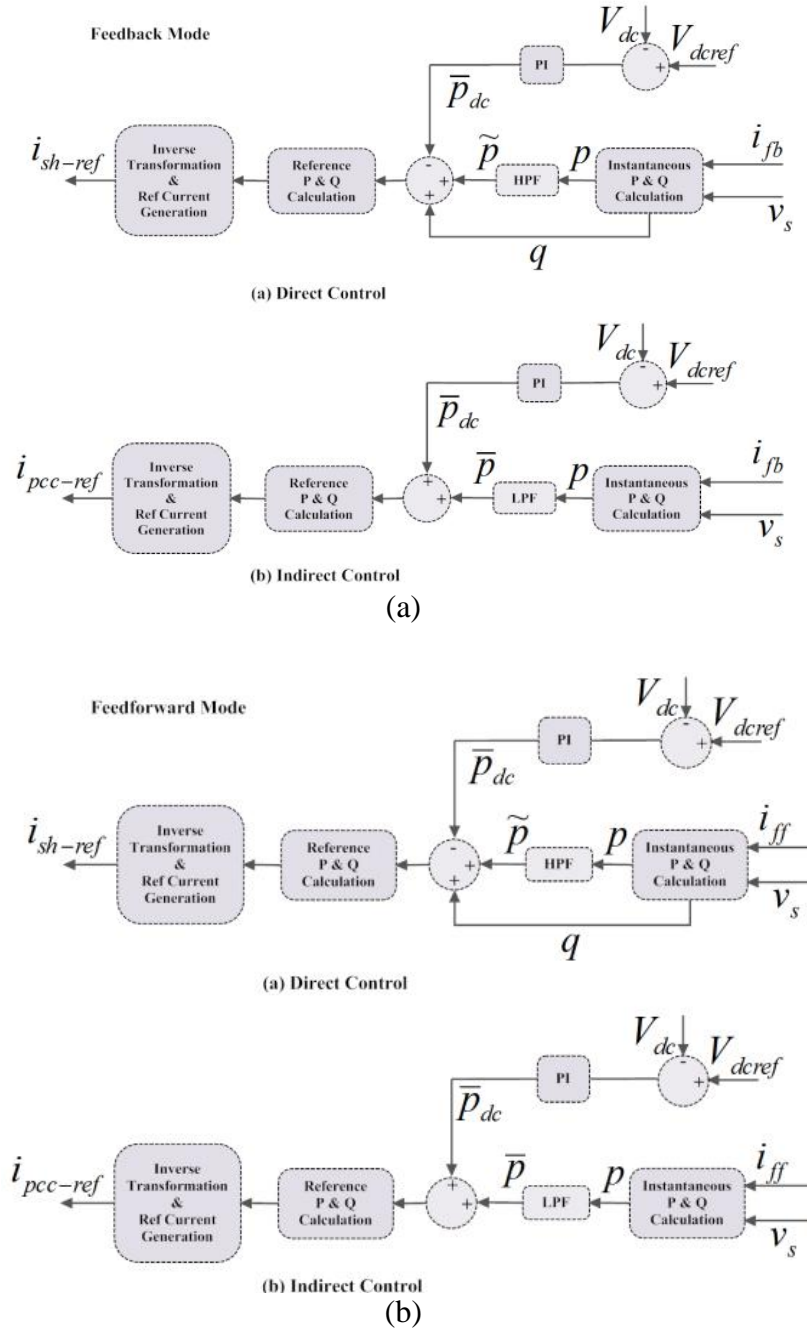
Fig 3.12 Generation of reference current in (a) FB and (b) FF mode for shunt part of UPQC
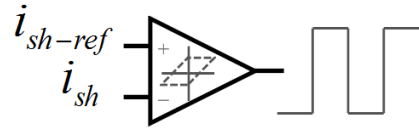
(a) Direct Control
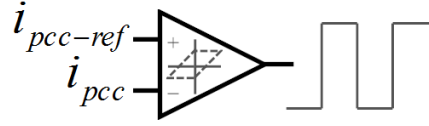
(b) Indirect Control

Fig 3.13 Hysteresis control to generate the gate pulses for shunt part of UPQC

3.4.2.2 Harmonic current compensation

Fig 3.15 shows the respective harmonic current compensation based on the generated reference current shown in Fig 3.14. Both, Fig 3.14 and 3.15, show how the placement of the DG source, the UPQC and its sensors affects the performance of the UPQC. Apart from position 3, the placement of the DG source/UPQC has an impact on both direct and indirect control in the FB mode. The reason for this is because the FB sensor for these positions measures the current difference between the load and DG source rather than the actual load current. Therefore, the sensing current and generating reference current are always varying with the DG input. In these cases, the UPQC controller should have a better dynamic/transient performance. The main advantage of these positions with the FB mode is that the UPQC can compensate the current harmonics (if any) generated by the DG converter.

Table 3.6 Impact of UPQC sensors and DG source on reference current generation

Position	Direct Control		Indirect Control	
	FB mode	FF mode	FB mode	FF mode
1	√	X	√	√
2	√	√	√	√
3	X	X	X	X
4	√	X	√	√
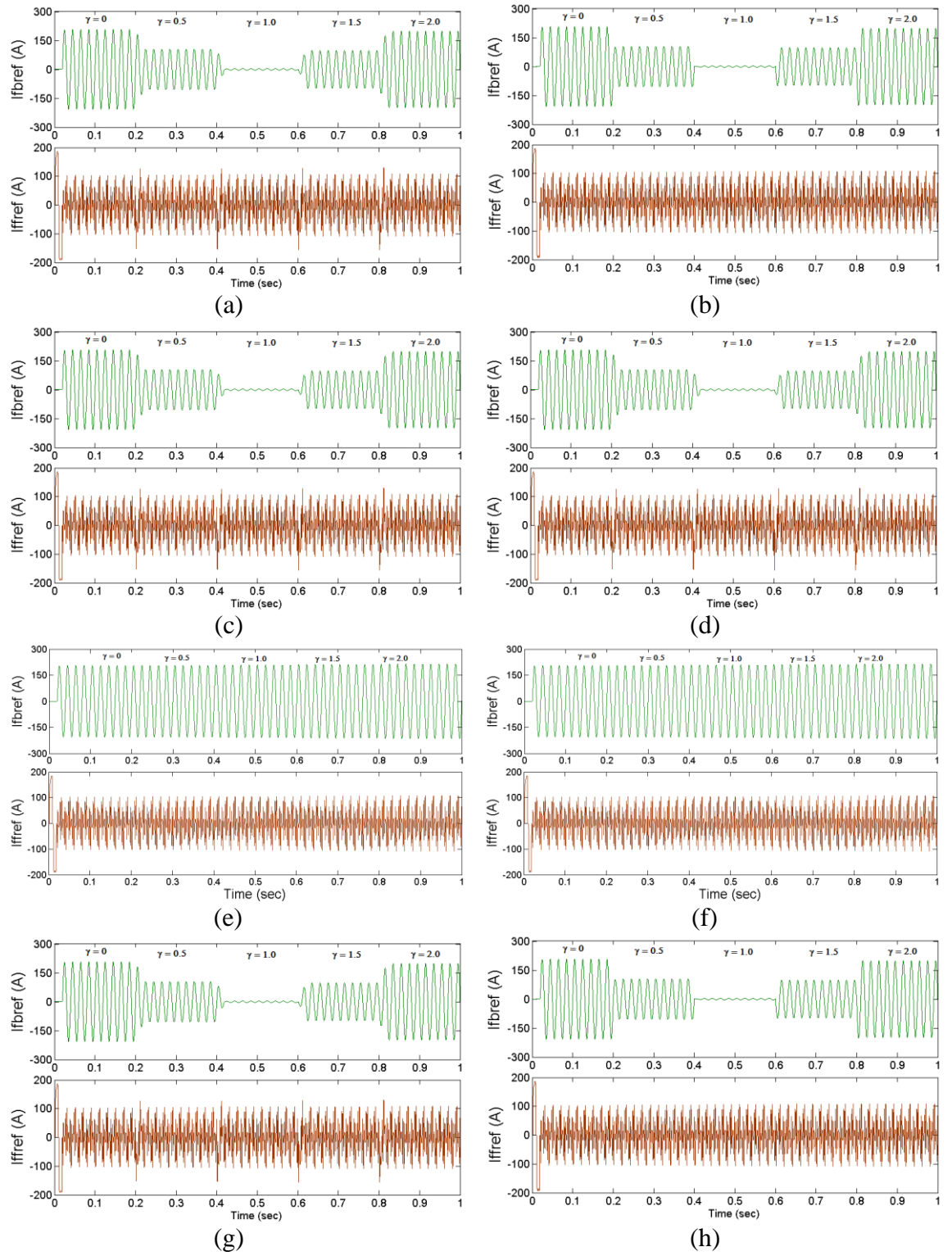
Fig 3.14 Generation of Reference Current in Position1 - (a) FB and (b) FF sensor; in Position 2 - (c) FB and (d) FF sensor; in Position 3 - (e) FB and (f) FF sensor; in Position 4 - (g) FB and (h) FF sensor.
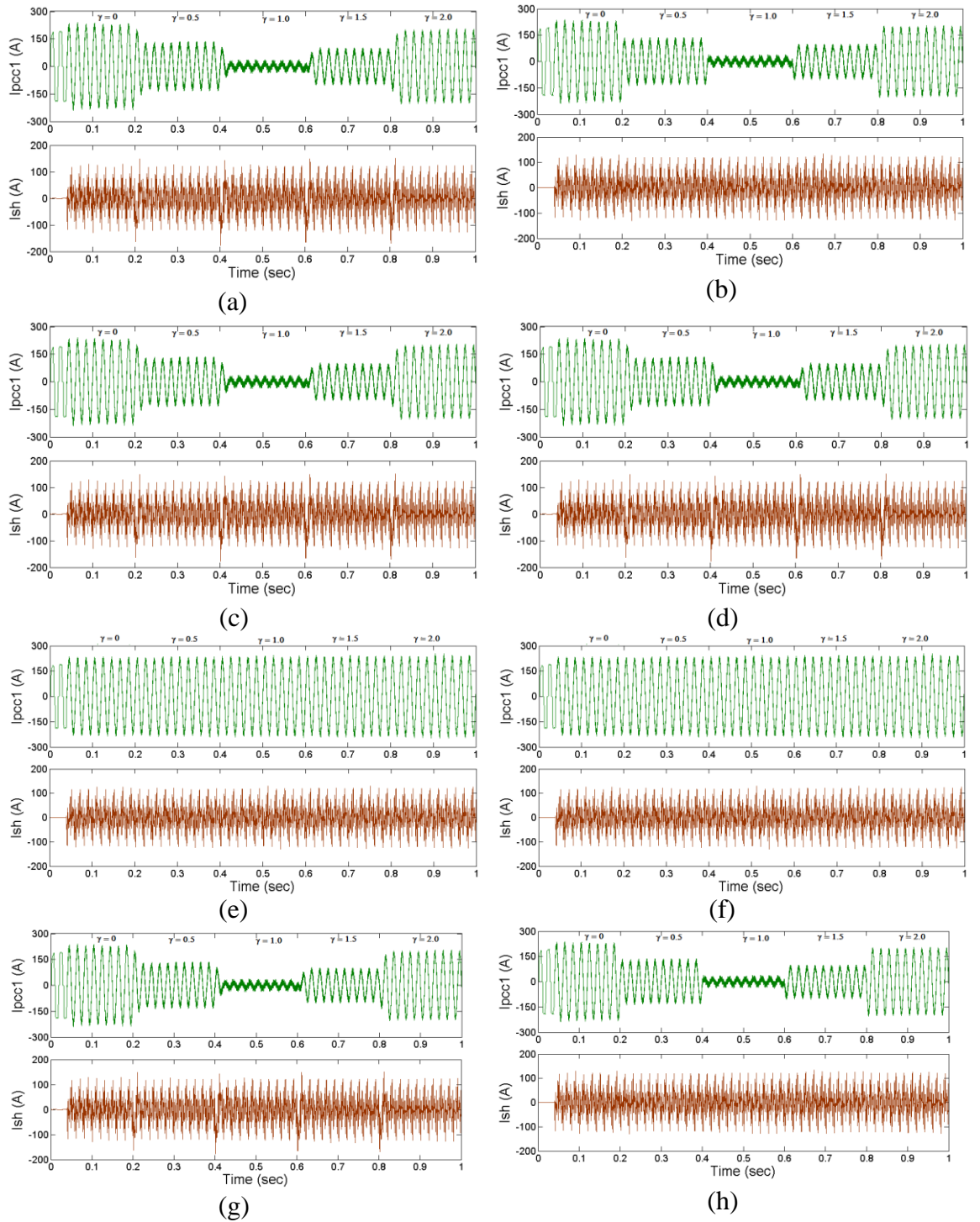
Fig 3.15 Harmonic Current compensation in Position1 - (a) FB and (b) FF mode; in Position 2 - (c) FB and (d) FF mode; in Position 3 - (e) FB and (f) FF mode; in Position 4 - (g) FB and (h) FF mode.

3.4.2.3 THD at PCC1

Table 3.7 shows the performance of the UPQC in terms of THD / TDD (%) at i_{pcc1} when no DG sources are connected to the system. In that case, only one position for the UPQC exists. Both the direct and indirect control with FB and FF mode shows almost the same performance in terms of reactive and harmonic current compensation.

In the presence of a DG source, the measured THD@ipcc1 is shown in Fig 3.16 where the DG input has been increased step by step up to a level equal to twice the load fundamentals. The shaded portion in the upper part of each figure is presented as a zoomed-in-version in the lower part of the respective figures. Results (in terms of THD) indicate that the FB mode can be better than the FF mode. But, as already mentioned, the FB mode becomes unstable during certain grid conditions and conventional supply current detection [31, 85]. This performance can be improved by introducing a closed-loop compensation method for selected line current harmonics which is proposed in [83]. But, still there is a possibility of unstable grid conditions due to the presence of a DG source (DG output is not constant) after the UPQC. Therefore, the FF mode can be a better option for the selection of the position. In that case, position1 and 2 with FF mode will be the best choice.

The other finding is that in the presence of a DG source and for any position and mode of control, the UPQC helps to keep the THD level within 5% (as required by the harmonic standards) except for the period when γ is within the range (0.5 to 1.5). This is reflected in the shaded portions (zoomed-in-version) of the Fig 3.16. Therefore, the μGrid designer needs to maintain this condition while designing a system.

Table 3.7 When UPQC is working; $i_{dg1} = 0$ and $i_{dg2} = 0$;

	Direct Control		Indirect Control	
THD / TDD (%)	FB Mode	FF Mode	FB Mode	FF Mode
@ i_{pcc1}	2.8	2.7	2.8	2.7

3.4.2.4 TDD at PCC1

Like THD, TDD measurement also depends on the sensor position. But for some positions it gives the real value of the harmonic contents. For example, in the case of Position 1, the FF sensor will sense the real load current and thus it can calculate the real load fundamentals to calculate the TDD. Thus, for this mode, TDD will reflect the

real condition of harmonics for any value of γ, as shown in Fig 3.17. For FB sensor, TDD will be same as THD. Similarly, for position 2 and 3, TDD and THD are same. Position 4 will show the results as shown for position 1. Therefore, instead of THD, it is better to measure TDD for such a DG integrated network with a power quality compensator.
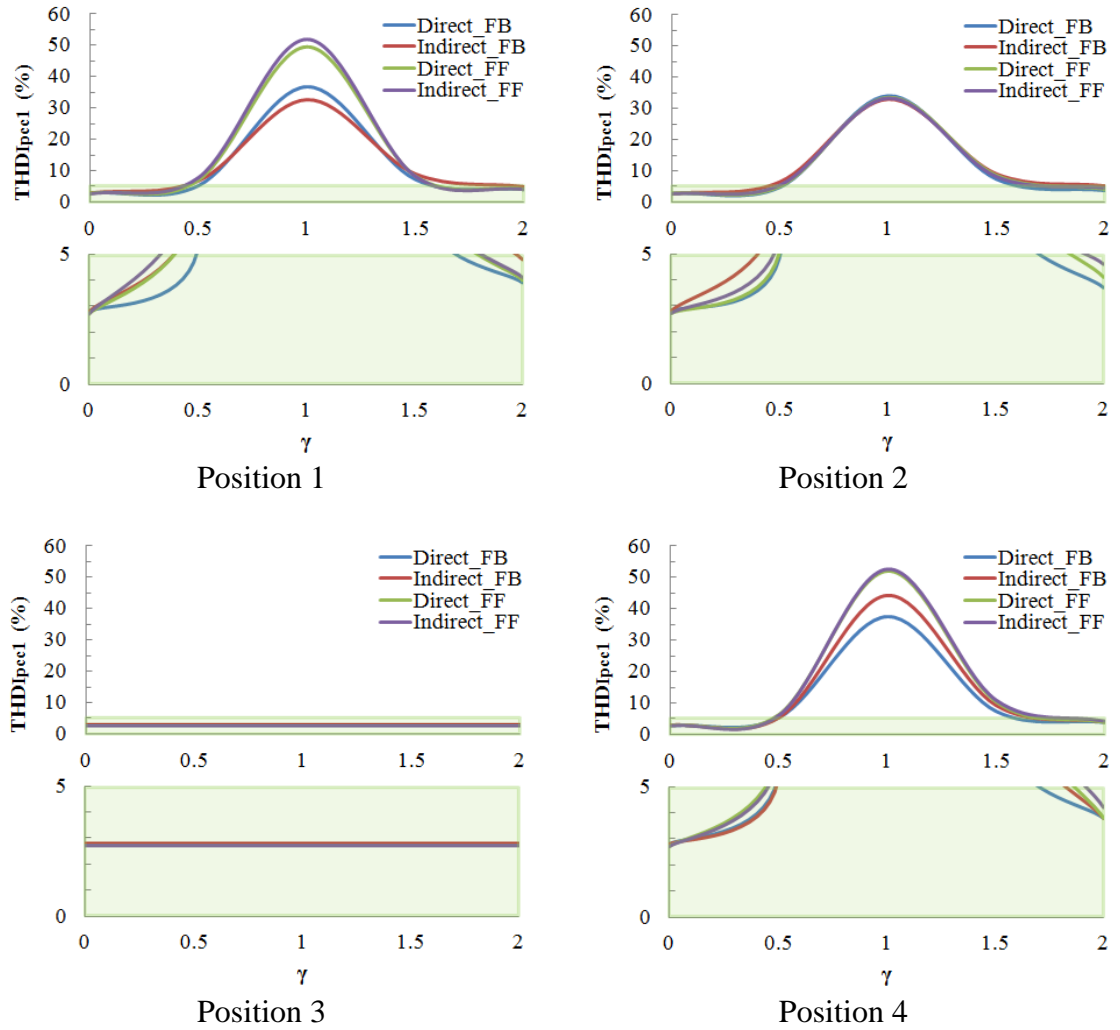
Fig 3.16 THD @ ipcc1 for all position and control of UPQC in presence of DG source. Lower part of each figure is the zoomed-in-version of the upper shaded part.
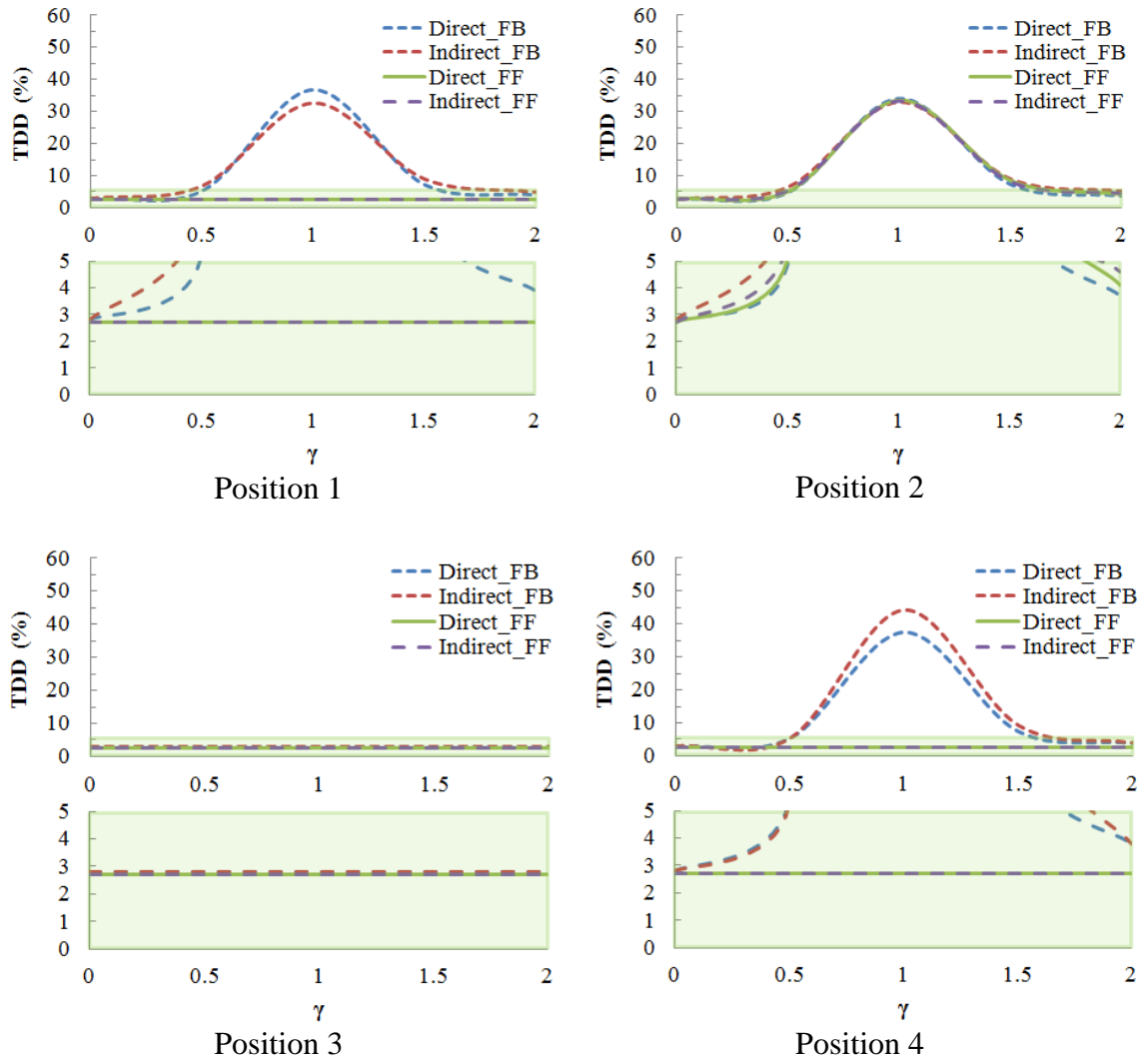
Fig 3.17 TDD for all position and control of UPQC in presence of DG source.

3.4.3 Performance of UPQC with bi-directional power flow

The UPQC will observe bi-directional power flow only when the DG source is placed after the UPQC. This will happen only for Position 1 and 2. Fig 3.18 - 3.21 show the performance of the UPQC in FF mode during reverse current flow due to the condition that $\gamma > 1$ and the dynamic change of i_{dg}. It is observed that for all the cases the response of the UPQC in position 1 with FF mode (a) is better than the position 2 (b). In terms of harmonic current compensation (THD value) as shown in Fig 3.16, direct control gives a better performance than indirect control.
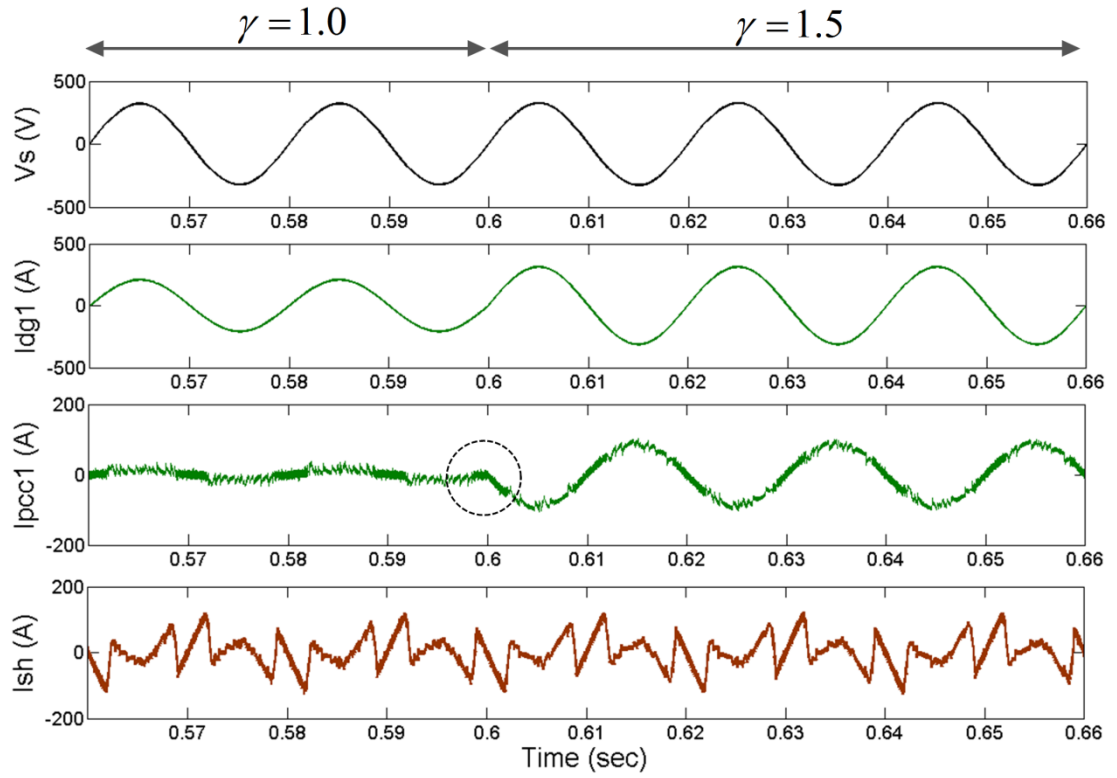
(a)
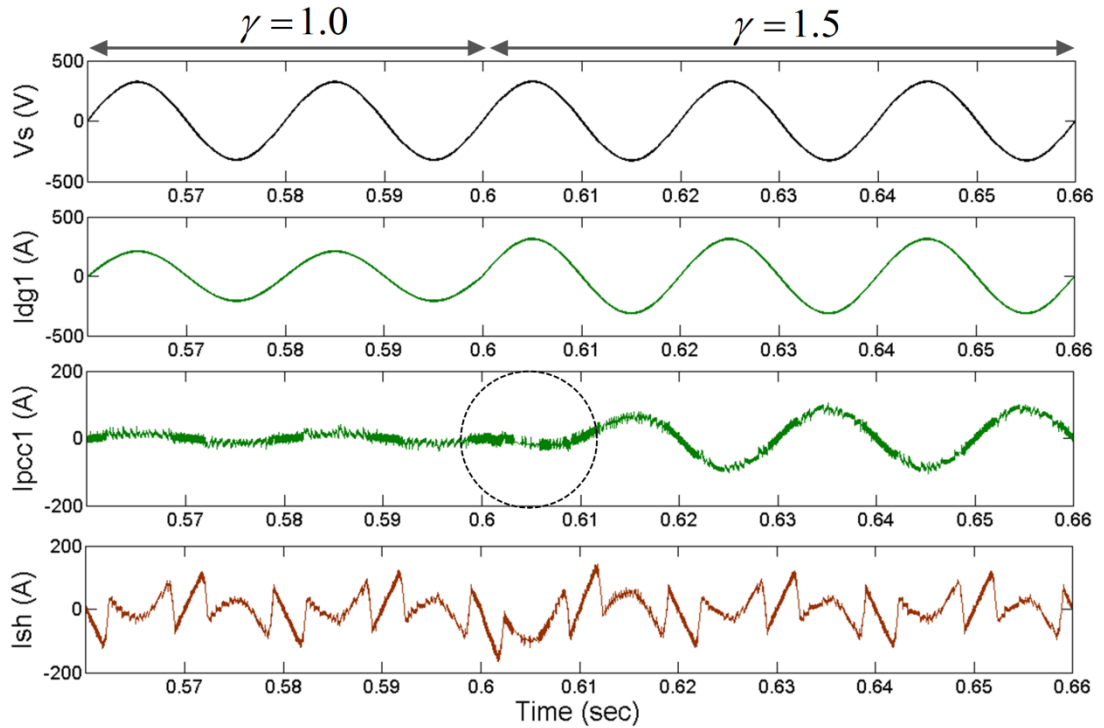
(b)

Fig 3.18 Performance of UPQC in reverse current flow (γ > 1) and FF mode for (a) Position 1 and (b) Position 2 with direct control;
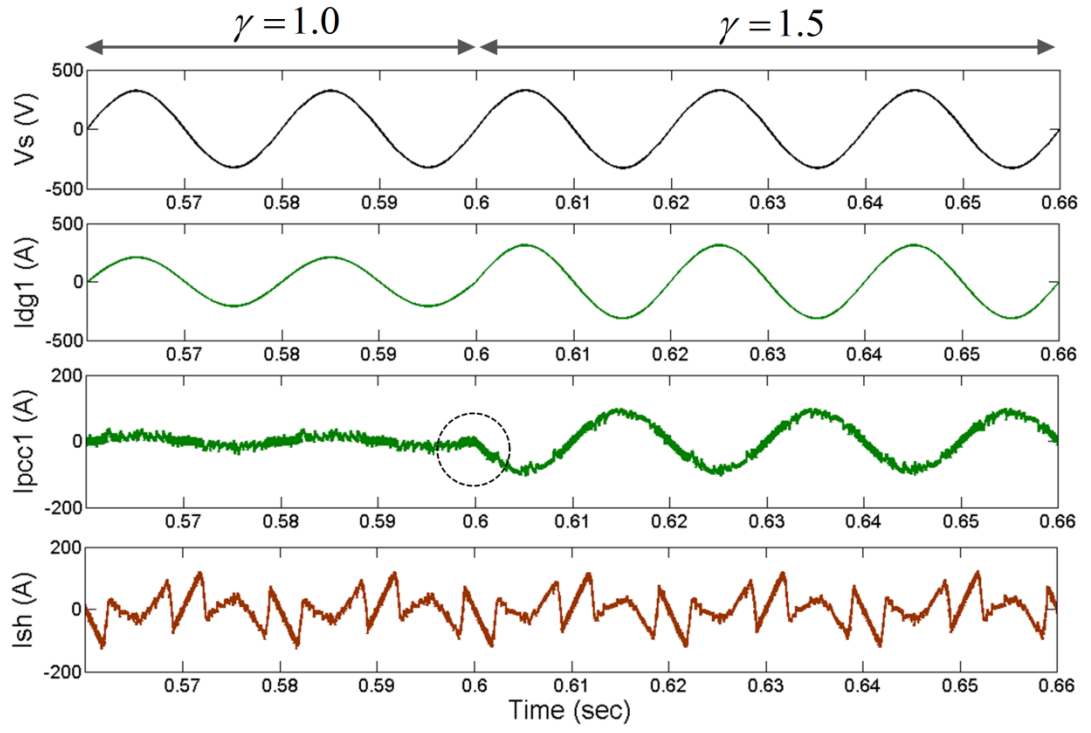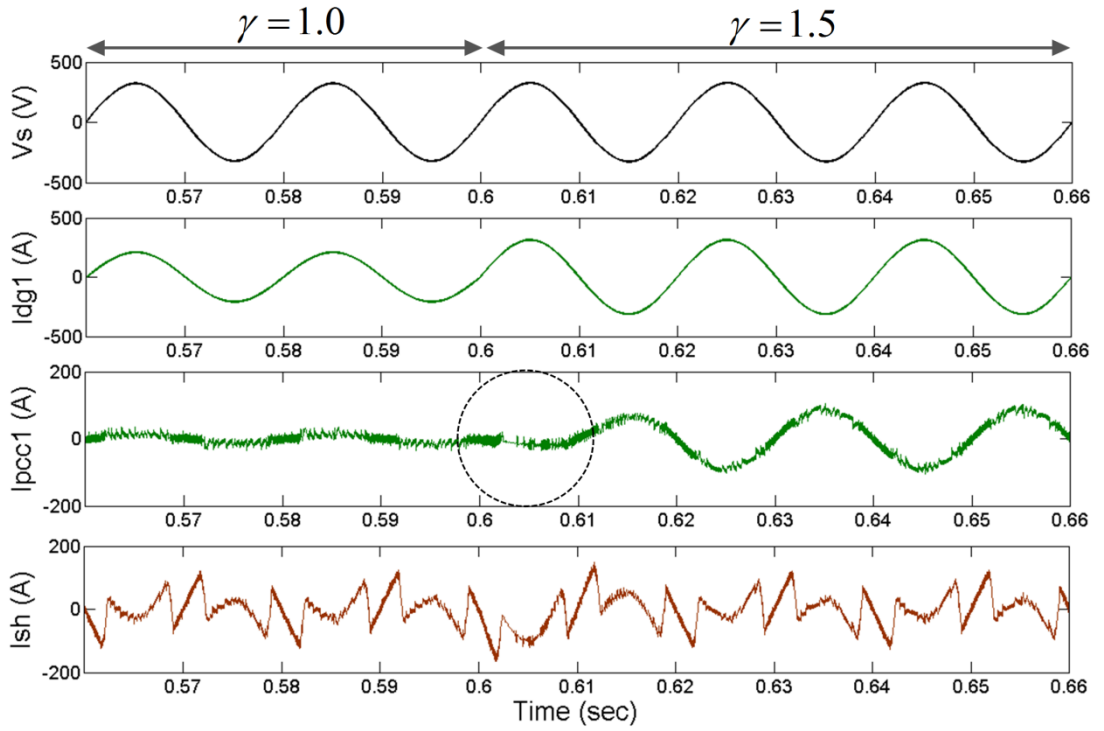
Fig 3.19 Performance of UPQC in reverse current flow (γ > 1) and FF mode for (a) Position 1 and (b) Position 2 with indirect control
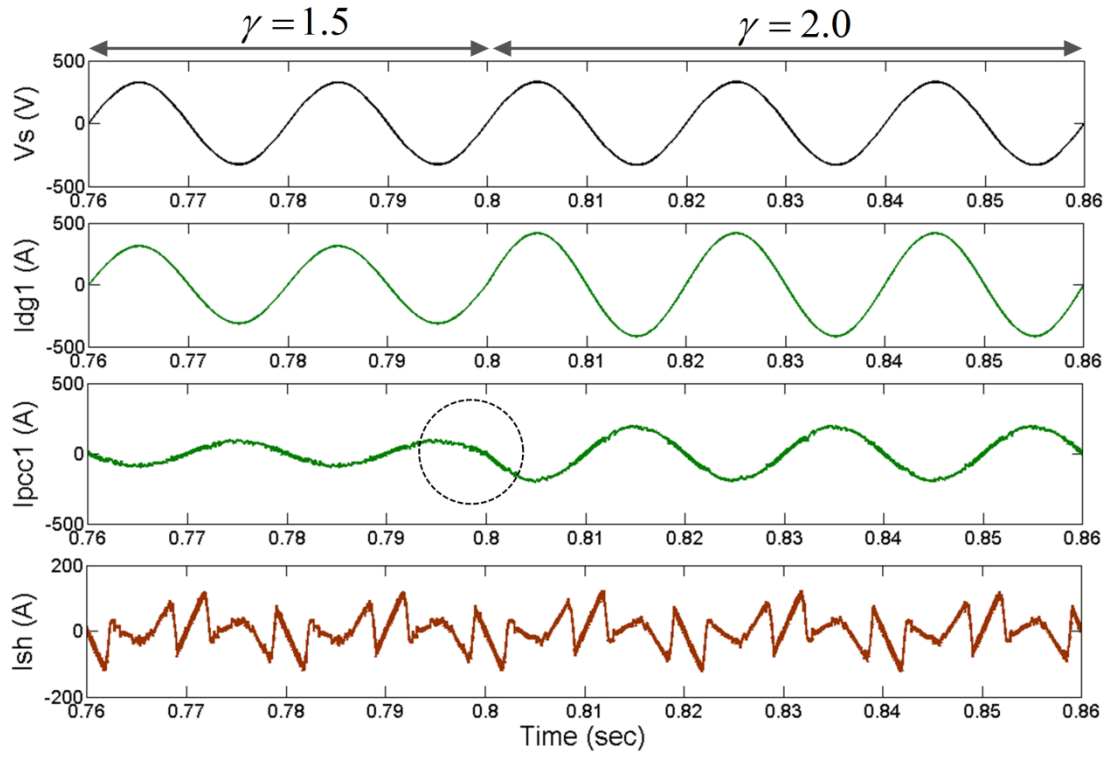
(a)
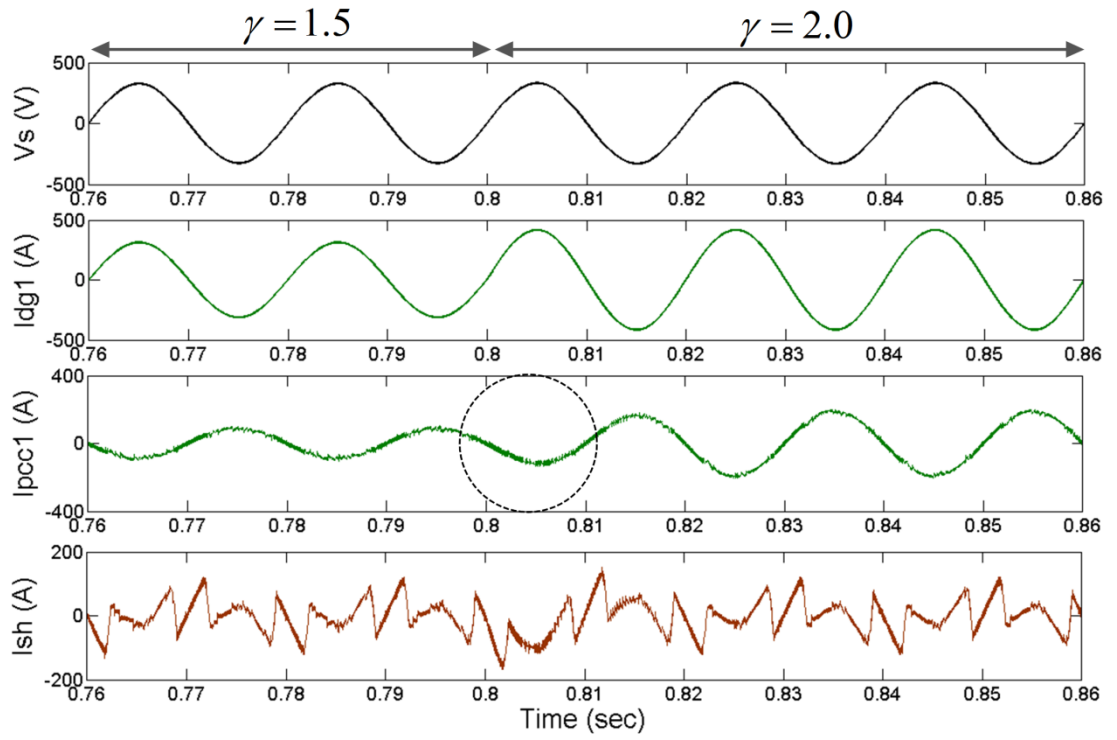
(b)

Fig 3.20 Performance of UPQC in reverse current flow ($i_{dg} > i_{load}$) with dynamic change of i_{dg} and FF mode for (a) Position 1 and (b) Position 2 with direct control
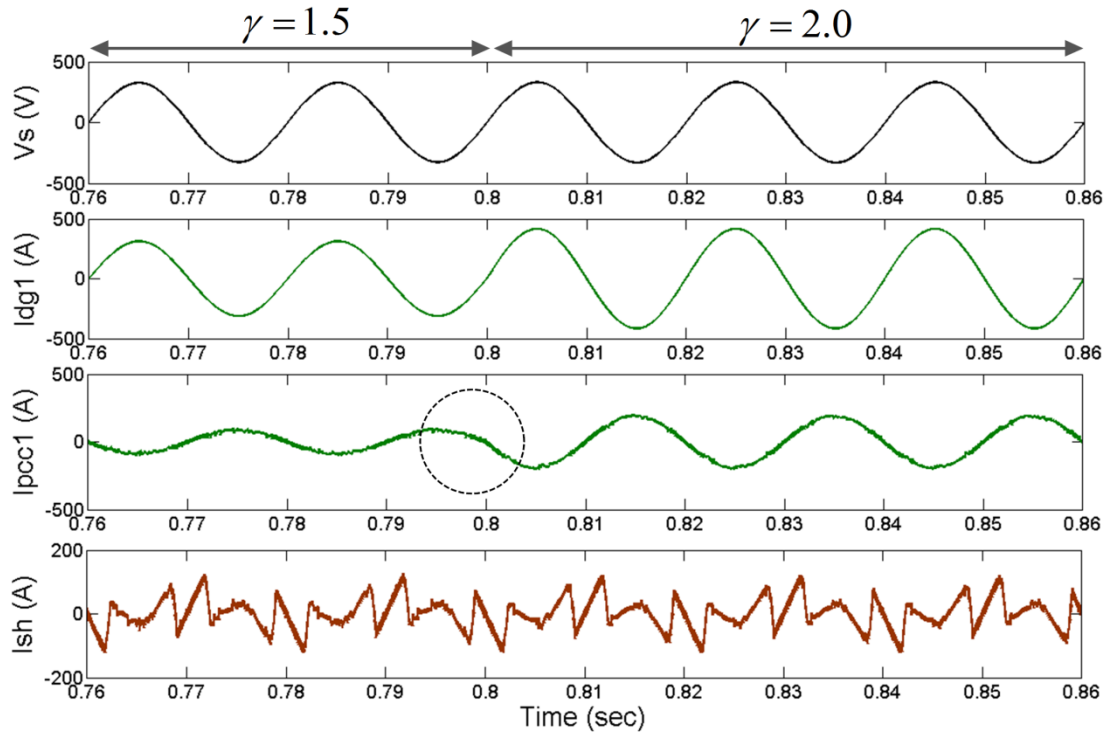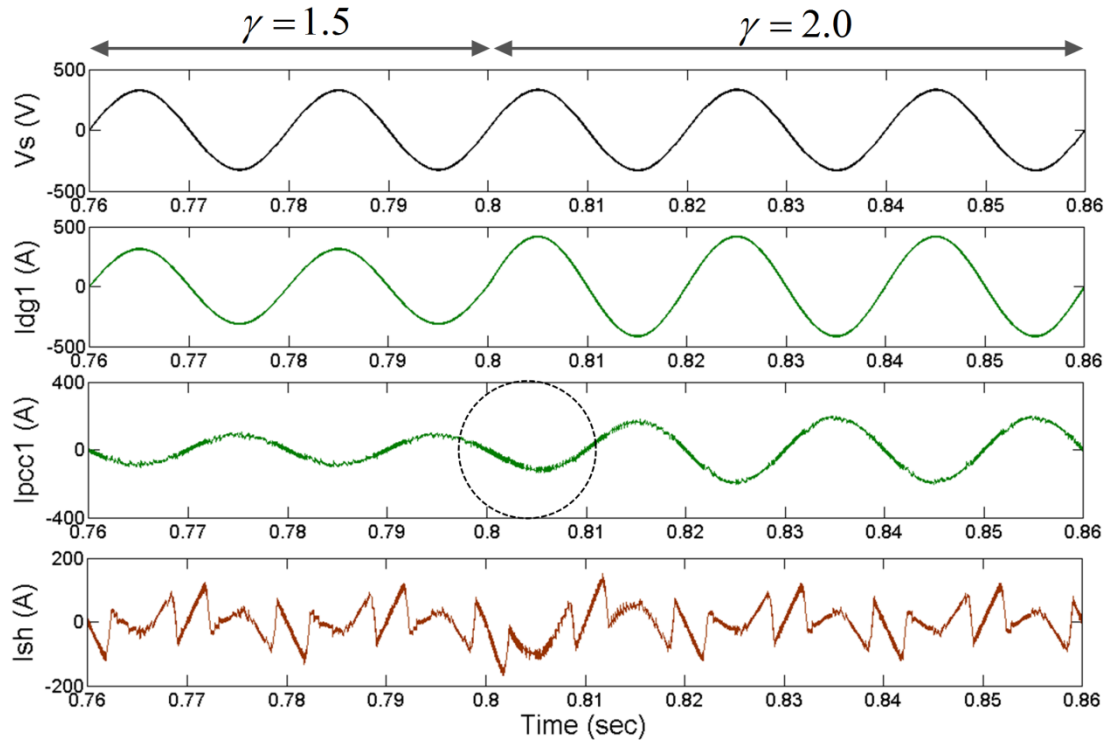
Fig 3.21 Performance of UPQC in reverse current flow ($i_{dg} > i_{load}$) with dynamic change of i_{dg} and FF mode for (a) Position 1 and (b) Position 2 with indirect control

3.4.4 Advantages of DG sources/µGrid systems

In terms of the DG source, it is better to place the DG source after the UPQC and therefore Positions 1 and 2 are preferable. This will have the following advantages;

(i) UPQC can compensate the voltage/current distortion generated by the DG source, and therefore the grid can be shielded from any disturbance created by the DG source/µGrid.

(ii) DG converter will not be exported to any grid voltage sag/swell or unbalance conditions and therefore will be safe from grid faults.

(iii) µGrid system can achieve some operational flexibility by exchanging the sag/swell, islanding and reconnection information between the UPQC and DG converters.

3.5 **Conclusion**

Based on the study and analysis for the placement of UPQC in DG connected µGrid/µGen network, it can be concluded that the network arrangement of PCC-UPQC-DG-Load (Position 1 and 2) can be a better choice for the overall performance of a UPQC and DG connected grid network. In terms of sensor placement, control and performance study (THD/TDD measurement at PCC), Position 1 gives the better result than that in Position 2. While designing a system, µGrid designer needs to maintain the condition that the measured current THD at PCC will be higher than the IEEE / EU limit while DG in connected to the network and provides 0.5 to 1.5 times of the load fundamental current. In the case of bi-directional power flow, Position 1 with direct control shows the better performance than indirect control. Finally, in a DG connected µGrid/µGen system, strategic positioning of UPQC can provide some control flexibility for DG inverters for islanding detection and reconnection. This scope is further explored in Chapter 5.

Chapter 4

Parallel Operation of Inverters and Active Power Filters in Distributed Generation Systems

4.1 **Introduction**

It is now more common to have grid connected inverters facilitating distributed generation (DG) or in microgrid systems. In some cases, grid connected inverters may extend the energy availability, increase the energy security and improve the system reliability. The power quality, at all time, is a matter of concern. DG inverters may introduce more harmonics into the grid. On the other hand, in microgrids or DG systems, load demands are also increasing. Therefore, to cope up with the increasing load demand, multiple low power inverters are on the rise instead of large capacity centralised inverters. Different controlling mechanism and topologies are available in handling the difficulties of parallel operation of inverters either in active load sharing or distributed mode. Research has also been carried out on parallel operation of shunt APF in active load sharing or distributed mode. Therefore, a technical review on parallel operation of power electronics inverter and APF for load sharing conditions in a distributed generation (DG) network has been carried out here.

This chapter is organized as follows: in Section 4.2, the principle of parallel operation of inverters with their possible problems is discussed. Active load sharing and a droop control method for parallel operation of inverters are presented in brief in Section 4.3. It is found that droop control is very suitable for both DG and off-grid conditions. Section 4.4 deals with the working principle of the droop control method.

Control strategies for parallel operation of APF are presented broadly in Section 4.5. Finally, concluding remarks are made in Section 4.6.

4.2 **Principle of Parallel Operation of Inverter**

Balance between generated and consumed real (P) and reactive (Q) power indicates the stable operation of a power system. Therefore, implementing effective control over P and Q is very important from the operational and control points of view. The real (P_1) and reactive (Q_1) power transferred between the inverter and common bus or grid can be explained [87] from the following diagram, Figure 4.1
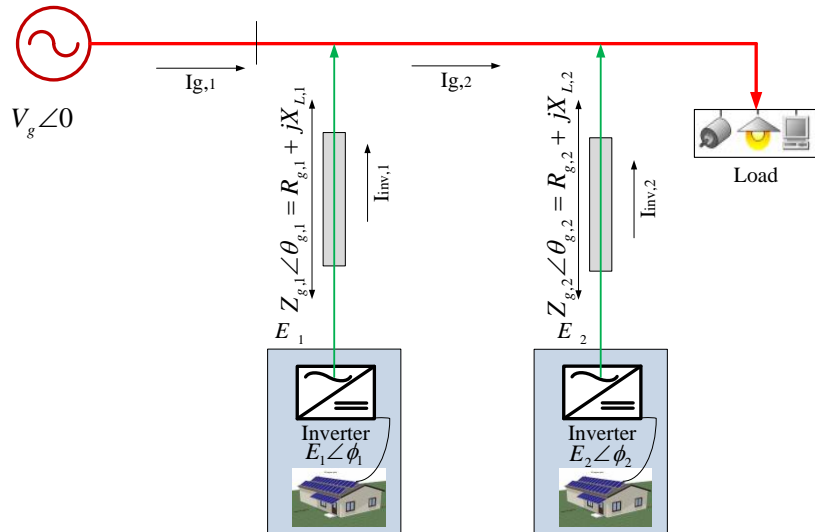
Fig 4.1 Equivalent circuit of parallel inverter connected to the grid

$$P_1 = \left[\left(\frac{E_1 V_g \cos\phi_1}{Z_{g,1}} - \frac{V_g^2}{Z_{g,1}} \right) \cos\theta_{g,1} + \frac{E_1 V_g}{Z_{g,1}} \sin\phi_1 \sin\theta_{g,1} \right] \tag{4.1}$$

$$Q_1 = \left[\left(\frac{E_1 V_g \cos\phi_1}{Z_{g,1}} - \frac{V_g^2}{Z_{g,1}} \right) \sin\theta_{g,1} - \frac{E_1 V_g}{Z_{g,1}} \sin\phi_1 \cos\theta_{g,1} \right] \tag{4.2}$$

Here P_1 and Q_1 are the transferred real and reactive power from the inverter, E_1. For only real power transfer, V_g and E should have the same amplitude but with a different phase. The different amplitude with same phase will give a reactive power circulation.

When both differ, it causes real and reactive power flow. Control of frequency dynamically controls the power angle and hence, the real power flows. As the output impedance of the inverter is very low, a small change in ϕ could result in a very large imbalance in the active power flow [28]. For parallel operation, the output voltage of all inverters must be kept strictly in phase in order to guarantee equality of the output active power for the corresponding inverters. Reactive currents can circulate between inverters if their output voltage magnitudes differ from each other, as shown in Figure 4.2, which can overload the inverters unnecessarily.
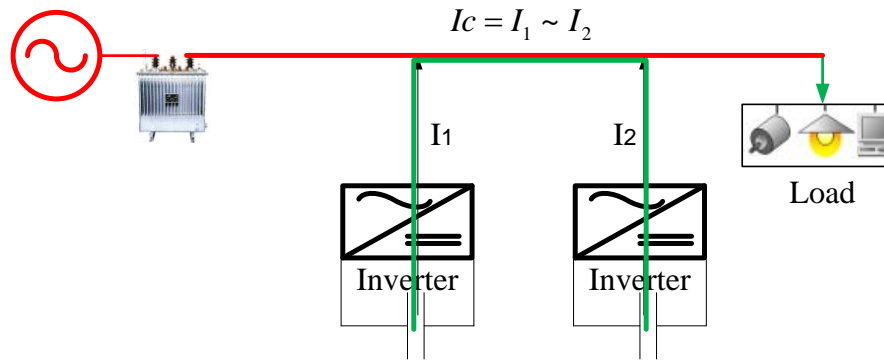
Fig 4.2 Circulating current flow between the parallel inverters

To suppress the circulating current and prevent the dc-link overvoltage, an isolation transformer can be used as a passive control [88 - 90] but then the size of the transformer for high power application could be a problem. Some active methods are also described in [91 - 104] and most of these are based on PWM control. A simple protective control algorithm has also been proposed in [94], Figure 4.3, where the regeneration protection concept based on the rising dc-link voltage is considered. If V_{dc} is greater than V_{dcref}, the battery converter stops delivering power from the battery side. Here a proportional controller detects the error signal of the dc-link voltage.
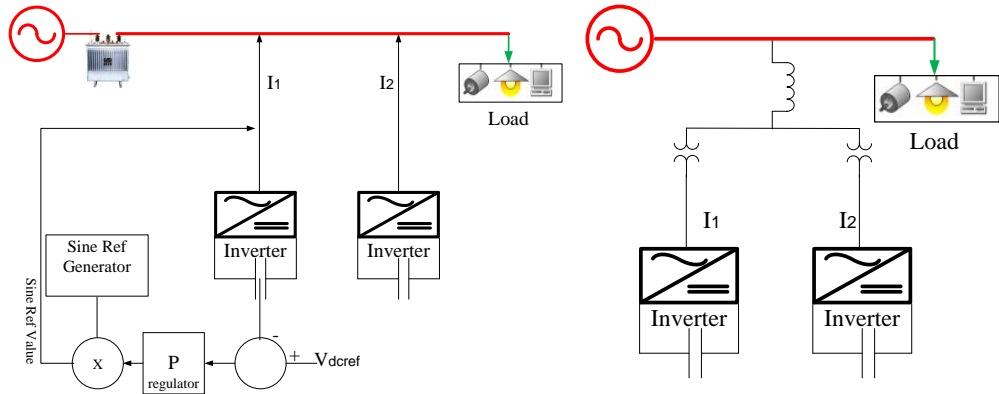
Fig 4.3 a) Regenerative control structure to avoid dc-link overvoltage / to prevent circulating current; b) passive control using isolation transformer

4.3 **Control Strategies in Parallel Operation of Inverter**

Distributed generation (DG) systems, either connected to or off the grid, may have more than one inverter acting in parallel. Therefore in distributed Uninterruptible Power Supply (UPS) systems, the parallel operation of a voltage source inverter with other inverters or with the grid, are sensitive to disturbances from the load or other sources and can easily be damaged by over-current. Hence, careful attention should be given to system design and the control method of parallel operating inverters. Several control methods are proposed and discussed in [89, 93 - 112]. Two or more inverters operating in parallel must achieve the following features: 1) amplitude, frequency and phase synchronization among the output voltages of inverters, 2) proper current distribution according to the capacities, 3) flexibility and 4) hot-swap ability at any operating time [105].

The purpose of active power filters (APF) with its multiple configurations differ from inverter operation, but as the inverter is also a part of the active power filter, the controlling methods of inverters and APF in parallel operation could have some similarities. Therefore the details of controlling methods are described in the APF section. Some of the outcomes of recent research on parallel operation of inverters are given below. The conventional control strategies for the parallel-connected inverters can

be classified into two types; active load sharing/current distribution and droop/wireless control.

4.3.1 Active load sharing / current distribution

The object of the active current distribution control is to generate a reference current for each parallel-connected inverter and it can be subdivided into;

i)   Central Limit Control (CLC)

ii)   Master-Slave Control (MSC)

iii)   Average Current Sharing (ACS) / Distributed Logical Control (DLC)

iv)   Circular Chain Control (3C)

In CLC mode, all the modules should have the same configuration and each module tracks the average current of all the modules to achieve an equal current distribution [94]. Perfect and equal current distribution can be achieved by using DSP-based control for the voltage and current controller and by tracking the averaged inductor current of the inverters. Thus the system stability and robustness can be improved [106]

In the MSC method, one inverter is specified as the master, and all others as the slaves. The master inverter supplies a reference current to the slave inverters. Thus the master module is responsible for the output voltage regulation [107]. In such a system, if the master module fails, the system will shut down and this is a major drawback. This can be partially overcome by introducing a separate current-controlled PWM inverter unit to generate the distributing current nearly independently for the slave inverters. Hence, precise current division between the inverters are very much important. This strategy is easy to implement in the parallel operation of UPS [108]. In other cases, another module can take the role of master in the event of a main master unit failure. The control scheme can be of dedicated, rotary or high-crest current type [109].

In the MSC and CLC methods, the output currents of all parallel-connected inverters must be collected, and the number of parallel-connected inverters must be pre-known. If one of the parallel-connected inverters fails, the parallel-connected system will fail. This problem can be overcome by the DLC mode where redundancy is also achievable.

In the ACS/DLC mode, an individual control circuit is used for each inverter. The current control mode is used to control its output current and to trace the same average reference current. When a defect is found in any module, others can still operate in parallel [107 - 110]. It can also be used as a power-sharing technique where each inverter controls the active and reactive power flow in order to match the average active power of the system [105].

In 3C mode, the successive module tracks the current of the previous module to achieve an equal current distribution, and the first module tracks the last one to form a circular chain connection. The output voltage and current of each inverter can also be varied and internally controlled to achieve a fast dynamic response [103, 109]. A coordinate control strategy for different load sharing controls can be applied to eliminate the circulating currents due to unbalance of parallel inverters [103].

4.3.2 Droop control

The droop control method for the parallel-connected inverters can avoid the communication of the reference current. It is also defined as Wireless Control (WC) with no interconnection between the inverters. In this case, inverters are generally operated in the voltage-mode of control and the phase and amplitude of the inverter's output voltage are the control parameters. This control is defined in such a way that the amplitude and frequency of the reference voltage signal will droop as the load current increases and these droops are used to allow independent inverters to share the load in proportion to their capacities [110]. This technique is then improved for non-linear

loads where harmonic components can be shared properly [111]. The load sharing is also affected by the line impedance [112, 113]. The impact of line impedance on reactive power sharing in the conventional frequency/voltage droop concept is further enhanced in [114 - 116] to make the controller ideally suited for distributed ac power supply systems.

4.3.3 Outcomes

A detailed review and performance comparison that has been presented in [114] which shows that within active load sharing control schemes, current-sharing control is good for output voltage regulation and harmonic current control. However it requires high speed communications. Active power sharing requires low bandwidth communication for active and reactive power sharing, but the harmonic power sharing is poor and therefore sharing non-linear loads with a high crest factor is a problem. Active synchronization is also a major problem for both the schemes.

Within the active load sharing scheme, the centralized and the master-slave controller need a main inverter module to be set as the central control unit and this would lower the system reliability. Modularity and redundancy are very low for both of the controllers. For the average current sharing/distributed logic controller, although there is no central controller and thus has higher modularity, it requires a current sharing control loop to manage the transient and stability problems. The circular current control strategies require more communication between each of the inverters as well as a circular path for current distribution. This is suitable when forming an ac power ring.

In general, though the active current distribution control method is perfect for well balanced current distribution, the inter-communication process of the generated reference current of parallel-connected inverters can be susceptible to interference, and thus the system reliability will be degraded. In addition, the communication of the

reference current among the parallel-connected inverters is difficult in some applications such as distributed generation systems.

On the other hand, droop control or the wireless control with no interconnection lines could be more useful for both active load sharing or in distributed generation networks connected to the grid or off-grid. Some improvement in control has also been achieved to overcome its limitations, such as poor transient response. Hot-swap operation is another benefit of the droop control method. Low sensitivity to line impedance unbalances and harmonic power sharing capability are the other advantages of a droop controller.

4.4 Working Principle of Droop Control Method

The idea of the droop control method in the parallel operation of an inverter or APF is to control the system without interconnection between units. Inverters can be placed in different locations within the microgrid or DG system. In that case, the droop control method is very effective for the inverters where active and reactive power flow predominantly depends on power angle/frequency and the output voltage amplitude of the inverters. Here, inverters are generally operated in the voltage-mode control and the phase and amplitude of the inverter's output voltage are the control parameters. The controller is defined in such a way that the amplitude and frequency of the reference voltage signal will droop as the load current increases. It should be noted that the conventional voltage and frequency droop methods of achieving load sharing have a slow and often oscillating transient response.

An inverter connected to the common bus through a decoupling impedance is shown in Figure 4.4. Usually the inverter output impedance is highly inductive, and hence, the active and reactive powers drawn to the bus can be expressed from equation 4.1 and 4.2 as [87];

$$P = \frac{EV}{X} \sin \phi \tag{4.3}$$

$$Q = \frac{EV \cos \phi - V^2}{X} \tag{4.4}$$

where X is the output reactance of an inverter, ϕ is the phase angle between the output voltage of the inverter and the voltage of the common bus, and E &V are the amplitude of the output voltage of the inverter and the grid/load voltage, respectively. From the above equations, it is found that the active power is predominantly dependent on the power angle ϕ, while the reactive power mostly depends on the output-voltage amplitude E. Consequently, most of the wireless-control of paralleled-inverters uses the conventional droop method, which introduces the following droops in the amplitude E and the angular frequency ω of the inverter output voltage [110];

$$\omega = \omega^* - m(P_{0i} - P_i) \tag{4.5}$$

$$E = E^* - n(Q_{0i} - Q_i) \tag{4.6}$$

being ω^* and E^* are the output voltage angular frequency and amplitude at no load, and m and n are the droop coefficients for the frequency and amplitude, respectively. P_{0i}, Pi & Q_{0i}, Qi represent the power rating and actual power output for active and reactive power respectively. If droop coefficients are increased, then good power sharing is achieved at the expense of degrading the voltage regulation, which can be acceptable if, for instance, the frequency and amplitude deviations ($\Delta\omega$ and ΔE) are mostly at 2% and 5%, respectively [115].

The output impedance angle θ determines the droop control law, as shown in Table 4.1. Fig. 4.5 shows the droop control functions depending on the output impedance. The controller gains m and n are chosen as a function of the nominal values

of P and Q, and the maximum allowed deviations in frequency $\Delta\omega$ and amplitude ΔE (Table 4.I). Fig. 4.6 shows a simple block diagram of a droop controller.
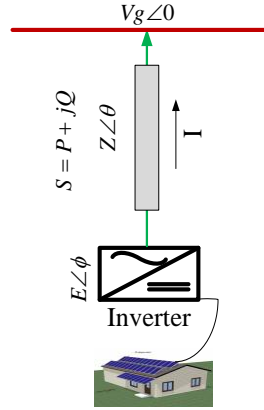
Fig 4.4 Inverter connected to the grid (droop control)
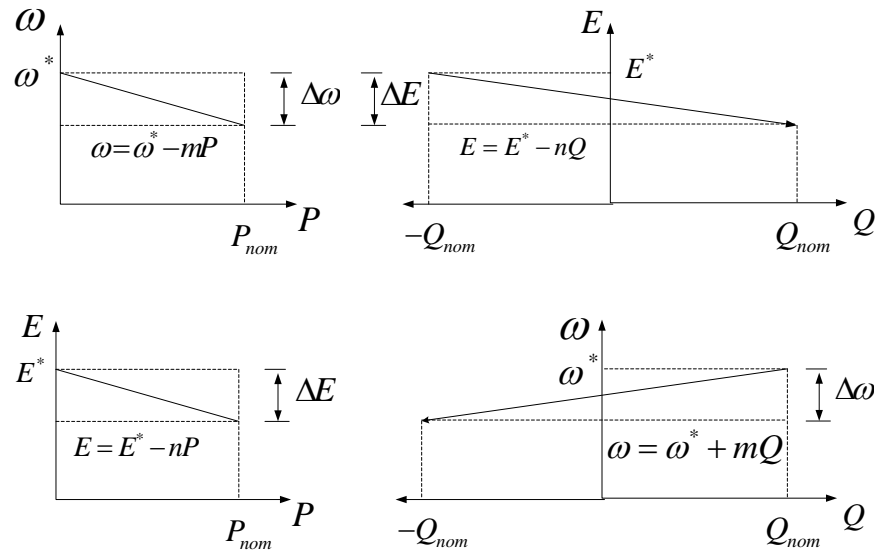
Fig 4.5 Static droop characteristics
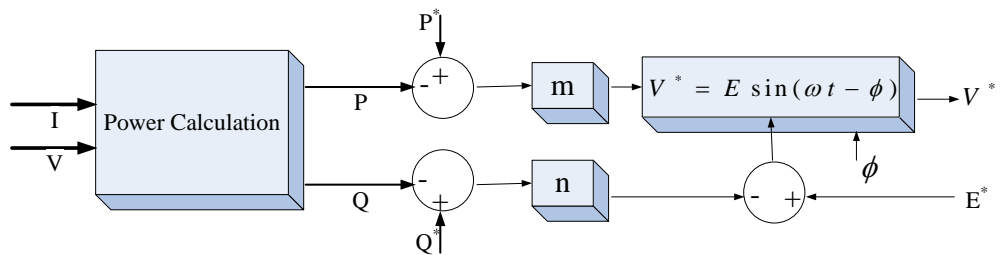
Fig 4.6 A simple block diagram of P/Q droop controller

Table 4.1 Output impedance impact over power flow controllability [104]

Output Impedance (Z)	$Z = jX$ (inductive: $\theta = 90^0$)	$Z = R$ (resistive: $\theta = 0^0$
Active Power (P)	$P = \dfrac{EV}{X}\sin\phi \cong \dfrac{EV}{X}\phi$	$P = \dfrac{EV\cos\phi - V^2}{R} \cong \dfrac{V}{R}(E-V)$
Reactive Power (Q)	$Q = \dfrac{EV\cos\phi - V^2}{X} \cong \dfrac{V}{X}(E-V)$	$Q = \dfrac{EV}{R}\sin\phi \cong -\dfrac{EV}{R}\phi$
Frequency droop (ω)	$\omega = \omega^* - mP$	$\omega = \omega^* + mQ$
Amplitude droop (E)	$E = E^* - nQ$	$E = E^* - nP$
m	$\Delta\omega \big/ P_{nom}$	$\Delta\omega \big/ 2Q_{nom}$
n	$\Delta E \big/ 2Q_{nom}$	$\Delta E \big/ P_{nom}$

4.5 **Control Strategies in Parallel Operation of APF**

Like inverters and UPS, Custom Power Devices (CPD) are finding greater applications as interfacing and compensating devices in the distributed generation system for power quality improvement as well as storing energy to work as a back-up UPS system during islanded mode of operation. The power rating and switching frequency of active power filter (APF) converters are determined by the magnitude of harmonic currents and required filter bandwidth. In high power applications, the filtering task cannot be performed for the whole spectrum of harmonics by using a single converter due to the limitations on switching frequency and power rating of the semiconductor devices. Therefore, to handle a larger portion of load power, increasing its capacity is essential. The solutions suggested in the literature to this typical design problem of APFs are a hybrid configuration, which reduces converter power rating; step-down transformer, which usually increases the cost; series or parallel connection of switching devices, which results in more complex gate drives; multilevel inverter, which reduces voltage rating of the switches; or splitting filtering on the spectrum range among a number of APF. The approaches with multiple inverters have already been demonstrated to be very effective for increasing the capacity.

The concept and a design analysis with experimental validation of a multi-module parallelable three-phase active power filter (centre mode) has been proposed first in [117] to solve the problems of capacity enlargement and load unbalance compensation encountered by the shunt APF with a three-arm topology. But the disadvantage of the proposed method was that the malfunction of any inverter will cause erroneous compensation due to the generation of a current command which is not independent to other inverters. Therefore another proposal was made by the same author in [118] with a capacity limitation technique. In that case, APFs are connected in a cascade mode which shows the advantages of high flexibility, reliability due to no control interconnection and reduced power capacity demand of APFs. But the disadvantage was that one APF treats other APFs on its load side as a part of its load. The third approach has been proposed in [119] which is based on power splitting. An overview of these techniques has been given below and present research outcomes along with the advantages and disadvantages of these techniques are also described later.

4.5.1 Frequency splitting (FS) / Centre mode control (CMC)

A central control unit is used to measure the total harmonic components and then each APF is assigned to compensate a specific harmonic component. Therefore it requires the minimum number of harmonic detection sensors, shown in Figure 4.7(a). It can also be referred to as concentrated control. The technique for reference current generation has been presented in Figure 4.7(b). If the sensing load current is i_L then the harmonic current will be, $i_{Lh} = i_L - i_{L1}$ where i_{L1} is the fundamental component of the load current and h is the number of harmonic components. In this mode, if there are 2 APFs working in parallel and one is responsible for reactive power compensation, then the other one will compensate the harmonics [88, 120].

The operational advantage is that the APF module which deals with the higher order harmonics should have the higher switching frequency. Since the harmonic

current magnitude is inversely proportional to the harmonic order, the power rating is low. Thus it also helps to reduce the switching losses. The main disadvantage is that the APF modules are not identical and therefore replacement requires a similar one.

a)

b)
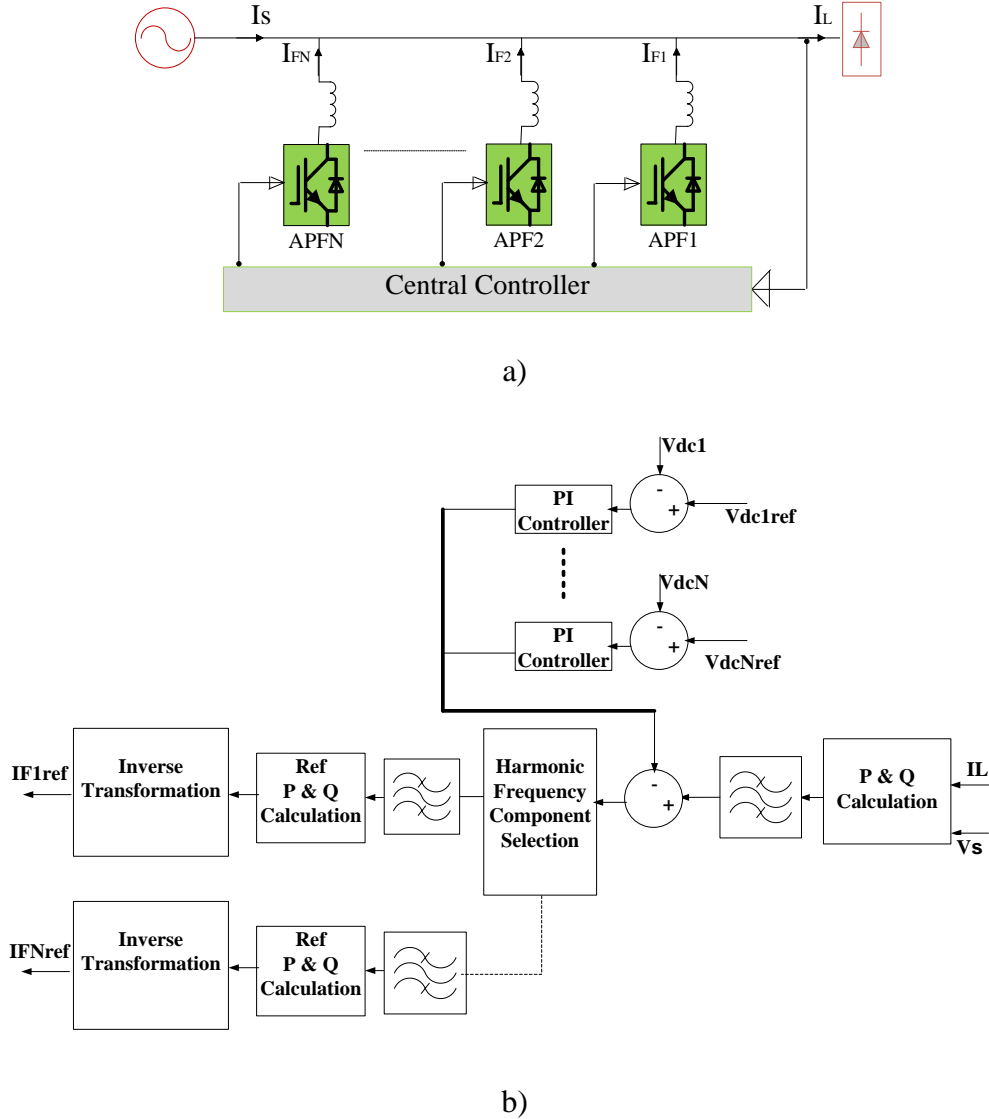
Fig 4.7 a) Centre Mode Control Technique; b) Reference Current Generation technique

4.5.2 Power splitting (PS) / Distributed control (DC)

In that case, compensating total harmonic current is equally distributed to the APFs and therefore identical modules are required. If there are N modules operating then the current reference of each module will be,

$$I_{FN} = {i_{Lh}}/{N} \qquad (4.7)$$

Since it maintains interconnection between the inverters, the number of sensors are also higher than the central control mode, shown in Figure 4.8(a). The reference current generation technique has been depicted in Figure 4.8(b). The main advantage is its ease of maintenance and installation. It is clear that in both central and distributed control systems, the reference current of each APF result from the same P&Q calculating algorithm block and therefore all the APFs maintain interconnection control. Hence a fault in any communication or malfunctioning of any APF can cause the system to halt.

a)

b)
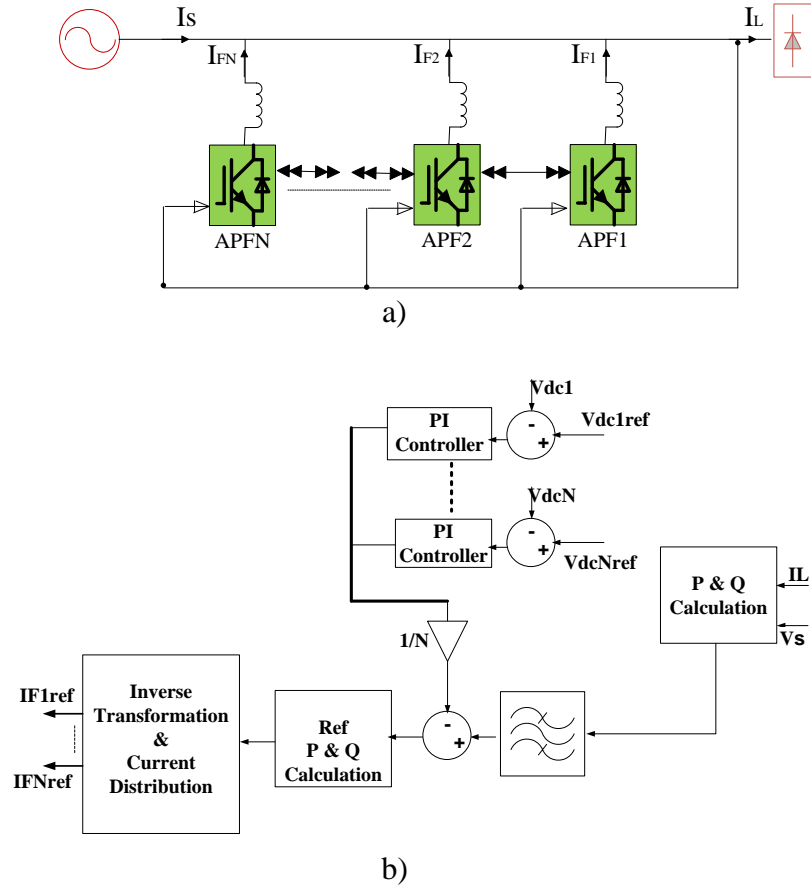
Fig 4.8 a) Distribute Control Technique; b) Reference Current Generation technique

4.5.3 Capacity limitation control (CLC) / Master – Slave control (MSC)

In this mode, each APF compensates harmonic current according to its power rating. Each APF are independent and sense the current at the up/downstream side of the node and therefore the maximum number of sensors are required, Figure 4.9(a).

Each APF only has to compensate the harmonic component left by the previous APF on its load side. Therefore generation of reference current for each APF requires separate P&Q calculation as shown in Figure 4.9(b). The rating of each APF module is defined as;

$$P = \frac{\sqrt{3}}{2} V_{dc} I_{F\max} \qquad (4.8)$$

In general, APF near the load has higher capacity and the lowest bandwidth. As the APFs are not identical and work independently therefore power capacity enlargement is easier and the system reliability is also high. Also there is no central control and no information sharing between the APFs. Poor dynamic characteristics is the main disadvantage of this mode. But for steady-state conditions, CLC and PS show a better performance than the FS [121].

Fig 4.9 a) Capacity Limitation Control Technique; b) Reference Current Generation technique

Furthermore, a common dc link capacitor can be used for parallel inverters, shown in Figure 4.10, to reduce the system cost [122], but it then raises the hardware design

and control complexity due to the zero sequence current circulation between the inverters [123].
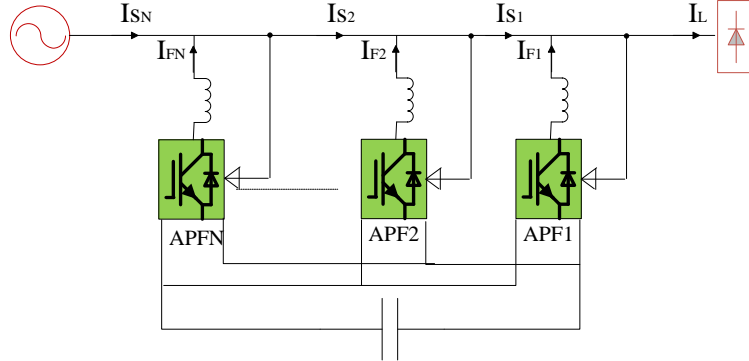
Fig 4.10 Parallel inverters with common dc link capacitor

A new modular based APF controlled strategy with a combination of central control and master-slave mode has been proposed in [124] where each APF can operate independently and compensate the load harmonic current according to its own capacity. The output current of each APF is optimized in such a way that the APF with large capacity compensates more current and the one with small capacity compensates less current. In this way, the feasibility and security of modular APF can be guaranteed. Figure 4.11 shows the new control strategy where the total harmonic compensating current, $I_F = I_{F1} + I_{F2} + \ldots + I_{FN}$. Here,

$$I_{F1} = K_1 I_F ; I_{F2} = K_2 I_F ; \ldots ; I_{FN} = K_N I_F \tag{4.9}$$

and $K_N = \dfrac{I_{rN}}{\displaystyle\sum_{j=1}^{N} I_{rj}} \dfrac{I_{rN}}{I_{FNref}}$ (4.10)

where, I_r and I_{FNref} represent the rated current and the compensating current reference of the selected APF.
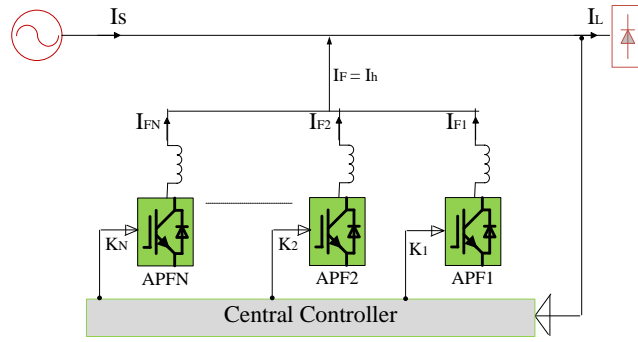
Fig 4.11 Parallel operation of APF with a combination of central control and capacity limitation

Controlling strategies are applicable only for the active load sharing mode when multiple APFs are placing close to each other either at the point of common coupling or close to a large capacity load. When these APFs are working in different feeders or deal with individual loads, (Figure 4.12), then no other controlling mechanism is needed even though they are seen to be in parallel operation [125].
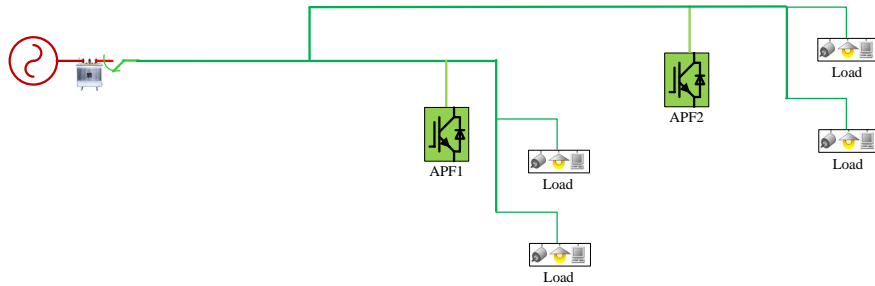
Fig 4.12 Parallel operation of APFs with different feeder

Depending on the placement of the harmonic current sensor, there could be two types of harmonic compensation loops for dual shunt APF in parallel mode, either feedforward or feedback [123, 83, 126]. In general, feedforward topology is extensively used for its good stability characteristics and easy installation where the controlling method is based on a current-controlled source. On the other hand, feedback control is better for stationary conditions but become unstable during unknown grid conditions. A combination of both controllers for two parallel APF rather than a single unit gives a better compensating result for both low and high order harmonics and it also stable for

grid operation [126]. A comparative analysis with advantages and disadvantages of these techniques with topologies has been presented in the Table 4.2.

All the above approaches are for harmonic current compensation which is the primary function of the parallel APF. Shunt APF can also be used as a compensator for voltage harmonics from the grid/DG source/load. Therefore, controlling of parallel APF for voltage harmonic compensation in a distribution line is another important issue. To detect the harmonic voltages, the active filter is characterized as behaving like a resistor for harmonic frequencies [127 - 129]. A cooperative controller based on voltage THD is proposed in [130] for parallel operation of multiple APF in a radial distribution feeder. A radial power distribution system with active power filter for voltage harmonic mitigation is shown in Fig. 4.13. The real-time communications among the APF units are required to coordinate the operations, which is overcome by introducing droop control method [131, 132].

a)

b)
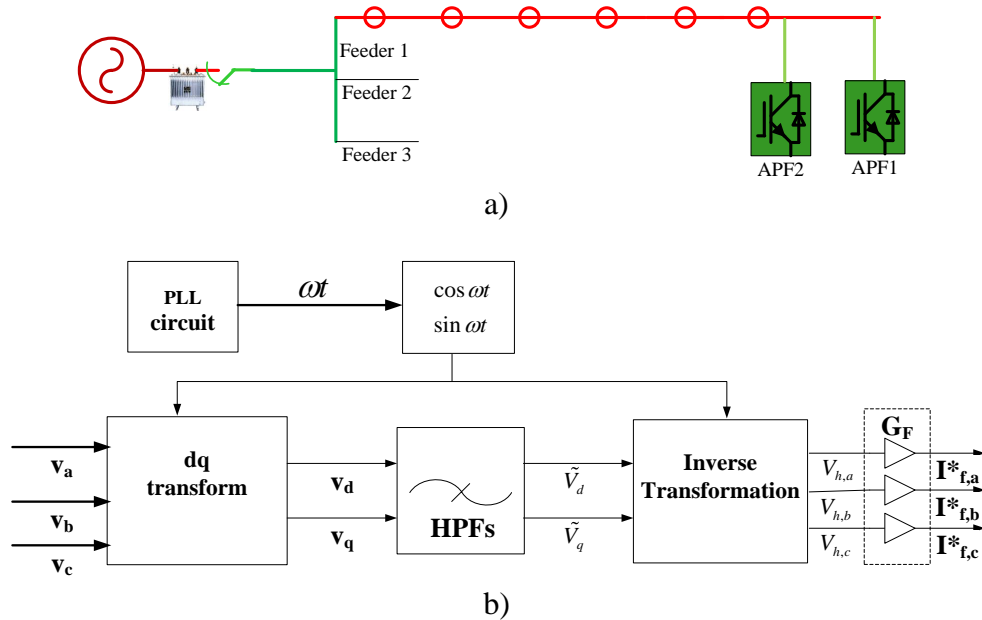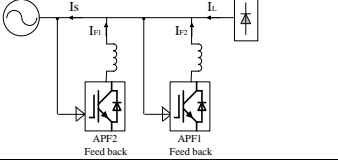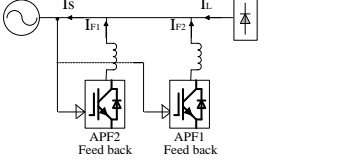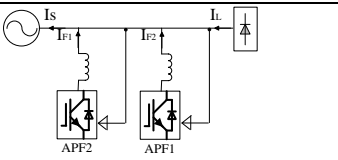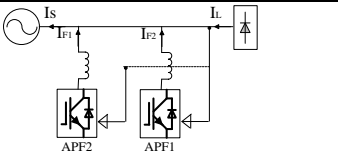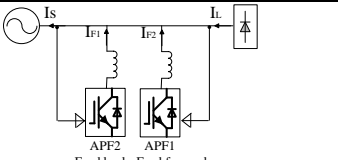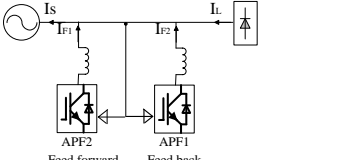
Fig 4.13 a) A radial power distribution system with active power filter; b) a simple control circuit of the shunt APF as a voltage harmonic compensator

Table 4.2 Comparative analysis of parallel APFs controlling scheme with topologies

Harmonic Compensation Loop	CS	Advantages	Disadvantages
(circuit diagram: APF2 Feed back, APF1 Feed back)	MSC	i. compensate damping resonance (due to grid and filtering capacitor at the load side) ii. better transient response in steady state condition iii. reliable and redundant	i. HDS - 4, thus increase the hardware complexity ii. unstable for unknown grid condition
(circuit diagram: APF2 Feed back, APF1 Feed back)	FS / PS	i. HDS - 3, thus reduces the hardware design complexity ii. reduce switching losses, if two inverters operate at different frequency iii. good for load sharing between the filters	i. design for reference current selection is critical; both inverters should be rated at same nominal power. ii. unstable for unknown grid condition iii. requires identical replacement
(circuit diagram: APF2 Feed forward, APF1 Feed forward)	MSC	i. does not depend on the voltage harmonic distortion ii. Good stability	i. HDS - 4, thus increase the hardware complexity ii. load sharing between the filters is difficult
(circuit diagram: APF2 Feed forward, APF1 Feed forward)	FS / PS	i. HDS - 3, thus reduces the hardware design complexity ii. easy maintenance and installation iii. good for load sharing between the filters	i. design for reference current selection is critical; both inverters should be rated at same nominal power.
(circuit diagram: APF2 Feed back, APF1 Feed forward)	MSC	i. harmonic compensation is better than that of the above four configuration	i. HDS - 4, thus increase the hardware complexity
(circuit diagram: APF2 Feed forward, APF1 Feed back)	FS / PS / MSC	i. harmonic compensation is better then all other configurations. ii. HDS - 3, thus reduces the hardware design complexity iii. reduce the line current ripple if the inverters have the same switching frequency	i. redundancy is possible in load sharing mode but may not be cost-effective. ii. higher rated power for APF2 is required for load sharing condition

CS – Controlling Scheme; HDS – Harmonic Detection Sensors

4.5.4 THD based cooperative control

The study in [128] shows that installation of an active or passive filter on a long-distance power distribution feeder may result in a certain phenomenon: voltage harmonics are mitigated at the point of installation, whereas they are magnified on other buses where no filter is connected and the phenomenon is termed as whack-a-mole. (The problem might be resolved at one location but re-appears elsewhere.) This voltage harmonic distortion can be damped by introducing an active filter at the end of a radial feeder [128, 130, 131]. The active filter detects voltage harmonics, V_h at the point of installation, and then injects a compensating current, I_F as follows:

$$I_F = G_F.V_h \tag{4.11}$$

where G_F is the control gain/conductance of the active filter. An automatic gain adjustment was also proposed in [131] to damp out harmonic propagation without considering the circuit parameters of the distribution feeder.

The purpose of cooperative control is to reduce the values of voltage THD over balancing the compensating currents. At first, THD controller is used to reduce the THD at the installation bus of one active filter to be lower than a specified value. Then the current controller generates equal compensating currents for the APFs. Thus the cooperative controller makes a significant contribution to reduce the required current rating of each active filter. Figure 4.14 shows a block diagram of cooperative control to reduce the voltage THD.
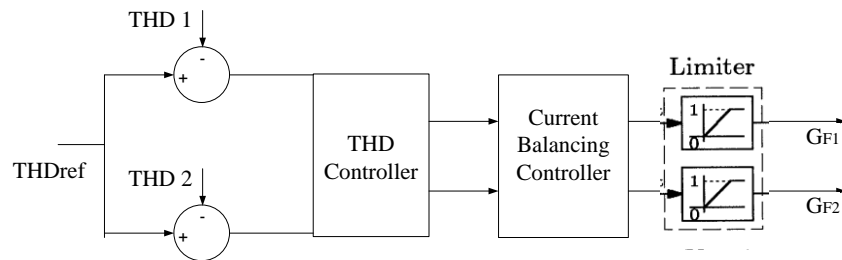
Fig 4.14 Block diagram of cooperative control

4.5.5 Droop control for APF

It is already mentioned that droop characteristics relate the output phase angle of the inverter with active power and the output phase voltage with reactive power flow. The function of the APF is to compensate harmonic load current. The APF can also be used to control voltage harmonics at the point of installation. Therefore, the droop control can be implemented for both purposes of the APF. The basics of these controls are briefly described below;

4.5.5.1 Voltage harmonics control

Using a high pass filter (HPF), V_h can be extracted from the supply voltage and then I_{Fref} is generated. The final voltage command, V_F is calculated as [132] and the PWM then generates the corresponding gating signals.

$$V_F = \frac{L_F}{\Delta T}(I_{Fref} - I_F) + V_s \tag{4.12}$$

where L_F is the interfacing inductor and ΔT is the sampling period of the controller. A droop relationship between the G_F and the VA consumption, Q_F of the APF can be derived as;

$$G_F = G_0 + n_F.(Q_F - Q_{F0}) \tag{4.13}$$

where G_0 is the rated conductance, n_F is the slope of the droop equation and Q_{F0} is the rated capacity of the APF. The value of n_F is determined by the VA rating of the APF to ensure the sharing of filtering workload in proportion with the capacity of the each APF. The droop relation between the G and Q is also depicted in Figure 4.15.
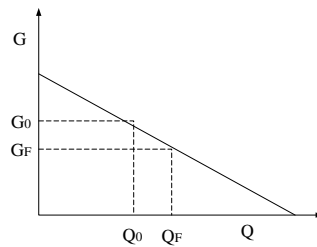
Fig 4.15 Droop characteristics between G – Q

4.5.5.2 Current harmonics control

To work as a harmonic current compensator, the APF current should deal with the node voltage, V_L or voltage at the point of installation. In that case, the injected compensating current will be,

$$I_F = G_F . V_L \tag{4.14}$$

The droop relation will be based on the conductance and non-fundamental power, Q_{hF} of the APF and this can be derived as [133];

$$G_F = G_0 + n_F . (Q_{hF} - Q_{hF0}) \tag{4.15}$$

where Q_{hF0} is the rated non-fundamental power of the APF. Non-fundamental power can be calculated as;

$$Q_{hF} = \sqrt{Q_F^2 - Q_{1F}^2} \tag{4.16}$$

$$Q_F = V_F . I_F \tag{4.17}$$

here, V_F is the output phase voltage of APF.

4.5.5.3 Droop control for multiple parallel APF

When multiple APFs with different ratings are used to compensate the reactive and harmonic components in a distributed environment then the control should be based on locally available information. In that case, the droop controller can be effectively used for harmonic voltage and current compensation which is similar to the adjustment of fundamental voltage amplitude and frequency. Here, the droop coefficient values have to be adjusted according to the following relationships [108, 134];

$$n_1 . Q_{10} = n_2 . Q_{20} .... = n_i . Q_{i0} \tag{4.18}$$

The relation between the VA of the APF and rated capacity can also be expressed as;

$$\frac{Q_1}{Q_{10}} \approx \frac{Q_i}{Q_{i0}} \tag{4.19}$$

Using the droop characteristic to share the current of a certain harmonic frequency has also been presented in [134]. The main advantages of droop control for multiple parallel APFs is that it can be used either when the APFs are in close position at the point of installation [128, 130, 131] or in distributed mode with no interconnection between each other [133].

APFs in a distributed mode can be termed as Distributed Active Filter System (DAFS). Figure 4.16 shows the DAFS system where multiple APFs are installed at different locations of the distribution line.
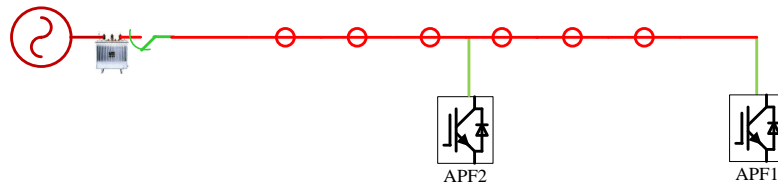
Fig 4.16 Distributed APFs System

The filtering capacity of the APFs is further improved by introducing a dynamic tuning method in the DAFS [131], Figure 4.17, where the voltage THD at the installation point of each APFs is used to dynamically adjust the VA capacity and the slope of droop characteristic. Here, the APFs can dynamically adjust their filtering capability in response to increasing or decreasing of nonlinear loads in the system to maintain the voltage distortion at the allowable level. A discrete frequency tuning active filter is also proposed in [132] to suppress power system harmonics effectively. Here, the active filter operates as a variable conductance for each individual harmonic frequency. Each harmonic conductance is dynamically adjusted according to the corresponding harmonic voltage distortion of the active filter at the installation point in response to an increase or decrease of nonlinear loads or variation of resonant frequency in the power system.
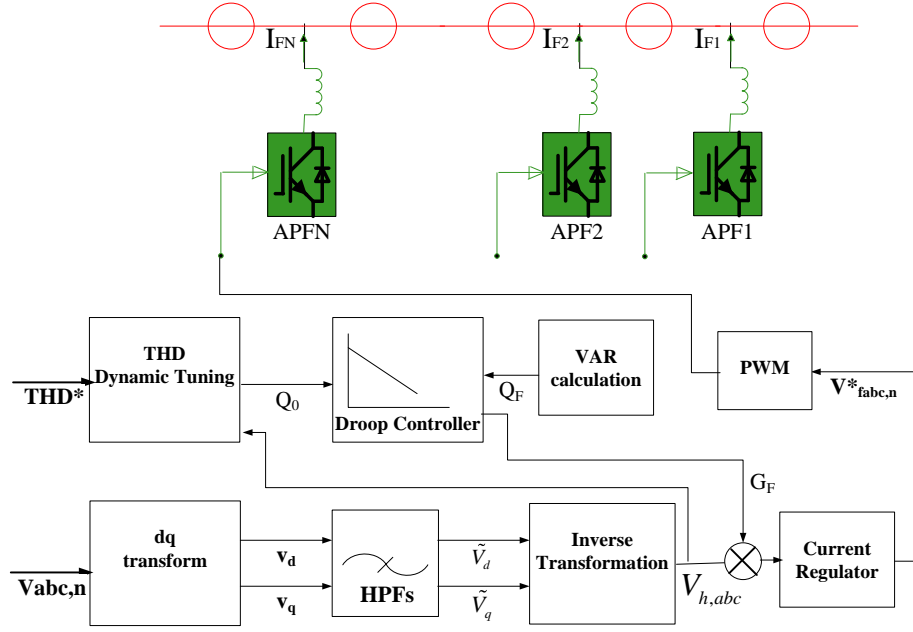
Fig 4.17 A Dynamic tuning of THD for DAFS.

4.6 **Conclusion**

In this section, the control strategies of parallel operation of DG inverters are initially described. Techniques for harmonic voltage and current compensation using APFs in parallel mode are also presented. From the inverter control strategies it is found that active load sharing control techniques have some limitations and control to overcome these problems is complicated due to the inter-communication between the inverters. Active load sharing techniques for parallel operation of a fixed number of inverters can be better due to their robust control but expansion of capacity due to the additional load may not be easy. On the other hand, droop control seems better for most purposes. Research indicates that most efforts are being put on droop control technique due to its capacity expansion flexibility, independent inverters, hot-swap facilities etc.

In the case of APFs in parallel operation, active harmonic load sharing techniques become more complicated due to the placement of harmonic current sensors or compensation topology. A comparative summary table has been given and it is found that a combination of feed-forward and feedback topology gives better results. For

multiple APF, these controller designs will be more difficult. Therefore, research efforts have concentrated more on the droop control method. Implementing the basic ideas of droop control for parallel inverter operation, placement and controlling of APF has been advanced to Distributed Active Filter Systems which is very much suitable for distributed generation integration on a network or off-grid operation.

Chapter 5

UPQC$_{\mu G}$ - A new proposal for integration of UPQC in DG connected Micro-grid or Micro-generation network

5.1 Introduction

As a part of the integration of the UPQC in a DG system, research to date has been carried out on two techniques; i) (DG-UPQC)$_{DC\text{-linked}}$ [73-78, 135-138] and ii) (DG-UPQC)$_{Separated}$ [79-81, 139, 140]. The advantages and disadvantages of these configurations are given details in [19]. The main disadvantages for both of the configurations are i) the control complexity for active power transfer, ii) inability to provide harmonic and reactive power compensation during the islanded mode and iii) difficulty in the capacity enhancement in multi-level or multi-module mode.

According to IEEE standard 1547-2003, interconnecting distributed resources with electric power systems (EPS), DG interconnection systems shall detect the unintentional islanding and cease to energize the islanded area within two seconds of the formation of an island [8]. One of the reasons is that the controller of the grid-tie DG inverter is designed to provide only the active power to the load and grid in the interconnected mode. For a seamless power transfer between the grid-connected operation and islanded mode, that is transfer between the current and voltage control modes of operation along with the robustness against the islanding detection and reconnection delays, research on hybrid control inverter is underway [141, 142]. Clearly this will further increase the control complexity of the inverter. However, the DG

inverter needs to be disconnected or to change its control strategy to work in the islanding mode after detecting the unintentional islanding.

To extend the operational flexibility of the DG inverter and to improve the power quality in grid connected DG based μGrid/μGen systems, a new hierarchical control method and integration technique of UPQC have been proposed here. The μGrid/μGen system (with or without storage), the load and shunt part of the UPQC (APF$_{sh}$) will be placed at or after the PCC. The series part of the UPQC (APF$_{se}$) will be placed before the PCC and in series with the grid. The UPQC current sensor, for reactive and harmonic power compensation, will measure only the load current. Islanding detection and reconnection techniques are introduced in the normal UPQC and hence is termed UPQCμ$_G$. Depending upon the control strategy and integration technique, the operation of UPQC$_{μG}$ can be of two types;

5.1.1 UPQCμ$_{G-I}$

- UPQC will compensate voltage interruptions in addition to voltage sags/swells, harmonic and reactive power compensation in the interconnected mode. Therefore, the DG inverter can still be connected to the system during the voltage sag/interrupt condition. Thus it will extend the operational flexibility of the DG inverter/μGrid/μGen system (hereafter referred as μG).

- The shunt part of the UPQC will also compensate the reactive and harmonic (QH) power of the load in islanded mode. Therefore, primary control will be based on the functionality of the series and shunt part of the UPQC.

- An islanding detection technique is introduced in the UPQC as a secondary control. Thus it will reduce the area of NDZ (non-detection zone) to be islanded. Therefore, the DG inverter will then be more flexible to be islanded. Otherwise, the DG inverter can remove the islanding detection technique from its control system.

- Both in the current and voltage control modes, the μG system will provide only the active power to the load. Therefore, it can reduce the control complexity of the inverter.

- Only the grid resynchronization/reconnection method will be part of the control of the μG.

5.1.2 UPQCμG-IR

- In addition to the previous method and technique, the reconnection method will also be part of the UPQC and hence the UPQCμG-IR will have to totally control the islanding operation and reconnection for a seamless operation of μG with a high quality power service.

- The system can even work in the presence of a phase jump or a phase difference (within limit) between the grid and μG.

For both cases, a communication between the UPQC and μG is required for secondary control. Fig 5.1 shows the integration technique of the proposed UPQC$_{\mu G}$.

The remainder of this Chapter has been organized as follows. The working principle/procedure of the proposed system is described in section 5.2. Based on the working principle, some of the design issues and rating selection have been discussed in section 5.3. Section 5.4 discusses the control method and technique in detail for all the elements of the UPQC$_{\mu G}$. The proposed control method and integration techniques have been verified by simulation using RT-LAB tools and simulation for UPQC$_{\mu G-I}$ is discussed in section 5.5 which is followed by simulation for UPQC$_{\mu G-IR}$ in section 5.6 . Section 5.7 shows real-time results by partial hardware test using real-time simulator in SIL (hardware synchronization) mode.

5.2 **Working Principle**

The integration method of the proposed UPQC$_{\mu G}$ to a DG connected micro-grid or micro-generation is presented in Fig 5.1. For both of the proposed systems, the DG system with or without storage can be connected in parallel to the grid, load and shunt APF part of the UPQC at or after the PCC. The series APF part of the UPQC will be placed before the PCC. Both the systems can work in interconnected and islanded modes. But as one can detect islanding only (UPQC$_{\mu G\text{-}I}$) and the other can detect islanding and reconnect also (UPQC$_{\mu G\text{-}IR}$), the working principle and control method have some differences. The working principle for both of the configurations is given below.

5.2.1 Interconnected mode

In this mode, as shown in Fig 5.2, the following will happen.

i. The DG source will deliver only the fundamental active power to the grid, storage and load.

ii. The shunt APF will compensate the reactive and harmonic (QH) power of the non-linear load to keep the THD at the PCC within the IEEE standard limit.

iii. Voltage sag/swell or interruption can be compensated by the active power from the grid through the series APF. Therefore, the DG converter will not sense any kind of voltage disturbance at the PCC and hence will remain connected during the voltage sag/swell condition.

iv. Islanding detection during the grid failure will be a part of the UPQC and hence the series APF will be deactivated and disconnected from the system, if islanding occurs.

The power transfer between the grid, UPQC$_{\mu G}$ and μG, during the interconnected mode, can be represented as;

$$P_{grid} + P_{DG} = (P + Q + H)_{load} + P_{loss} + P_{series} + P_{storage} \qquad (5.1)$$

$$(Q + H)_{shunt} = -(Q + H)_{load} \tag{5.2}$$

where *P, Q* and *H* represent active, reactive and harmonic power.
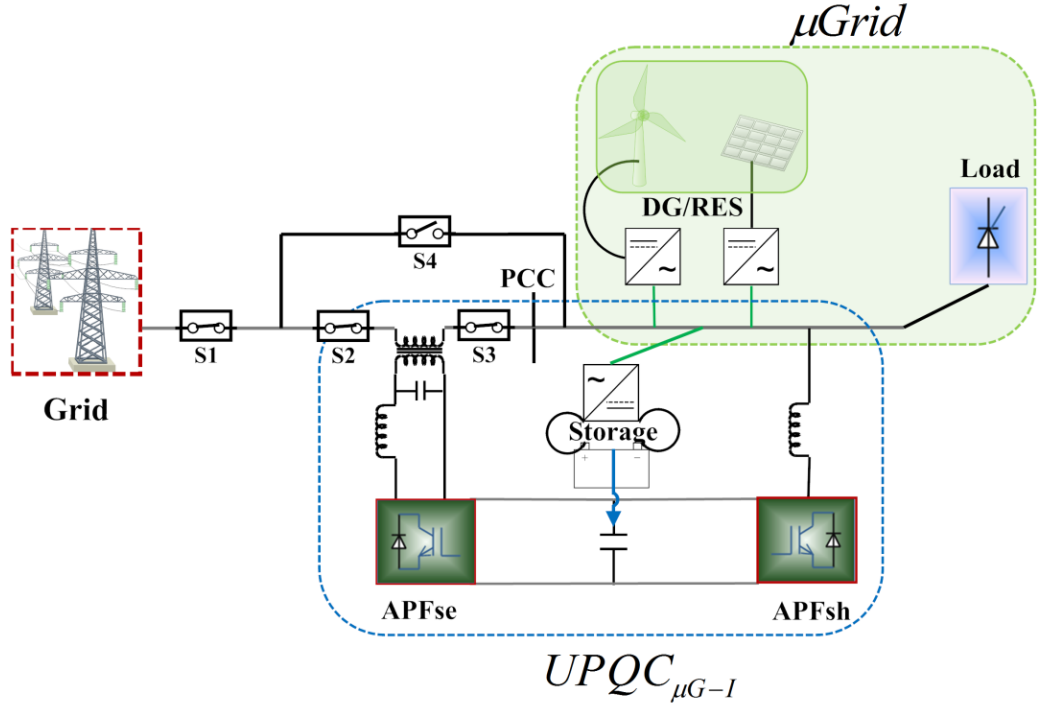
(a)
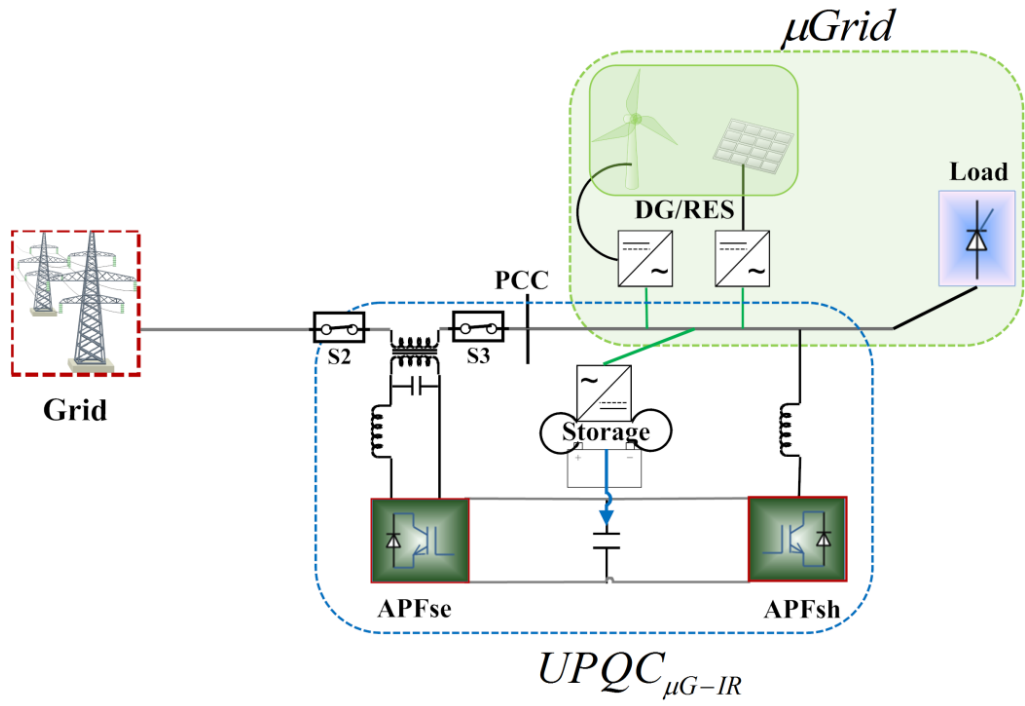
(b)

Fig 5.1 Integration technique of the proposed UPQC$_{\mu G}$
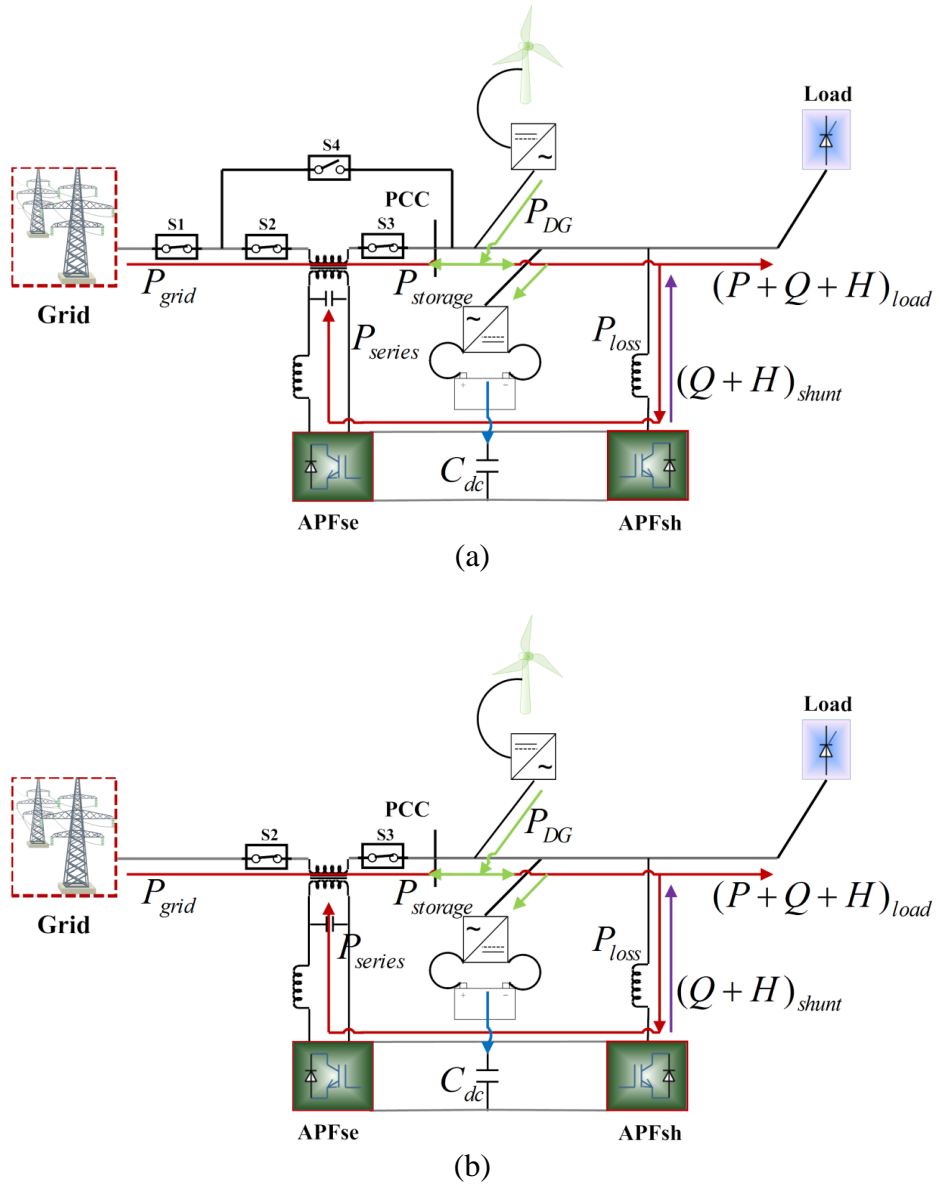
Fig 5.2 Working principle of (a) UPQCµG-I and (b) UPQCµG-IR in interconnected mode

5.2.2 Islanded mode

In this case, as shown in Fig 5.3, the following will occur.

i. The series APF will be disconnected during the grid failure and DG inverter will remain connected and maintain the required voltage at PCC.

ii. The shunt APF will still compensate the non-active power of the non-linear load to provide or maintain undistorted current at PCC for other linear loads (if any).

iii. Therefore, DG inverter (with storage) will deliver only the active power and hence does not need to be disconnected from the system.

iv. The series APF will be reconnected once the grid power is available.

The power transfer between the microgrid and UPQC$_{\mu G}$, during the islanded mode, can be represented as;

$$P_{DG} + P_{storage} = (P + Q + H)_{load} + P_{loss} \tag{5.3}$$

$$(Q + H)_{shunt} = -(Q + H)_{load} \tag{5.4}$$
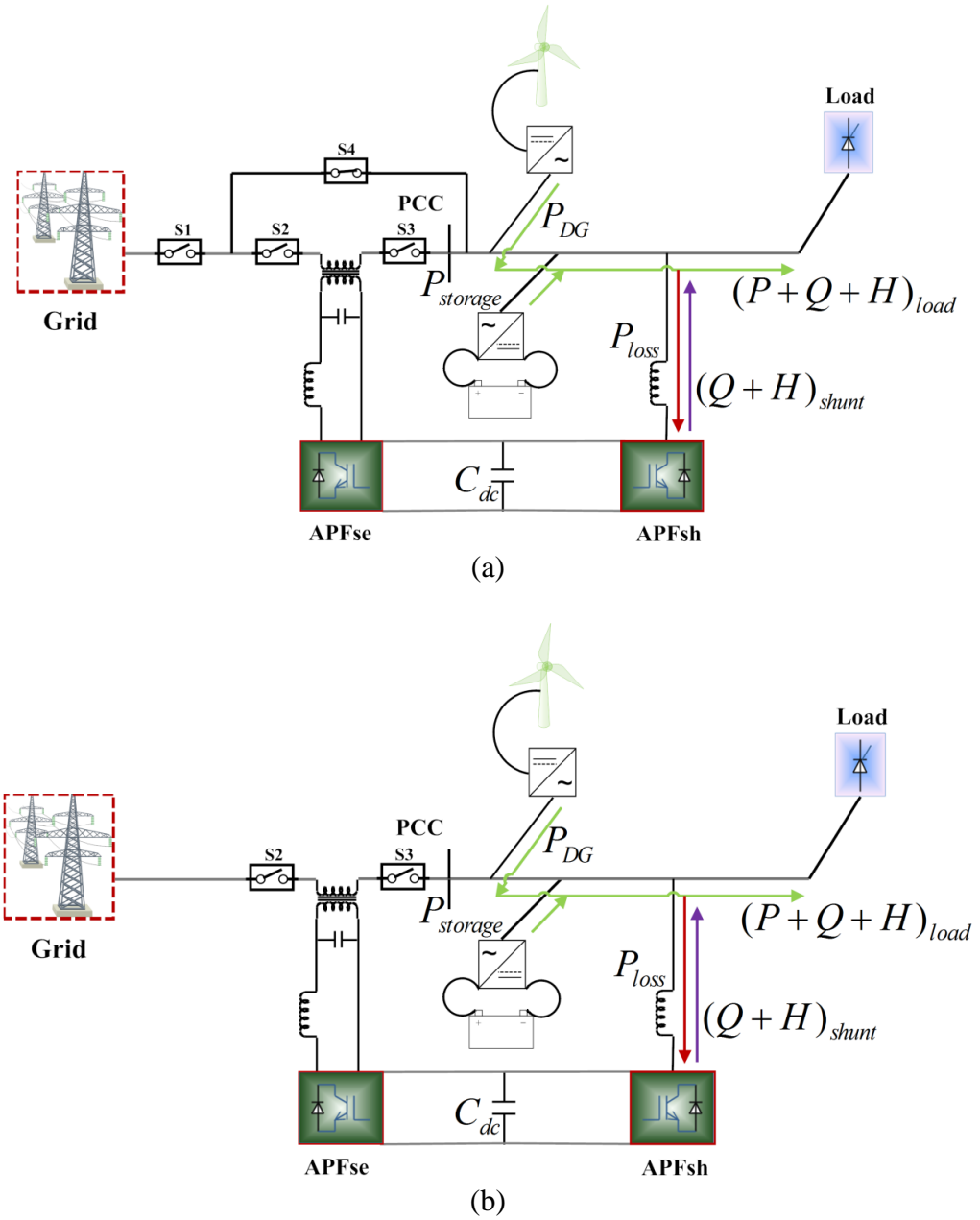
Fig 5.3 Working principle of (a) UPQCµG-I and (b) UPQCµG-IR in islanded mode

5.3 Design Issue and Rating Selection

From Fig 5.1, it is clear that the UPQC$_{\mu G-I}$ requires four switches whereas UPQC$_{\mu G-IR}$ needs only two. As the synchronization and reconnection control are part of the DG inverter, after synchronization the inverter is directly reconnected (through S4 and S1) to the grid and then sends an activation signal to UPQC$_{\mu G-I}$ to prepare for reconnection. After a suitable time, series APF of UPQC$_{\mu G-I}$ reconnects through S2 and S3 (by deactivated S4). Details of the switching mechanism is discussed in the control method section. Due to the full control of islanding detection and reconnection after a grid failure, UPQC$_{\mu G-IR}$ uses only two switches for its operation.

The fundamental frequency representation of the proposed system is shown in Fig 5.4 and the relations are derived in (5.5, 5.6). According to the functionality/working principle, both of the proposed UPQC$_{\mu G}$ should be able to work during interruption, compensate sag/swell up to a certain level and then islanded. The shunt APF will always have to compensate QH power of the load. Therefore, design and rating selection for the shunt and series APF and series transformer together with the sizing of DC link capacitor/storage system are very important. These are discussed below.
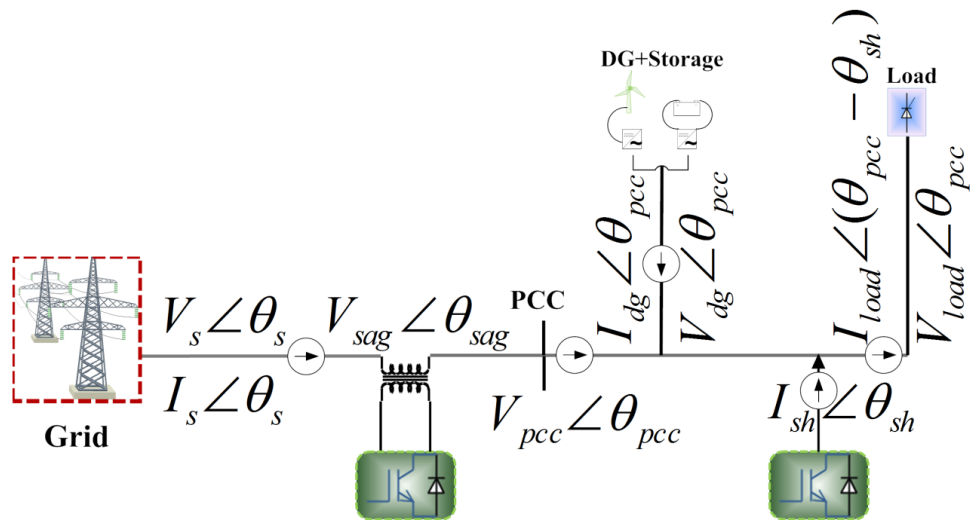
Fig 5.4 Fundamental frequency representation of proposed system

$$V_{pcc}\angle\theta_{pcc} = V_s\angle\theta_s + V_{sag}\angle\theta_{sag} \tag{5.5}$$

$$I_{load}\angle\theta_{load} = I_s\angle\theta_s + I_{dg}\angle\theta_{pcc} + I_{sh}\angle\theta_{sh} \tag{5.6}$$

For proper operation and under any condition, $V_{pcc} = V_{dg} = V_{load}$ and assuming $\theta_{pcc} = 0^0$, the phasor diagram of the proposed system is shown in Fig 5.5.
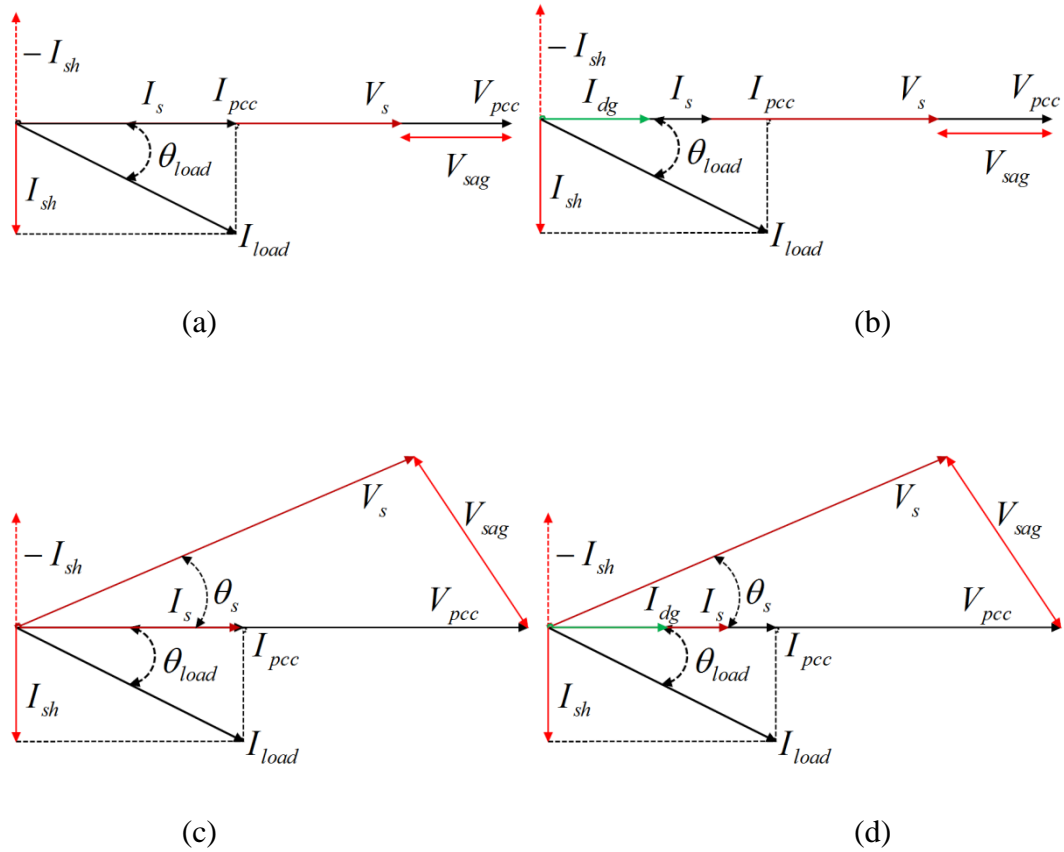
Fig 5.5 Simple phasor diagram of UPQCµG when (a) no DG and $\theta_s = \theta_{pcc}$ (b) with DG and $\theta_s = \theta_{pcc}$ (c) no DG and $\theta_s \neq \theta_{pcc}$ (d) with DG and $\theta_s \neq \theta_{pcc}$

5.3.1 Shunt APF (APF$_{sh}$)

It is shown in Fig 5.5 that for any condition shunt APF will compensate the reactive and harmonic power of the load by injecting I_{sh} in quadrature to the I_s. When a voltage sag appears in the supply side, series APF compensates the sag by injecting the required voltage to maintain the constant voltage and zero phase at PCC. To complete the task, series APF draws additional current from the source, I'_s in phase to the V_s. This

can further change the phase angle of the load, θ'_{load} which has an effect on I_{sh}, as shown in Fig 5.6. In this case,

$$I'_s = I'_{load} \cos(\theta'_{load}) \tag{5.7}$$

$$I'_{sh} = I'_{load} \sin(\theta'_{load}) \tag{5.8}$$

This ultimately increases the current at PCC and thus creates a VA loading impact on the shunt APF.
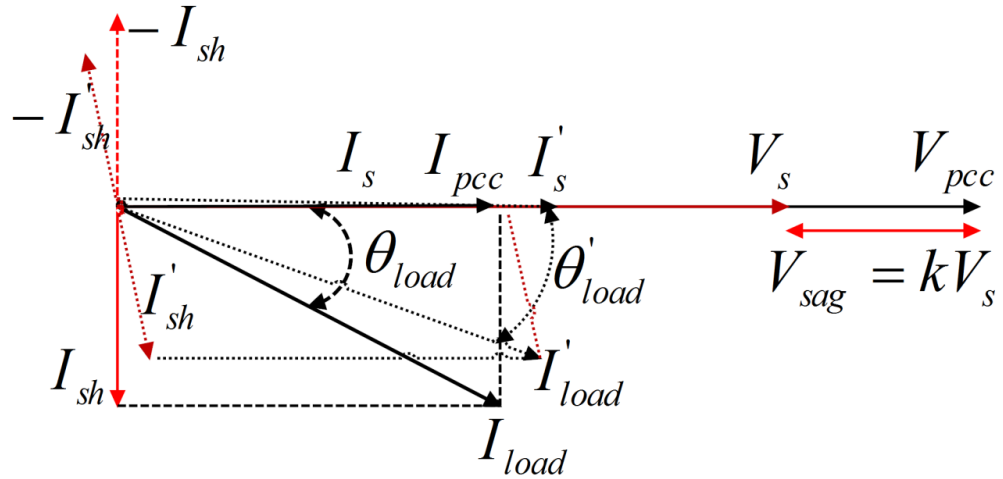
Fig 5.6 Phasor diagram of UPQC during in phase voltage sag compensation

5.3.2 Series APF (APFse)

The series APF always appears in series with the load. In the proposed integration technique when no energy is available from the DG unit and shunt the APF compensates the reactive and harmonic part of the load current, the active fundamental part of the load current flows through the series APF. Therefore, the APF must have at least the same current rating as the active load fundamental requirement,

$$I_{APFse,min} = I_{loadfp} \tag{5.9}$$

From Fig 5.5 (c and d), the general equation for voltage sag compensation by the series APF can be written as;

$$V_{sag} = \sqrt{V_s^2 + V_{pcc}^2 - 2V_s V_{pcc} \cos(\theta_s - \theta_{pcc})} \tag{5.10}$$

The voltage rating of the series APF should be equal to the highest value of the injected sag voltage, thus,

$$V_{APFse,rated} = V_{sag,max} = kV_{load,rated} \tag{5.11}$$

Assume k is the fraction of V_s that appears as a voltage sag, $V_{sag} = kV_s = kV_{load}$ and $k < 1$.

Therefore the VA rating of the series APF will be,

$$S_{APFse,rated} = I_{APFse,rated}V_{APFse,rated} = kP_{loadf,rated} \tag{5.12}$$

Fig 5.7 shows the phasor diagram for active power exchanges in the proposed system. From Fig 5.5 and 5.7, the active power transfer through the series APF can be calculated for the worse case when $P_{dg} = 0$;

$$P_{APFse} = S_{APFse}\cos(\theta_{APFse}) = P_{loadf}\left[\frac{kV_s}{V_{load}}\cos(\theta_s - \theta_{pcc} + \theta_{seAPF})\right] \tag{5.13}$$

Under stable and in-phase operating conditions, assume that $\theta_s = \theta_{pcc} = 0$, and then $\theta_{APFse} = 0$

$$P_{APFse} = \frac{kP_{loadf}V_s}{V_{load}} \tag{5.14}$$

(a)

(b)
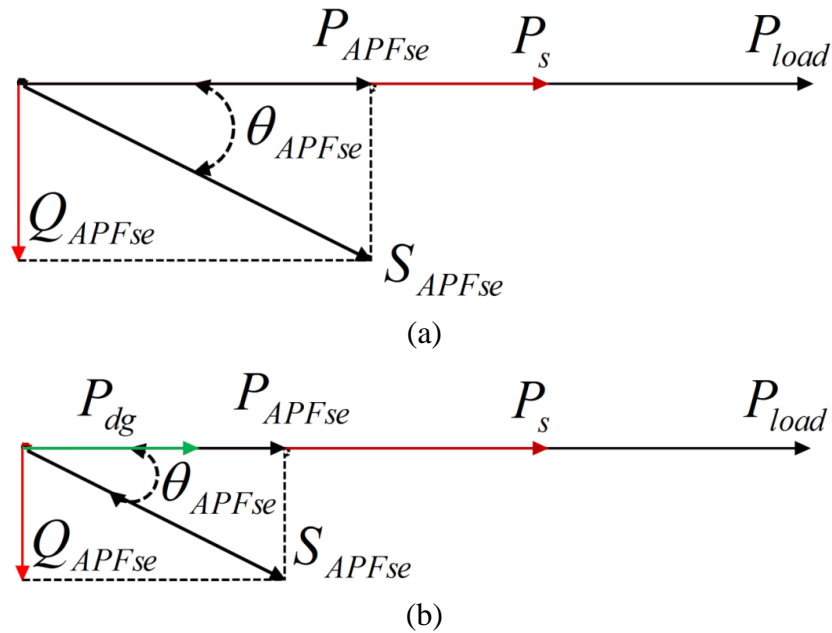
Fig 5.7 Phasor diagram for active power exchanges in the proposed system (a) in absence of DG source and (b) in presence of DG source and / or storage

Therefore, during voltage sag compensation, the required source current that will be transferred through the series transformer of the APF$_{se}$ (shown in Fig 5.6) can be calculated as,

$$I_s' = \frac{P_{loadf}}{(1-k)V_s} = \frac{I}{(1-k)} I_{loadfp} \tag{5.15}$$

Thus the size and VA rating of the series transformer depends on the amount of sag to be compensated. Fig 5.8 shows how the source current increases with the value of k.
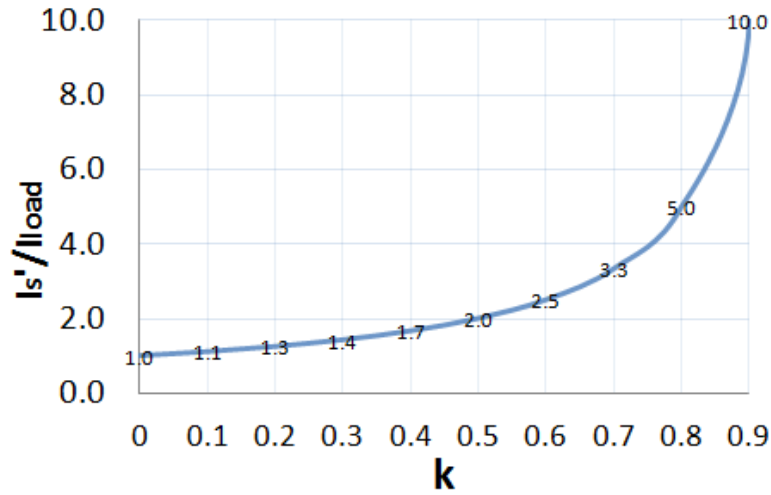
Fig 5.8 Relation between source current, load current and k for voltage sag compensation

Based on (10 - 15), and for a given value of k, there can be of multiple solutions for V_{sag}, I_s' and P_{APFse}. Control strategies are based on the minimization of the energy exchange during compensation, even to zero or by reducing the voltage rating [51, 61, 143 - 147].

The voltage rating of the series APF is an important design parameter, as it determines some other characteristics, such as compensating range, the need to include (and size of) energy storage devices, and the overall size of the series transformer. Again, losses tend to increase if the voltage rating of the series APF is increased. Therefore, the voltage injection capability should be chosen as low as necessary in order to reduce equipment cost and standby losses.

5.3.3 DC link capacitor

According to the working principle of the proposed UPQC$_{\mu G}$, the series APF should be able to work during ahigh sag/swell condition and even in the case of an interruption (depending on the interruption time) before it goes to islanding mode. At this stage, the DC link capacitor should be able i) to maintain the DC voltage with minimal ripple in the steady state, ii) to serve as an energy storage element to supply the reactive power of the load as a compensation and iii) to supply the real power difference between the load and source during the sag/swell or interruption period. Therefore, the size of the DC side capacitor should be selected, and the controller should be designed in such a way, that the series active filter can compensate the real power difference for a short period (typically a number of msec.) and by this time the controller should be able to adjust the reference current. Thus V_{dc} can be maintained at a reference value.

In general, the energy handling capacity determines the size of the capacitor. The basic equation can be written as;

$$C_{dc} = \frac{2.S.n.T}{V_{dcmax}^2 - V_{dcmin}^2} = \frac{2.S.n.T}{4.c.V_{dc}^2} \qquad (5.16)$$

where S is the power required to be i) compensated during the steady state condition, ii) supplied to the load during the transient condition and iii) compensated active power during voltage sag/swell condition, as explained in Chapter 2 (section 2.2.3). For a specific system, it is better to consider the higher value of C_{dc} so that it can handle all of the above conditions. It also helps to get a better transient response and lower the steady-state ripples. For the proposed system, the required capacitor size will be;

$$C_{dc} = \frac{2S_{load}.n.T}{4.c.V_{dc}^2} \qquad (5.17)$$

where S_{load} is the total P, Q and H power of the load.

It indicates that the size of the capacitor can be adjusted by the selection of interrupt cycles for which the series APF will compensate. One of the purposes of the proposed integration technique of the UPQC$_{\mu G}$ into the μG system is to maintain

smooth power supply during sag/swell or interruption and extend the flexibility of the DG inverter operation during the interconnected and islanded modes. For the supply continuity the DG storage system has also been introduced. Therefore a DC link connection between the capacitor and the DG storage has been proposed for the system. It will help to reduce the size of the capacitor and provide power during the sag/interrupt condition. Therefore, the source current will maintain the required load current active component and the additional current will be provided by the DG inverter or storage, as shown in Fig 5.7(b). Thus it will ultimately help to reduce the rating of the series APF converter.

5.4 **Controller Design**

The block diagram of the proposed UPQC$_{\mu G}$ Controller is shown in Fig 5.9. It has the same basic functionality as the UPQC controller except for the additional islanding detection and reconnection capabilities. It was already mentioned that a communication channel between the proposed UPQC$_{\mu G}$ and the μG is required for the detection of islanding and reconnection where islanding detection is a part of the UPQC. The detection and reconnection functions (for UPQC$_{\mu G\text{-}IR}$) are based on the sag/swell/interrupt/supply failure conditions. This task is performed in Level 2 (secondary control) of the hierarchical control [148]. Level 1 deals with the primary control of the series and shunt APF to perform their basic functions in the interconnected and the islanded mode. Also note that, the control strategy is the same for both of the proposed UPQC devices. The only difference is in the $S_{\mu G\text{-}R}$ signal generation. In UPQC$_{\mu G\text{-}I,}$ this signal is generated by the μG controller and then received by the UPQC to be acted upon. On the other hand, in the UPQC$_{\mu G\text{-}IR,}$ this signal is generated by the UPQC and is sent to the μG to be active/change its control strategy to operate in the interconnected mode. The overall control strategy is to improve the power

quality during interconnected and islanded modes. This involves detecting islanding and then ensuring that the DG inverter remains connected and supplying active power to the load. This reduces the control complexity of the inverter as well as the power failure possibility in the islanded mode. The five main elements of the proposed UPQC$_{\mu G}$ Controller are;

a. Positive Sequence Detection (PSD)

b. Series APF Control (APFseC)

c. Shunt APF Control (APFshC)

d. Islanding Detection (IsD)

e. Synchronization and Re-connection (SynRec)

The details of control structures are given in the following sections.
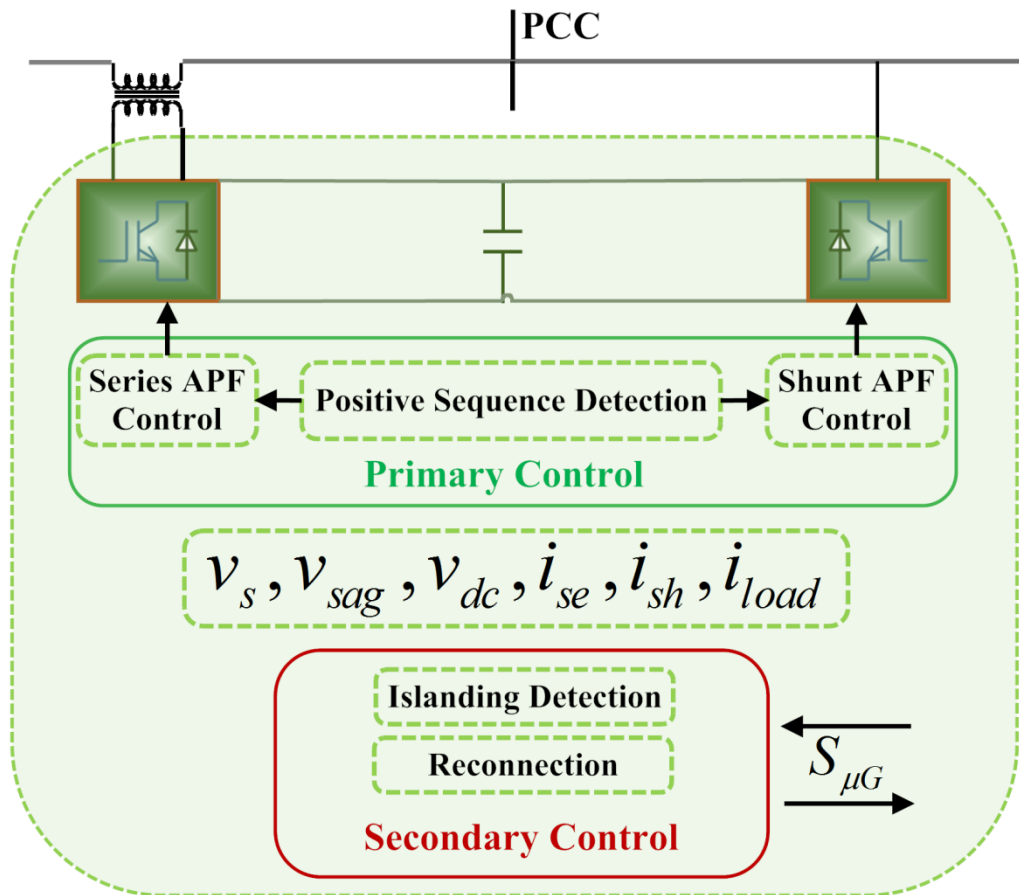
UPQCµG - Controller

(a)
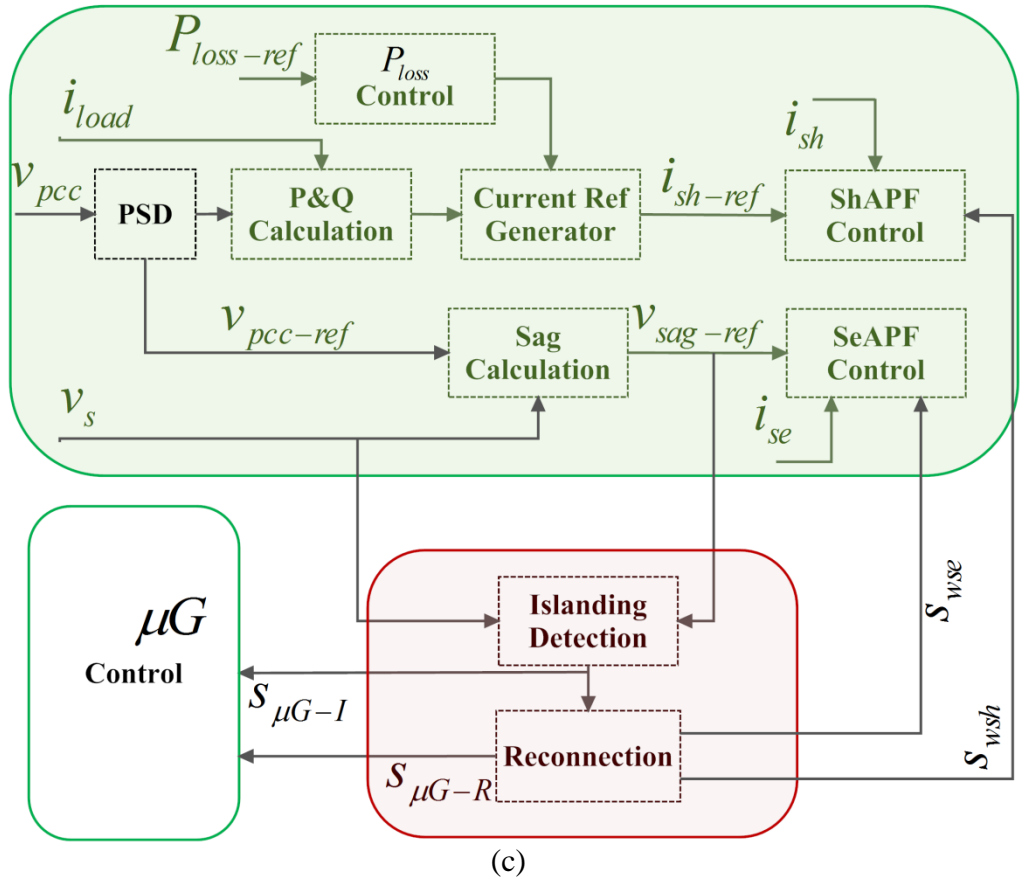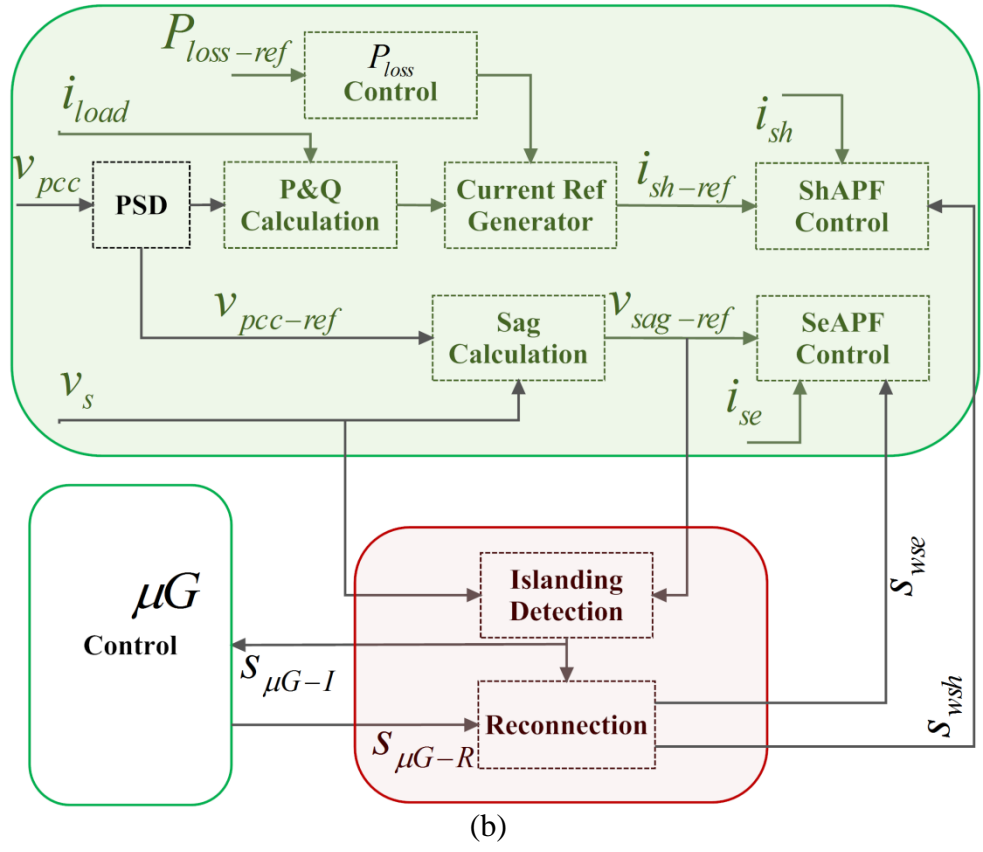
Fig 5.9 Block diagram of proposed UPQC$_{\mu G}$ a) Controller, b) UPQC$_{\mu G-I}$ - Control method and c) UPQC$_{\mu G-IR}$ - Control method

5.4.1 Positive Sequence Detection (PSD)

The positive-sequence detector determines instantaneously and accurately the amplitude, frequency and phase angle of the fundamental positive sequence component of the voltage at the measurment point. Fig 5.10 shows the basic block diagram of the positive sequence detection and reference voltage generation for the series part of the UPQC. Details of this method can be obtained from the Instantaneous Reactive Power Theory (IRP) [26]. The generated v_{s-ref} then determines the reference of sag/swell $v_{sag-ref}$ for compensation. This reference is also used to detect the islanding condition.
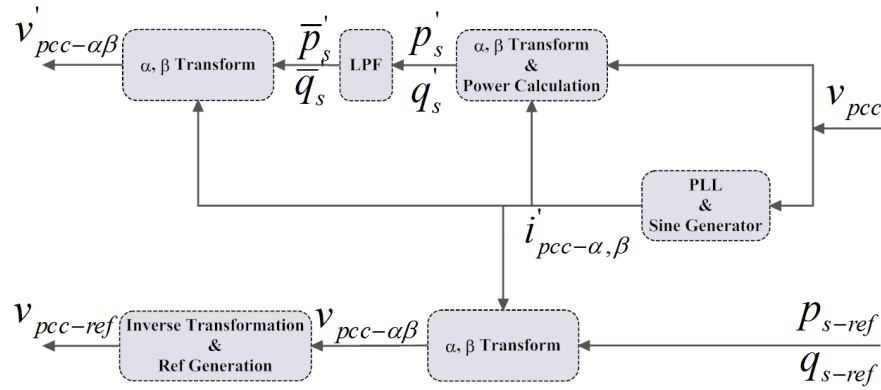
Fig 5.10 Positive Sequence detection and Reference source voltage generation

5.4.2 Series APF Control (APFseC)

The purpose of the series APF is to compensate unwanted voltage components at the PCC (i.e., everything apart from the fundamental positive sequence component). Therefore, the controller receives the generated positive sequence reference voltage from the PSD and then generates the required compensating voltage based on the block diagram shown in Fig 5.11.

5.4.3 Shunt APF Control (APFshC)

The shunt APF deals with the reactive and harmonic current of the load side and prevents these current components being injected into the grid or PCC so that the other loads do not sense any current related disturbance at the PCC. The basic block diagram

to generate the reference compensating current together with the compensator control is shown in Fig 5.12. Because of its simpler implementation, enhanced system stability, increased reliability and response speed, hysteresis control [24, 41] has been chosen here as a current controller. (A PWM based current controller can also be used.) The IRP theory [26], which is valid for both the steady-state and transient operation and is characterised by relatively simple computation, has been used to generate the reference current. Here P_{loss} has been considered as a power loss due to the overall system and VSI operation [75] which should be compensated to maintain the dc-link voltage during operation of the series inverter.

Fig 5.11 Generation of reference voltage for series VSI and Series APF control

Fig 5.12 Generation of reference current for shunt VSI and Shunt APF control

5.4.4 Islanding Detection (IsD)

In order to ensure the reliable and safe transfer of electrical energy to the grid and load during the interconnected mode, all DG systems should comply with a series of standard requirements given in the international regulations such as [149];

- IEEE 929-2000 : Recommended Practice for Utility Interface of PV systems

- IEEE 1547-2003 : Standard for Interconnecting Distributed Resources with Electric Power Systems

- IEC 61727 : Characteristics of Utility Interface

- VDE 0126-1-1 Safety

- IEC 61000 Electromagnetic Compatibility

- EN 50160 Public Distribution Voltage Quality

Particularly in low power DG systems, the anti-islanding detection is essential. It is clear that the DG inverter should detect the islanding and then cease to energize the area within 2 sec. For any other voltage disturbance at the PCC, the maximum trip time is also defined and is given in Table 5.1. In the case of a high power DG system, such as a wind farm, the requirement is different. In these cases the connection during a grid fault should be maintained. Considering the future trends towards the smart microgrid operation in connection with the distribution grid, the capability of (i) maintaining connection during grid fault condition, (ii) automatically detecting the islanded condition and (iii) reconnecting after the grid fault should be an important feature of the autonomous microgrid system. In that case, the placement of series APF in the proposed integration method of the system will play an important role by extending the operational flexibility of the DG inverter in the μG system. Several active and passive methods have been developed and studied to detect the islanding condition [142, 149 - 155]. In general, islanding is detected by measuring the voltage amplitude, phase and frequency of the source and comparing these with some standard values (Table 5.1). The accuracy of measurement and detection are improved by the development from simple the PLL (Phase locked loop) to SOGI-PLL (Second Order Generalized Integrator PLL) [149], DQ-PLL [156, 157], FLL (Frequency locked loop) [158], SOGI-FLL [159], DSOGI-FLL [160]. The reliability of these methods can be represented by

the proper selection of a non-detection zone (NDZ), as shown in Fig 5.13, which is defined by the power mismatch space at the PCC where the islanding is not detectable [149].
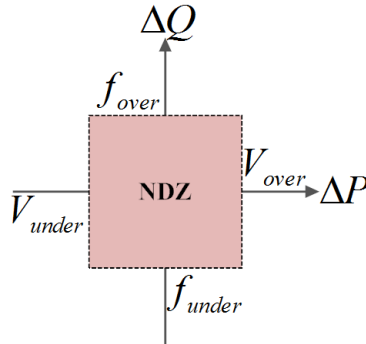
Fig 5.13 Non-detection Zone

However, in addition to the islanding detection, changing the controlling strategy from current to voltage control may result in serious voltage deviations and it becomes severe when the islanding detection is delayed in the case of hierarchical control [172]. Therefore seamless voltage transfer control between the grid-connected and isolated controlled modes is very important [142, 173]. Both indirect and direct current control techniques are proposed in [142, 172, 173 - 175] to mitigate the voltage transients in transition mode. These controllers increase the control complexity of the µG converters.

Table 5.1 DG response to abnormal utility conditions [6, 8]

Voltage at PCC	Clearing Time (sec)
V < 50%	0.16
50% < V < 88%	2.00
88% < V < 110%	Normal Operation
110% < V < 120%	1.00
120% < V	0.16
Frequency at PCC	
< 49.5 Hz	0.16
49.5 - 50.5 Hz	Normal Operation
> 50.5 Hz	0.16

In the case of power quality problems, the typical characteristics of electrical grid voltage phenomena is shown in Table 5.2. It is reported in [161] that more than 95% of

voltage sags can be compensated by injecting a voltage of up to 60% of the nominal voltage, with a maximum duration of 30 cycles. Therefore, based on the previous discussion on islanding detection requirement and sag/swell or other voltage disturbance compensation, an algorithm for the proposed UPQC$_{\mu G-I}$ can be developed to detect the grid fault or failure using the reference from the PSD signal. As the series APF takes the responsibility for compensating sag/swell/voltage unbalance / frequency disturbances (depending on the controller), islanding detection is quite flexible and simple for the proposed system.

Table 5.2 Typical characteristics of electrical grid voltage phenomena [IEEE 1159-1995]

Category	Typical Duration	Typical Voltage magnitude
Short Duration - sag / swell	0.5 - 30 cycles	0.1 - 0.9 pu / 1.1 - 1.8 pu
Interruption	3sec - 1 minute	< 0.1 pu
Long Duration - under / over voltage	> 1 minute	0.8 - 0.9 pu / 1.1 - 1.2 pu

Fig 5.14 shows the algorithm (with an example) that has been used to detect the islanding condition to operate the UPQC$_{\mu G-I}$ in the islanded mode. As the voltage at PCC is taken here as the reference and it is always in phase with the source and the DG converter (in UPQC$_{\mu G-I}$), the difference between the $V_{pcc-ref}$ (pu) and V_s (pu) is V_{error}. This error is then compared with the pre-set values (0.1 to 0.9) and a waiting period (n =1 to 50 cycle) is used to determine the sag/interrupt/islanding condition. In this example, (i) if V_{error} is less than or equal to 0.6, then 60% sag will be compensated for up to 50 cycles; (ii) if V_{error} is between 0.6 to 0.9, then compensation will be for 30 cycles; (iii) otherwise ($if\ V_{error} \geq 0.9$) it will be interrupt/black out for islanding after 1 cycle. The algorithm is simple and can be adjusted for any time length and V_{error} condition. Thus the flexibility of time for compensating the sag can be achieved before islanding. As the seamless voltage transfer from grid connected to isolated mode is one of the critical tasks in transition period, the transfer will be completed at the zero

crossing position of the APF$_{se}$. Therefore, no voltage fluctuation or abrupt conditions will occur. Development of this algorithm in MATLAB-Simulink is shown in Fig 5.15. The other advantage is that, this islanding detection and reconnection method have been carried out as a secondary control in Level 2, i.e. these can also be added in standard UPQC system as an additional block to convert it to UPQC$_{\mu G}$.
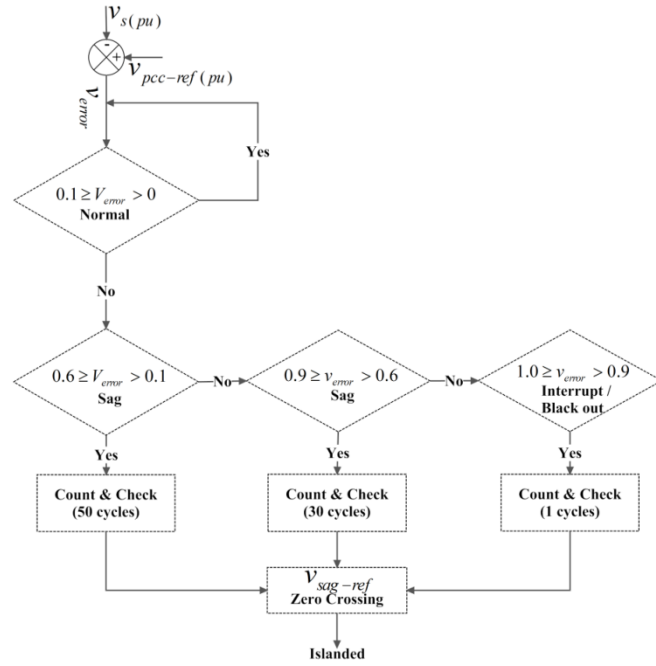

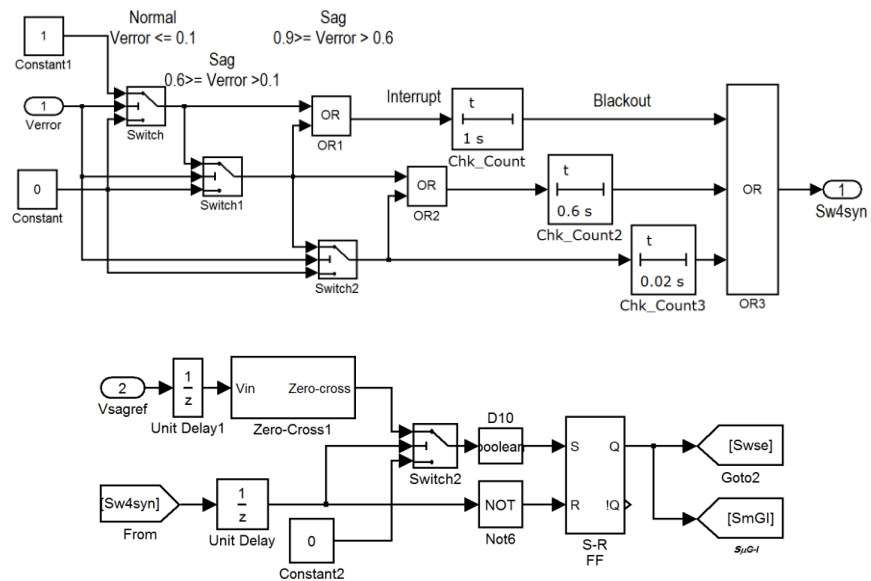Fig 5.14 Islanding detection algorithm

Fig 5.15 Development of Islanding detection method in simulink

5.4.5 Synchronization and Re-connection (SynRec)

When a problem (sag/interrupt) occurs at the main grid, the usual practice is that the μGrid/μGen should be disconnected and operated in an island mode, supplying the local demand either totally or partially. In that case, the DG Inverter needs to change its control strategy. Once the grid system is restored, the μGrid/μGen may be reconnected to the main grid and return to its pre-disturbance condition. Normally a re-closer is used as a protection device to disconnect the system against high current faults or absence of power in the grid system and reconnect when the grid becomes stable. The main problem occurs when the re-closer is closed after a delay. If both the utility grid and μGrid/μGen system are not synchronized, a high current flows, causing surges and power oscillation, which can trip the re-closer again. Some of the results due to this problem has been discussed and analyzed in [162 - 164]. This can be minimized by the coordinated operation between the two system (utility and μGrid/μGen).

A smooth connection can be achieved when the difference between the voltage magnitude, phase and frequency of the two buses are minimized or close to zero. It is also defined as parallelization of two synchronous systems. With some additional control, if a perfect parallelization is reached, no power flow will be observed at the re-closer immediately after its operation [164]. In an autonomous μG system, DG converter is generally synchronized with the grid voltage to avoid hard transients [165, 166]. Once the DG is synchronized with the grid, the DG inverter is connected back to the PCC. The parameter limits for synchronous reconnection are also given in Table 5.3. The seamless reconnection also depends on the accuracy and performance of the synchronization method. This method is started by simple PLL and improved to SRF-PLL [167], DDSRF-PLL [168], positive sequenced SRF-PLL [169], DPLL [170]. A serious requirement of these PLL schemes is to synchronize the system during phase jump conditions which can be overcome by SOGI-FLL [160], power PLL [171]. This

synchronization can also be done remotely [162]. This may require a major investment

to develop the communication system.

DG Rating (kVA)	Frequency Difference (Hz)	Voltage Difference (%)	Phase angle difference (deg)
0 - 500	0.3	10	20
> 500 - 1500	0.2	5	15
> 1500 - 10000	0.1	3	10

5.4.5.1 SynRec for UPQC$_{\mu G-I}$

In the case of the UPQC$_{\mu G-I}$, the synchronization for reconnection is done by the

DG converter. Once the voltage magnitude, phase angle and frequency differences are

within the pre-defined range or are close to zero, then reconnection is made through S4

and S1 as shown in Fig 5.3. The μG control system then sends a signal $S_{\mu G-R}$ to the

UPQC$_{\mu G}$. The Series APF is then activated and switches S2 and S3 are reconnected to

the system by deactivating S4. This switching transition is controlled and performed at

a zero crossing condition of V_s. As an example, Fig 5.16(a) shows a simple

synchronization method for reconnection and $S_{\mu G-R}$ is the signal generated by the DG

inverter. This signal is activated when the phase difference between the utility (V_s) and

PCC are within 2 deg in phase and corresponding voltage amplitude difference is within

11.24V. These are observed at a zero crossing of V_s. 5.16(b) shows the reconnection

method of series APF for the UPQC$_{\mu G-I}$. The activated $S_{\mu G-R}$ signal is taken from the μG

and passed through a S-R Flip Flop to generate the active signal (Swsesyn) for APF$_{se}$ at

the V_s zero crossing condition. This Swsesyn signal is then XOR to the Swse (as shown

in Fig 5.15) to generate the real activation signal for the APF$_{se}$.

(a)

(b)
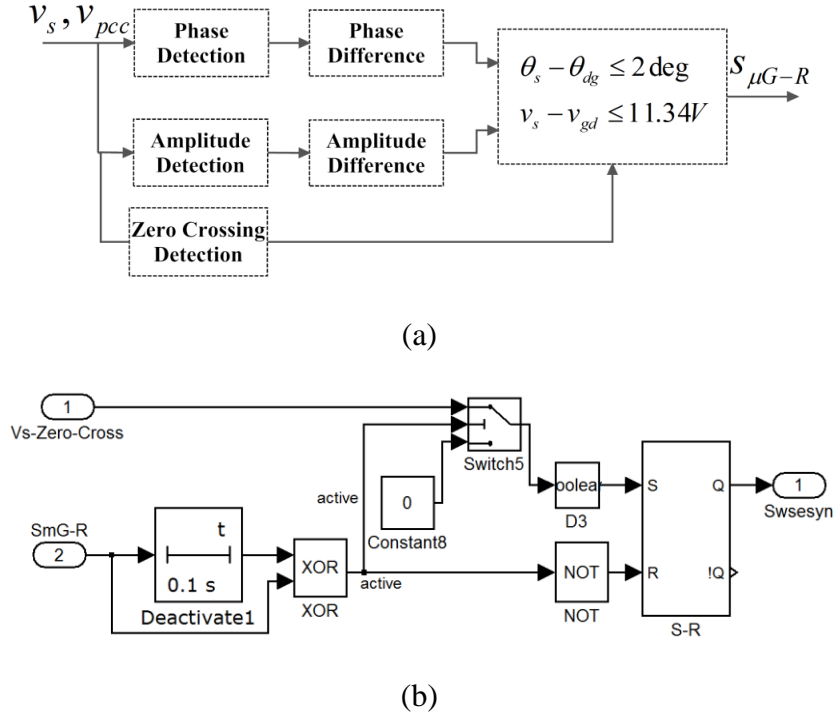
Fig 5.16 Synchronization method for reconnection and signal generation: (a) in DG inverter
(b) in UPQC$_{\mu G\text{-}I}$

5.4.5.2 SynRec for UPQCµG-IR

In case of UPQC$_{\mu G\text{-}IR}$, reconnection is performed by the the APF$_{se}$ of the UPQC. As the method of islanding detection and reconnection are within the control capability of the proposed UPQC$_{\mu G\text{-}IR}$, in this case switches S1 and S4 can be omitted. Moreover, due to the control of sag/swell by the APF$_{se}$, this UPQC$_{\mu G\text{-}IR}$ has the advantage of reconnection even in case of phase jump or phase difference (up to a certain limit) between the voltage of the utility and at the PCC. This obviously increases the operational flexibility of the proposed µG system with high power quality. The phase difference limit depends on the rating of the APF$_{se}$ and the level of $V_{sag\text{-}max}$ required for compensation. This limit can be calculated from Fig 5.5(c) and (5.10, 5.11). Assuming that the possible $V_{sag\text{-}max} = V_s = V_{pcc}$, the $\theta_{sag\text{-}max}$ can be found as;

$$\theta_{sag-max} = \cos\big[(\theta_s - \theta_{pcc})\big]^{-1} = {}^{1}\!/_{2} = 60^0 \tag{5.18}$$

Note that, in islanding detection algorithm, V_{error} is calculated from the per unit value of the voltage at the PCC and the source (as shown in Fig 5.14). And the $V_{sag-ref}$ is calculated from ($V_{pcc-ref}$ - V_s) as shown in Fig 5.11 and 5.12. Therefore, the reconnection is possible at this phase difference.

On the other hand, if $V_{sag-ref}$ is considered as the V_{error}, then according to the islanding detection algorithm, $V_{sag-max}$ will be allowed for up to 0.6 sec and then the system will be re-islanded after 50 cycles. Therefore, when there is a phase difference between the utility and PCC, the allowed $V_{sag-max}$ should not go beyond the sag compensation limit ($0.6V_s$). In that case, the $\theta_{sag-max}$ will have a limit and can be calculated from (5.10),

$$V_{sag} = 0.6V_s = V_s\sqrt{2(1 - cos\theta_{sag-limit})} \tag{5.19}$$

$$\theta_{sag-limit} = \cos\left[1 - \frac{0.36}{2}\right]^{-1} = 35^0 \tag{5.20}$$

The relation for the phase difference and magnitude between V_s, V_{pcc} and V_{sag} are also depicted in Fig 5.17. It also shows the zero-crossing point of the $V_{sag-ref}$ depending upon the phase. This zero-crossing detection also indicates the point at which the instantaneous voltage difference between the utility and the PCC becomes zero. Detection of this zero-crossing point and activation of the switches S2 and S3 at the same time are the key control of this reconnection method for a seamless transfer from the off-grid to the on-grid condition as well as changing the controller of the DG inverter from voltage to current control mode.

The reconnection method is shown in Fig 5.18. Conditions for reconnection are set as; (i) assuming the phase difference between the utility grid and DG unit should be within $\theta_{sag-max}$, (ii) the instantaneous value of the two bus voltages becomes equal and (iii) these should occur at the zero crossing condition. Once the utility grid supply is available after a blackout, a synchronization pulse (Sw4syn, as shown in Fig 5.15) is enabled to start synchronization. A simple logic sequence is then created, based on the

condition shown in Fig 5.18, to generate the active pulse for S2 and S3 to return the system in the interconnected mode. The development of the logical condition in MATLAB-Simulink is shown in Fig 5.19.

It is to be noted that, once the proposed $UPQC_{\mu G\text{-}IR}$ reconnects the system with phase/voltage difference between the grid and PCC, then the $UPQC_{\mu G\text{-}IR}$ has to supply the active power to maintain the gap which is not desirable.
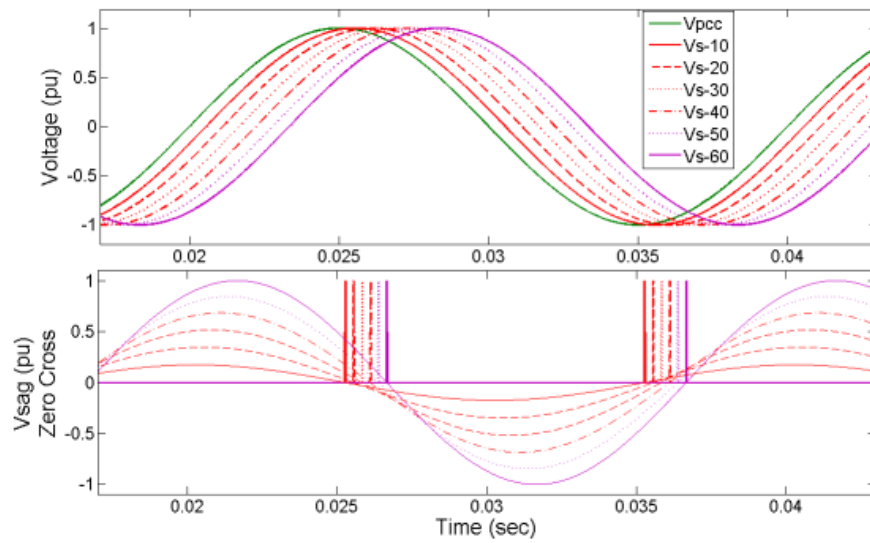
(a)
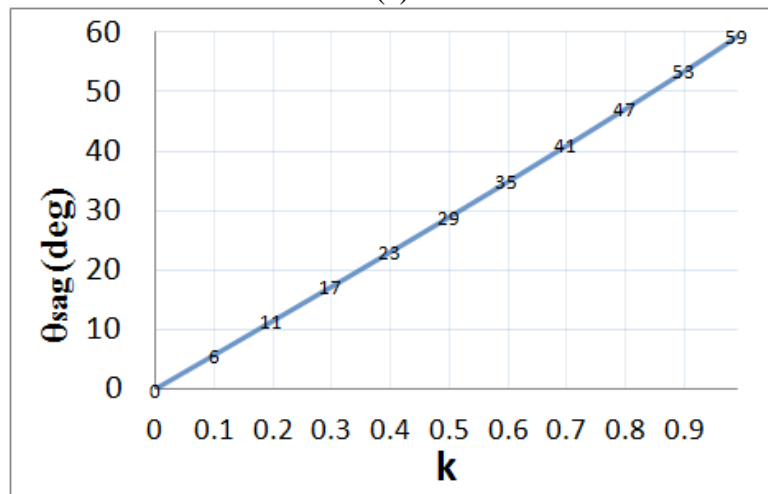
(b)

Fig 5.17 (a) Relation between V_s, V_{pcc} and V_{sag} and the point of zero-crossing; (b) relation between acceptable limit of $\theta_{sag\text{-}max}$ for possible voltage sag (k) during reconnection
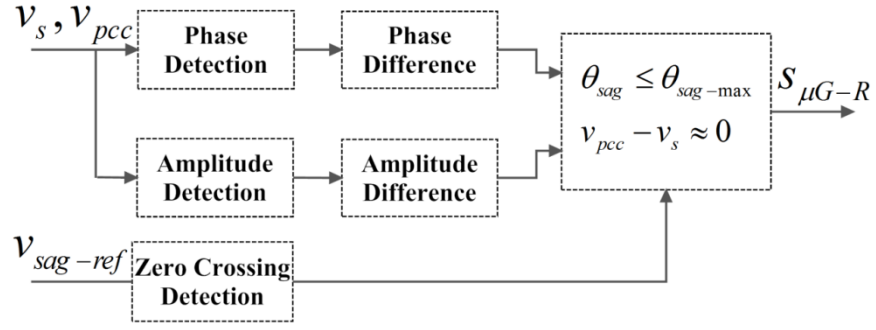
Fig 5.18 Logical condition for reconnection method
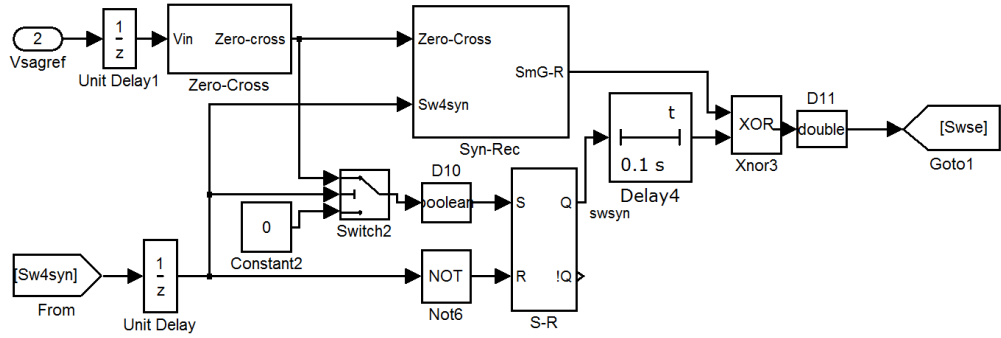
Fig 5.19 Development of reconnection method in MATLAB

5.5 Simulation Study - UPQC$_{\mu G-I}$

The power circuit of the proposed UPQC$_{\mu G-I}$ and the microgrid, as shown in Fig 5.1(b), have been developed in the MATLAB environment. The total system is modelled as a three-phase, three-wire system. Detailed simulation has been performed to analyze the operation of the proposed system. The circuit parameters that were used in the simulation are shown in Table 5.4.

The working principle of the proposed system is already described in the previous section. Fig 5.2 and 5.3 also explain the operational concept during interconnected and islanded modes. Details of the performance with the simulation results are given below. All the simulations have been performed for up to 2 sec. Table 5.5 also shows the timeline for the respective operating conditions.

Table 5.4 Overall network parameters for the simulation

Section	Parameter	Value / phase
Grid (3 phase)	Voltage (rms)	$230V_{L-N}$
	Line Frequency	50Hz
Load (µGrid)	Load current (max)	200A
	Harmonic Current (max)	100A
UPQC	DC link Voltage	600 V
	Series Inductance	0.15 mH
	Series Transformer	1:1
	Switching frequency	10 kHz
	Max Sag Compensation	100%
	Shunt Inductance	0.42 mH
	Hysteresis band	7.5 A
	Switching frequency	16 kHz
	Max Compensating Current	100 A

Table 5.5 Timeline of the Operating Conditions

The operating positions (0 for open and 1 for close) of the switches during the operation are very important in detecting the islanded, synchronization, reconnection and interconnected modes. These positions depend on the magnitude and time length of V_{error} (as shown in Fig 5.14 and 5.15) and the S_{w4syn} switch (as shown in Fig 5.15). Based on the algorithm for islanding detection and the reconnection method, Fig 5.20 shows the switch positions during the operation from 0 to 2 sec where both the interconnected and islanded modes are observed. Fig 5.21 shows the performance of the proposed UPQC$_{\mu G}$ for voltage sag compensation, as shown in Fig 5.21(a) and harmonic current compensation, as shown in Fig 5.21(b) along with the islanding detection, performance in islanded condition based on the Table 5.5 and Fig 5.20. Performance

during the reverse current flow due to the high penetration of DG is also shown by the red circle in Fig 5.21(b). Details of the synchronization condition and reconnection process are discussed in a later section. Performance of the proposed UPQC$_{\mu G}$ during interconnected and islanded mode has been discussed below. Generally waveforms are shown for phase A only.
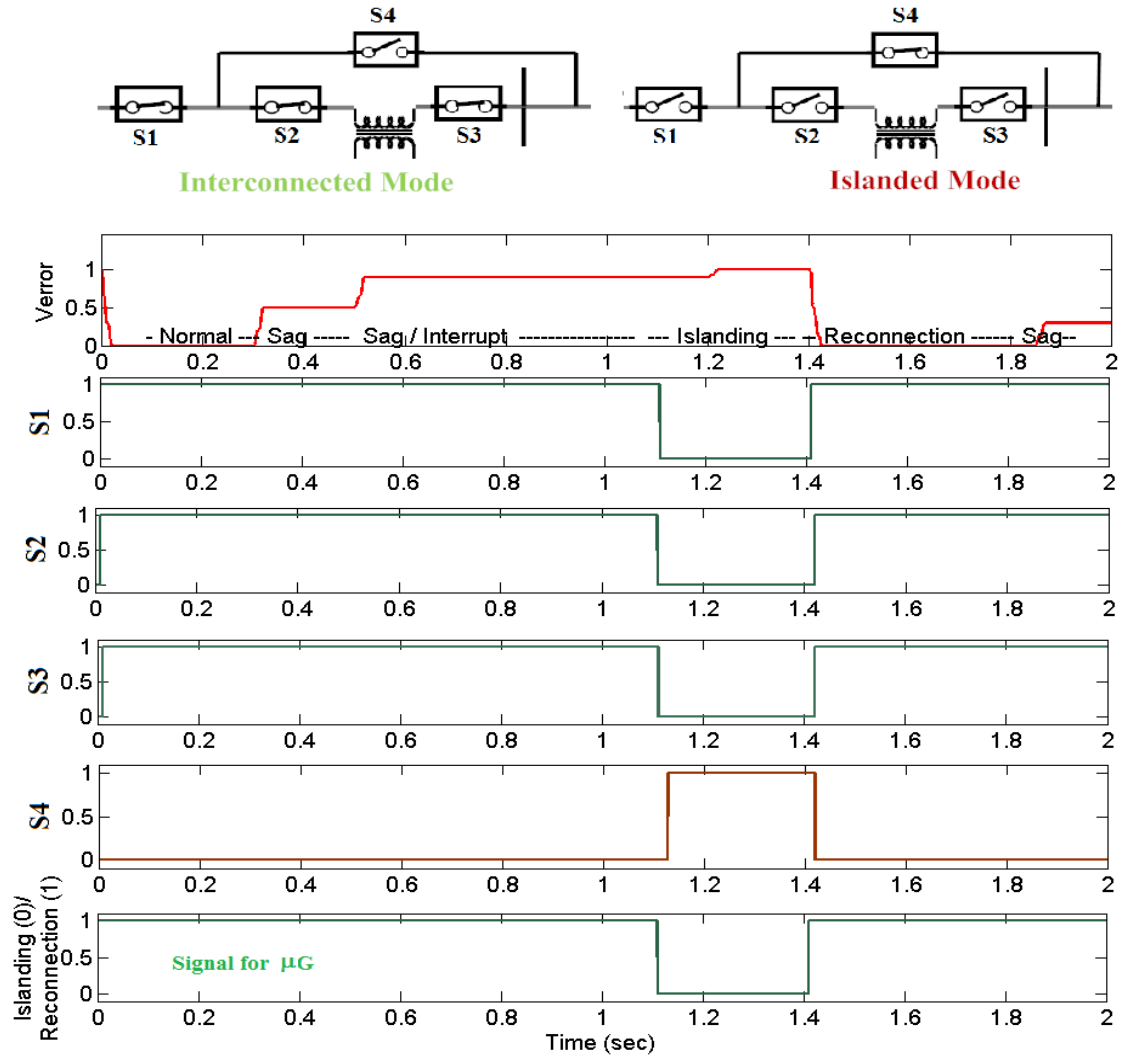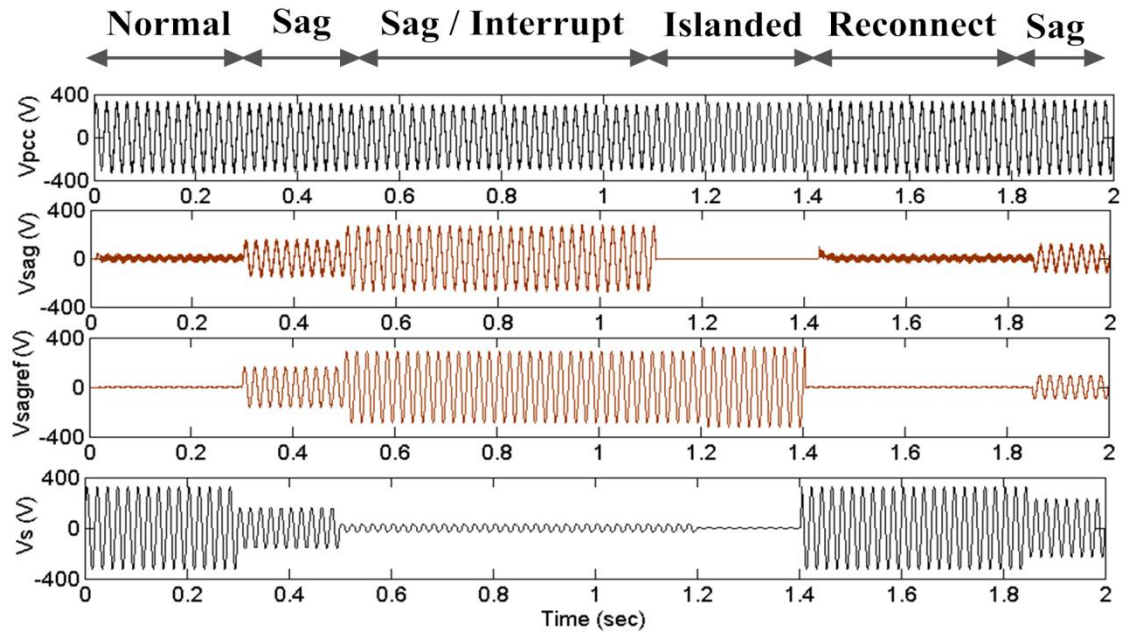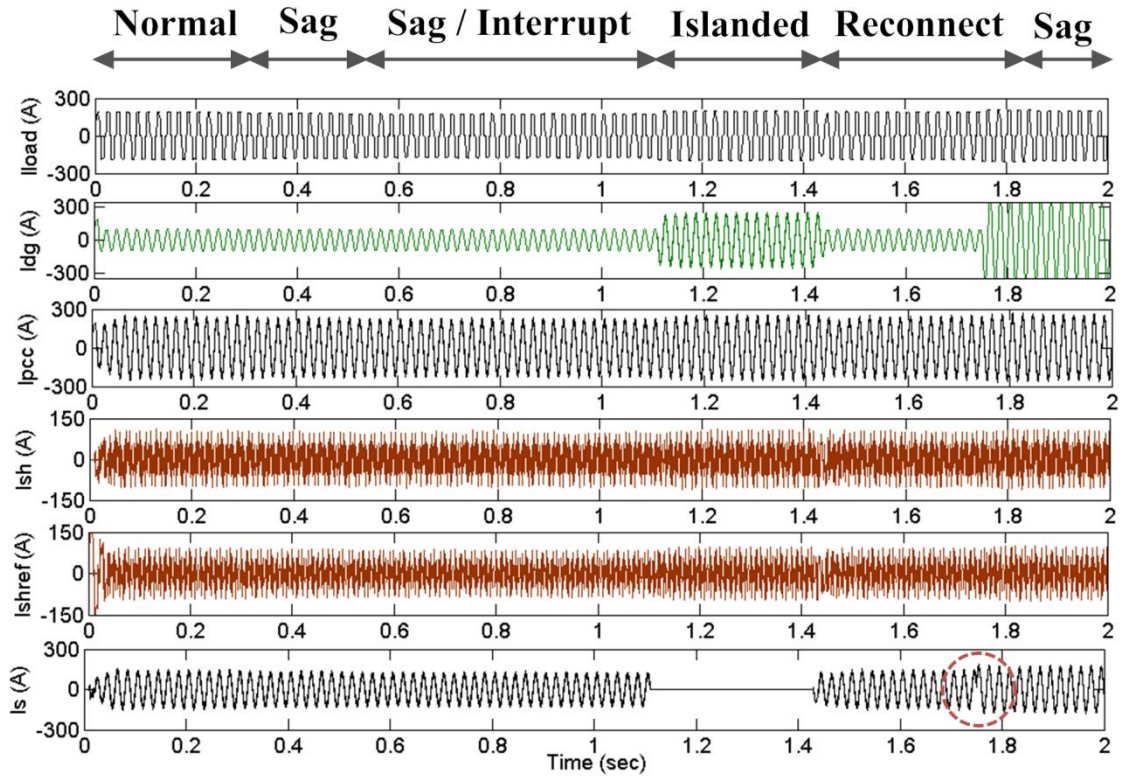

Fig 5.20 Switching positions during the operation from 0 to 2 sec.

(a)

(b)

Fig 5.21 Complete performance of UPQC$_{\mu G\text{-}I}$ during interconnected and islanded mode, (a) voltage waveform and (b) current waveforms at difference conditions and positions in the network.
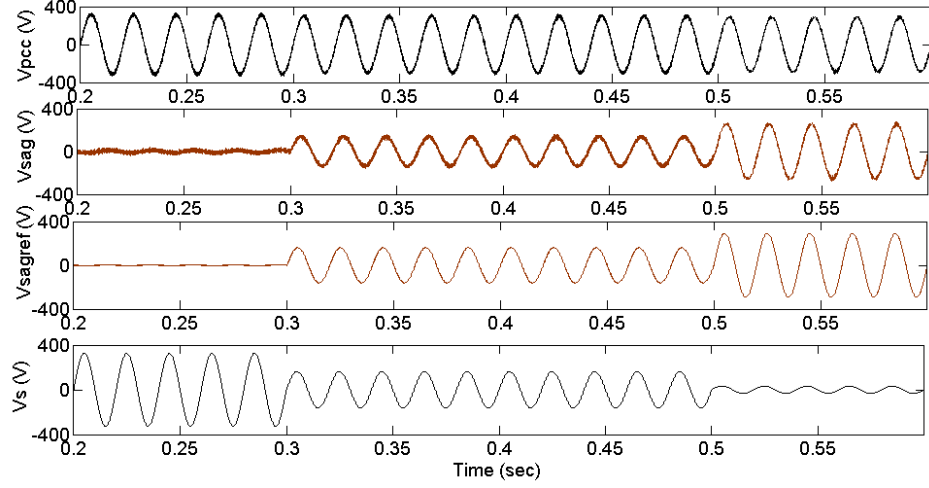
5.5.1 Interconnected Mode

Depending on the power availability, the DG source can supply power to the load and grid, and therefore by-directional power flow can occur. Hence, the performance of the proposed UPQC should be observed in both cases. For a better understanding, according to the direction of power flow, operation in the interconnected mode can be divided into two parts: (i) forward-flow mode and (ii) reverse-flow mode.

5.5.1.1 Forward-flow mode

In this case, the available DG power is less than the required load demand. Therefore, the utility grid supplies the rest of the power to the load which is not met by the DG supply. Depending on the microgrid energy management and control strategy, the DG storage system can be charged through utility and/or DG units. Fig 5.22 shows the initial condition from 0.2 to 0.6 sec of the simulation study where the voltage sag and interruption events occurs and are used to study the performance of the UPQC. Fig 5.22(a) shows the output waveforms of the voltage in different branches of the proposed system, whereas current waveforms are shown in Fig 5.22(b). A 50% sag is applied at 0.3 sec, 90% at 0.5 sec and then at 1.2 sec the utility is disconnected. In general, the APF_{se} can also compensate the voltage distortion, created by the utility, at the PCC. Therefore, this advantage can also be implemented in the series APF control part of the proposed system. Fig 5.22(a) shows the performance of the series APF part of the proposed UPQC in maintaining the constant and stable load voltage. Fig 5.22(b) shows the performance of the shunt APF part in compensating the reactive and harmonic current generated by the load. This compensation helps the UPQC system to maintain the grid current THD level within the IEEE limit. As is mentioned in the timeline table, the DG unit supplies $0.5I_{loadf}$ (half of load fundamental in current control mode) during this time frame. Therefore the remainder of the current is supplied by the utility grid and storage. During a 90% sag condition, the total power for the load demand is still met by

the µG system and the utility where the storage system provides the power for sag compensation through the DC link.

(a)
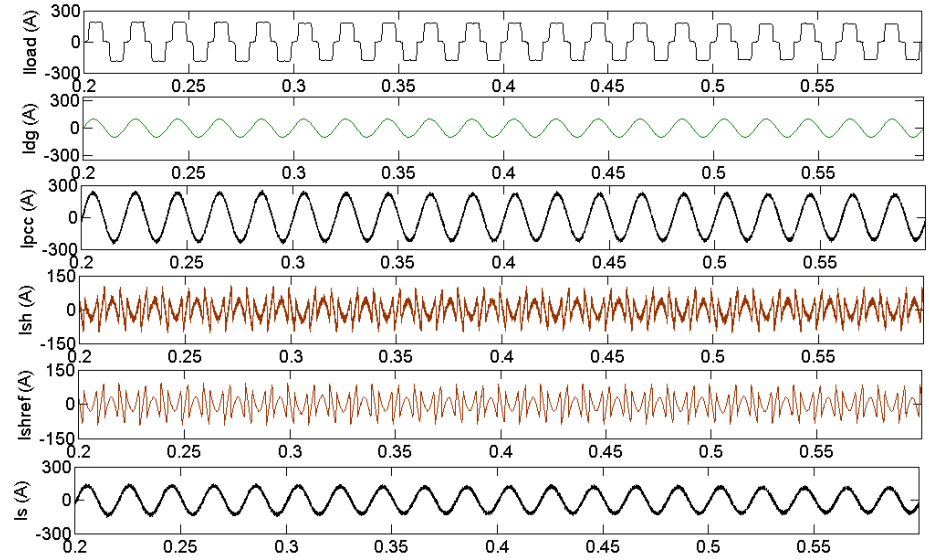
(b)

Fig 5.22 Performance of the proposed UPQC$_{\mu G}$; a) series APF and b) shunt APF; from 0.2 to 0.6 sec during interconnected and forward flow mode.

5.5.1.2 Reverse-flow mode

When the available DG power becomes higher than the required load demand, the extra energy is transferred to the grid and storage and this is termed the reverse-flow mode. At this stage, the grid current becomes out of phase with the grid voltage or the

voltage at the PCC. Fig 5.23 shows the performance of the UPQC when DG current becomes 1.5 times of the load fundamental at 1.75 sec and a 30% sag is also applied at 1.85 sec.
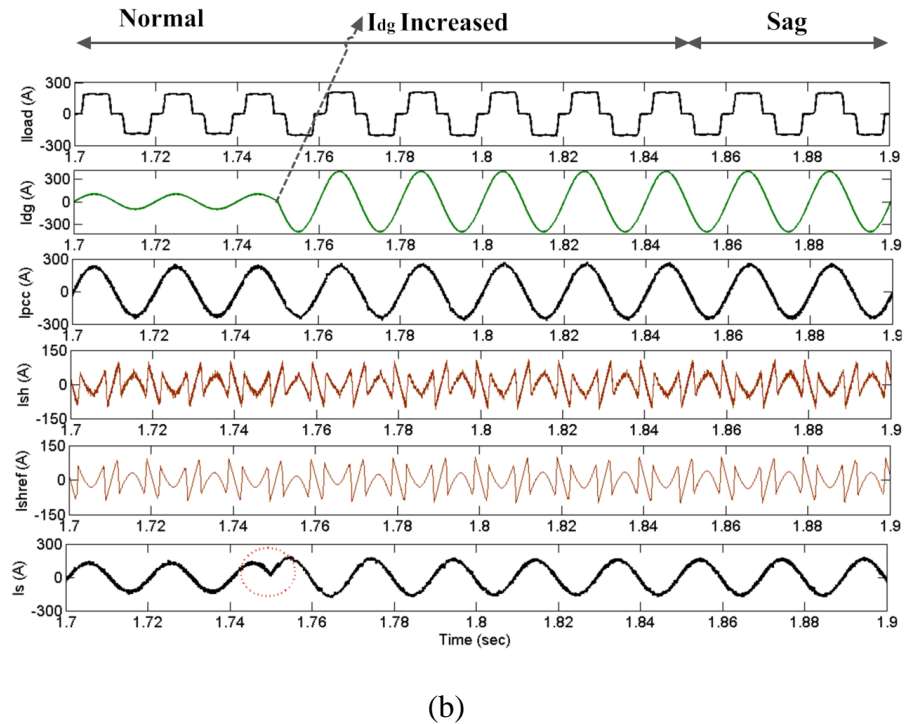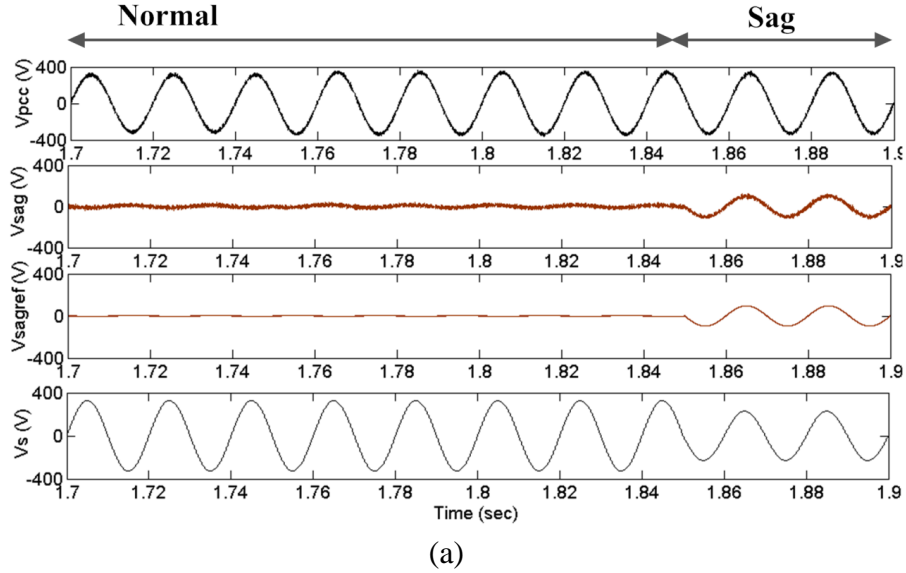

(a)

(b)

Fig 5.23 Performance of the proposed UPQC$_{μG}$; a) series APF and b) shunt APF; during interconnected and reverse flow mode.

In this case, the performance of the shunt APF remains the same even when the utility current becomes out of phase, as shown by the red circle in Fig 5.23(b). Fig

5.23(a) shows that the series APF performs voltage sag compensation during the reverse flow mode also.

5.5.2 Islanded Mode

It was mentioned earlier that a 90% sag compensation has been introduced at 0.5 sec of the simulation time period. According to the islanding detection method, the series APF compensates the sag for up to 0.6 sec (30 cycles) and then the system goes into islanded mode. A utility disconnection is applied at 1.11 sec just after completing the 30 cycle count and then detecting the zero crossing of $V_{sag\text{-}ref}$ where S1, S2 and S3 are opened. This is depicted in Fig 5.20 and 5.24. At disconnection, the system immediately operates in an isolated microgrid condition. At this stage, if the available DG power is lower than the load demand, the additional required power is supplied by the storage. If the DG power is higher than the load, then the additional power goes to the storage. The shunt APF still performs the compensation of reactive and harmonic power. Therefore, DG converter does not need to be disconnected or change the control strategy (supplying only the fundamental active power) to supply power to the load.

Fig 5.24 shows the performance of the proposed UPQC during 1.0 to 1.2 sec where the islanding is detected just immediately after 1.1 sec at zero crossing detection. The islanding mode is observed between 1.11 and 1.405 sec. During this period the APF_{se} is disconnected, as shown in Fig 5. 24(b) where $V_{sag} = 0$, utility current become zero, as shown in Fig 5.24(c). The APF_{sh} continues to operate, as shown in Fig 24(c), and the load demand is met by the DG with the storage unit.
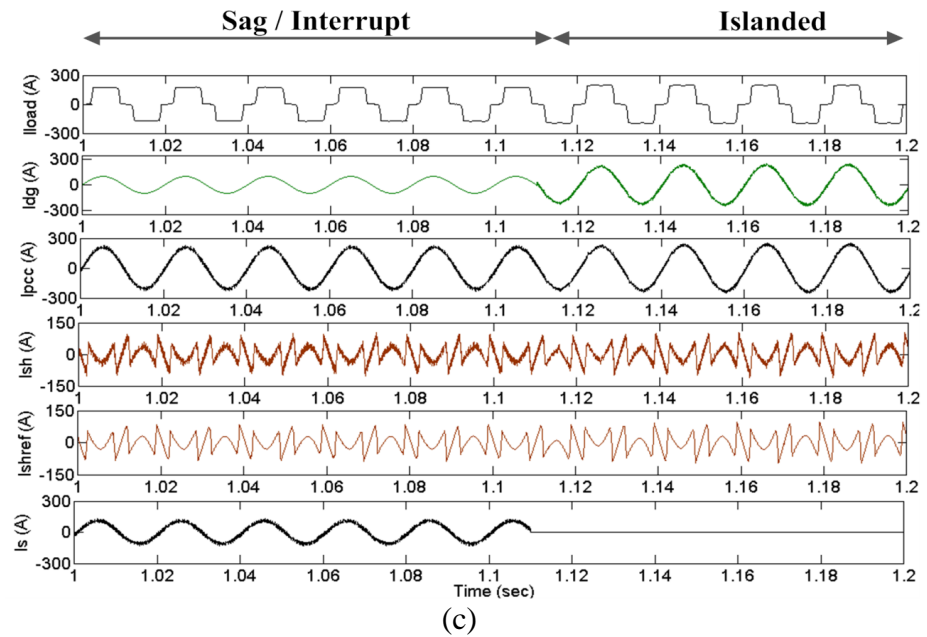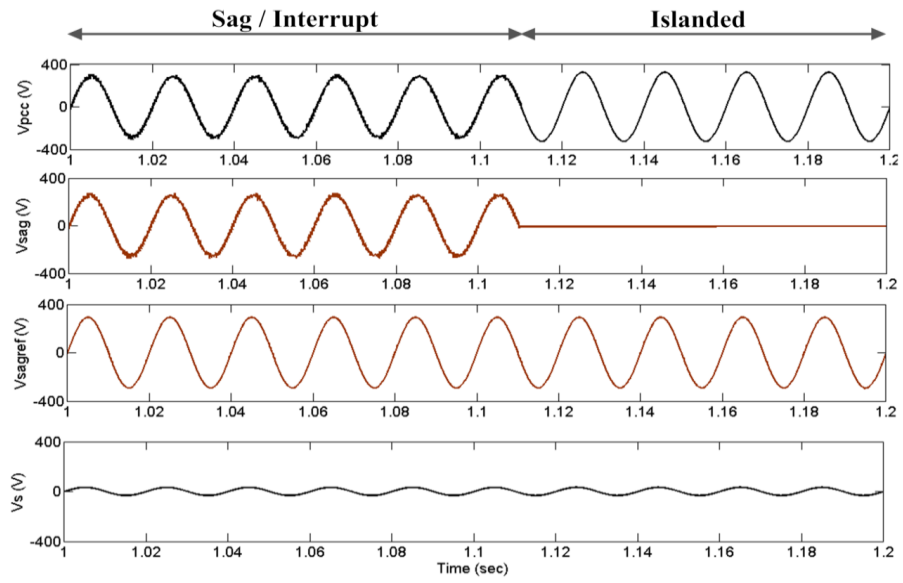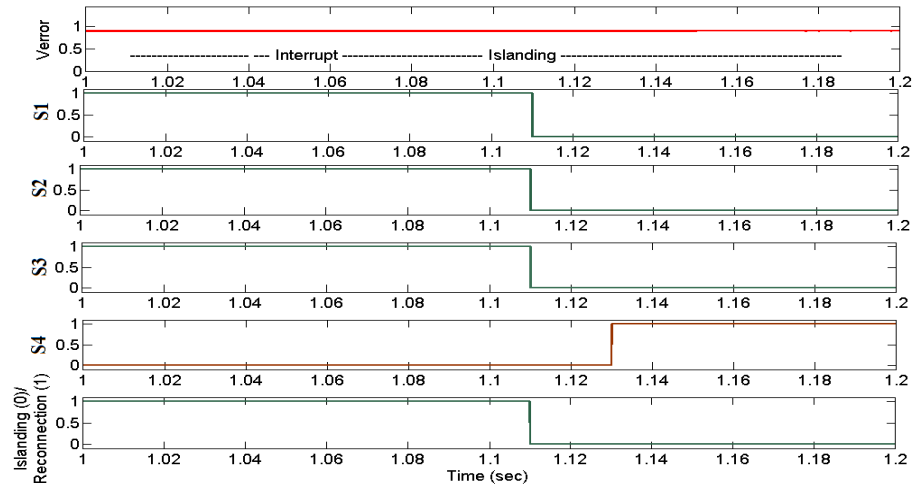
Fig 5.24 Performance of the proposed UPQC$_{\mu G}$; (a) switching condition; b) series APF; c) shunt APF during islanded mode.

5.5.3 Reconnection

One of the most important parts of the proposed UPQC$_{\mu G}$ is the reconnection process. This has to occur without disconnecting the DG units or changing its control strategy during isolated or grid connected μGrid/μGen operating conditions. Fig 5.25 shows the different signals for the reconnection process based on the algorithm and developed method showed in Fig 5.18 and 5.19. To check the performance of the reconnection process for the worst condition, the utility grid (V_s) is powered on at 1.405 sec where the magnitude is at a maximum, as shown by the red circle in Fig 5.26(a). Immediately, the S_{w4syn} pulse is activated and the reconnection algorithm starts generating active pulses as the phase and amplitude differences start to be within the required limits. Zero crossing detection is also shown. The DG unit sends a reconnection signal to the UPQC unit. Based on the logic given in Fig 5.19, the actual switch S1 is activated at 1.43 sec and the V_{sag} starts operation, as shown by the red circle in Fig 5.26(a). S2 and S3 are activated after the synchronization by the DG unit. S4 is disconnected simultaneously at 1.44 sec. This simple algorithm with a combined logic gate ensures the utility connects with the μGrid smoothly after the utility system is restored.

Fig 5.26(a) shows that the series APF unit is immediately reactivated when the grid voltage is available at 1.405 sec but it starts operation when the S2 and S3 switches are closed at 1.43 sec. It is expected that, according to the smooth reclosing condition, no power flow will occur at the point of reclosing. The switching is carried out successfully within the limiting condition as shown in Fig 5.26(b). The circle at 1.43 sec for I_{dg} and I_s in Fig 5.26(b) indicates the smooth transition from islanded to interconnected mode. DG inverter also changes its control from voltage to current control mode but only transfers the active fundamental current. The performance of the APF$_{sh}$ is also uninterrupted during the transition period.
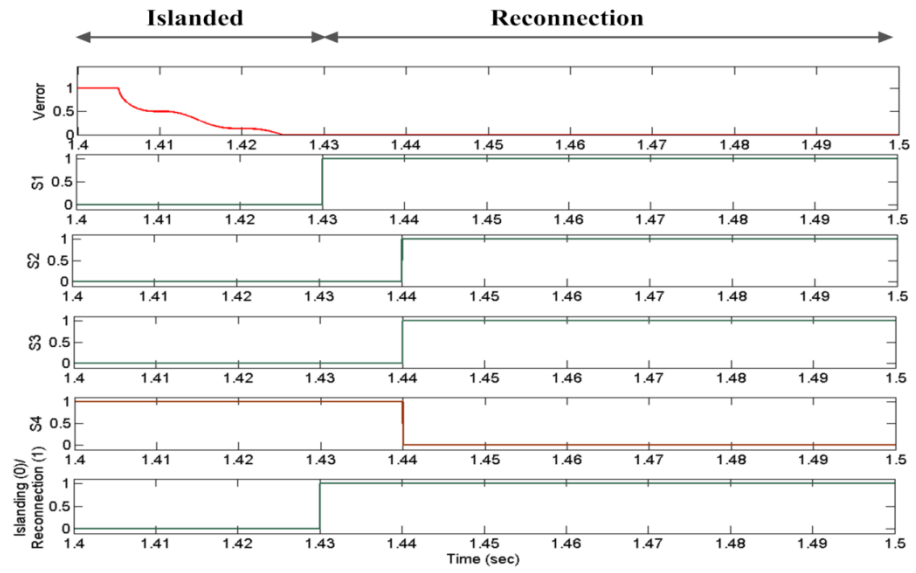
Fig 5.25 Condition of different signals for reconnection process based on Fig 5.19.
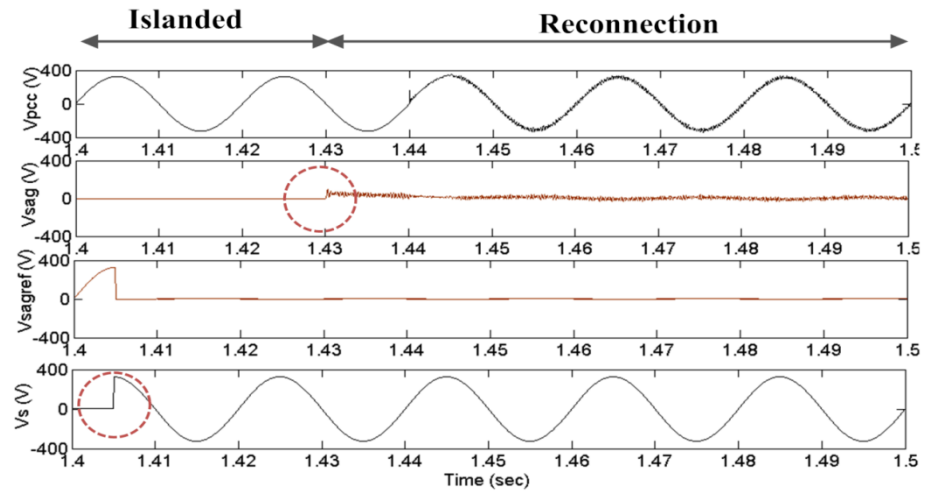
(a)
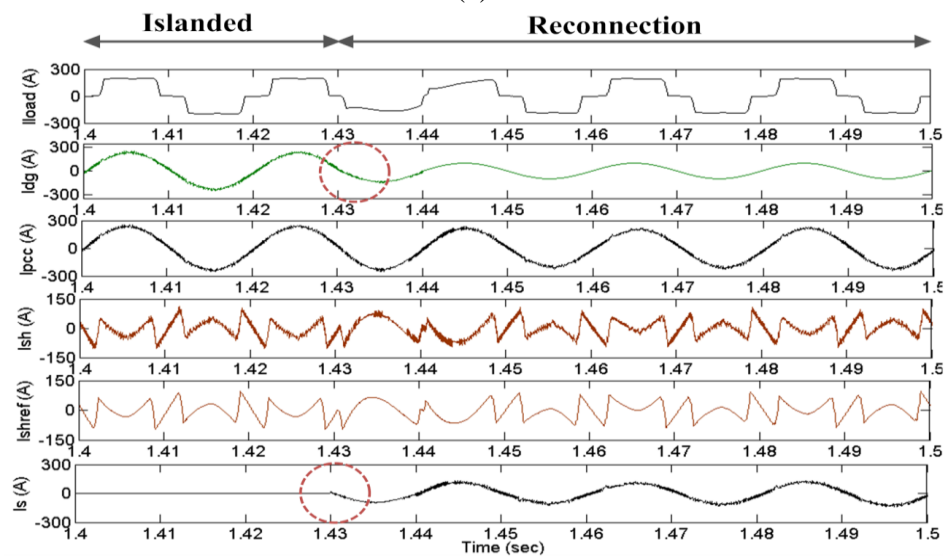
(b)

Fig 5.26 Performance of the proposed UPQC during reconnection, (a) series APF, (b) shunt APF

147

5.5.4 Power Flow

The power flow diagram is shown in Fig 5.27 for the complete simulation time where the green line represent the active power (P) and red line (dash) for reactive and harmonic power (QH). This also validates the operation and performance of the APF_{se} and APF_{sh} part of the proposed $UPQC_{\mu G\text{-}I}$ along with the islanding detection and reconnection.
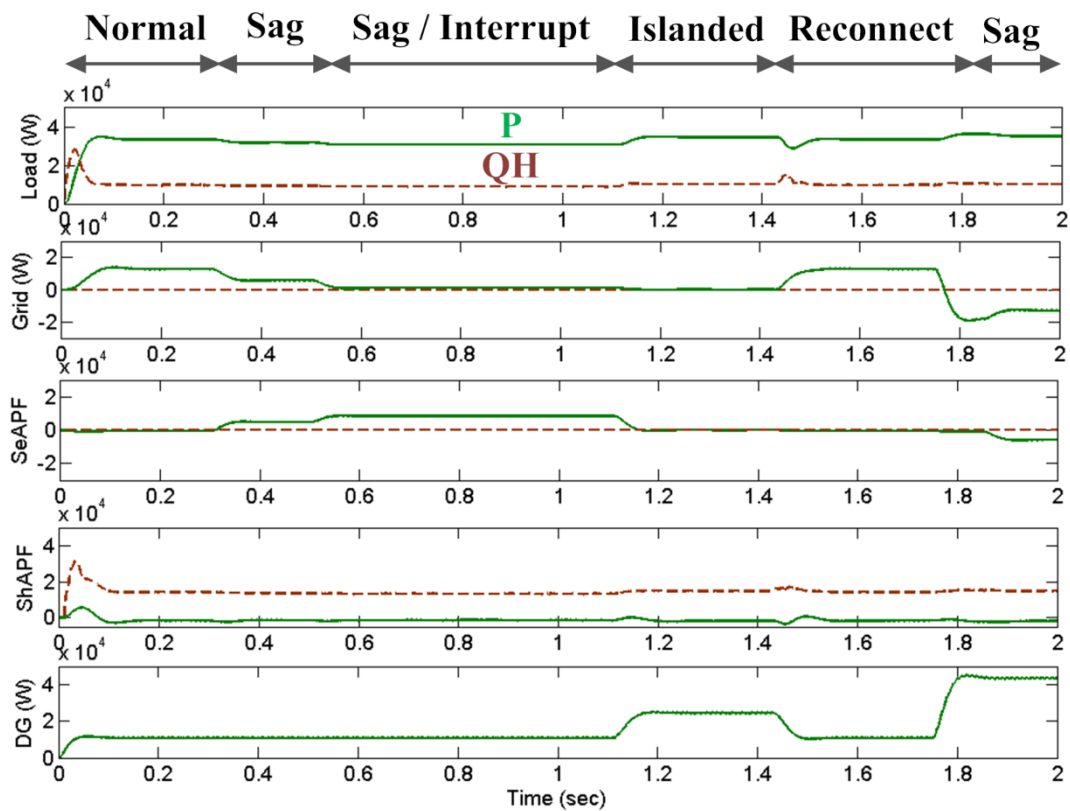
Fig 5.27 Power flow during the simulation time

5.6 Simulation Study - UPQC$_{\mu\text{G-IR}}$

The working principle of the proposed system is already described in the previous section. Fig 5.2 and 5.3 also explain the operational concept during interconnected and islanded mode. Details of the performance with the simulation results are given below. All the simulations have been performed for up to 2 sec. Table 5.6 also shows the timeline for the respective operating conditions.

It is to be noted that, operation-wise, the simulation and performance of the UPQC$_{\mu\text{G-I}}$ and UPQC$_{\mu\text{G-IR}}$ are the same for the cases of forward flow, reverse flow mode and up to the islanded condition with islanding detection. These are repeated here for the UPQC$_{\mu\text{G-IR}}$. The difference will be observed in the case of reconnection mode.

Table 5.6 Timeline of the Operating Conditions

| Operating Condition	Interconnected									Islanded					Interconnected					
	Time (sec)																			
	0.1	0.2	0.3	0.4	0.5	0.6	0.7	0.8	0.9	1.0	1.1	1.2	1.3	1.4	1.5	1.6	1.7	1.8	1.9	2.0
Normal Operation	Phase = 0 deg															Phase = 40 deg				
Sag			50%																	
Sag / Interrupt							90%													
Islanding																				
Synchronization																				
Reconnection																				
DG-input		0.5 I$_{load}$				Grid + 0.5 I$_{load}$ + Storage					I$_{dg}$ + Storage					0.5 I$_{load}$			1.5 I$_{load}$		

The operating positions (0 for open and 1 for close) of the switches during the operation are very important in detecting the islanded, synchronization, reconnection and interconnected modes. These positions depend on the magnitude and time length of V_{error} (as shown in Fig 5.14 and 5.15) and the S_{w4syn}, $S_{\mu\text{G-R}}$ switches (as shown in Fig 5.15, 5.17). Based on the algorithm for islanding detection and the reconnection method, Fig 5.28 shows the switch positions during the operation from 0 to 2 sec where both the interconnected and islanded modes are observed. Fig 5.29 shows the performance of the proposed UPQC based on the Table 5.6 and Fig 5.28. A 40 degree phase shift of the utility supply (V_s and I_s) is applied during the reconnection process.

Though the voltage magnitudes at the utility and the PCC are the same, a voltage sag appears due to the phase difference between them. Therefore, in that position the proposed UPQC$_{\mu G\text{-}IR}$ reconnects the system starting with voltage sag compensation, as shown in Fig 5.29(a). Reverse current flow also occurs (when the DG supplies more than the required load fundamental) during the voltage sag compensation, as shown by the circle in Fig 5.29(b). Details of the synchronization condition and the reconnection process are discussed in a later section. Performance of the proposed UPQC$_{\mu G}$ during interconnected and islanded mode has been discussed below. Generally waveforms are shown for phase A only.

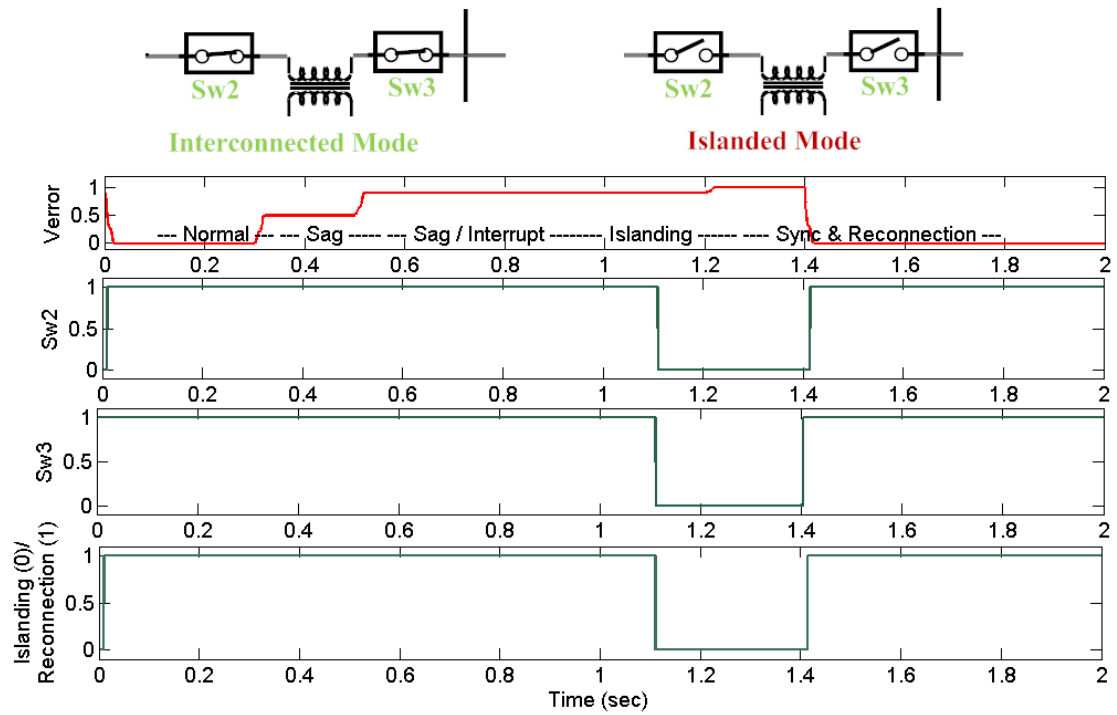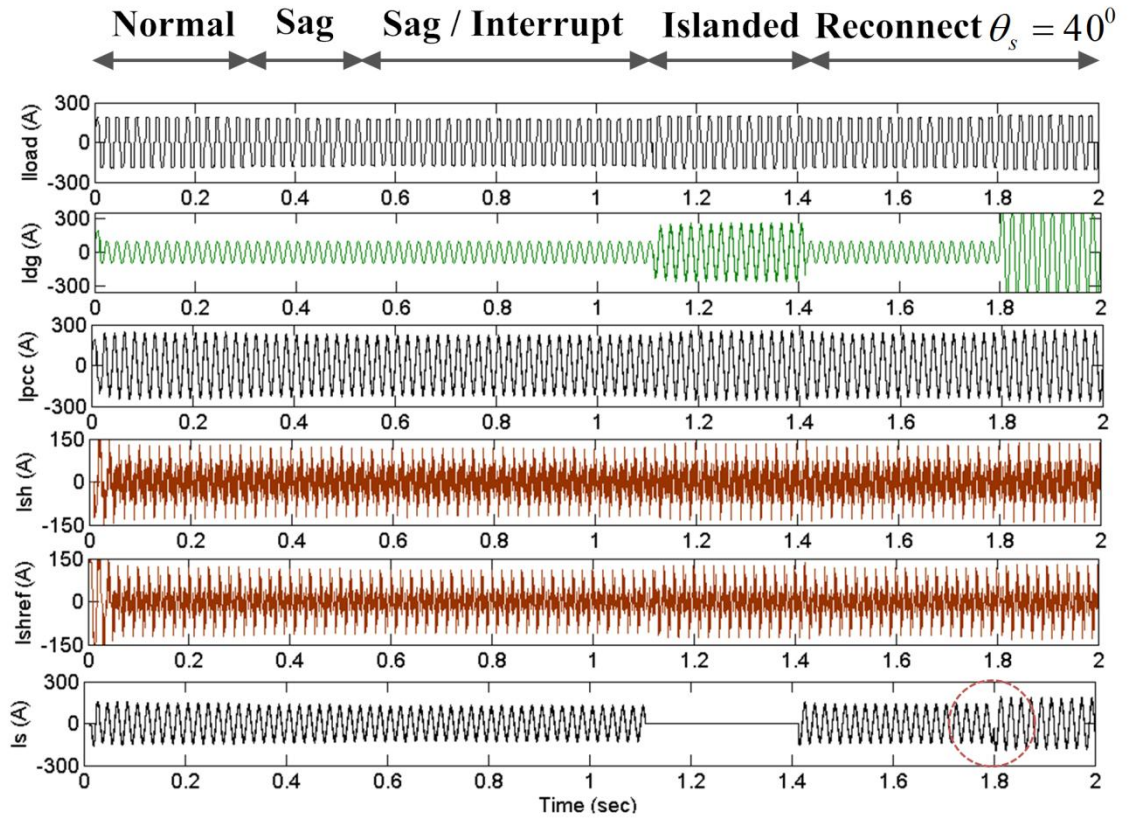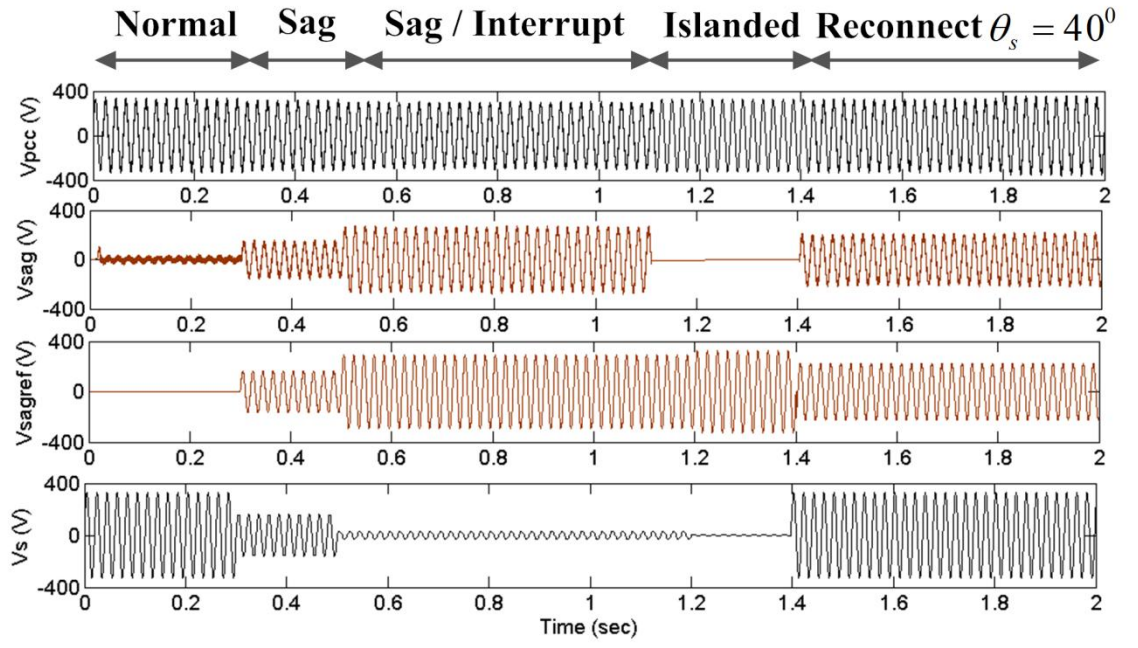Fig 5.28 Switching positions during the operation from 0 to 2 sec.

(a)

(b)

Fig 5.29 Complete performance of UPQC$_{\mu G\text{-}I}$ during interconnected and islanded mode, (a) voltage waveform and (b) current waveforms at difference conditions and positions in the network.

5.6.1 Interconnection mode

Depending on the power availability, the DG source can supply power to the load and grid, and therefore by-directional power flow can occur. Hence, the performance of the proposed UPQC should be observed in both cases. For a better understanding, according to the direction of power flow, operation in the interconnected mode can be divided into two parts: (i) forward-flow mode and (ii) reverse-flow mode.
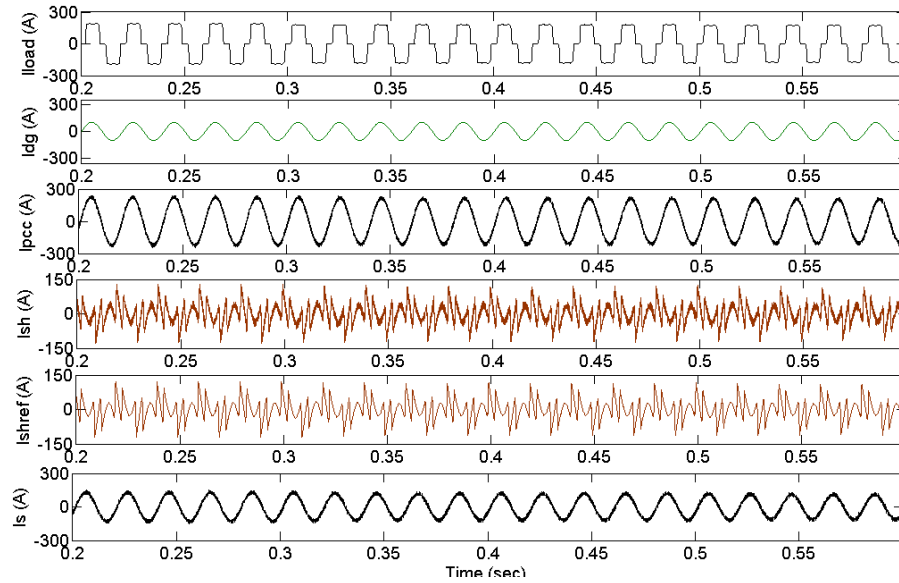
5.6.1.1 Forward-flow mode

In this case, the available DG power is less than the required load demand. Therefore, the utility grid supplies the rest of the power to the load which is not met by the DG supply. Depending on the microgrid energy management and control strategy, the DG storage system can be charged through the utility and/or the DG units. Fig 5.30 shows the initial condition from 0.2 to 0.6 sec of the simulation study where the voltage sag and interruption events occur and are used to study the performance of the UPQC. Fig 5.30(a) shows the output waveforms of the voltage in different branches of the proposed system, whereas the current waveforms are shown in Fig 5.30(b). A 50% sag is applied at 0.3 sec, 90% at 0.5 sec and then at 1.2 sec the utility is disconnected. In general, the series APF can also compensate the voltage distortion, created by the utility, at the PCC. Therefore, this advantage can also be implemented in the series APF control part of the proposed system. The other advantage of this configuration is that the shunt APF can compensate the voltage distortion created by the DG converters. Fig 5.30(a) shows the performance of the series APF part of the proposed UPQC in maintaining the constant and stable load voltage. Fig 5.30(b) shows the performance of the shunt APF part in compensating the reactive and harmonic current generated by the load. This compensation helps the UPQC system to maintain the grid current THD level within the IEEE limit. As is mentioned in the timeline table, the DG unit supplies $0.5I_{loadf}$ (half of load fundamental in current control mode) during this time frame.

Therefore the remainder of the current is supplied by the utility grid and storage. During a 90% sag condition, supply from the DG unit and the utility remains unchanged and the storage system provides the power for sag compensation (through the DC link) which is reflected in Fig 5.30(b).
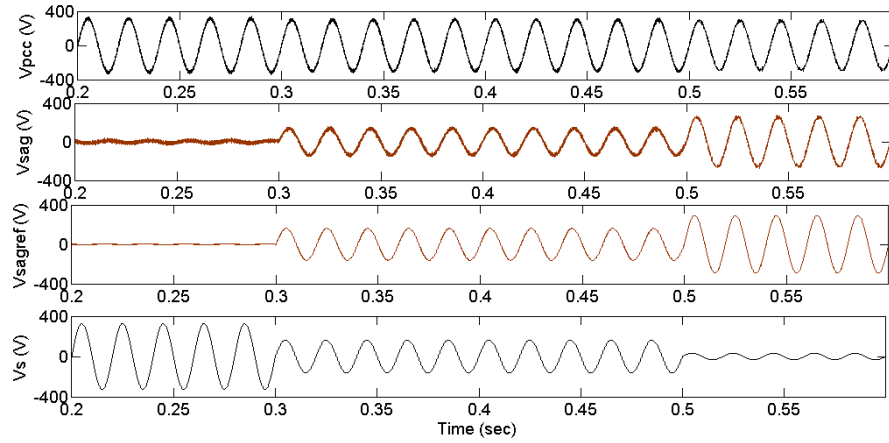
(a)

(b)

Fig 5.30 Performance of the proposed UPQC$_{\mu G}$; a) series APF and b) shunt APF; from 0.2 to 0.6 sec during interconnected and forward flow mode.

5.6.1.2 Reverse-flow mode

At this stage, the grid current becomes out of phase with the grid voltage or the voltage at the PCC. Fig 5.31 shows the performance of the UPQC when the DG current

becomes 1.5 times of the load fundamental at 1.75 sec and a 40% sag already exists after reconnection at 1.41 sec. In this case, the performance of the shunt APF remains the same even when the utility current becomes out of phase, as shown in Fig 5.31(b). Fig 5.31(a) shows that the series APF performs voltage sag compensation during the reverse flow mode also.
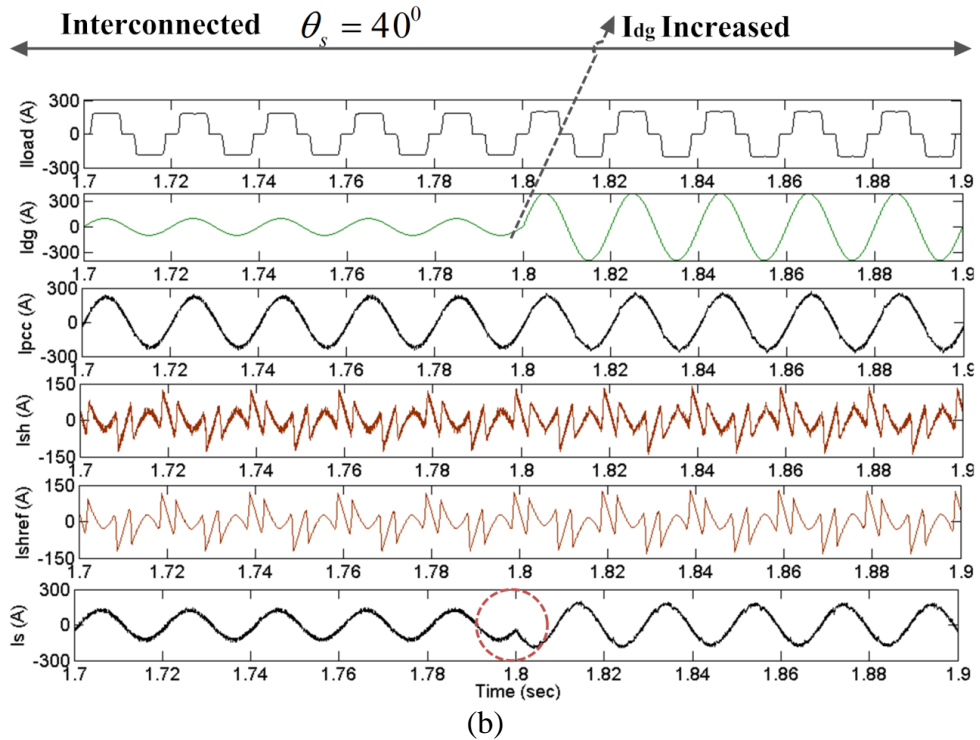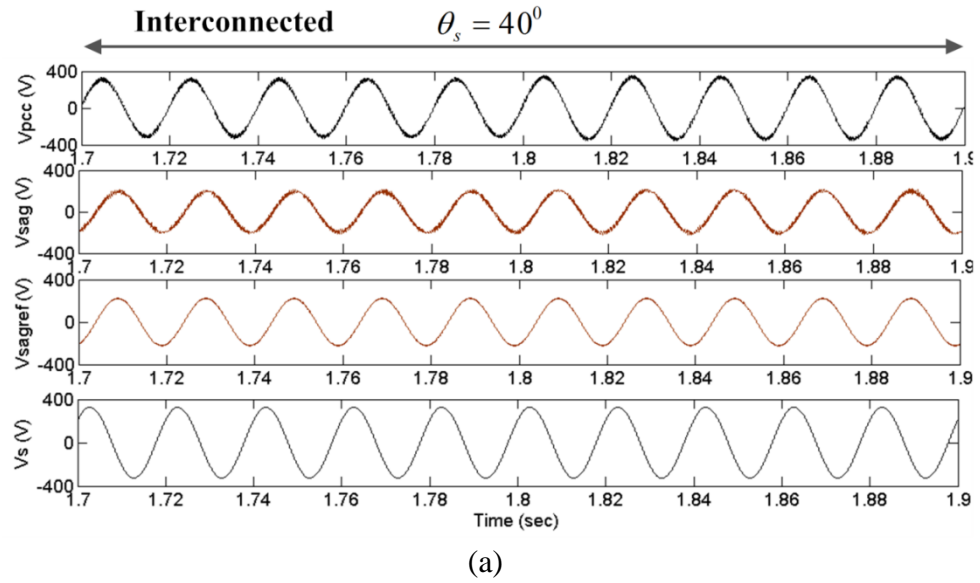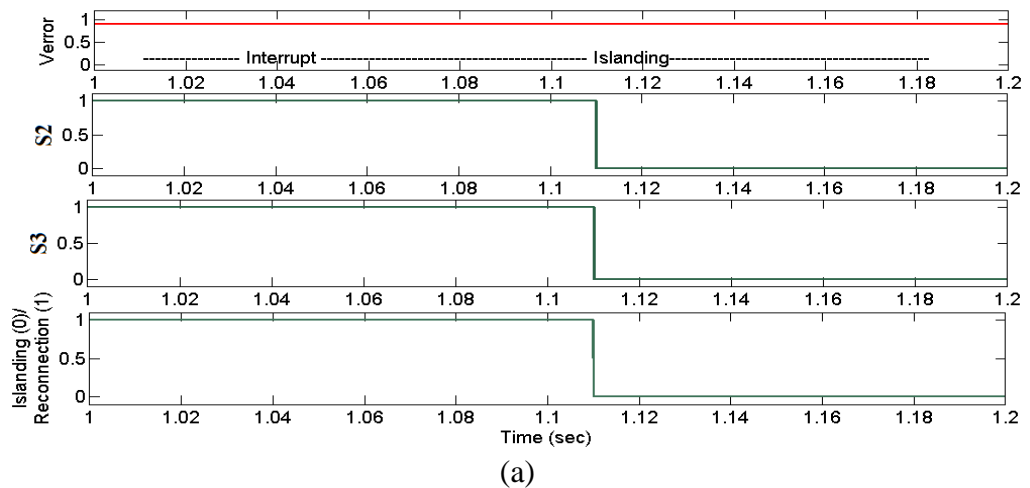

Fig 5.31 Performance of the proposed UPQC$_{\mu G}$; a) series APF and b) shunt APF; during interconnected and reverse flow mode.

5.6.2 Islanded Mode

It was mentioned earlier that a 90% sag compensation has been introduced at 0.5 sec. According to the islanding detection method, the series APF compensates the sag for up to 0.6 sec (30 cycles) and then the system goes into islanding mode. A utility disconnection is applied at 1.1 sec just after completing the 30 cycle count and then detecting the zero crossing of $V_{sag\text{-}ref}$ (at 1.11) where S2 and S3 are opened. This is depicted in Fig 5.28 and 5.32(a). At disconnection, the system immediately operates in an isolated microgrid condition. At this stage, if the available DG power is lower than the load demand, the additional required power is supplied by the storage. If the DG power is higher than the load, then the additional power goes to the storage. The shunt APF still performs the compensation of reactive and harmonic power. Therefore, the DG converter does not need to be disconnected or change the control strategy (supplying only fundamental active power) to supply power to the load.

Fig 5.32 shows the performance of the proposed UPQC during 1.0 to 1.2 sec where the islanding is detected just immediately after 1.1 sec at zero crossing detection. The islanding mode is observed between 1.11 and 1.40 sec. During this period the series APF is disconnected, as shown in Fig 5.32(c) where $V_{sag} = 0$, and the utility current become zero, as shown in Fig 5.32(b). The shunt APF continues to operate, as shown in Fig 5.32(b), and the load demand is met by the DG with the storage unit.

(a)
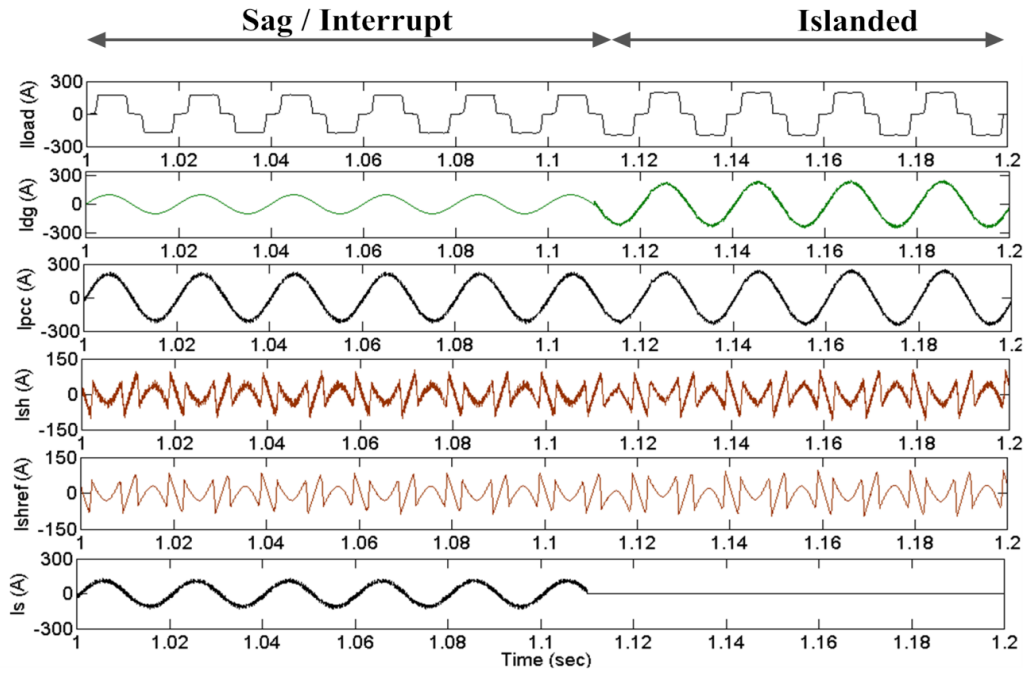
(b)
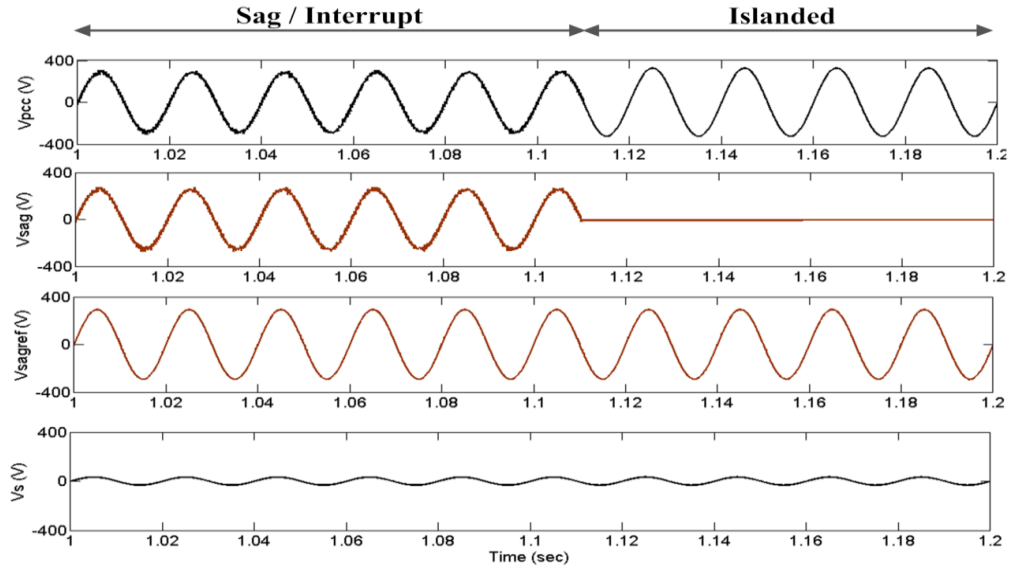
(c)

Fig 5.32 Performance of the proposed UPQC$_{\mu G}$; a) switching condition, b) shunt APF and (c) series APF; during islanded mode.

5.6.3 Reconnection

One of the most important parts of the proposed UPQC$_{\mu G\text{-}IR}$ is the reconnection process. This has to occur without disconnecting the DG units or changing its current control strategy during isolated or grid connected μGrid / μGen operating conditions. Fig 5.33 shows the different signals for the reconnection process based on the algorithm

and developed method showed in Fig 5.18 and 5.19. To check the performance of the reconnection process for the worse condition, the utility grid (V_s) is powered on at 1.40 sec with a 40 degree out of phase from the PCC. Immediately, the S_{w4syn} pulse is activated and the reconnection algorithm starts generating active pulses as the phase and amplitude differences are within the required limits. Zero crossing detection is also shown. UPQC unit sends a reconnection signal to the DG unit. Based on the logic given in Fig 5.19, the actual switch S2 and S3 are activated at 1.405 and 1.415 sec respectively. This simple algorithm with a combined logic gate ensures the utility connects with the μGrid smoothly after the utility system is restored.

Fig 5.34(a) shows that the series APF unit is immediately reactivated and starts operation when the grid voltage is available and S3 is connected at 1.405 sec, as shown by the circle in V_{sag} waveform. The power transfer starts when the S2 is closed at 1.415 sec, as shown in Fig 5.34(b). It is expected that, according to the smooth reclosing condition, no power flow will occur at the point of reclosing. The switching is carried out successfully within the limiting condition as shown in Fig 5.34(b). The circle at 1.415 sec for I_{dg} and I_s in Fig 5.34(b) indicates the smooth transition from islanded to interconnected mode. The DG inverter also changes its control from voltage to current control mode but only transfers active fundamental current. The performance of APF$_{sh}$ is also uninterrupted during the transition period.
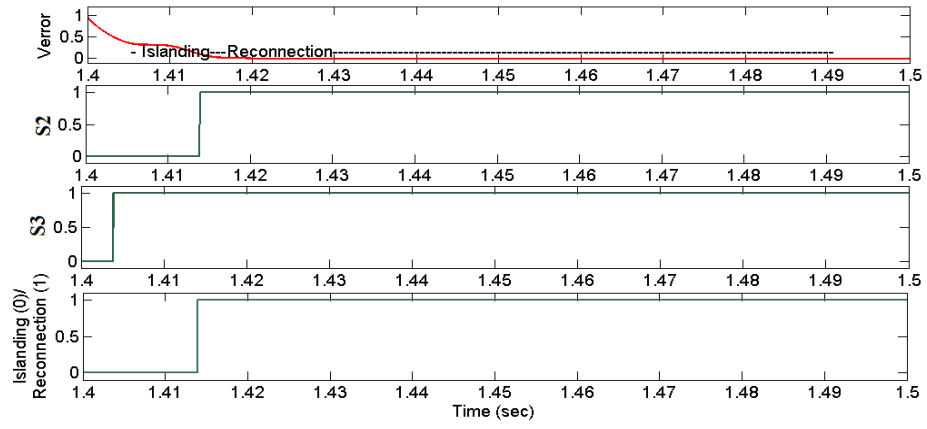
Fig 5.33 Condition of different signals for reconnection process based on Fig 5.19.
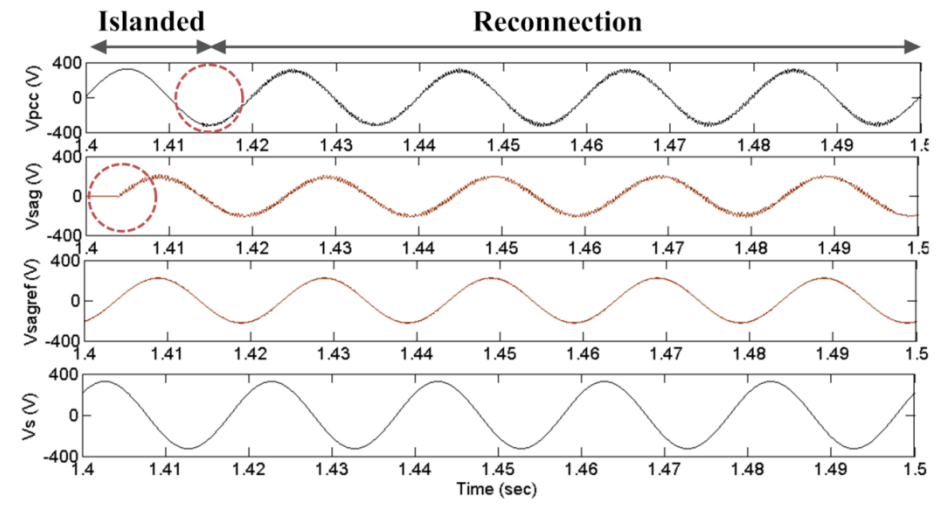
(a)
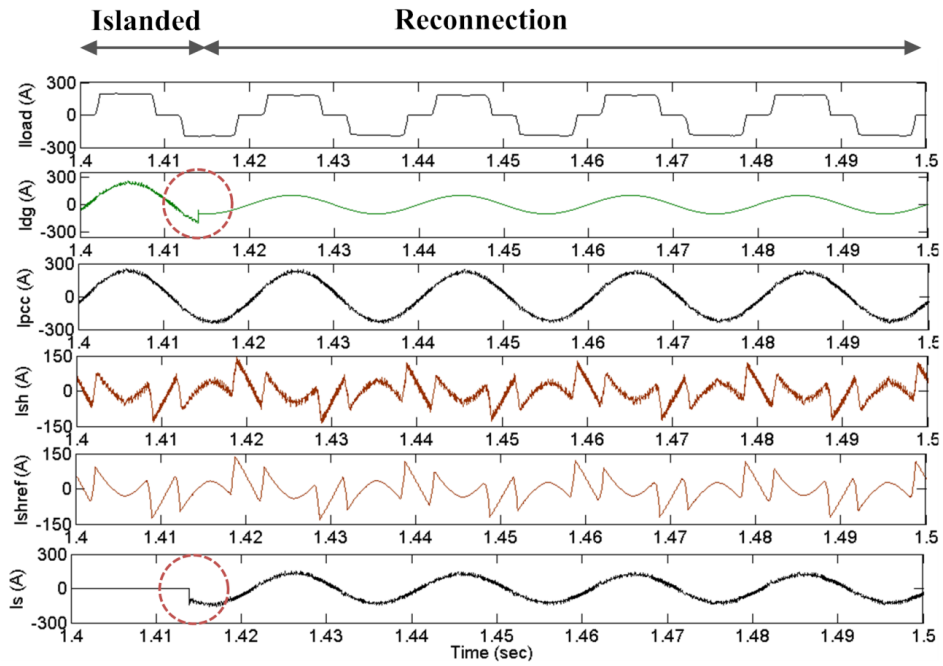
(b)

Fig 5.34 Performance of the proposed UPQC during reconnection, (a) series APF, (b) shunt APF

5.6.4 Power Flow

The power flow diagram is shown in Fig 5.35 for the complete simulation time where the green line represents the active power (P) and red line (dash) for reactive and harmonic power (QH). This also validates the operation and performance of the APF$_{se}$ and APF$_{sh}$ part of the proposed UPQC$_{\mu G\text{-}I}$ along with the islanding detection and reconnection.
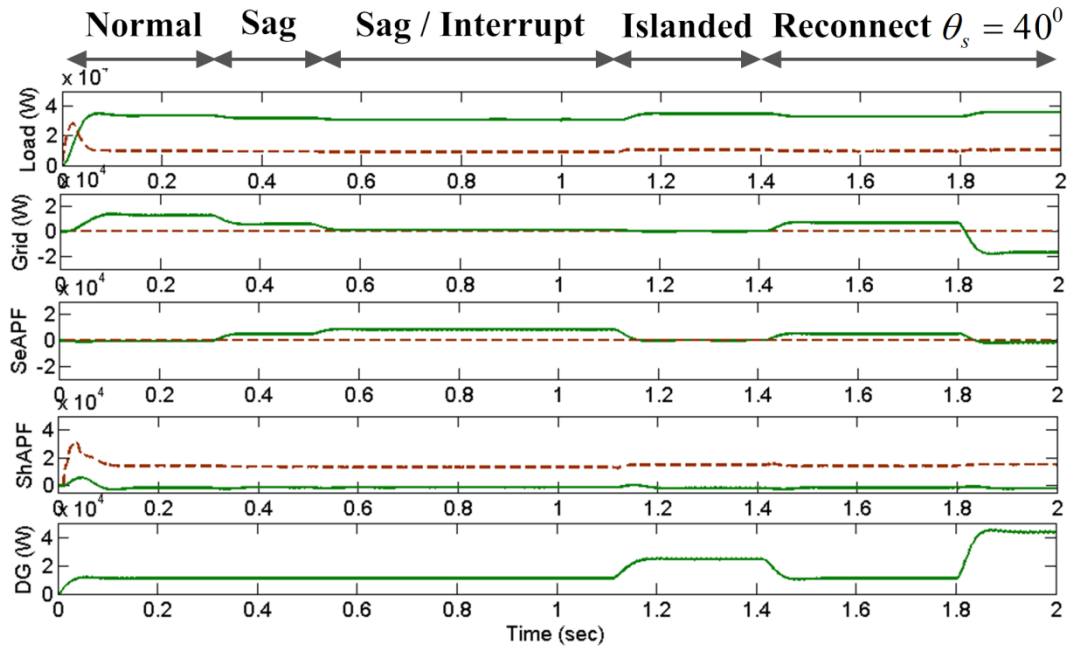
Fig 5.35 Power flow during the simulation time

5.7 Hardware Results

Due to the limitations of hardware facilities as well as the existing real-time simulators capabilities, real-time test of the proposed UPQC$_{\mu G}$ is performed partially. The performance of the APF$_{se}$ and APF$_{sh}$ of the UPQC$_{\mu G}$ is obtained during interconnected and islanded mode. All the tests are performed in SIL (software-in-loop) configuration using hardware synchronized mode, as discussed in Chapter 1 (section 1.1.5). Details of the simulation and set up are given in Appendix 2.

5.7.1 Interconnected mode

Fig 5.36 shows the performance of APF$_{se}$ during the voltage sag (40%) condition where v_s, v_{sag}, v_{pcc}, i_{load}, i_{dg} are presented. The performance is obtained when the APF$_{sh}$ is not working and the system is in a steady-state condition. For measurement, the system is stepped down by 100, i.e., each division of the scope represents the value (x 100) in the original system. For current, 1V = 100A.
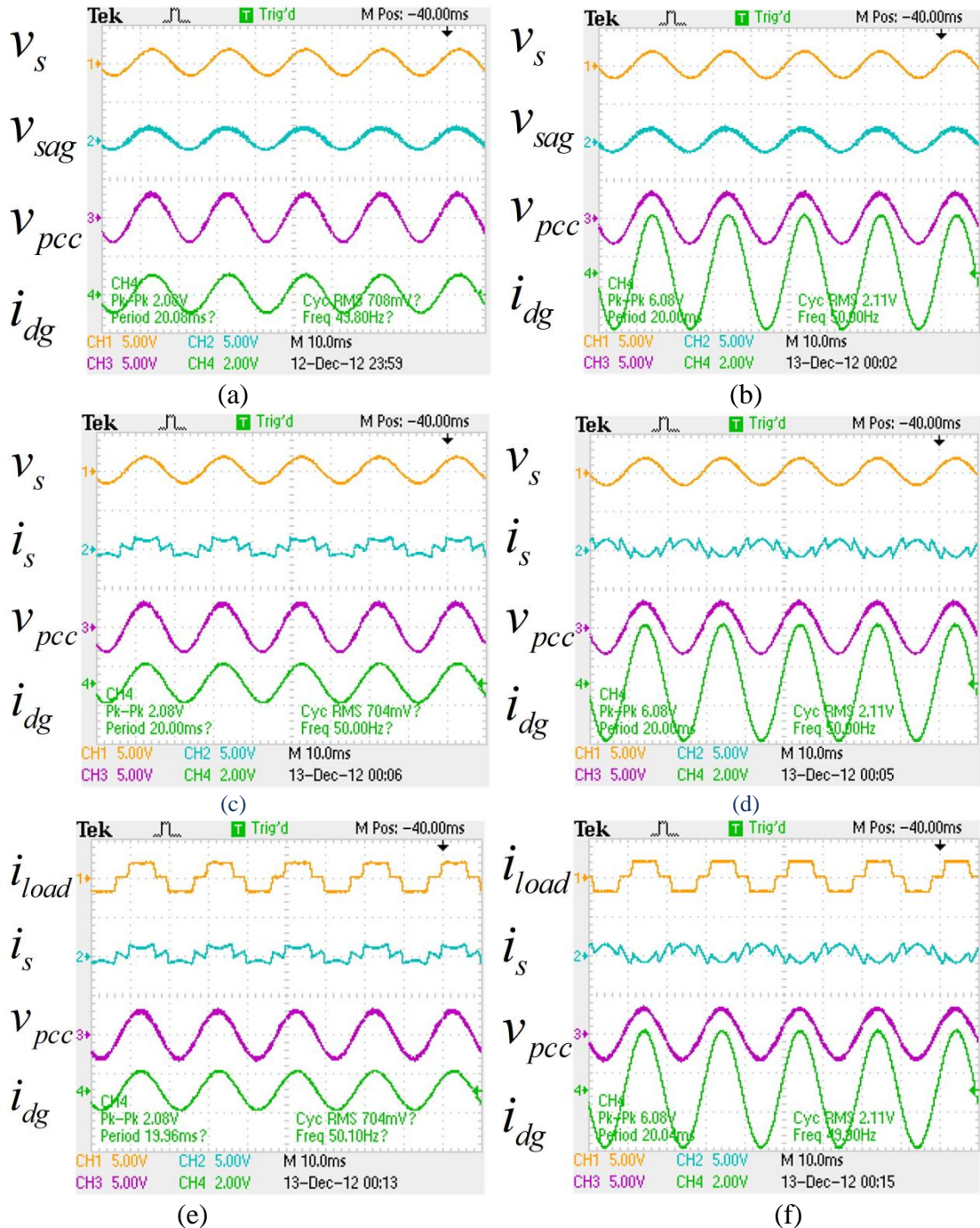
Fig 5.36 Performance of APF$_{se}$; (a, c, e) $i_{dg} < i_{loadf}$; (b, d, f) $i_{dg} > i_{loadf}$ when APF$_{sh}$ is off

Fig 5.36(a, c, e) shows the condition of utility voltage, current and load current during voltage sag compensation in forward flow mode. Fig 5.36(b, d, f) shows the voltage sag compensation during reverse flow mode where the utility current becomes out of phase.

Fig 5.37 shows the dynamic response of the APF$_{se}$ for voltage sag (40%) compensation. Fig 5.37(a) shows a complete response between the sag occurrence and normal condition of the utility supply. Voltage at PCC is maintained constant. Fig 5.37(a) and (b) show the response of APF$_{se}$ during pre-sag and post-sag condition. This performance is observed at forward flow condition, where $i_{dg} < i_{loadf}$. Similar performance is obtained for the APF$_{se}$ in reverse flow condition where, $i_{dg} > i_{loadf}$. The result is shown in Fig 5.38.

Although the APF$_{se}$ has been designed for 100% sag condition, due to the hardware limitations and the capabilities available to the existing real-time simulator, the performance of APF$_{se}$ was further obtained for 80% voltage sag compensation. The results are shown in Fig 5.39 and 5.40. Fig 5.39 shows the performance during forward flow condition, whereas Fig 5.40 shows the results in the reverse flow condition.

Fig 5.41 shows the performance in forward-reverse flow condition during a voltage sag (80%) compensation. The performance is obtained with the dynamic change of DG current (i_{dg}). From forward to reverse flow is created by increasing i_{dg} during the sag compensation, as shown in Fig 5.41(b). Performance in reverse conditions is also shown in Fig 5.41(c).

Fig 5.42 shows the performance of the APF$_{sh}$ in interconnected mode. In this case, the values of APF$_{sh}$ are stepped down by 10. Fig 5.42(a) shows the harmonic current compensation when the DG supply is zero. Fig 5.42(b) shows the performance in forward flow mode whereas Fig 5.42(c) represents the results for reverse flow mode.
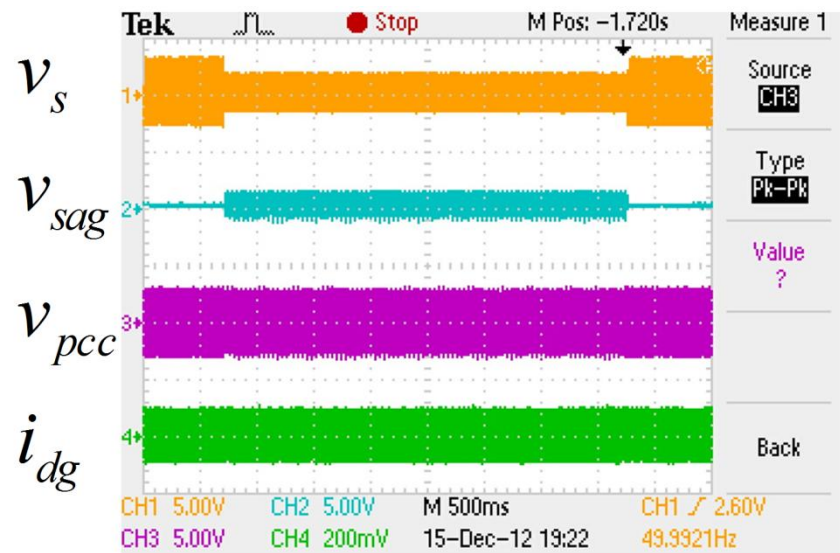
(a)
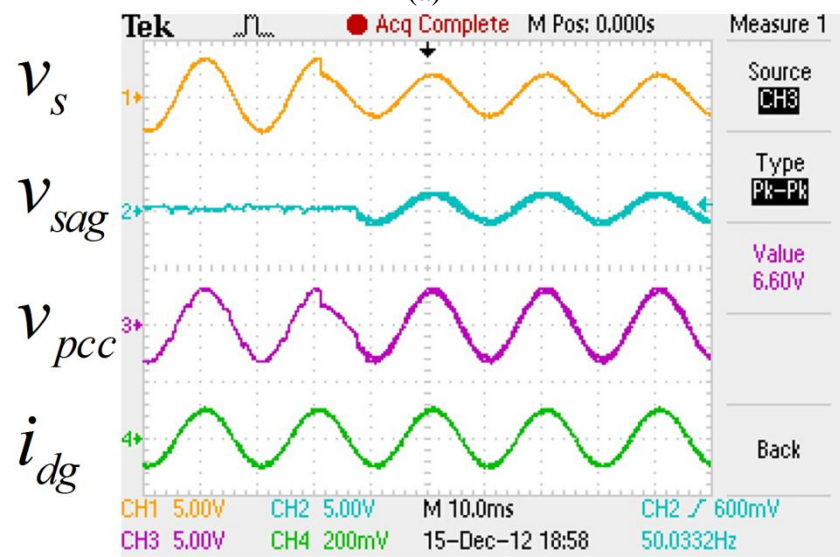
(b)
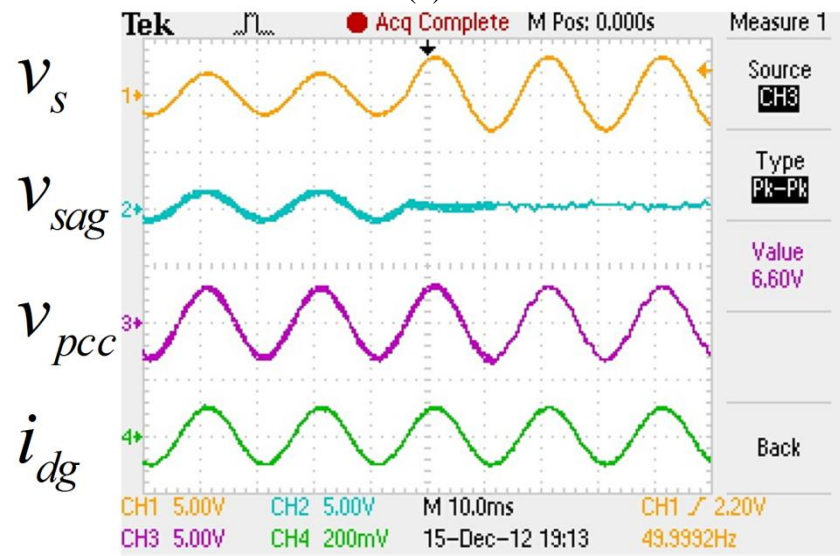
(c)

Fig 5.37 Performance of APFse in forward flow condition (a) compensating voltage sag (40%), (b) during pre-sag and (c) post -sag condition
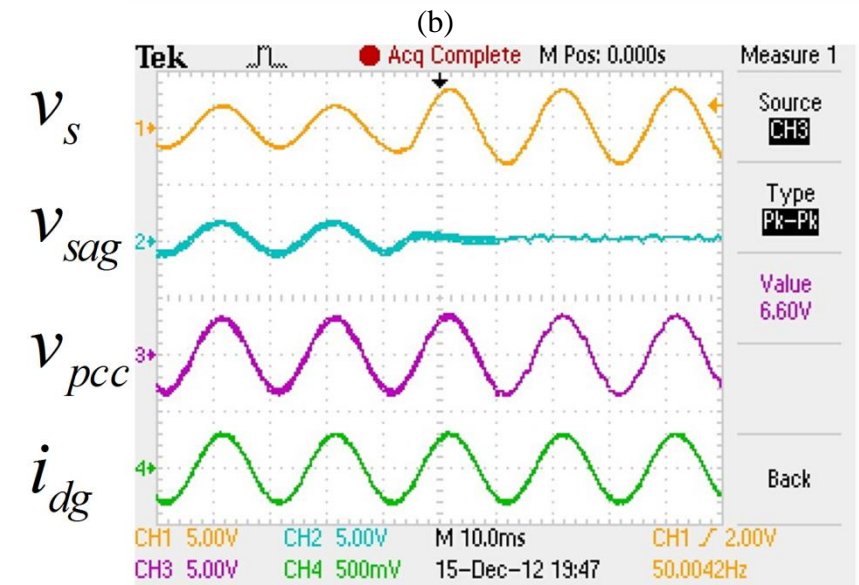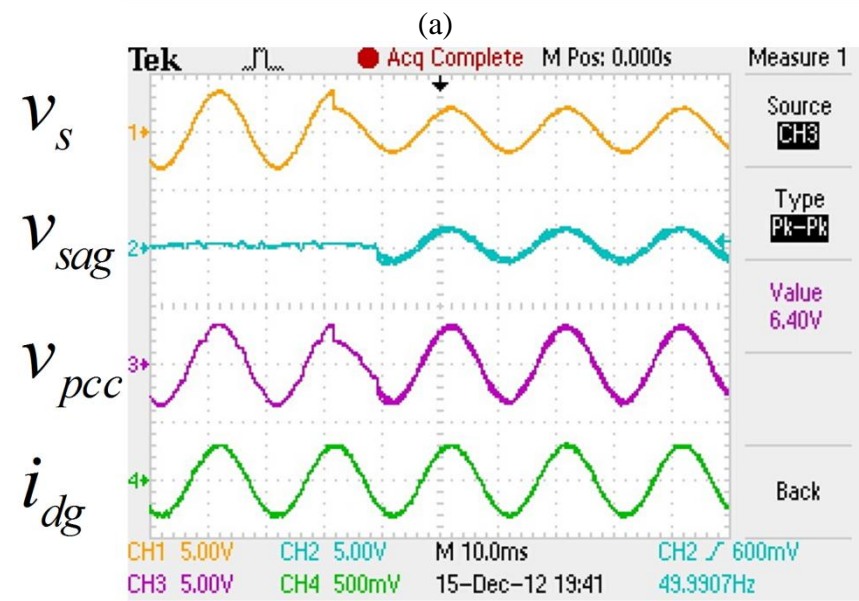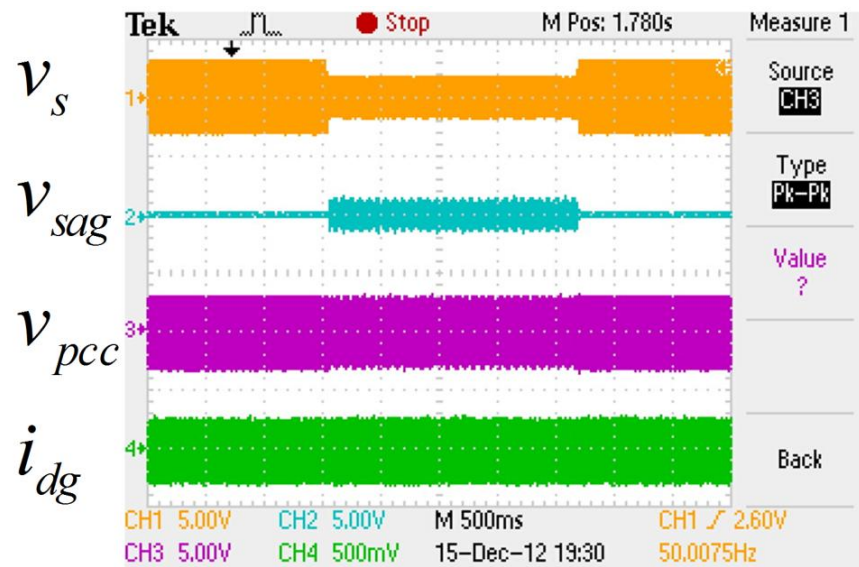
Fig 5.38 Performance of APFse in reverse flow condition (a) compensating voltage sag (40%), (b) during pre-sag and (c) post -sag condition
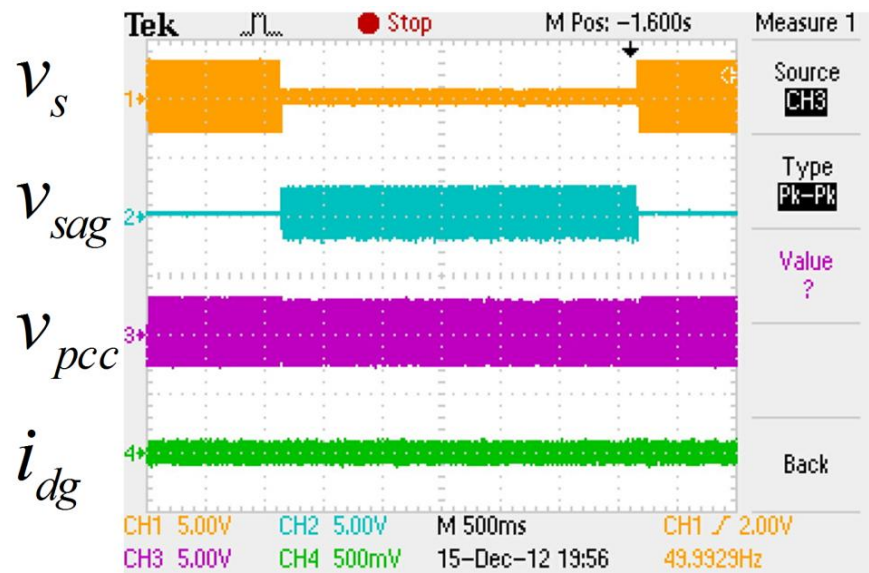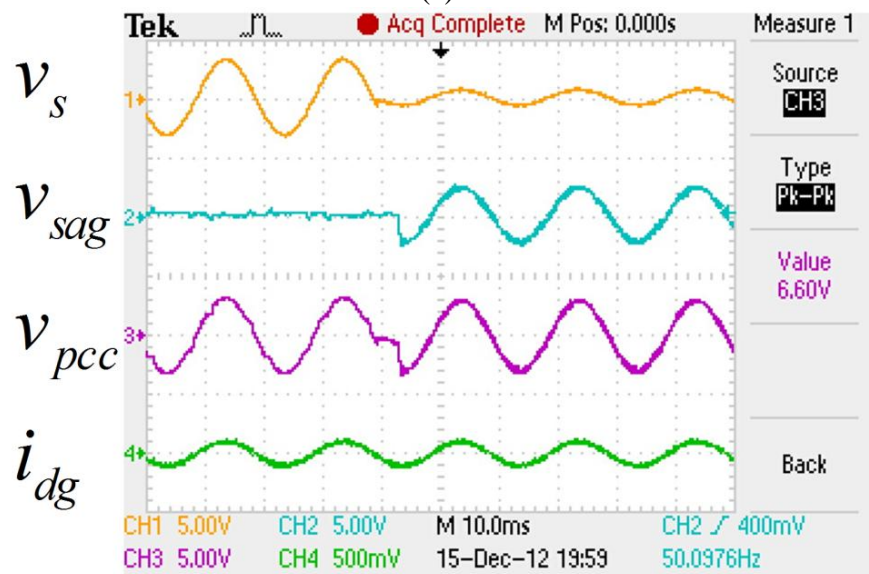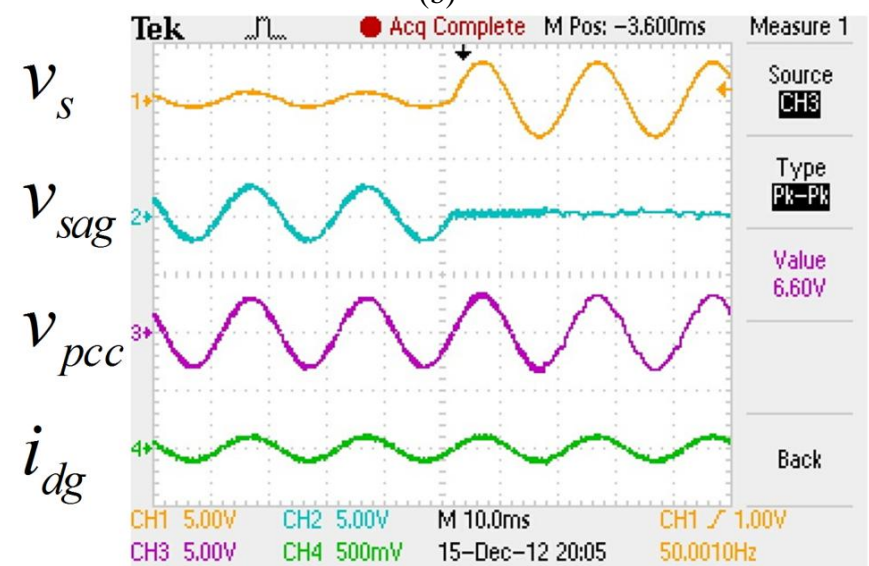
Fig 5.39 Performance of APFse in forward flow condition (a) compensating voltage sag (80%), (b) during pre-sag and (c) post -sag condition
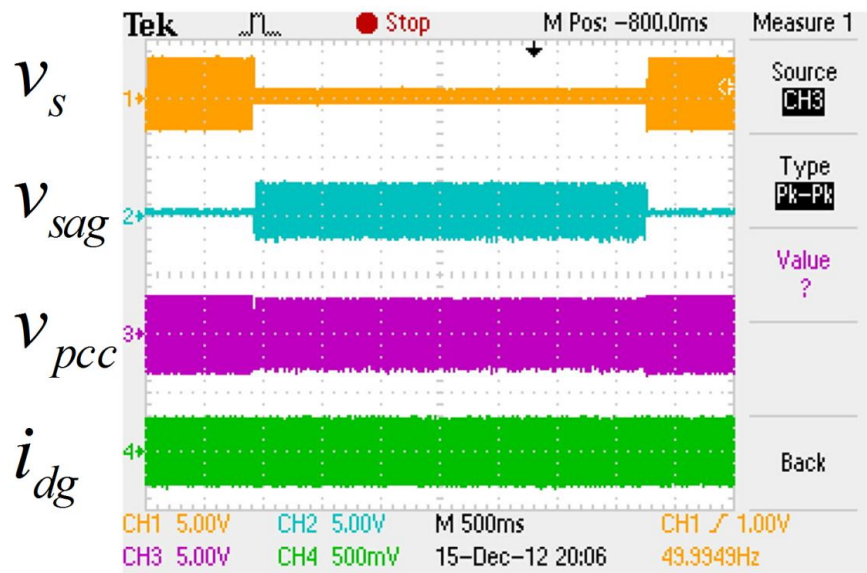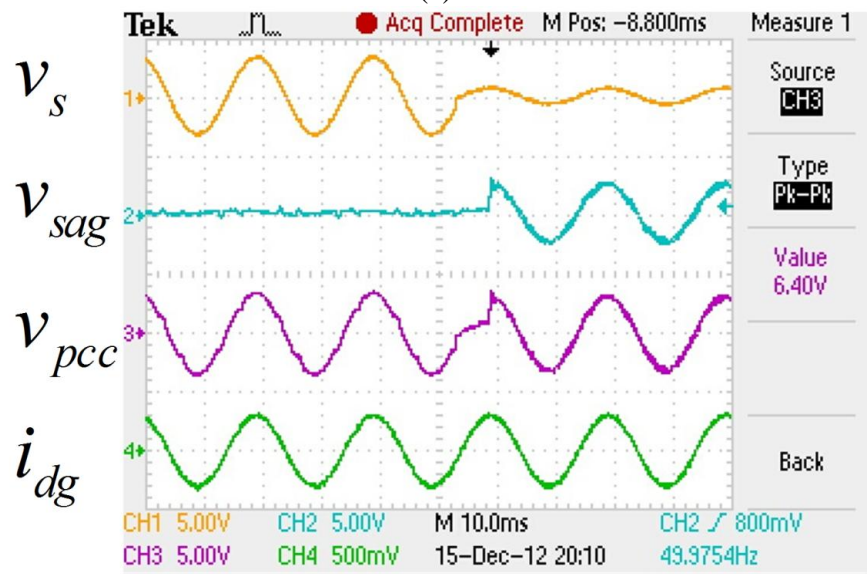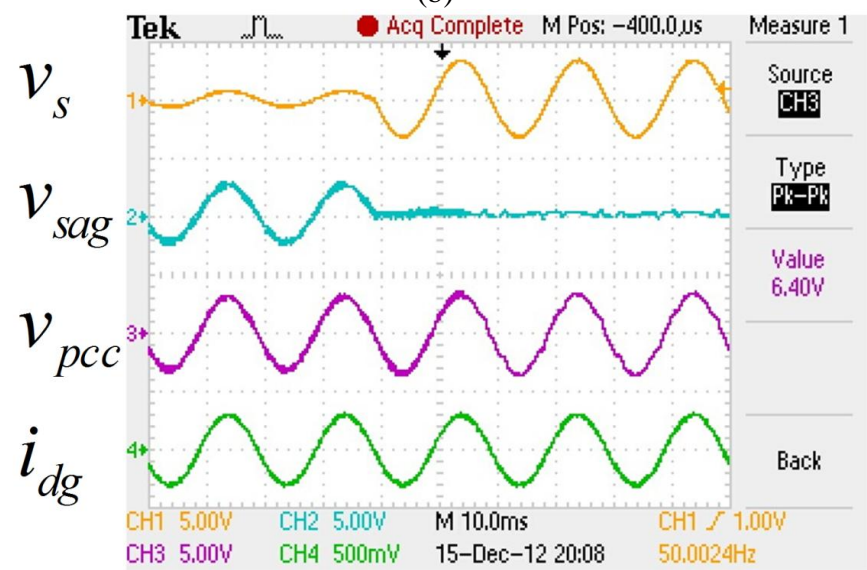
Fig 5.40 Performance of APFse in reverse flow condition (a) compensating voltage sag (80%), (b) during pre-sag and (c) post -sag condition
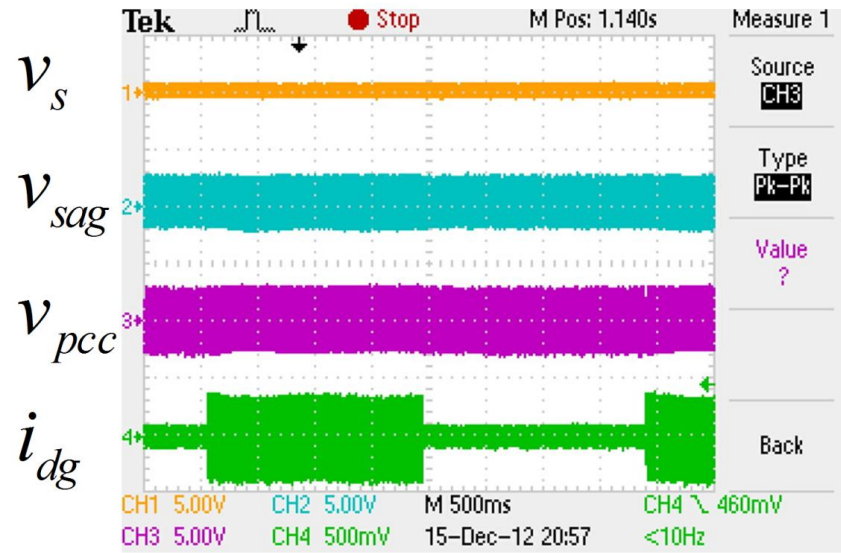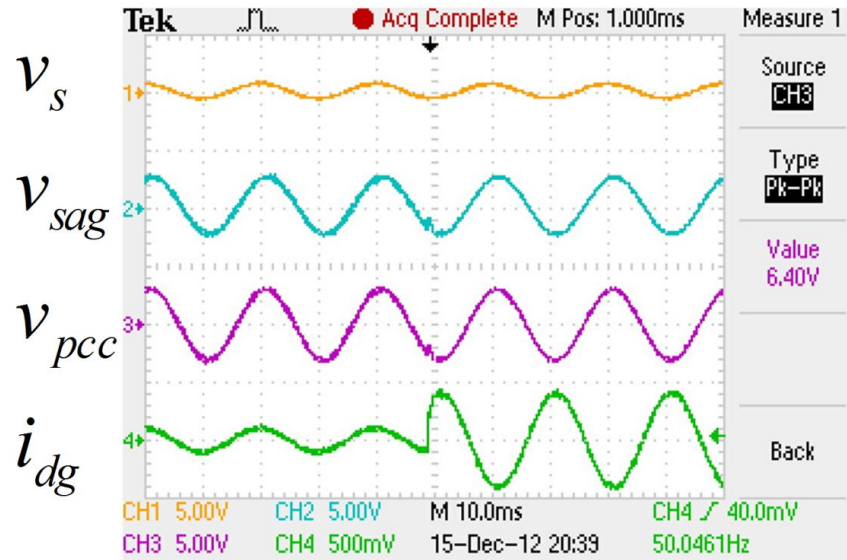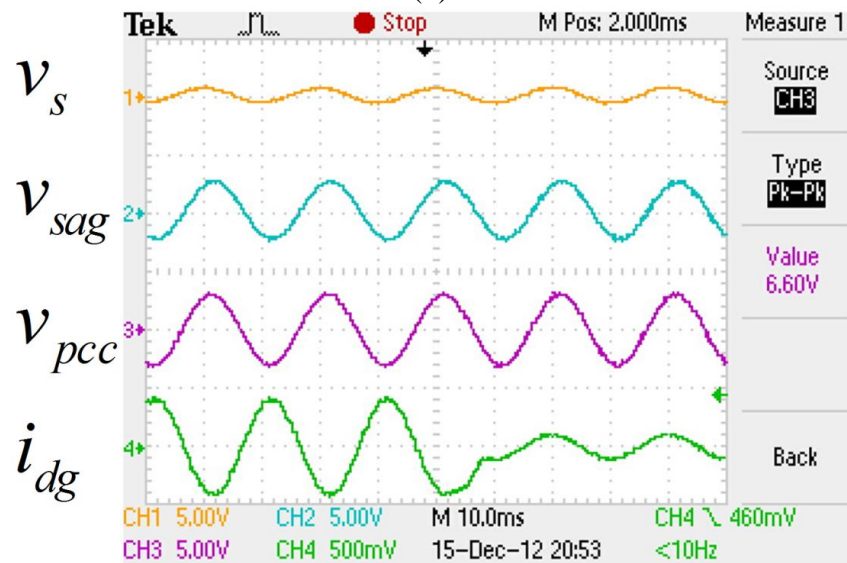
Fig 5.41 Performance of APFse in forward-reverse flow condition and compensating voltage sag (80%)
(a) dynamic change of i_{dg} (b) i_{dg} increasing: forward-reverse, (c) i_{dg} decreasing: reverse-forward flow
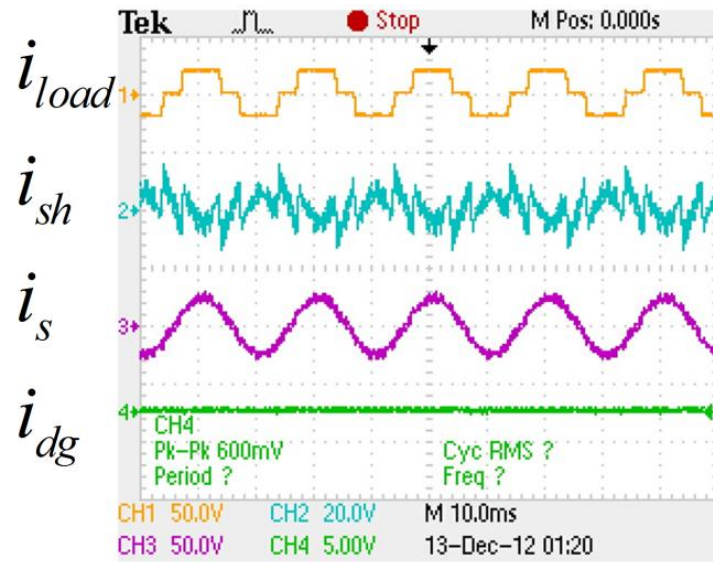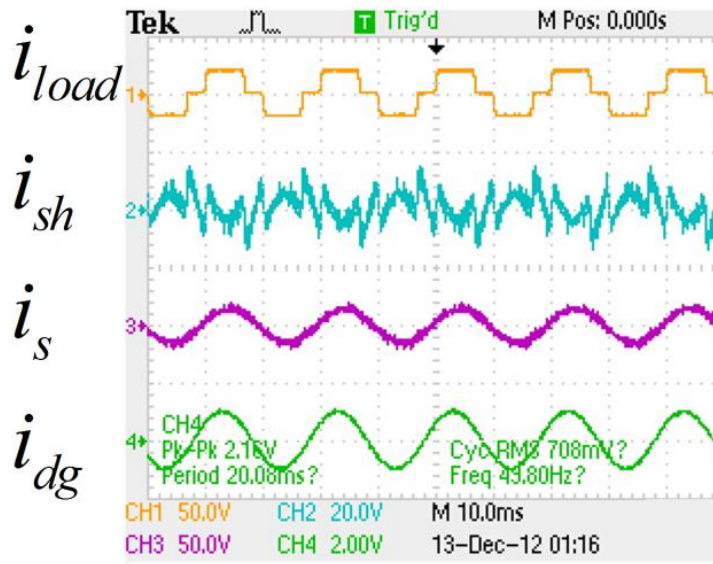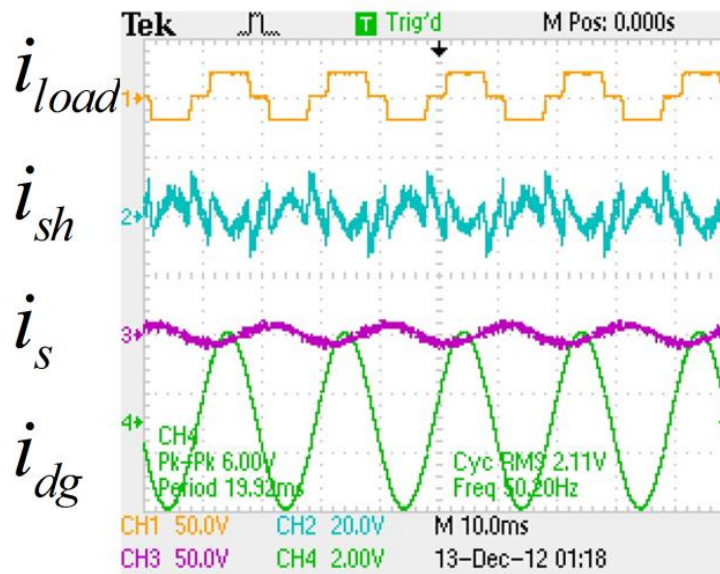
Fig 5.42 Performance of APF$_{sh}$ (a) during $i_{dg} = 0$, (b) forward flow (c) reverse flow mode.

5.8 **Conclusion**

This chapter describes the working principle, operation and performance of the proposed UPQC$_{\mu G}$ in the grid connected microgrid condition. The simulation has been performed in MATLAB and the results show that the proposed system can compensate the voltage disturbance at the PCC, the reactive and harmonic current compensation of the load that could inject at the PCC during the interconnected mode. The DG current does not have any effect in degrading the performance of the system in the interconnected reverse-flow mode. During the islanded mode, the DG converter also only supplies the active power to the load and the shunt APF performs the reactive and harmonic power compensation. Therefore, the grid-tie DG converter does not need to be disconnected or change its control strategy to keep the microgrid operating during the islanding detection and operation in islanded mode. The proposed UPQC$_{\mu G}$ thus will reduce the control complexity of the grid-tie converter and improve the power quality of a grid connected μGrid or μGen system.

Chapter 6

Distributed UPQC (D-UPQC): A way to enhance capacity and achieve flexibility

6.1 Introduction

In high power applications, the filtering task cannot be performed for the whole spectrum of harmonics by using a single converter due to the limitations on switching frequency and power rating of the semiconductor devices. Therefore, compensating the reactive harmonic components to improve the power quality of the DG integrated system as well as to avoid the large capacity centralised APF, has meant that parallel operation of multiple low power APF units is increasing. Like APF, UPQC can also be placed at the PCC or at a high voltage distribution line as a part of a DG integrated network or in microgrid system to work both in interconnected or islanded mode.

The UPQC units developed so far for capacity expansion is mainly for medium or high voltage distribution lines where both the current and voltage are high. Therefore, it may be easier to use these multi-level or multi-modular type UPQC systems [59,60,176-181]. But these configurations may not be suitable for low voltage distribution lines where the 3-phase voltage (typically $400V_{L-L}$) is low, but the required compensating current is comparatively high (100A or more). In that case, multi-level or module type series APF may not be required. But for high current compensation, multiple Shunt APF units in a distributed (parallel) mode and connected with a common dc linked capacitor can be a solution in developing a Distributed UPQC (D-UPQC).

This chapter deals with the following sections. Limitations of the centralised system and the advantages of distributed approach are discussed in section 6.2. Section 6.3 describes the review of the UPQC capacity enhancement techniques. The new proposal of capacity enhancement, D-UPQC, is described in Section 6.4. Section 6.5 deals with the simulation study and real-time performance of the proposed system and the conclusions are made in Section 6.6.

6.2 Centralised and Distributed Systems

6.2.1 Limitations of centralized system (APF)

- One large unit is required to compensate the reactive and harmonic power arising from all critical loads rather than the specified loads.

- Impractical for some applications because of its high initial cost,

- Difficulties in installation due to large size and weight

- Single-point-of-failure reduces its reliability.

- High relative cost for achieving redundancy and increasing the capacity with expansion of the load.

6.2.2 Distributed/Multi-unit parallel approach

- In a distributed approach, many separate APF units operate in parallel. APF units are placed flexibly in the system to form a critical network.

- Highly reliable because of redundancy and also easy to achieve this redundancy

- Highly flexible and easy to increase the capacity when the load increases

- User-friendly in terms of maintenance

6.3 **Capacity enhancement techniques**

At this place, capacity enhancement is achieved by using Multi-level/module topologies to reach the higher power levels. These options are as follows:

i. Multi-level converter based UPQC

ii. Multi-module converter based UPQC

iii. Multi-module (power cell) unit based UPQC

A multi-level converter is proposed to increase the converter operation voltage, avoiding the series connection of switching elements. However, the multilevel converter is complex to form the output voltage and requires an excessive number of back-connection diodes or flying capacitors [59] or cascade converters [176]. A basic form of a multi-level UPQC is shown in Fig 6.1.

A multi-module H-bridge UPQC can also be connected to the distribution system without series injection transformers. It has the flexibility in expanding the operation voltage by increasing the number of H-bridge modules [177], as shown in Fig 6.2. Here each phase consists of several pairs of H-bridge modules isolated through a single-phase multi-winding transformer.

These Multi-module techniques [59,60,176-179] allow the symmetrical distribution of the load power among the components of the topology, but the classical design procedure must be modified or refined to ensure the power cell components should be within its maximum ratings. Therefore, a new design procedure of UPQC with a feature of extending capacity based on a modular approach is presented in [180,181], shown in Fig 6.3, where H-bridge power cells are added in each single phase arrangement depending on the required compensating power. Some advantages and disadvantages are also outlined in Table 6.1.
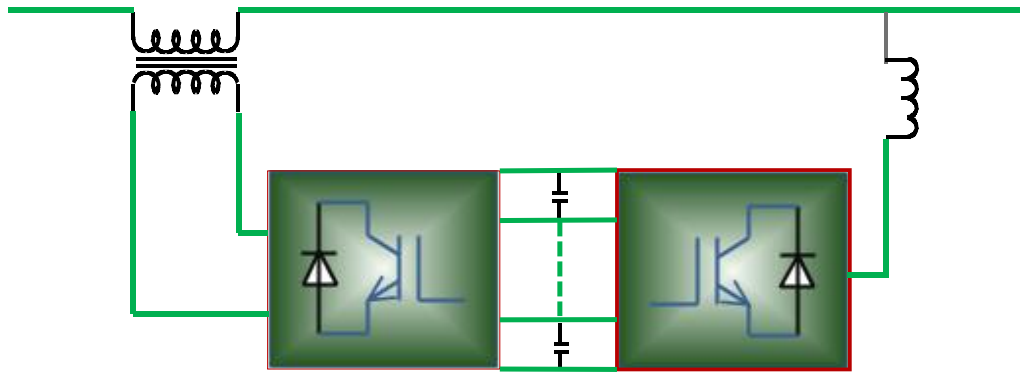
Fig 6.1 Multi-level Converter based UPQC
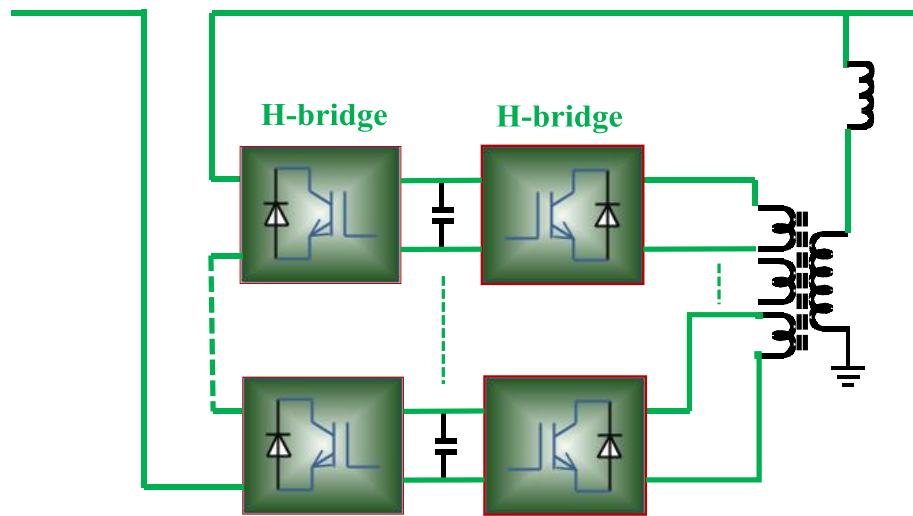
Fig 6.2 Series transformer-less Multi-module H-bridge
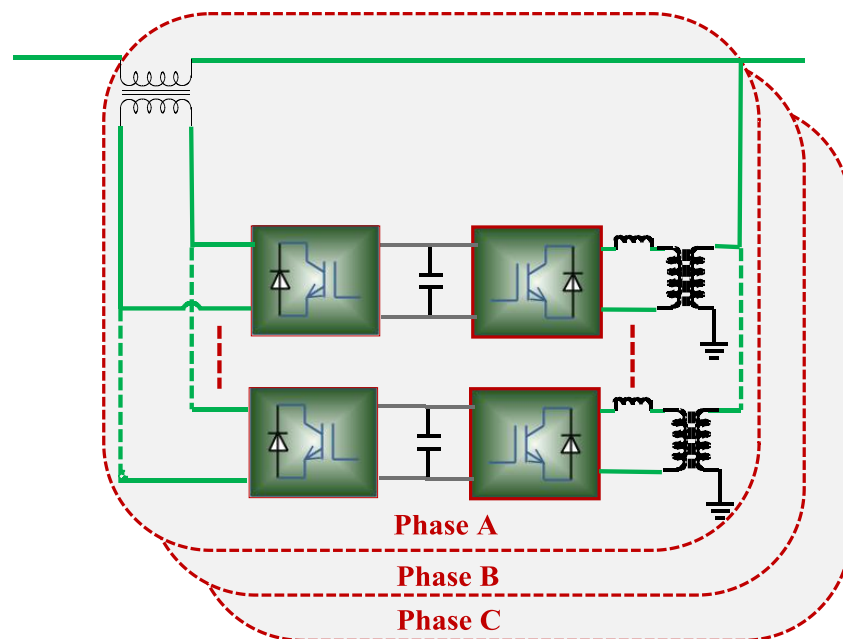
Fig 6.3 Modular approach of UPQC based on power cells

Table 6.1 Advantages and disadvantages of different capacity enhancement techniques

Type of UPQC	Advantages	Disadvantages
Multi-level Converter based	i. High voltage and current can be achieved ii. Can be developed in different ways – diode clamp / flying capacitor / cascade inverter based	i. Voltage unbalance could occur between the different levels ii. Requires excessive number of diode / flying capacitor / inverter iii. Central control is required and it is complicated iv. Conduction loss is high v. Capacity expansion is difficult vi. Centralized approach
Multi-modular transformer-less	i. No series transformer is required, thus reduces the cost ii. Capacity expansion is easier than multi-level converter iii. Redundancy is possible	i. It requires high number of switching devices to enhance the capacity ii. Central control is required iii. Conduction loss and switching loss also high iv. Due to symmetrical distribution of the load power among the H-bridge inverters, modules may not work at its maximum rating
Multi-modular (power cell)	i. power cell topology helps the unit to work at its maximum rating ii. Capacity expansion is easier iii. Redundancy is possible iv. Central and distributed controls are possible v. Conduction loss can be reduced	i. Number of H-bridge switching device increases, thus increase the switching loss ii. Transformer for each shunt part of the power cell could increase the loss as well as make the system bulky iii. Additional single shunt unit may not be included if compensating current increases

6.4 Distributed - UPQC (D-UPQC)

Capacity enhancement of UPQC can be achieved using multi-level or multi-module and central control mode. However, the flexibility of the UPQC to increase its capacity in future and to cope up with the increased load demand at a low voltage distribution level has not been achieved. Fig 6.4 shows the proposed configuration of a modular D-UPQC where a single unit of series APF_{se} and multiple units of shunt APF_{sh} are placed in a distributed approach. The connection between the series and shunt part of the UPQC is maintained through a DC link capacitor.

The main advantage of the proposed system is that the APF_{sh} units can be controlled to compensate (i) the reactive and harmonic current individually according to their capacity, or (ii) the combined reactive and harmonic current can be shared among the APF_{sh} units. Therefore, the installed APF_{sh} units can be switched on or the

additional APF$_{sh}$ units can be integrated into the D-UPQC system according to the requirement of the compensating current. Thus the capacity enhancement and flexibility of the proposed UPQC operation can be achieved. It is to be noted that, for any system, there is a limit up to which the capacity enhancement is possible. For the proposed D-UPQC, the capacity enhancement limit and the possible flexibility have been described in the design issues in section 6.4.1.
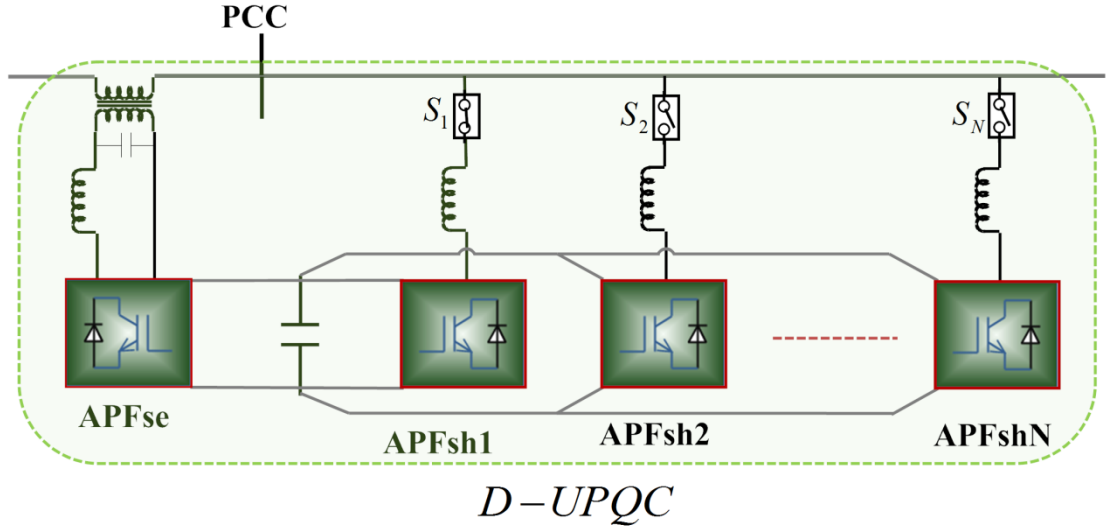
Fig 6.4 Configuration of the proposed Distributed UPQC (D-UPQC)

6.4.1 Design Issues

Fig 6.5 shows the working diagram of the proposed modular D-UPQC with electrical network and Fig 6.6 shows the equivalent electrical circuit of the system assuming that the reactive part of the load current will be compensated by the APF$_{sh1}$ and the harmonic part will be equally divided and compensated by the rest of the APF$_{sh}$ units. Here f, p, q and h represent the fundamental, active, reactive and harmonic part of the respective parameters. Fig 6.7 shows the tetrahedron diagram of the load current and it also reflects the amount and components of the load current that will be compensated by the APF$_{sh}$ units of the proposed D-UPQC. Thus the source will provide the active fundamental part of the load current in phase with the voltage to maintain the unity power factor at the PCC and the THD_{Ipcc} will be kept within the IEEE limit.
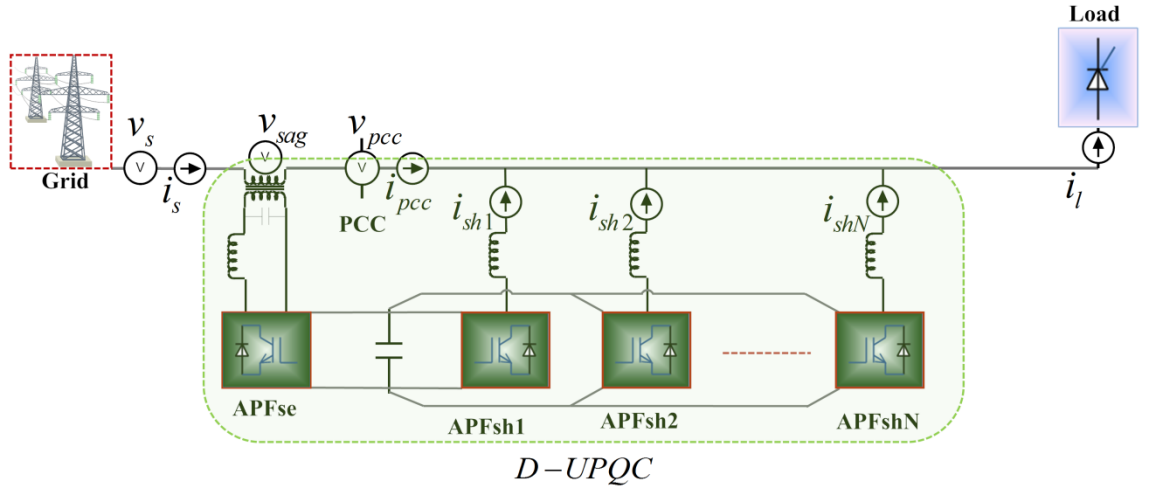
Fig 6.5 Working diagram of the D-UPQC with an electrical network
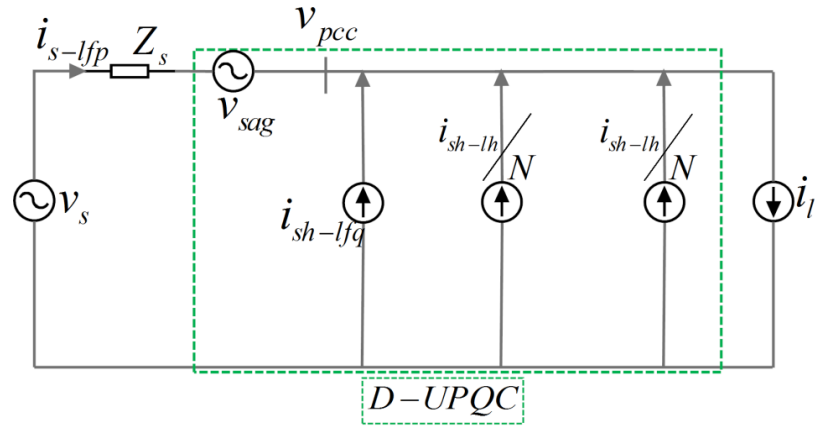
Fig 6.6 Equivalent electrical circuit of the system shown in Fig 7.5
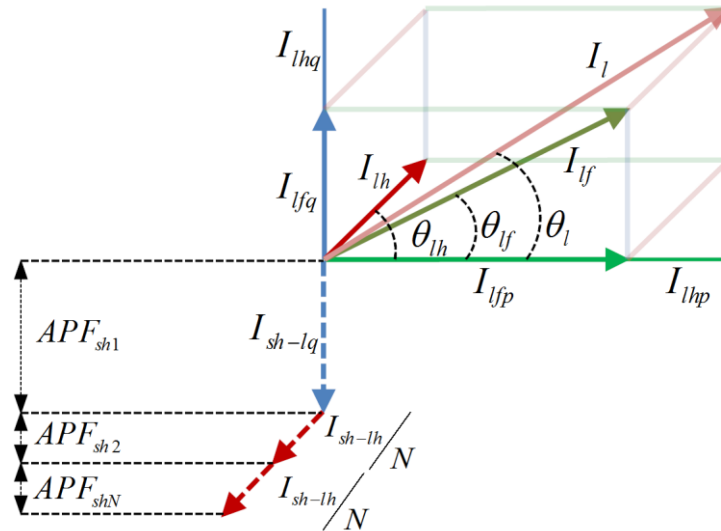
Fig 6.7 Tetrahedron diagram of the load current and the compensating part of the APF$_{sh}$ units

The integration of APF$_{sh}$ as a part of the possible capacity enhancement and achievable flexibility in operation of D-UPQC is mainly dependent on the rating of

APF$_{se}$ or the size of the series transformer. Therefore the design issues related to the APF$_{se}$ and APF$_{sh}$ are discussed below.

6.4.1.1 APF$_{se}$

Rating selection procedure of the APF$_{se}$ was already discussed in section 5.3.2 for a UPQC when it is integrated to a DG connected microgrid system. In general, the full load current flows through the series transformer of the APF$_{se}$ when APF$_{sh}$ is inactive. As the APF$_{sh}$ units compensate the reactive and harmonic part of the load current,, the minimum current rating of the APF$_{se}$ should be equal to the load active fundamental current (5.9), as shown in Fig 6.8. The voltage rating of the APF$_{se}$ should be equal to the highest value of the injected sag voltage (5.11). If k is the fraction of V_s that will appear as a voltage sag, then the required source current that will be transferred through the series transformer of the APF$_{se}$ (shown in Fig 5.6 and Fig 6.9) can be calculated as (5.15). This source current will be the current rating of APF$_{se}$ to compensate the k amount of voltage sag. Therefore,

$$I_{APFse} = I_s' = \frac{1}{(1-k)} I_{lfp} \tag{6.1}$$

$$V_{APFse} = kV_s \tag{6.2}$$

The current carrying capacity of the series transformer will be;

$$I_{Tr-se} = I_{APFse} + I_{loss} \tag{6.3}$$

where I_{loss} represents the amount of fundamental current that is required to maintain the operation of the UPQC. It is reflected as a P_{loss} in the control method. Therefore, this I_{Tr-se} will be the maximum rating for the APFse as shown in Fig 6.9. It also indicates the maximum limit of the active fundamental component of the load current that can be used in the network followed by the UPQC.

The sag compensation strategy by I_s' can create an additional VA loading effect on the APF$_{sh}$ control also [61]. This can be minimized by introducing a direct link between

the DC capacitor and the storage system (if the proposed D-UPQC is placed in a μGrid system), as discussed in 5.3.
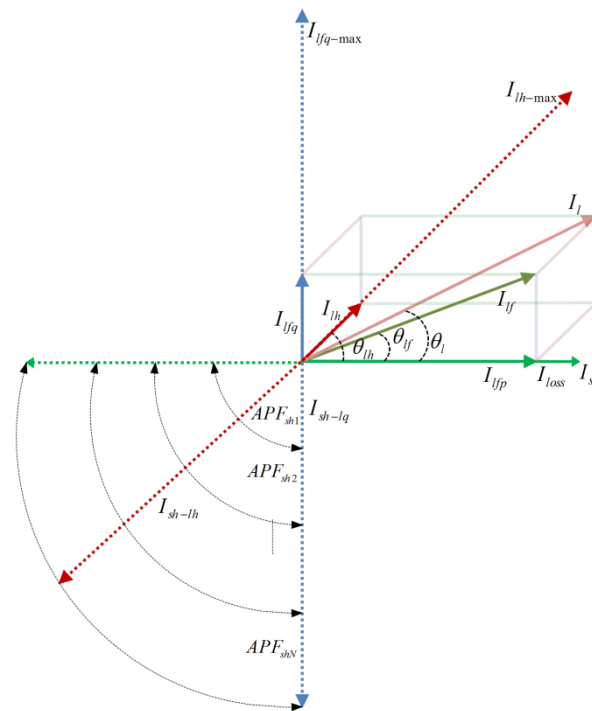
Fig 6.8 Compensating capacity of APF$_{sh}$ for the D-UPQC when $V_{sag} = 0$;
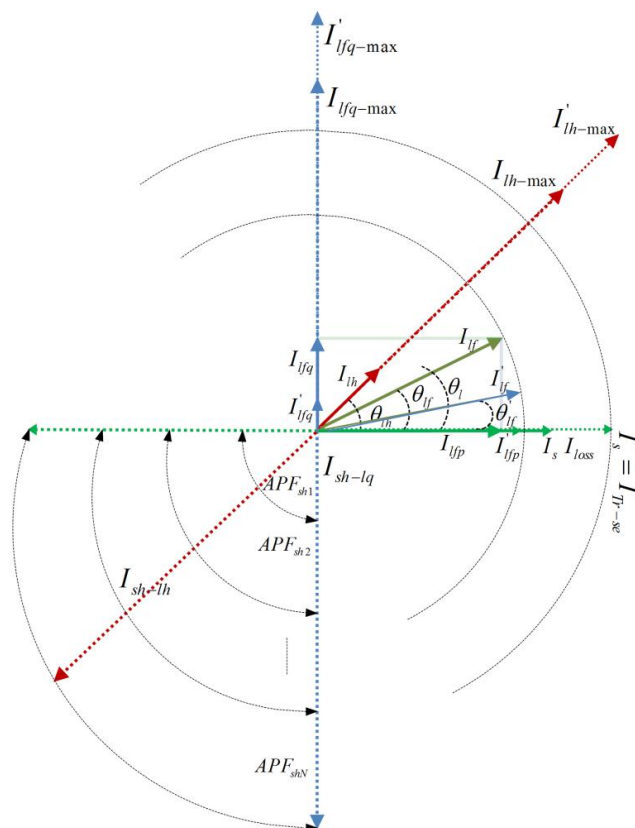
Fig 6.9 Compensating capacity of APF$_{sh}$ for the D-UPQC when $V_{sag} = kV_s$

6.4.1.2 APF_{sh}

According to the tetrahedron diagram of the load current shown in Fig 6.7.

$$I_l = \sqrt{I_{lp}^2 + I_{lq}^2} \; ; \text{here, } I_{lp} = I_{lfp} + I_{lhp} \text{ and } I_{lq} = I_{lfq} + I_{lhq}$$

$$I_{lf} = \sqrt{I_{lfp}^2 + I_{lfq}^2} \; ; \text{here, } I_{lfp} = I_{lf}\cos\theta_{lf} \text{ and } I_{lfq} = I_{lf}\sin\theta_{lf}$$

$$I_{lh} = \sqrt{I_{lhp}^2 + I_{lhq}^2}$$

In stable operating conditions, when no voltage sag appears in the network, the APF_{sh} units compensate the reactive and harmonic parts of the load current. According to Fig 6.7, the load current is composed of active, reactive and harmonic components. The source supplies the active load fundamental ($i_s = I_{lf}\cos\theta_{lf}$) and I_{loss} through the series transformer. Both the source and APF_{se} do not deal with the reactive and harmonic part of the load. Therefore, I_s and I_{APFse} are not directly related to the selection of maximum current rating of the APF_{sh} ($I_{lfq-max}$ and I_{lh-max}). The size of the series transformer actually imposes the limit of maximum I_{loss} that can be used for the operation of UPQC. The possible maximum I_{loss} can be found from (6.3) as;

$$I_{loss-max} = I_{Tr-se} \text{ while } I_{APFse} = 0$$

Again, the I_{loss} depends on the rating of APF_{sh} and can be related as;

$$I_{loss} = \alpha I_{APFsh}; \text{ where } \alpha \text{ is a fraction of } I_{APFsh}$$

Therefore, the possible $I_{APFsh-max}$ to integrate in the UPQC system and to compensate the reactive and harmonic components of the load current ($I_{lfq-max}$ and I_{lh-max}), as shown in the Fig 6.8 can be written as;

$$I_{APFsh-max} = \frac{1}{\alpha}I_{Tr-se}; \text{ while } I_{APFse} = 0 \tag{6.4}$$

This rating can further be increased when the UPQC will have the capacity of voltage sag compensation, as shown in Fig 6.9.

The flexibility can be achieved by integrating multiple APF$_{sh}$ units in the proposed D-UPQC system. Depending upon the control strategy, the APF$_{sh}$ units can be switched on and off to compensate the required current up to the maximum level. By turning off the additional APF$_{sh}$ units, the modular D-UPQC can avail of lower switching losses and retain high efficiency performance when the load VAR demands are low. For example, as shown in Fig 6.10, the load has been changed from I_{l1} to I_{l2} (where $I_{l2} = I_{l1}$; $I_{lfq2} > I_{lfq1}$; $I_{lfp1} > I_{lfp2}$ and $I_{lh2} > I_{lh1}$). Then, if the rating of APF$_{sh1}$ (I_{sh-lq1}) is smaller than the I_{lfq2}, APF$_{sh2}$ will be switched on. Similar approachs can be implemented for the harmonic current compensation separately or in combination with reactive compensation. These are mainly dependent on the implemented control strategy. Thus instead of design of a normal single unit UPQC, the proposed modular D-UPQC can be designed to maximize the efficiency. It will also work with a higher performance and reduced power loss.
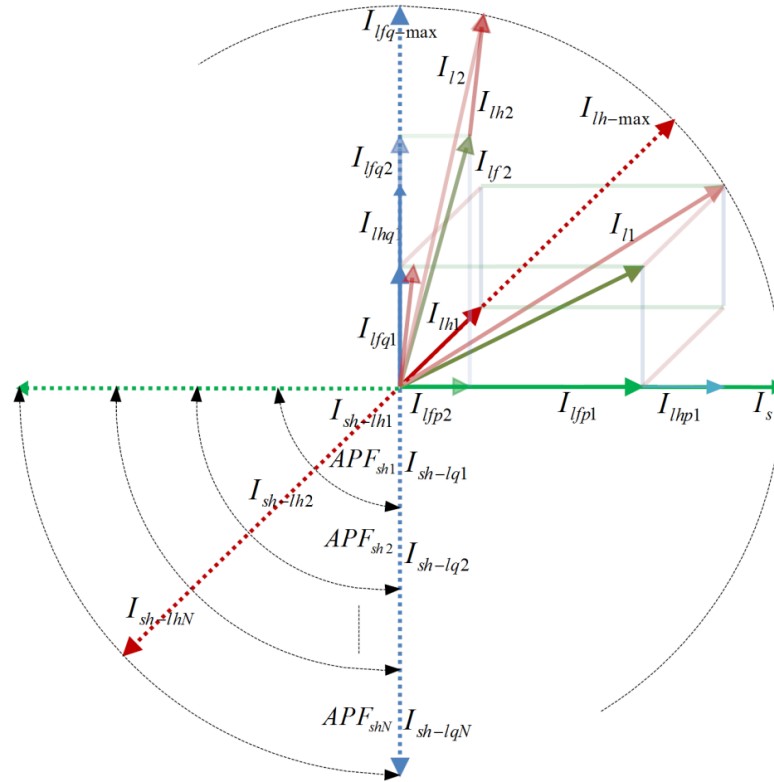
Fig 6.10 Compensating strategy of APF$_{sh}$ units for the D-UPQC

Therefore, in the case of a D-UPQC system, the current rating of the APF_{sh} units can be found as;

$$\sum_{N=1,2,3\ldots} I_{APFshN} = I_{lfq-max} = \frac{1}{\alpha} I_{Tr-se} \qquad (6.5)$$

While, $I_{lfp} = 0;\ I_{lfh} = 0;\ and\ V_{sag} = kV_s$

$$\sum_{N=1,2,3\ldots} I_{APFshN} = I_{lfh-max} = \frac{1}{\alpha} I_{Tr-se} \qquad (6.6)$$

While, $I_{lfp} = 0;\ I_{lfq} = 0;\ and\ V_{sag} = kV_s$

6.4.1.3 DC link Capacitor

In general, the energy handling capacity determines the size of the capacitor. The basics for the selection of capacitor size has already been described in sections 2.2.3.5 and 5.3.3. The size of the capacitor will increase when (i) the number of APF_{sh} units (or the reactive and harmonic current compensation capacity) increases and/or (ii) the required voltage sag compensation capacity is increased. If the proposed D-UPQC is placed in a DG connected μGrid network, the storage system of the μGrid can be connected directly to the DC link as discussed in 5.3.3. This will also reduce the control complexity of the UPQC.

6.4.2 Control issues

Like UPQC, the proposed D-UPQC also ha controllers for the APF_{se} and APF_{sh} units. The control of APF_{se} is the same as the normal UPQC and has already been discussed in 2.5.2 and 5.3.2. The control strategy for multiple parallel APF units has also been described in 4.6. For most of the control methods the APF units are controlled with a separate DC link capacitor. In the proposed D-UPQC, due to the DC link between the APF_{sh} units, a circulating current (CC) could flow among the filter units. Control of this flow can be part of the control of multiple APF_{sh} units with a common DC link. Therefore, the following sections will be discussed (i) the derivation model for

circulating current flow, (ii) the control issues for the circulating current flow, (ii) the selection of control method for APF$_{sh}$ units and (iv) the control of switches.

6.4.2.1 Model for circulating current (CC) flow

The working principle of an APF unit in parallel (shunt) to the load to compensate the reactive and harmonic current has already been discussed in section 2.2.1. Depending upon the switching condition, there are two possible modes of operation: capacitive mode (where the current flows from the capacitor) and inductive mode (the current flows towards the capacitor). During compensation, each APF unit completes one capacitive and one inductive mode of operation in a single switching cycle. When multiple APF units work in a current sharing mode, there could be four possible modes of operation: (i) capacitive-capacitive, (ii) inductive-inductive, (iii) capacitive-inductive and (iv) inductive-capacitive. As an example, Fig 6.11 shows a single line diagram of a 3-phase system where 2 APF units with a common dc link are working together in parallel operation mode. Here, i_{cc} represents the circulating current flow between the APF units. It is to be noted that, in the case of a 3-phase system this circulating current flow exists as a zero sequence harmonics in the zero sequence current flow when a circulating loop is created within the APF$_{sh}$ units and hence it is termed zero sequence circualting current (ZSCC) flow. In general these harmonics are (3+n*6) order, where n = 0, 1, 2 ....
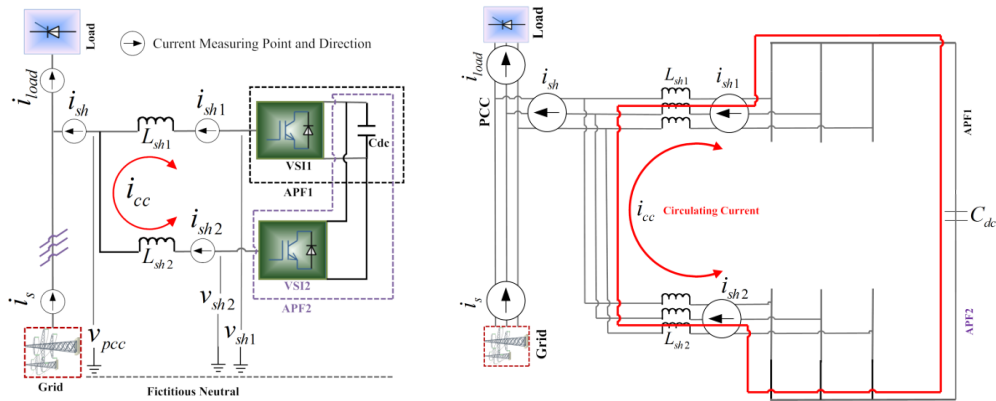
Fig 6.11 Single line diagram of a 3ph 2 units APF$_{sh}$ with common DC-link presenting CC flow

For simplicity, derivation of CC flow has been carried out on a per phase a basis. Fig 6.12 shows the possible mode of operation between the APF units (1 phase) where *sh-i* and *sh-c* represent the corresponding inductive and capacitive mode respectively. From Fig 6.12 (a and b), during the capacitive mode, the current flow can be obtained as;

$\frac{di_{sh-c}}{dt} = \frac{v_{sh-c} - v_{pcc}}{L_{sh1}||L_{sh2}}$ while $v_{sh-c1} = \delta_1 v_{dc} = v_{sh-c2} = (1 - \delta_2)v_{dc} = v_{sh-c}$; here δ is the ducy cycle, i.e, the 2 APF ac voltages are equal.

Similarly, Fig 6.12 (c and d) shows that when both the APF units work in inductive mode during its switching cycle, the resulting current flows can be found as;

$\frac{di_{sh-i}}{dt} = -\frac{v_{sh-i} + v_{pcc}}{L_{sh1}||L_{sh2}}$ while $v_{sh-i1} = (1 - \delta_1)v_{dc} = v_{sh-i2} = \delta_2 v_{dc} = v_{sh-i}$;

If there is a differnce in any of the parameters, such as switching frequency, current sharing, interfacing inductor, hysteresis band (in case of hysteresis current controller) then the APF units can operate in inductive-capacitive or capacitive-inductive mode. In these cases, CC will flow and these are reflected in Fig 6.12 (e - h). From Fig 6.12(e and f), the circulating current flow in capacitive-inductive mode can be obtained as;

$\frac{di_{cc-c}}{dt} = \frac{v_{cc-c}}{L_{sh1} + L_{sh2}} = \frac{v_{sh-c1} - v_{sh-i2}}{L_{sh1} + L_{sh2}} = \frac{(\delta_1 - \delta_2)v_{dc}}{L_{sh1} + L_{sh2}}$; while $v_{sh-c1} > v_{sh-i2}$

Similarly, the circulating current flow for inductive-capacitive mode is;

$\frac{di_{cc-i}}{dt} = \frac{v_{cc-i}}{L_{sh1} + L_{sh2}} = \frac{v_{sh-i1} - v_{sh-c2}}{L_{sh1} + L_{sh2}} = -\frac{(\delta_1 - \delta_2)v_{dc}}{L_{sh1} + L_{sh2}}$; while $v_{sh-i1} > v_{sh-c2}$

Therefore, in general, the equation for the CC flow can be written as;

$$\frac{di_{cc}}{dt} = \frac{\delta_{cc} v_{dc}}{L_{sh1} + L_{sh2}} \tag{6.7}$$

where $\delta_{cc} = \delta_1 - \delta_2$ for capacitive mode and $\delta_{cc} = \delta_2 - \delta_1$ for inductive mode.
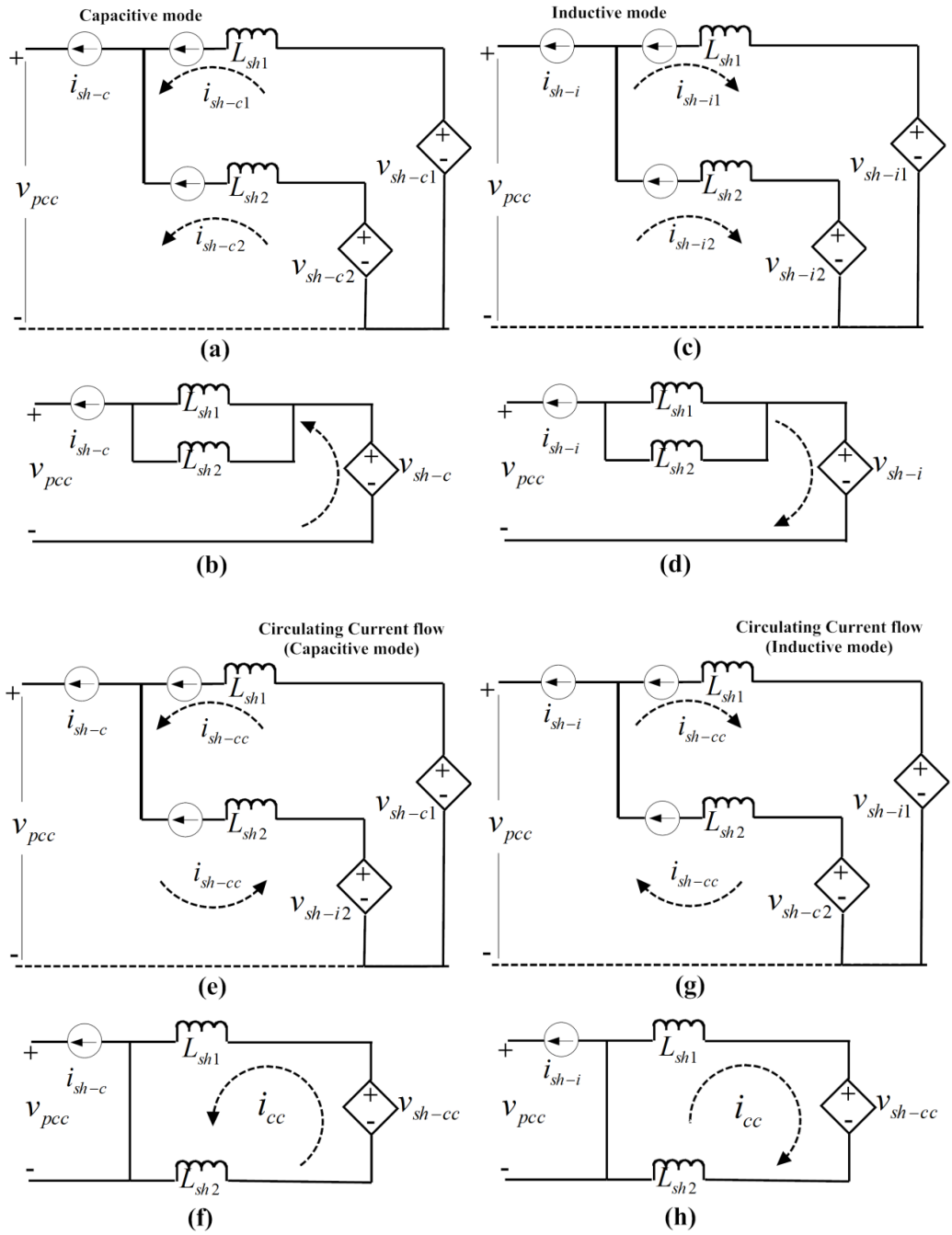
Fig 6.12 Possible mode of operation between two APF units to calculate circulating current

The possible maximum value for CC can be obtained as;

$$I_{cc-max} = \frac{V_{dc}}{L_{sh1} + L_{sh2}} \quad (6.8)$$

For 3-phase system, the ZSCC can be found as;

$$ZSCC = i_{sh1-zs} \sim i_{sh2-zs} \quad (6.9)$$

where i_{sh1-zs} and i_{sh2-zs} are the zero sequence component of the APF$_{sh}$ units.

This is also confirmed in [182] for shunt APF topology analysis based on a parallel interleaved inverter. It is also similar to the rectifier analysis in [90].

In most of the research articles, derivation or CC cancellation has been carried out for two inverters or APF units [90, 104, 182, 183]. But none of these discuss the cases when more than 2 APF/inverter units are integrated. Based on the previous analysis, it can be shown that if more than 2 APF units are connected in parallel then the additional units will work in either capacitive or inductive mode also and will be parallel to any of the other units as shown in Fig 6.13. In these cases additional circulating current flow loops will form. The CC flow for these loops can also be derived in similar way as found in (6.7).

Moreover, the control methods discussed in the literature are mainly for PWM based control system. None of them discuss the CC flow issues for the parallel operation of APFs based on hysteresis control. Therefore, an attempt has been made here to discuss the issues related to hysteresis control.
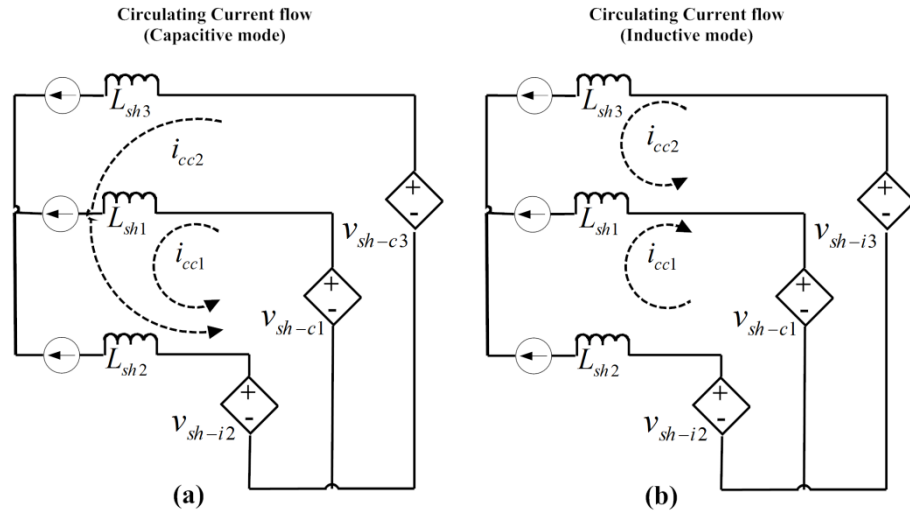
Fig 6.13 Circulating current flow when 3 APF units work in parallel

6.4.2.2 Control issues for the circulating current (CC) flow

There are mainly two ways to eliminate or reduce the CC flow: (i) breaking the route of CC flow by introducing physical devices such as an isolation transformer or common mode inductor or (ii) by proper control methods. These are reviewed in section 4.2. From the derivation of CC flow it is found that the CC value depends on (i) the duty cycle (δ) or switching frequency (f_{sw}), DC link voltage (V_{dc}) and the interfacing inductor (L_{sh}) of the APF units. Therefore, before going to select the control method for multiple APF$_{sh}$ units with a common dc link, some design consideration should be made to reduce the CC flow. The design options that can be implemented to reduce the CC flow are;

i. Decrease the V_{dc}: According to the design criteria of single/3-phase APF$_{sh}$ system there is a minimum value of V_{dc} that has to be maintained to compensate the reactive and harmonic current.

ii. As the $\delta = \frac{\tau}{T} = \tau f_{sw}$, reduce the f_{sw} and decreasing the difference between the f_{sw} or δ will reduce CC flow.

iii. Reduced f_{sw} will further increase the L_{sh} (in the case of hysteresis current control) and it will then in turn reduce the circulating current flow. But increased L_{sh} will reduce the VAR rating of APFsh.

It is also clear from the derivation that the CC flow does not directly depend on the compensating current rating of the APF$_{sh}$ units. Therefore, once the current or VAR rating of APF$_{sh}$ is fixed, the design components (f_{sw} and L_{sh}) should be chosen in such a way so that the L_{sh} is possibly high and the f_{sw} difference between the APF$_{sh}$ units are as low as possible. In that case, introducing the common mode inductor in the APF$_{sh}$ units can be a better choice. Implementation of a CC control method in the APF$_{sh}$ control strategy will further reduce the CC flow. But it will then increase the control complexity.

6.4.2.3 Selection of control method for APF$_{sh}$ units

With the control issues of the CC flow in mind, selection of a control strategy for the APF$_{sh}$ units should be made. Different control strategies for parallel operation of multiple APF units were reviewed in section 4.6. In general, control can be based on active current sharing where the compensating power/current can be divided equally or up to the compensating capacity of the APF units. Another prominent control is droop control where information exchange between the APF units is required. For simplicity, a current sharing (power splitting) method based on hysteresis current control has been chosen for the remainder of the analysis.

6.4.2.4 Control of switches

The control of switches mainly depends on the control method for the APF units. In the case of the current sharing method, the switching can be determined by current sharing (equally distributed) or a capacity limitation technique. As for example, if I_{sh}, I_{sh-ref}, $I_{APFsh-rated}$ and I_{sw-ref} are the rms values of APF compensating current, reference compensating current, rated current and the switching reference current for ON/OFF condition, then,

$I_{sh} \leq I_{sw-ref}$ for thecurrent sharing technique where $I_{sw-ref} = {I_{sh-ref}}/{N}$ and

$I_{sh} \leq I_{APFsh-rated}$ for the capacity limitation technique

6.4.3 Simulation Study

An electrical power system including D-UPQC, as shown in Fig 6.5, has been modelled in MATLAB using RT-LAB (real-time simulation) tools to observe the performance in the real-time environment. Within the available facilities, the proposed system is then partially tested in SIL with the hardware synchronization mode which is similar to hardware-in-loop (HIL) test.

In depth information on parallel operation of multiple APF$_{sh}$ based on hysteresis current controller is not available yet, specially in the case of CC flow. Therefore, in the present work, the objective is to reduce the CC flow based on the design options mentioned in 6.4.2.2. Two units of APF$_{sh}$ have been modelled here to operate in power sharing mode. In terms of sharing following proportions have been chosen:

(A) $I_{APFsh1} = I_{APFsh2} = 0.5 * I_{lqh-max}$ and $I_{lqh-max} = 100A$; each APF$_{sh}$ compensates half of the load reactive and harmonic components.

(B) $I_{APFsh1} = 0.75 * I_{lqh-max}$; $I_{APFsh2} = 0.25 * I_{lqh-max}$ and $I_{lqh-max} = 100A$;

(C) $I_{APFsh1} = 0.6 * I_{lqh-max}$; $I_{APFsh2} = 0.4 * I_{lqh-max}$; and $I_{lqh-max} = 100A$

(D) $I_{APFsh1} = 0.6 * I_{lqh-max}$; $I_{APFsh2} = 0.4 * I_{lqh-max}$; and $I_{lqh-max} = 200A$

In the case of a hysteresis current control based APF$_{sh}$, according to the selection of design parameters for APF$_{sh}$, described in 2.2.3 and the control issues of CC flow, the CC flow can be reduced by the proper selection of the design components including f_{sw}, L_{sh}, h and V_{dc}. As the V_{dc} is fixed, variation of other components has been made here to analyze the reduction of CC flow. Results and discussion are given below.

Table 6.2 shows the parameters that have been considered for the proportion A. Corresponding results have been given in Fig 6.14 and discussed below.

Table 6.2 A: $I_{APFsh1} = I_{APFsh2} = 0.5 * I_{lqh-max}$ and $I_{lqh-max} = 100A$

Frequency (kHz)	Cases	L_{sh1} / L_{sh2} (mH)	h1 / h2 (A)	THD@I_{pcc} (%)
$f_{sw1} = 17.3$	A1	0.625 / 0.625	5 / 5	2.57
$f_{sw2} = 17.3$	A2	1.25 / 1.25	2.5 / 2.5	2.02
	A3	1.25 / 0.625	2.5 / 5	1.74
$f_{sw1} = 17.3$	A4	1.25 / 1.25	2.5 / 3.75	1.67
$f_{sw2} = 11.6$	A5	1.25 / 1.875	2.5 / 2.5	2.35
$f_{sw1} = 13.0$	A6	1.67 / 0.625	2.5 / 5	2.88
$f_{sw2} = 11.6$	A7	1.67 / 1.25	2.5 / 3.75	2.82
	A8	1.67 / 1.875	2.5 / 2.5	3.76
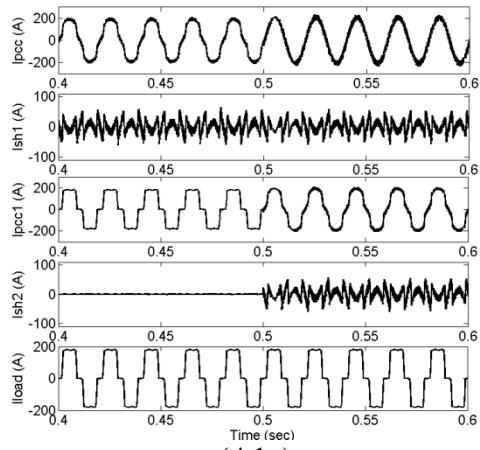
(A1a)
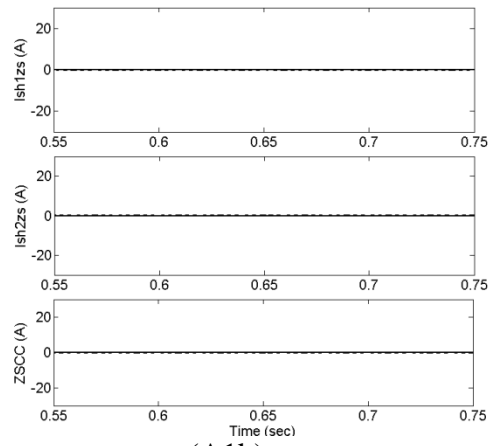
(A1b)
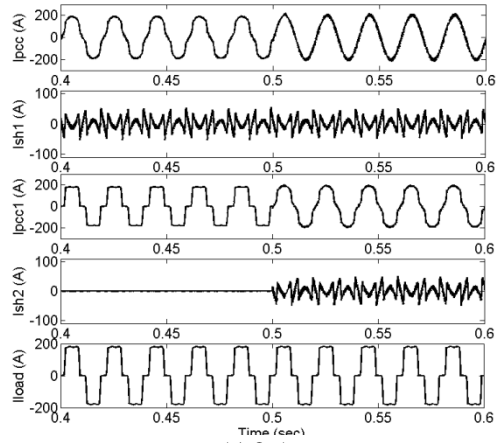
(A2a)

(A2b)

(A3a)

(A3b)

(A4a)

(A4b)

188
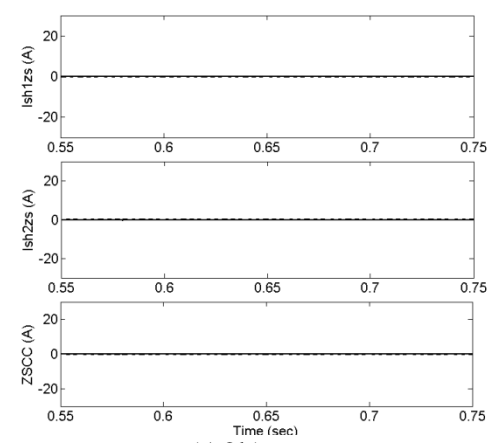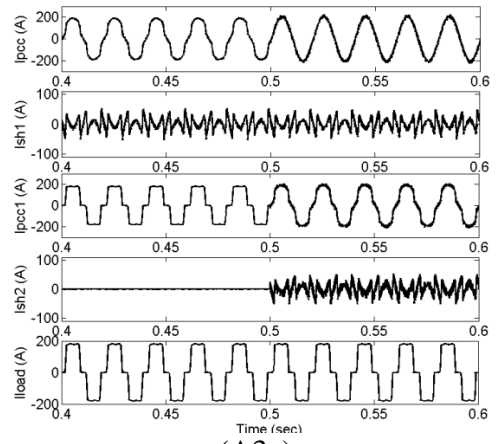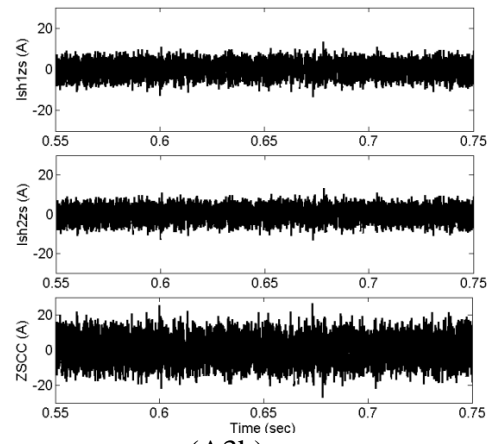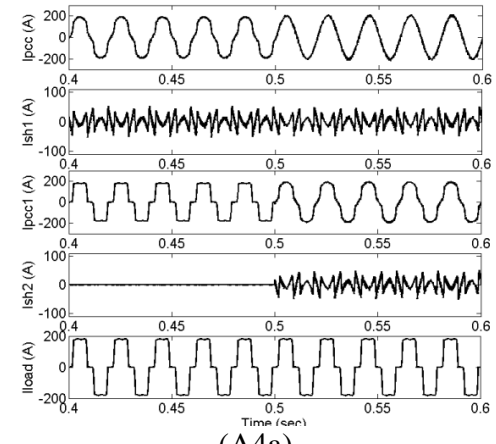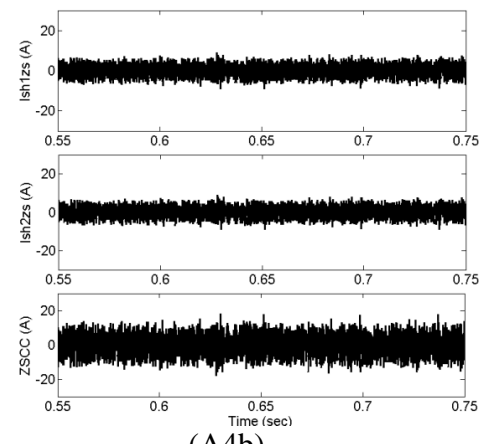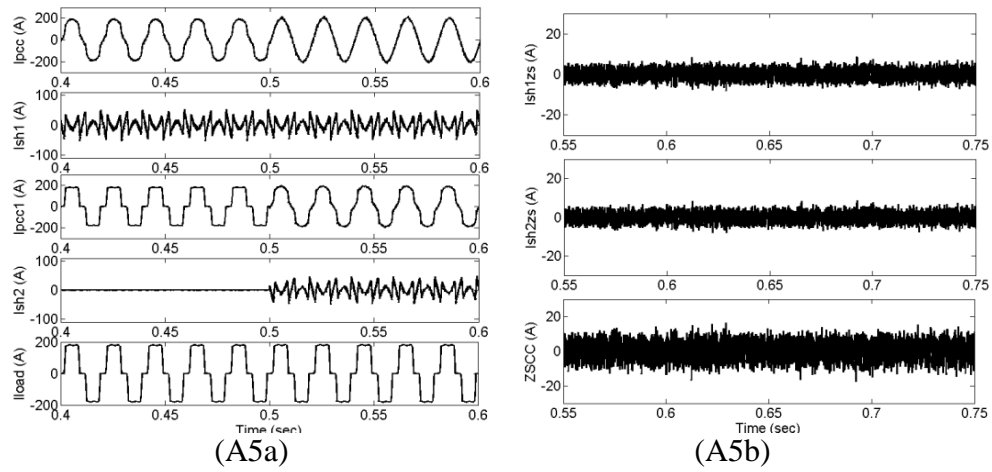
Fig 6.14 Performance of APF$_{sh}$ for the cases (A1 - A5) and the corresponding CC flow

Fig 6.14 shows the performance study of the two APF$_{sh}$ units in power sharing mode for the cases (A1 - A5) where each of the units compensates half of the load reactive and harmonic components. For the cases (A1-A3), the switching frequency of both units was equal and the variations have been made for L_{sh} and h. Cases A1 and A2 show that the possible CC flow can be zero when $L_{sh1} = L_{sh2}$ and $h1 = h2$, i.e, both the APF$_{sh}$ units are identical. Although the rating and f_{sw} of each unit are the same, ZSCC can flow as shown in case A3. This happens due to the difference in design parameters L_{sh} and h. Cases A4 and A5 shows the results for different f_{sw}, L_{sh} and h. For both the cases, ZSCC flows. A comparison with A3, A4 and A5, A5 shows better results in the reduction of ZSCC flow. It is due to the higher values of L_{sh} and lower values of h, though the parameter f_{sw} is different.

Table 6.3 shows the parameters that have been considered for the proportion B. Corresponding results have been given in Fig 6.15 and discussed below.

Table 6.3 B: $I_{APFsh1} = 0.75 * I_{lqh-max}$; $I_{APFsh2} = 0.25 * I_{lqh-max}$ and $I_{lqh-max} = 100A$

Frequency (kHz)	Cases	L_{sh1} / L_{sh2} (mH)	H1 / h2 (A)	THD@I_{pcc} (%)
$f_{sw1} = 17.3$ $f_{sw2} = 17.3$	B1	0.835 / 2.5	3.75 / 1.25	1.74
	B2	0.418 / 1.25	7.5 / 2.5	1.81
	B3	0.835 / 1.25	3.75 / 2.5	2.25
$f_{sw1} = 17.3$ $f_{sw2} = 11.6$	B4	0.835 / 1.87	3.75 / 2.5	2.25
	B5	0.835 / 3.74	3.75 / 1.25	2.33
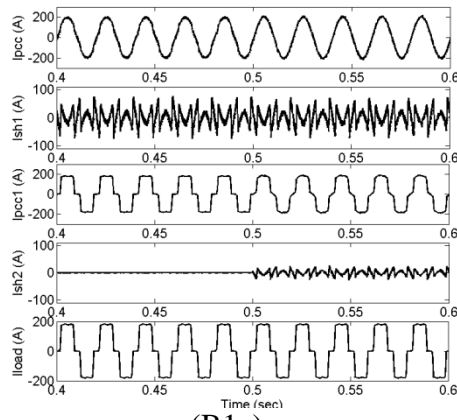
(B1a)
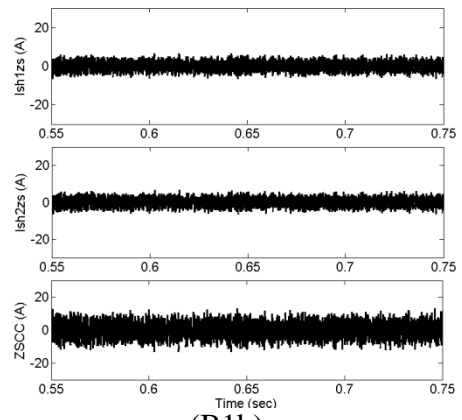
(B1b)
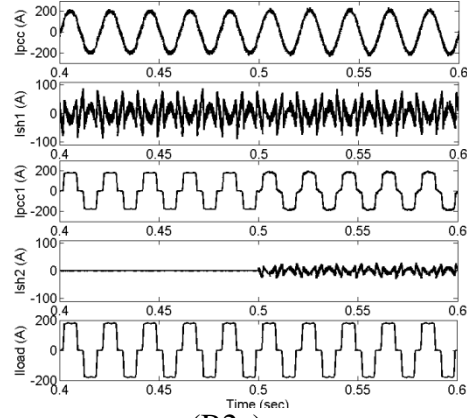
(B2a)

(B2b)

(B3a)

(B3b)

(B4a)

(B4b)
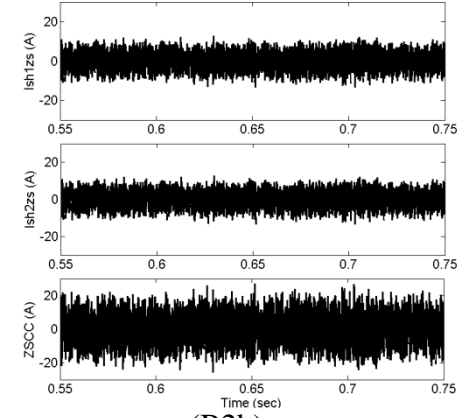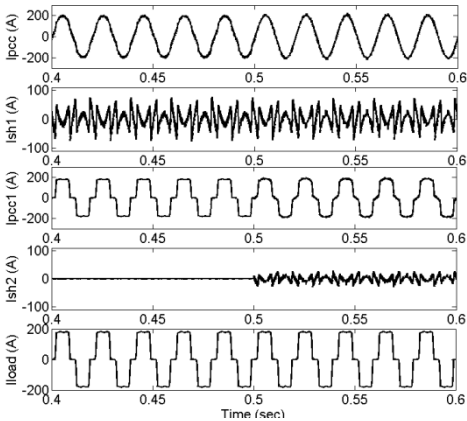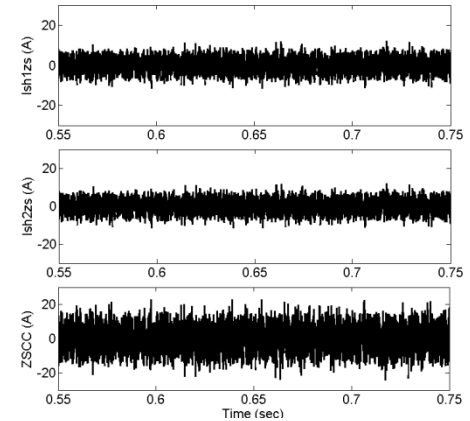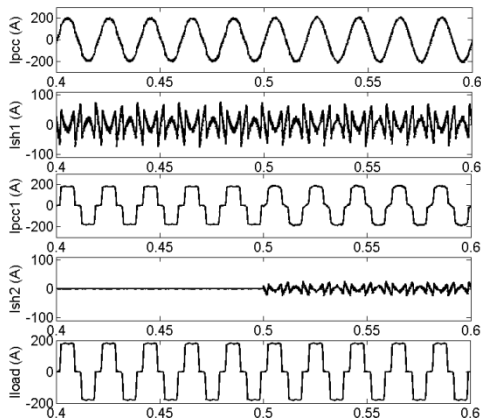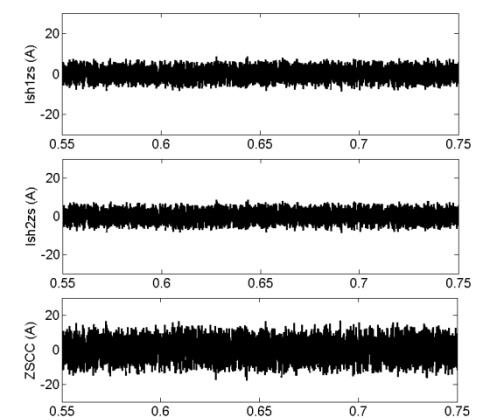
(B5a)   (B5b)
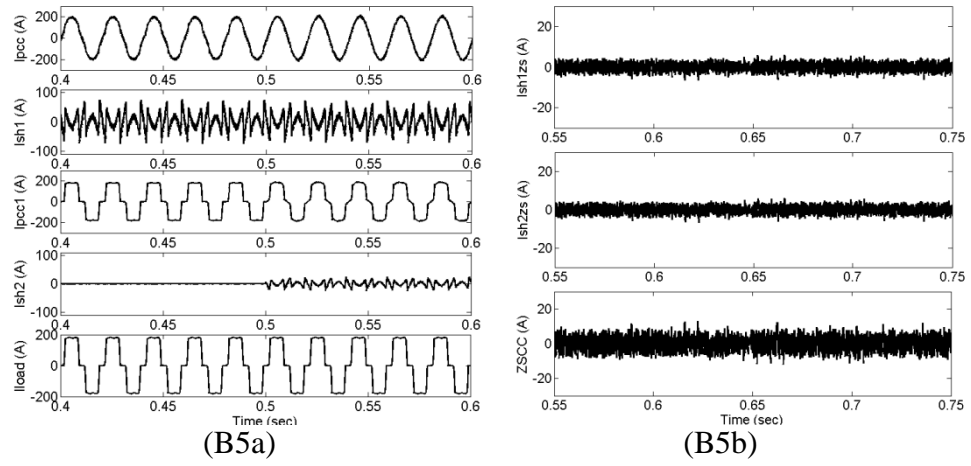
Fig 6.15 Performance of APF$_{sh}$ for the cases (B1 - B5) and the corresponding CC flow

Fig 6.15 shows that for all the cases, ZSCC flows. Even though the f_{sw} values are different, the reduced ZSCC flow occurs in the case of B5 where the values for L_{sh} are high and h are low compare to other cases. The worse case occurs for B2 where L_{sh} is low and h is high.

Tables 6.4 and 6.5 show the parameters for the cases C and D where the sharing proportion is different than that for A and B. For both the cases, values of L_{sh} are kept low wheres the values for h are high. In both cases, f_{sw} are the same. And the same components has been chosen for D where the compensating current is two times higher than that of case C.

Table 6.4 C: $I_{APFsh1} = 0.6 * I_{lqh-max}$; $I_{APFsh2} = 0.4 * I_{lqh-max}$; and $I_{lqh-max} = 100A$

Frequency (kHz)	Cases	L_{sh1} / L_{sh2} (mH)	H1 / h2 (A)	THD@I_{pcc} (%)
$f_{sw1} = 17.3$ $f_{sw2} = 17.3$	C1	0.625 / 0.625	5 / 5	2.65

Table 6.5 D: $I_{APFsh1} = 0.6 * I_{lqh-max}$; $I_{APFsh2} = 0.4 * I_{lqh-max}$; and $I_{lqh-max} = 200A$

Frequency (kHz)	Cases	L_{sh1} / L_{sh2} (mH)	H1 / h2 (A)	THD@I_{pcc} (%)
$f_{sw1} = 17.3$ $f_{sw2} = 17.3$	D1	0.625 / 0.625	5 / 5	2.12

Fig 6.16 shows the performances for the cases of C and D in terms of ZSCC flow. In both cases, ZSCC flow is the same even though for case D, APF$_{sh}$ units are compensating higher current than that of C. These results indicate that the ZSCC flow does not depends on the amount of compensating current. These ZSCC flows are higher than that for A and B and this is due to the lower values of L_{sh}.

(C1)   (D1)
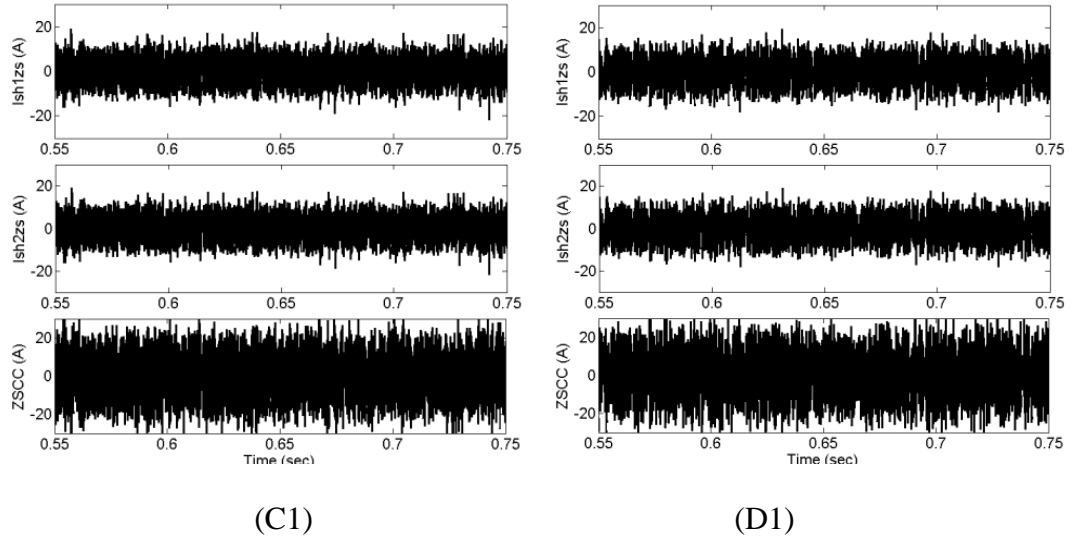
Fig 6.16 CC flow for the cases C and D

Finally, a comparison has been made for the ZSCC between the (A3 - A5) and (A6 - A8) cases, as shown in Fig 6.17. For A3, the f_{sw} is the same for both APF$_{sh}$ units, whereas for A4 and A5 it is different. But the values of L_{sh} are comparatively higher for A5. Therefore, within A3 to A5, the ZSCC flow is comparatively lower in the case of A5, as shown in Fig 6.17(a).

For the cases A6 - A8, the switching frequency (f_{sw1}) of APF$_{sh1}$ is reduced and therefore the value of L_{sh} increases. At the same time, the frequency difference between APF$_{sh}$ units are also reduced. The performance of the D-UPQC in terms of ZSCC flow for these cases is reflected in Fig 6.17(b). This shows that ZSCC flow can further be reduced by reducing the f_{sw} (to increase the value of L_{sh}) and the difference between the f_{sw} of the APF$_{sh}$ units. The reduction of zero sequence harmonics content for the cases (A6 - A8) are also shown in Fig 6.18 where it shows that the magnitude of zero

sequence harmonics is reduced gradually for the cases from A6 to A8. This also confirms the outcome as shown in Fig 6.17.
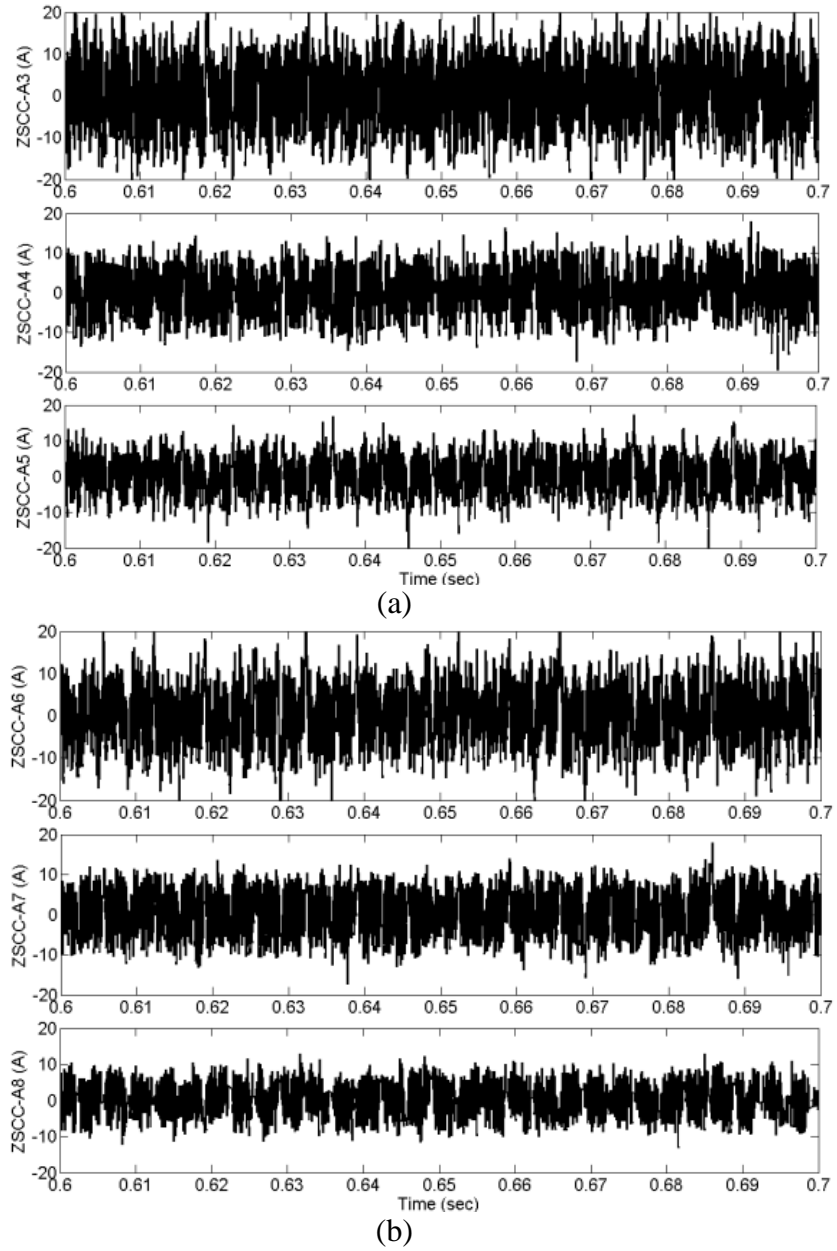
Fig 6.17 ZSCC comparison between the cases for (a) A3, A4, A5 and for (b) A6, A7, A8

But it also has to be kept in mind that increasing L_{sh} could increase the active power loss of the APF$_{sh}$ units (as discussed in Chapter 2, section 2.6) as well as increase the THD at the PCC, as given in Table 6.2. Therefore, in terms of design criteria for the selection of APF$_{sh}$ units to place in a D-UPQC system, one should consider the higher values of L_{sh} and lower the difference between f_{sw} of the APF$_{sh}$ units with care about THD.
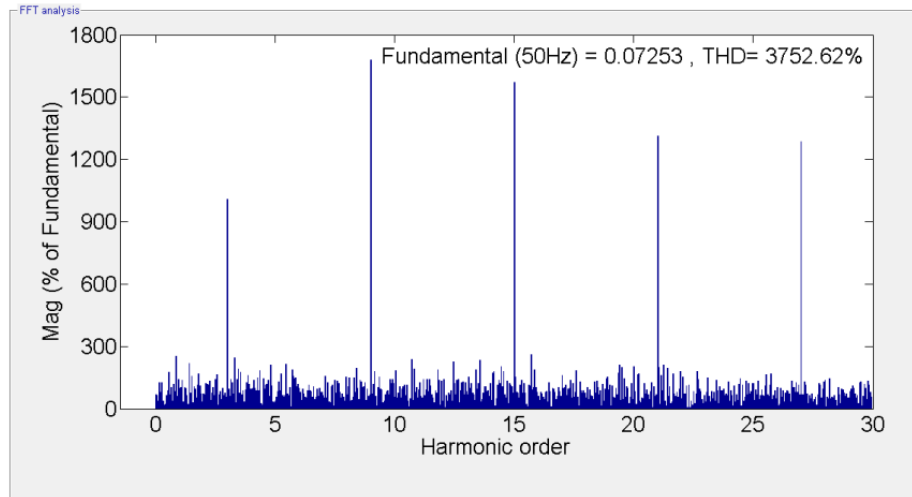
(a)
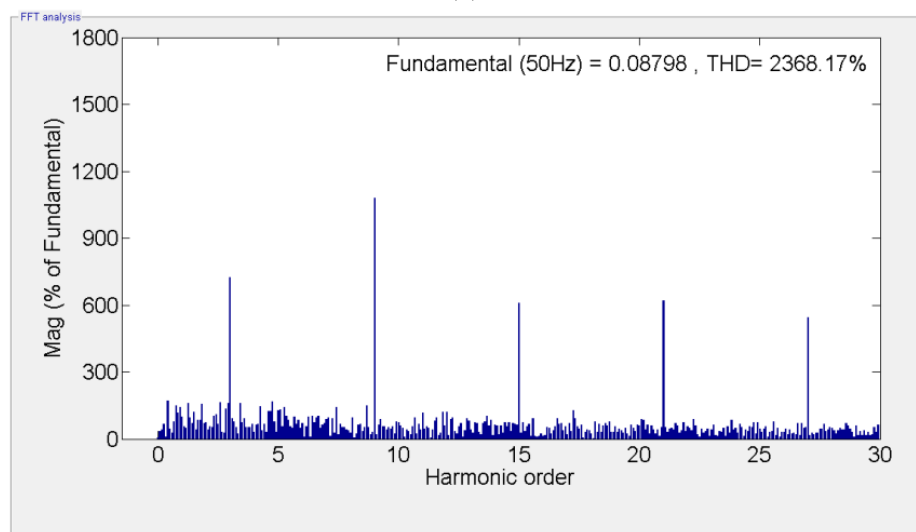
(b)
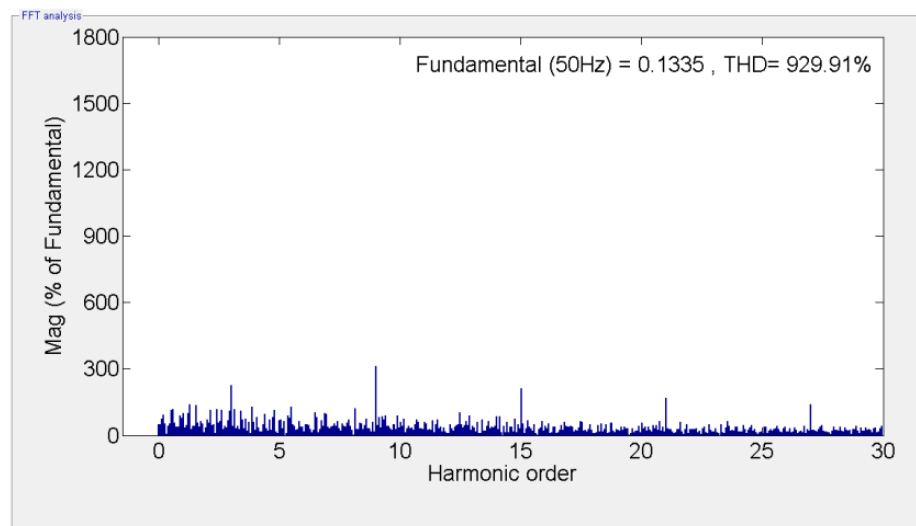
(c)

Fig 6.18 FFT analysis for the cases (a) A6, (b) A7 and (c) A8.

6.4.4 Hardware Results

Real-time tests have been performed for some of the analysis in SIL configuration (hardware synchronization mode). Fig 6.19 shows the results for the cases A6, A7 and A8 where both the APF_{sh} units are compensating harmonic current in a power sharing mode. The waveform of the utility current (i_s) contains fewer harmonics for A7 compared to A6 and A8. This happens because of the moderate value of L_{sh} and h for A7 compared to that of A6 (L_{sh} is too low) and A8 (L_{sh} is too high). Therefore, the THD value is also reduced.

For the case of A8, although the THD increases, ZSCC is reduced. Fig 6.20 shows the ZSCC flow for these (A6 - A8) cases and it clearly depicts the gradual reduction of ZSCC from A6 to A8. It is also clear from Fig 6.20 that a considerable amount of ZSCC can be reduced by proper selection of design parameters for the APF_{sh} units to operate in load sharing mode. Thus it validates the simulation, analysis of the performance and ZSCC flow study.

6.5 Conclusion

Capacity enhancement and operation flexibility are two of the important limitations of the centralized UPQC unit when placed in a DG integrated network, especially in the low voltage distribution level where the compensating current could be high. Therefore, a proposal has been made here to develop the modular based Distributed UPQC (D-UPQC) where multiple APF_{sh} units can operate in parallel. This can be controlled in an active load sharing mode (inter-communication is required) or in droop control mode. The most important part is common the DC link between the APF units. Therefore, a circulating current could flow. In the case of a hysteresis current controller based multiple APF_{sh} units in load sharing mode, this CC control is not yet achieved. One of the difficulties of this CC flow control or reduction is the variable

switching frequency of the APF$_{sh}$ units. By proper selection of design parameters, this CC flow can be reduced in an acceptable level.
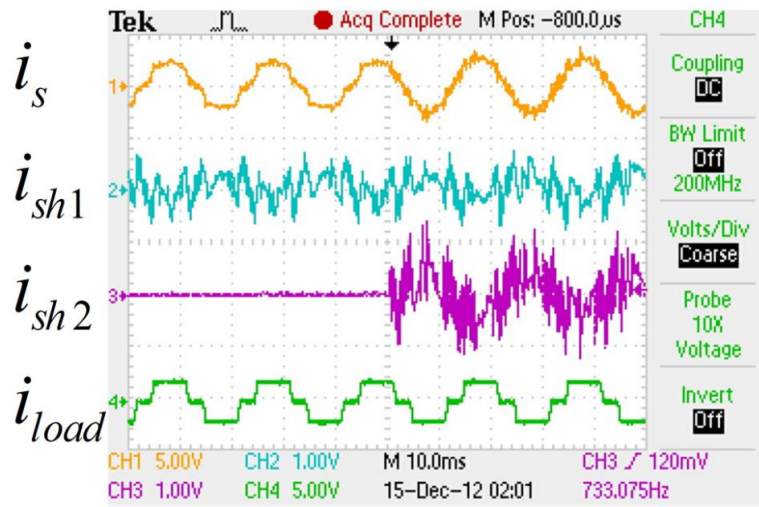
(a)
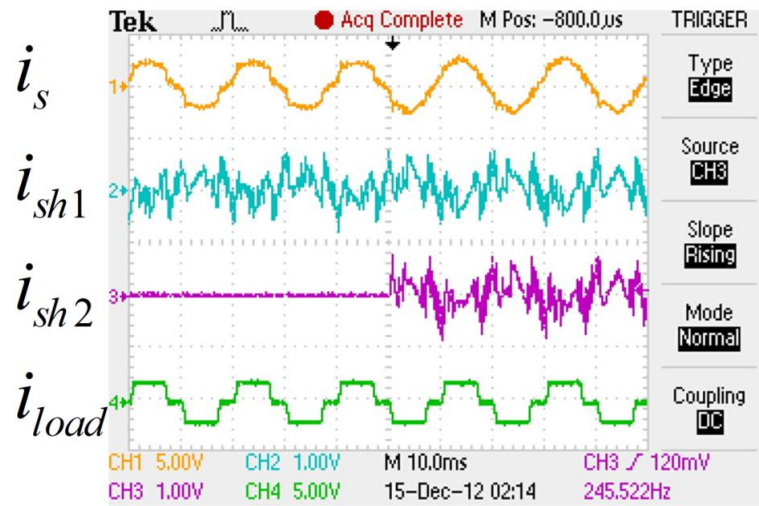
(b)
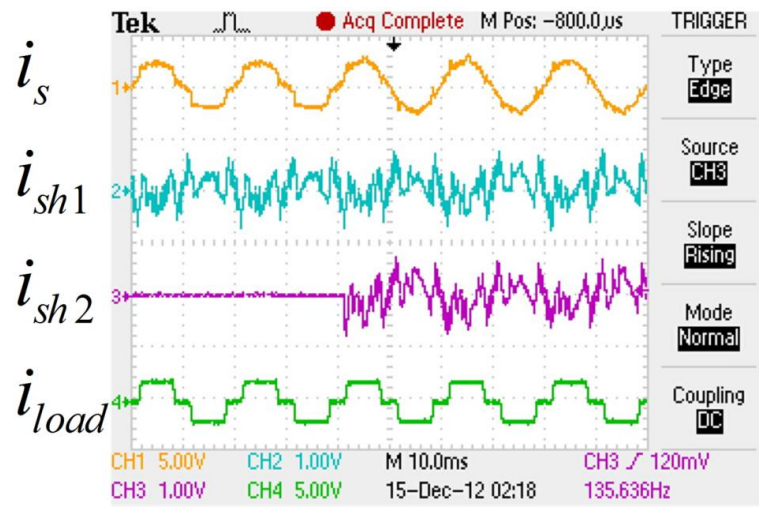
(c)

Fig 6.19 Performance of APFsh units in D-UPQC for the cases (a) A6, (b) A7 and (c) A8

196
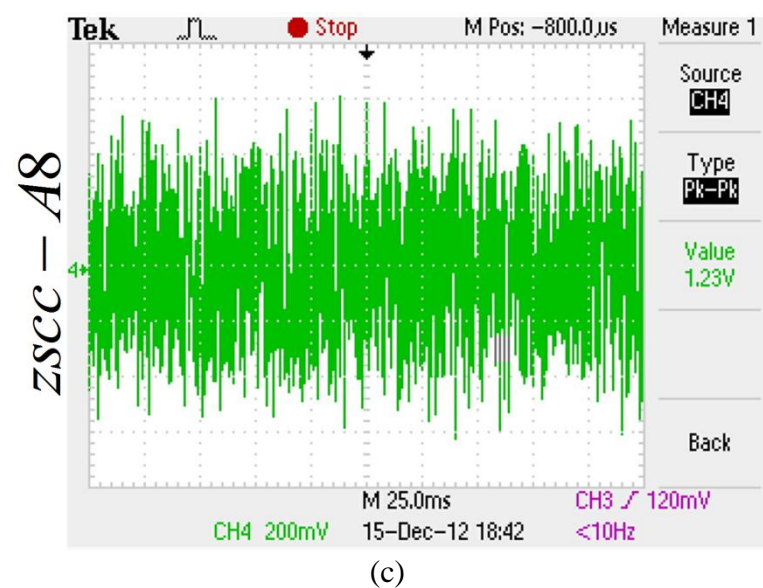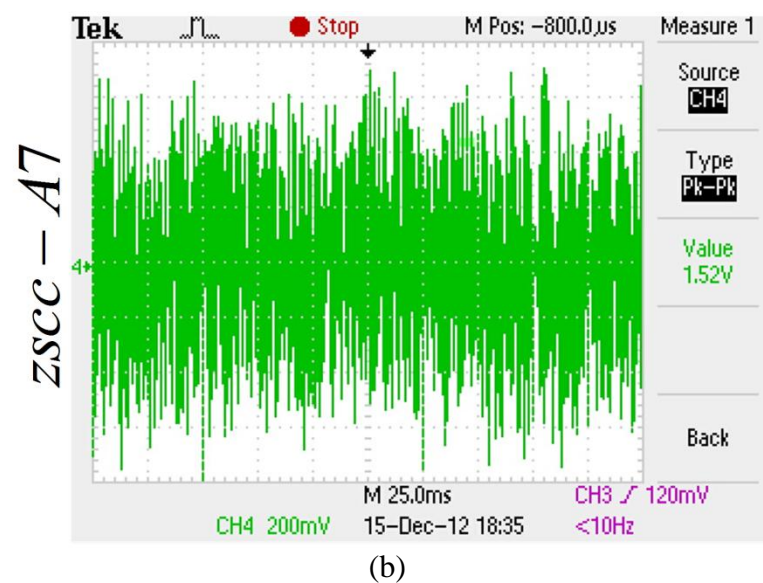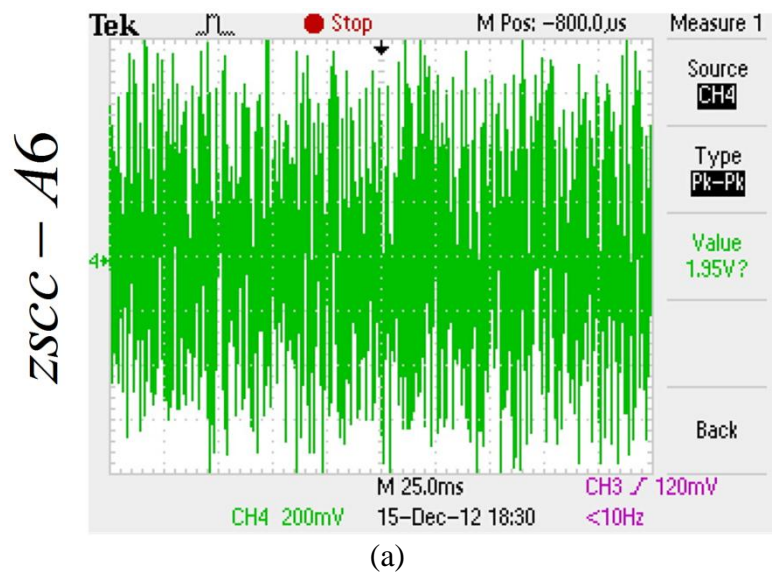
Fig 6.20 ZSCC flow for the cases of (a) A6, (b) A7 and (c) A8

Chapter 7

Conclusions and Future Work

7.1 **Conclusions**

The main objective of this research was to investigate the (i) placement (ii) integration (iii) capacity enhancement and (iv) real time control of the Unified Power Quality Conditioner (UPQC) to improve the power quality (PQ) of a distributed generation (DG) network connected to the grid or microgrid. The following developments have been achieved through this PhD research.

With the increased penetration of small scale renewable energy sources in the electrical distribution network, maintaining or improvement of power quality has become more critical than ever where the level of voltage and current harmonics or disturbances can vary widely. For this reason, Custom Power Devices (CPDs) such as the Unified Power Quality Conditioner (UPQC) can be the most appropriate solution for the dynamic performances of the distribution network, where prior knowledge of disturbances may not be accurately known. The UPQC is introduced at the PCC (a) to prevent propagation of the current harmonics generated by the non-linear loads into the grid, (b) to maintain the voltage and current THD at the PCC within the IEEE and IEC limits and (c) compensate the grid voltage sag/swell to provide a balanced and stable voltage at the PCC. In the presence of DG sources and the UPQC in an active distribution network, (A) the placement of UPQC and its sensors in the network, (B) its impact on the control method to perform the specified task, (C) its performance with bi-

directional power flow in the network and (D) the advantages of DG inverter in the presence of UPQC issues have been analysed. Depending on the location and integration technique of DG sources, the proper placement of UPQC has been identified in the DG integrated grid connected microgrid network together with the feedback sensors to cope with the bidirectional power flow without compromising the power quality controlling features.

A new integration method of UPQC has been developed that can help the DGs to deliver quality power in the case of islanding. It can also help to reintegrate with the grid seamlessly post fault. In the proposed new integration method, the DG Inverter (with or without storage) and the load and shunt part of the UPQC have been placed at or after the PCC and in parallel to the grid. The series part of the UPQC have been placed before the PCC and in series with the grid. Islanding detection and reconnection techniques together with the associated control have been introduced to the existing UPQC. Hence, this configuration is termed UPQC$_{\mu G}$. The control function has been performed with a hierarchical approach. The control method for islanding detection and reconnection is placed in the secondary level. Thus the additional control part can be placed in a conventional UPQC to improve its performance to a UPQC$_{\mu G}$. The advantages of the proposed UPQC$_{\mu G}$ configuration and associated integration system over the normal UPQC are to compensate voltage interruptions in addition to voltage sags/swells, and harmonic and reactive power compensation in the interconnected mode. The DG Inverter with storage then supplies the active fundamental power only and the shunt part of the UPQC compensates the reactive and harmonic power of the load in islanding mode. Therefore, the integrated system works both in interconnected and islanded mode. The other advantage is that the DG Inverter is not required to be disconnected during islanded mode and hence the islanding detection and reconnection need no longer be a part of the inverter. In all conditions, DG Inverter only provides the

active power to the load and grid. Thus it reduces the control complexity of the DG inverter as well as improving the PQ of the microgrid.

In the case of high power applications in low voltage distribution levels, the filtering task cannot be performed for the whole spectrum of harmonics by using a single converter due to the limitations on switching frequency and power rating of the semiconductor devices. The relative power loss of the APF unit is also high. Therefore, compensating the reactive harmonic components to improve the power quality of the DG integrated system as well as to avoid the large capacity centralised APF, parallel operation of multiple low power APF units in modular and distributed way are desirable. A novel method of capacity enhancement along with the operational flexibility of the UPQC in distribution level has been proposed, providing modularity and redundancy for better efficiency and reliability. This is termed Distributed-UPQC (D-UPQC). Here, multiple Shunt APF units in distributed (parallel) mode have been placed and connected with a common dc linked capacitor. In that case, the issue of circulating current flow arises. Control or reduction of circulating current flow in the case of hysteresis current control, where switching frequency varies, may be complicated. This flow can be reduced by proper selection of design parameters. Therefore, the design issues have been discussed here.

As a part of design and capacity enhancement, detailed switching dynamics with a parameter selection procedure of shunt APF units has been studied. Power flow between the shunt APF unit and the PCC has been derived and equations for reactive and harmonic current compensation capacity has been acquired. Active power loss associated with the design parameters has also been analyzed as a rating requirement of the shunt APF unit. In the case of hysteresis control with multiple APF units, the design issues have been discussed for the proper selection of design parameters to reduce the circulating current flow.

Implementation of the proposed integration and capacity enhancement methods, and the modification in design with an advanced and real time control strategy have been developed. The performance of the proposed UPQC (UPQC$_{\mu G}$ and D-UPQC) in an active DG integrated microgird network has been studied. The distribution network has been developed by RT-LAB tools and the whole system has been tested in real-time simulation in SIL configuration with a hardware synchronization mode from the OPAL-RT real time environment.

7.2 Future works

There are several important points which need to be investigated but could not be included in the scope of this research work. Thus, during this research, the following issues have been identified as possible topics of work in future in this area:

1. This research can be extended to investigate the case of 3-phase, 4-wire systems.

2. The proposed integration technique of UPQC$_{\mu G}$ along with the control of islanding detection and reconnection techniques can be tested with real controllable hardware switches as a validation of their effectiveness in the next step.

3. A control method should be developed to reduce the circulating current flow in D-UPQC system based on hysteresis current control.

4. A droop control method can be developed for reactive and harmonic current compensation for implementation in a D-UPQC system. The independent operation of a droop control based APF$_{sh}$ can further increase the operational flexibility of the proposed D-UPQC.

5. The proposed D-UPQC can be integrated as D-UPQC$_{\mu G}$ to check the performance of the system in DG integrated microgrid system.

References

[1] S Chowdhury, S P Chowdhury and P Crossley , Microgrids and Active Distribution Networks, 1st Edition, IET, UK, 2009

[2] S M Halpin, L L Grigsby, The Electric Power Engineering Handbook, CRC Press, 2001

[3] C Sankaran, Power Quality, CRC Press, 2002

[4] R D Henderson, P J Rose, Harmonics: The Effects On Power Quality And Transformers, IEEE Trans Industry Appl, vol 30(3), 1994, pp 528 - 532

[5] IEEE Std 519-1992, IEEE Recommended Practices and Requirements for Harmonic Control in Electrical Power Systems, 1992

[6] International Electrotechnical Vocabulary (IEV) – Chapter 121: Electromagnetism, IEC 600 50-121 Std., Available: http://www.electropedia.org.

[7] C Marshman, M Tyndall, EMC and EMF Regulatory Issues for the Power Industry, CIRED, 2009

[8] IEEE 1547, IEEE Standard for Interconnecting Distributed Resources with Electric Power Systems, 2003

[9] G Chicco, J Schlabbach, F Spertino, Experimental assessment of the waveform distortion in grid-connected photovoltaic installations, Solar Energy, vol. 83, 2009, pp 1026–1039

[10] J D Mondol, Y Yohanis, M Smyth, B Norton, Long term performance analysis of a grid connected photovoltaic system in Northern Ireland, ECM, 2006, vol. 47, pp. 2925–2947

[11] H Fechner, R Bründlinger, B Bletterie, Power quality and safety aspects for grid connection of Photovoltaic Systems, 2005, http://www.arsenal.ac.at/downloads/Publikationen/2005/Power Quality and Safety Aspects.pdf

[12] F Blaabjerg, Z Chen, S B Kjaer, Power Electronics as Efficient Interface in Dispersed Power Generation Systems, IEEE Trans. on PE, 2004, Vol. 19(4), pp 184 – 1194

[13] R Teodorescu, F Blaabjerg M Liserre, U Borup, A New Control Structure for Grid-Connected PV Inverters with Zero Steady- State Error and Selective Harmonic Compensation, IEEE PESC 2004, pp 1742 – 1747

[14] X Yuan, W Merk, H Stemmler, J Allmeling, Stationary Frame Generalized Integrators for Current Control of Active Power Filters with Zero Steady-State Error for Current Harmonics of Concern Under Unbalanced and Distorted Operating Conditions, IEEE Trans. on Ind. App., 2002, vol. 38(2), pp.523 – 532

[15] R Fadaeinedjad, G Moschopoulos, M Moallem, The Impact of Tower Shadow, Yaw Error, and Wind Shears on Power Quality in a Wind–Diesel System, IEEE Trans Energy Conv, 2009, Vol. 24(1), pp 102 – 111

[16] I M de Alegrıa, J Andreu, J L Martın, P Ibanez, J L Villate, H Camblong, Connection requirements for wind farms: A survey on technical requierements and regulation, Renewable and Sustainable Energy Reviews, 2007, vol. 11, 1858–1872

[17] F Blaabjerg, R Teodorescu, M Liserre, A V. Timbus, Overview of Control and Grid S7nchronization for Distributed Power Generation Systems, IEEE Trns Indust Elect, 2006, Vol. 53(5), pp 1398 – 1409

[18] S.P. Chowdhurya, S. Chowdhurya, P.A. Crossleyb, Islanding protection of active distribution networks with renewable distributed generators: A comprehensive survey, EPSR, 2009, vol 79, pp. 984–992

[19] S. K. Khadem, M Basu and M F Conlon, UPQC for Power Quality Improvement in DG Integrated Smart Grid Network – A Review, International Journal of Emerging Electric Power Systems, Vol. 13(1), 2012, Art 3

[20] A Baggini, Handbook of Power Quality, John Wiley & Sons Ltd, UK(2008), pp. 545 - 546

[21] J Manson, R Targosz, European Power Quality Survey Report, 2008, pp. 3 - 15

[22] L Yufeng, Evaluation of dip and interruption costs for a distribution system with distributed generations, ICHQP 2008.

[23] N G Hingorani, Introducing custom power, IEEE Spectrum, 1995, vol. 32(6), pp. 41-48.

[24] A Ghosh and G Ledwich, Power quality enhancement using custom power devices, Kluwer Academic, 2002

[25] A Ghosh, Compensation of Distribution System Voltage Using DVR, IEEE Trans on power delivery, 2002, vol. 17(4), pp. 1030 - 1036

[26] H Akagi, E H Watanabe and M Aredes, Instantaneous Power Theory and Applications to Power Conditioning. Piscataway, NJ: IEEE Press, 2007

[27] P Venne, J N Paquin, J Bélanger, The What, Where and Why of Real-Time Simulation, PES general meeting, 2010, pp. 37 - 49

[28] A Emadi, A Nasiri and S B Bekiarov, Uninterruptible Power supplies And Active filters, CRC Press LLC, 2005

[29] B Singh, K A Haddad and A Chandra, A Review of Active Filters for Power Quality Improvement, IEEE Trans Industrial Electronics, Vol. 46(5), 1999, pp. 960 – 971

[30] B singh, R Saha, A Chandra, K Al-Haddad, Static synchrounous compensators (STATCOM): a review, IET Power Electron, vol 2(4), 2009, pp. 297-324

[31] H Akagi, New Trends in Active Filters, EPE Conference, vol. 1, 1995, pp. 17– 26

[32] L Benchaita, A Salemnia, A comparison of voltage source and current source shunt active filter by simulation and experimentation, IEEE Trans PS, 1999, 14 (2), pp. 642 – 647

[33] A Ghosh and A Joshi, The use of instantaneous symmetrical components for balancing a delta connected load and power factor correction, EPSR, vol. 54, 2000, pp. 67–74

[34] M K Mishra, K Karthikeyan, An investigation on design and switching dynamics of voltage source inverter to compensate unbalanced and non-linear loads, IEEE Trans. Ind Electron, Vol. 56 (8), 2009, pp 2802 - 2810

[35] M Rastogi, R Naik, N Mohan, A comparative evaluation of harmonic reduction techniques in three-phase utility interface of power electronic loads, IEEE Trans Ind Appl, Vol. 30(5), 1994, pp. 1149 – 1155

[36] S J Chiang, J M Chang, Design and Implementation of the parallelable active power filter, IEEE PES Conference, vol. 1, 1999, pp. 406-411.

[37] S K Jain, P Agrawal, H O Gupta, Fuzzy logic controlled shunt activepower filter for power quality improvement, IEE Proc. Electr. Power Appl. Vol. 149(5), 2002, pp. 317 - 328

[38] G K Singh, A K Singh, R Mitra, A simple fuzzy logic based robust active power filter for harmonics minimization under random load variation, EPSR, Vol 77 (8), 2007, pp. 1101-1111

[39] M H Rashid, Power Electronics Handbook: devices, circuits, and applications, Elsevier, 2007

[40] J Arrillaga, Y Liu, and N R Watson, Self-Commutating Conversion, in Flexible Power Transmission: The HVDC Options, John Wiley & Sons, Ltd, Chichester, UK, 2007

[41] I Axente, J N Ganesh, M Basu, M F Conlon, K Gaughan, A 12-kVA DSP-Controlled Laboratory Prototype UPQC Capable of Mitigating Unbalance in Source Voltage and Load Current , IEEE Trans Power Electronics, Vol. 25(6), 2010, pp. 1471 - 1479

[42] IEEE std 519-1992, IEEE Recommended Practices and Requirements for Harmonic Control in Electrical Power Systems, 1993

[43] F Liu and A I Maswood, A novel variable hysteresis band current control of three-phase three-level unity PF rectifier with constant switching frequency, IEEE Trans. Power Electron., vol. 21(6), 2006, pp. 1727–1734

[44] N Belhaouchet, L Rahmani, S Begag, A novel adaptive HBCC technique for three-phase shunt APF, EPSR, Vol. 79, 2009, pp. 1097–1104

[45] S Ponnaluri, A Brickwedde, Generalized System Design of Active Filters, PESC, vol. 3, 2001, pp. 1414 – 1419

[46] K Chatterjee, B G Fernandes, G K Dubey, An Instantaneous Reactive Volt–Ampere Compensator and Harmonic Suppressor System, IEEE Trans Power Electron, Vol. 14 (2), 1999, pp. 381 – 392

[47] H Akagi, Y Kanazawa, A Nabae, Instantaneous Reactive Power Compensators Comprising Switching Devices without Energy Storage Components, IEEE Trans Ind Appl, Vol. 20 (3), 1984, pp. 625 – 630

[48] M H Bollen. Fast assessment methods for Voltage Sags in Distribution Systems, IEEE Trans Ind App, Vol. 32(6) 1996, pp. 1414 – 1423.

[49] J G Nielsen, Design and Control of a Dynamic Voltage Restorer, 2002, Aalborg University, Denmark

[50] C Zhan, V K Ramachandaramurthy, A Arulampalam, C Fitzer, S Kromlidis, Mike Barnes and N Jenkins , Dynamic Voltage Restorer Based on Voltage-Space-Vector PWM Control, IEEE Trans Ind Appl, Vol. 37(6), 2001, pp. 1855- 1863

[51] T Jimichi, H Fujita, H Akagi, Design and Experimentation of a Dynamic Voltage Restorer Capable of Significantly Reducing an Energy-Storage Element, IEEE Trans Ind App., Vol. 44(3), 2008, pp. 817 - 825

[52] F.A.L. Jowder, Design and analysis of dynamic voltage restorer for deep voltage sag and harmonic compensation, IET Gener. Transm. Distrib., 2009, Vol. 3(6), pp. 547–560

[53] C L Chen, C E Lin and C L Huang, Reactive and harmonic current compensation for unbalanced three-phase systems using the synchronous detection method, EPSR, Vol. 26, 1993, pp. 163-170.

[54] S Bhattacharya, D M Divan and B B Banerjee, Active filter solutions for utility interface, IEEE ISIE Conf, 1995, pp. 1–11

[55] S Bhattacharya, T M Frank, D M Divan, B Banerjee, Active filter system implementation, IEEE Trans. Ind Appl, Vol. 4 (5), 1998, pp. 47 – 63.

[56] Jou H, Performance comparison of the three-phase active-power-filter algorithms Generation, IEE T&D Conf, Vol. 142 (6), 1995, pp. 646–652

[57] V Khadkikar, A Chandra1, B N Singh, Generalised single-phase p-q theory for active power filtering: simulation and DSP-based experimental investigation, IET Power Electron., 2009, Vol. 2, No. 1, pp. 67–78

[58] M Basu, S P Das, G K Dubey, Comparative evaluation of two models of UPQC for suitable interface to enhance power quality, EPSR, Vol. 77, 2007, pp. 821 – 830

[59] J Lai, F Z Peng, Multilevel converters-a new breed of power converters, IEEE Trans Ind Appl, Vol. 32(3), 1996, pp. 509 - 517

[60] J A Munoz, J R Espinoza, Design of a Modular UPQC Configuration Integrating a Components Economical Analysis, IEEE Trans PD, Vol. 24(4), 2009, pp. 1763-1772.

[61] M Basu, S P Das, G K Dubey, Investigation on the performance of UPQC-Q for voltage sag mitigation and power quality improvement at a critical load point, IET Gen Trans and Dist, vol.2(3), 2008, pp.414-423.

[62] M Basu, M Farrell, M F Conlon, K Gaughan, E Coyle, Optimal Control Strategy of UPQC for Minimum Operational Losses, UPEC, 2004.

[63] M Basu, M F Conlon, K Gaughan, Converter Rating Optimasation of a Unified Power Quality Conditioner, UPEC, 2005.

[64] I Axente, Unified Power Quality Conditioner: Protection and Performance Enhancement, PhD Thesis, DIT, Ireland, 2008

[65] M Boost, P D Ziogas, State of the Art PWM Techniques: A Critical Evaluation, IEEE-PESC, 1986, pp. 425– 433.

[66] S M Muyeen, T Murata, J Tamura, M H Ali, Application of STATCOM/BESS for wind power smoothening and hydrogen generation, EPSR, 2009, vol. 79, pp 365–373

[67] H H Kuo, S N Yeh and J C Hwang, Novel analytical model for design and implementation of three-phase active power filter controller, Elec. Power Appl. Vol. 148(4), 2001, pp. 369 -383

[68] S K. Jain, P Agrawal and H O Gupta, Fuzzy logic controlled shunt active power filter for power quality improvement, IEE proc Elect Power Appl. vol 149 (5), 2002, pp. 317 - 328

[69] M Ucar, E Ozdemir, Control of a 3-phase 4-leg active power filter under non-ideal mains voltage condition, Electric Power Systems Research, Vol. 78, 2008, pp. 58–73

[70] A Ghosh, G Ledwich, Load Compensating DSTATCOM in Weak AC Systems, IEEE Trans Power Delivery, Vol. 18 (4), 2003, pp. 1302 - 1309

[71] M Cirrincione, M Pucci, G Vitale A Miraoui, Current Harmonic Compensation by a Single-Phase Shunt Active Power Filter Controlled by Adaptive Neural Filtering, IEEE Trans Ind Electron, Vol. 56 (8), 2009, pp. 3128 - 3143

[72] J Miret, L García, M Castilla, J Matas and J M Guerrero, Design of an Analog Quasi-Steady-State Nonlinear Current-Mode Controller for Single-Phase Active Power Filter, IEEE Trans Ind Electron, Vol. 56 (12), 2009, pp. 4872 - 4881

[73] B S Chen and Y Hsu, An Analytical Approach to Harmonic Analysis and Controller Design of a STATCOM, IEEE Trans Power Delivery, Vol. 22 (1), 2007, pp. 423 - 432

[74] M K. Mishra, A Joshi and A Ghosh, Control Schemes for Equalization of Capacitor Voltages in Neutral Clamped Shunt Compensator, IEEE Trans Power Delivery, Vol. 18 (2), 2003, pp. 538 - 544

[75] B Han, B Bae, H Kim, S Baek, Combined Operation of Unified Power Quality Conditioner with Distributed Generation, IEEE Trans Power Delivery, vol. 21(1), 2006, pp. 330 – 338

[76] G S Reddy, Feasibility analysis of DGSC-UPQC, Int Journal Research and Reviews in Applied Sciences, vol 4(1), 2010, pp. 32-47

[77] M Hosseinpour, M Rezapour, S Torabzade, Combined operation of Unifier Power Quality Conditioner and Photovoltaic Array, Journal of Applied Sciences, vol 9(4), 2009, pp 680-688

[78] M A Emran, M Forghani, M Abedi, G B Gharehpetian, Combined Operation of UPQC and Fuel Cell with Common DC Bus, Int Conf Renewable Energy and Power Quality, 2008

[79] M Hosseinpour, A Yazdian, M Hohamadian, J Kazempour, Desing and Simulation of UPQC to Improve Power Quality and Transfer Wind Energy to Grid, Jour of Applied Sciences, 2008, vol. 8(21), pp. 3770 – 3782.

[80] N G Jayanti, M Basu, M. F. Conlon and K. Gaughan, Rating requirements of the unified power quality conditioner to integrate the fixed speed induction generator-type wind generation to the grid, IET Renewable Power Generation, vol. 3(2), 2009, pp. 133-143

[81] M F Farias, P E Battaiotto, M G Cendoya, Wind Farm to Weak-Grid connection using UPQC Custom Power Device, Int Conf on Industrial Technology, 2010, pp. 1745 – 1750

[82] J K Kaldellis, K A Kavadias, Cost-benefit analysis of remote hybrid wind-diesel power stations: Case study Aegean Sea Islands, Energy Policy, vol 35, 2007, pp. 1525-1538

[83] P. Mattavelli, A closed-loop selective harmonic compensation for active filters, IEEE Trans. Ind. Appl. 37(1) (2001), pp. 81–89

[84] L Asiminoaei, E Aeloiza, J Kim, P H Enjeti, F Blaabjerg, L Moran, S Sul, Parallel Interleaved Inverters for Reactive Power and Harmonic Compensation, PESC, (2006), pp.1-7

[85] L Asiminoaei, C. Lascu, Performance Improvement of Shunt Active Power Filter With Dual Parallel Topology, IEEE Trans Power Electronics 22(1) (2007), pp. 247-259.

[86] B Singh, K Al-Haddad, Chandra, A, A new control approach to three-phase active filter for harmonics and reactive power compensation, Power Systems, IEEE Transactions on , vol.13, no.1, pp.133-138, Feb 1998

[87] A. R. Bergen, Power Systems Analysis. Englewood Cliffs, Prentice- Hall, NJ, 1986

[88] T. Kawabata and S. Higashino, Parallel operation of voltage source inverters, IEEE Trans. Ind. Appl. 24(2) (1988), pp.281-287

[88] M Basu, S P Das and G K Dubey, Parallel converter scheme for high-power active power filters, IEE Proc. Electr. Power Appl. 151(4) (2004), pp. 460 – 466

[89] C Rech and J R Pinheiro, Line current harmonics reduction in multipulse connection of asymmetrically loaded rectifiers, IEEE Trans. Ind. Electron. 52(3) (2005), pp. 640–652

[90] Z Ye, D Boroyevich, J Y Choi and F C Lee, Control of circulating current in parallel three-phase boost rectifiers, IEEE APEC (2000), pp. 506–512.

[91] C T Pan and Y H Liao, Modeling and coordinate control of circulating currents in parallel three-phase boost rectifiers, IEEE Trans. Ind. Electron. 54(2) (2007), pp. 825–838

[92] M Baumann and J W Kolar, Parallel Connection of Two Three-Phase Three-Switch Buck-Type Unity-Power-Factor Rectifier Systems With DC-Link Current Balancing, IEEE Trans Ind Electron 54(6) (2007), pp 3042 – 3053

[93] H P Glauser, M Keller, A Plüs, M Schwab and R Scherwey, New inverter module with digital control for parallel operation, IEEE TELES Conf (2000), pp. 265–269

[94] J. Holtz and K. H. Werner, Multi-inverter UPS system with redundant load sharing control, IEEE Trans. Ind. Electron., 37(6) (1990), pp.506-513

[95] C Jiann-Fuh and C. C Lung, Combination voltage-controlled and current-controlled PWM inverters for UPS parallel operation, IEEE Trans PE 10(5) (1995), pp. 547-558.

[96] H Hanaoka, M. Nagai, Development of a novel parallel redundant UPS, Telecommunications Energy Conference (2003), pp. 493 - 498

[97] W Tsai-Fu, C. Yu-Kai, 3C strategy for inverters in parallel operation achieving an equal current distribution, IEEE Trans Ind Elect 47(2) (2000), pp. 273-281

[98] K Siri, C Q Lee, T F Wu, Current distribution control schemes for parallel connected converter modules Part II: Central-limit control, IEEE Trans. A E Sys. 28 (1992), pp. 841–851

[99] C Yu-Kai, W Yu-En, ACSS for paralleled multi-inverter systems with DSP based robust controls, IEEE Trans A E Sys, Vol. 39(3) (2003), pp. 1002-1015

[100] K Siri, T F Wu, C Q Lee, Current distribution control schemes for parallel connected converter modules Part I: Master-slave control, IEEE Trans. A E. Syst. 28 (1992), pp. 829–840

[101] Ching-Tsai Pan, Yi-Hung Liao, Modeling and Coordinate Control of Circulating Currents in Parallel Three-Phase Boost Rectifiers, IEEE Trans Ind Elec , vol.54, no.2, pp.825-838, 2007

[102] Di Zhang, Fei Wang, Burgos R, Boroyevich, D, Common-Mode Circulating Current Control of Paralleled Interleaved Three-Phase Two-Level Voltage-Source Converters With Discontinuous Space-Vector Modulation, IEEE Trans PE, vol.26, no.12, pp.3925-3935, 2011

[103] C T Pan, Y Liao, Modelling and Control of Circulating Currents for Parallel Three-Phase Boost Rectifiers With Different Load Sharing, IEEE Trans IE, vol.55(7), pp.2776-2785, 2008

[104] Chen, T P, Circulating zero-sequence current control of parallel three-phase inverters, Electric Power Applications, vol.153, no.2, pp. 282- 288, 2006

[105] Y Pei, G Jiang, X Yang and Z Wang, Auto-master–slave control technique of parallel inverters in distributed AC power systems and UPS, IEEE PES Conf, 2004, pp. 2050–2053

[106] D Shanxu, M Yu, X Jian, K Yong and C Jian, Parallel operation control technique of voltage source inverters in UPS, PEDS Conf, 1999, pp. 883 - 887

[107] X Sun, Y S Lee and D Xu, Modelling, analysis, and implementation of parallel multi-inverter system with instantaneous average-current-sharing scheme, IEEE Trans. Power Electron. 18(3) (2003), pp. 844–856.

[108] Y J Cheng and E K K Sng, A novel communication strategy for decentralized control of paralleled multi-inverter systems, IEEE Trans. Power Electron. 21(1) (2006), pp. 148–156

[109] J Tao, H Lin, J Zhang and J Ying, A novel load sharing control technique for paralleled inverters, IEEE PES Conf. (2003), pp. 1432–1437.

 [110] M. C. Chandorkar, D. M. Divan, and R. Adapa, Control of parallel connected inverters in standalone ac supply systems, IEEE Trans. Ind. Appl. 29 (1993), pp. 136–143

[111] A. Tuladhar, H. Jin, T. Unger, and K. Mauch, Parallel operation of single phase inverters with no control interconnections, IEEE APEC (1997), pp. 94–100.

[112] A Tuladhar, H Unger, K Mauch, Control of Parallel Inverters in Distributed AC Power Systems with consideration of line impedance effect, IEEE Trans IA, 36(1), 2000, pp. 131-138

[113] L Corradini, M Corradin, P Mattavelli, F Polo, Analysis of Parallel Operation of Uninterruptible Power Supplies Loaded Through Long Wiring Cables, IEEE Trans PE, Vol. 25(4), 2010, pp. 1046-1054

[114] J M Guerrero, L. Hang, Control of Distributed Uninterruptible Power Supply Systems, IEEE Trans Industrial Electronics 55(8) (2008), pp. 2845-2859.

[115] J Guerrero, L Vicuna, A wireless controller to enhance dynamic performance of parallel inverters in distributed generation systems, IEEE Trans PE, vol. 19(5), 2004, pp. 1205-1213

[116] J M Guerrero, M. J. Matas, Wireless-Control Strategy for Parallel Operation of Distributed-Generation Inverters, IEEE Trans Ind Elect 53(5) (2006), pp. 1461-1470

[117] S J Chiang and J M Chang, Design and implementation of the parallelable active power filter, IEEE PES Conference 1 (1999), pp 406 – 411

[118] S J Chiang and J. M. Chang, Parallel operation of shunt active power filters with capacity limitation control, IEEE Trans. Aerospace and Electronic Systems 37(4) (2001), pp.1312-1320

[119] Y. Abdelli, M. Machoum, and M.S. Khoor, Control of a multimodule parallelable three-phase active power filters, Int Conf on Harmonics and Quality of Power (2004), pp.543-548.

[120] E C dos Santos, C B Jacobina and A M Maciel, Parallel connection of two shunt active power filters with losses optimization, APEC 1 (2010), pp. 1191 – 1196

[121] T Surgevil, K Vardar and E Akpnar, Analysis of Shunt Active Power Filters Using PSCAD for Parallel Operation, (2009), pp. 263 - 267

[122] H Akagi and K Nabae, Control strategy of active power filters using multiple voltage source PWM converters, IEEE Trans. Ind. Appl. l(3) (1985), pp. 460–466

[123] L Asiminoaei, E Aeloiza, J Kim, P H Enjeti, F Blaabjerg, L Moran, S Sul, Parallel Interleaved Inverters for Reactive Power and Harmonic Compensation, PESC, (2006), pp.1-7

[124] Xueliang Wei, Ke Dai, Xin Fang, Pan Geng, Fang Luo, Yong Kang, Parallel Control of Three-Phase Three-Wire Shunt Active Power Filters, IPEMC 2 (2006), pp. 1 -5

[125] R Pregitzer, J Pinto, G Sepulveda, M Joao A Fonso and L Joao, Parallel Association of Shunt Active Power Filters, ISIE (2007) pp. 2493 - 2498

[126] L Asiminoaei, C. Lascu, Performance Improvement of Shunt Active Power Filter With Dual Parallel Topology, IEEE Trans Power Electronics 22(1) (2007), pp. 247-259.

[127] H Akagi, H Fujita, K Wada, A shunt active filter based on voltage detection for harmonic termination of a radial power distribution line, IEEE Trans. IA, vol. 35(3) (1999), pp. 638–645

[128] K Wada, H Akagi, Considerations of a shunt active filter based on voltage detection for installation on a long distribution feeder, IEEE Trans. IA, vol.38(4), 2002, pp. 1123–1130

[129] P. Jintakosonwit, H. Akagi, H. Fujita, and S. Ogasawara, Implementation and performance of automatic gain adjustment in a shunt active filter for harmonic damping throughout a power distribution system, IEEE Trans. PE. Vol. 17(3) (2002), pp. 438–447

[130] P. Jintakosonwit, H. Fujita, H. Akagi, and S. Ogasawara, Implementation and performance of cooperative control of shunt active filters for harmonic damping throughout a power distribution system, IEEE Trans. Ind. Appl. 39(2) (2003), pp. 556–564.

[131] Po-Tai Cheng, Tzung-Lin Lee, Distributed Active Filter Systems (DAFSs): A New Approach to Power System Harmonics, IEEE Trans Ind Appl 42(5) (2006), pp. 1301 - 1309

[132] Tzung-Lin Lee, Po-Tai Cheng, H Akagi, H Fujita, A Dynamic Tuning Method for Distributed Active Filter Systems, IEEE Trans Ind Appl 44(2) (2008), pp. 612 - 623

[133] Falahi, G.; Mokhtari, H., Performance Improvement of Parallel Active Power Filters Using Droop Control Method, APPEEC (2009), pp 1- 4

[134] U Borup, F Blaabjerg, P N. Enjeti, Sharing of Nonlinear Load in Parallel-Connected Three-Phase Converters, IEEE trans Ind Appl, 37(6) (2001), pp. 1817 - 1823

[135] S W Park , I Y Chung , J H Choi , S I Moon and J E Kim, Control schemes of the inverter-interfaced multi-functional dispersed generation, PES meeting, pp.1924 -1929, 2003

[136] R. Mastromauro , M. Liserre and A. Dell, Single-phase grid-connected photovoltaic systems with power quality conditioner functionality, *Power Electron. Appl.*, pp.1 -11 2007

[137] M Davari , H Yazdanpanahi, G Gharehpetian, Modelling the combination of UPQC and photovoltaic arrays with multi-input single-output DC-DC converter, PS Conf, pp.1 -7 2009

[138] H Toodeji , S Fathi, G Gharehpetian, Power management and performance improvement in integrated system of variable speed wind turbine and UPQC, ICCEP, pp.609 -614, 2009

[139] P Paul, I Raglend, T Prakash, Universal Power Line Manager for wind turbine generator connected with strong grid, ICONRAEeCE, 2011, pp.448-453

[140] Ali Ajami, Mehdi Armaghan, Fixed speed wind farm operation improvement using current-source converter based UPQC, ECM, Vol 58, 2012, Pages 10-18,

[141] Xiaoxiao Yu; Khambadkone, A.M.; Huanhuan Wang; Terence, S, Control of Parallel-Connected Power Converters for Low-Voltage Microgrid—Part I: A Hybrid Control Architecture, IEEE Trans PE , vol.25 (12), 2010, pp.2962-2970

[142] A Kahrobaeian, Y Mohamed, Interactive distributed generation interface for flexible microgrid operation in smart distribution systems, IEEE Trans SE , vol.3(2), pp.295-305, 2012

[143] J Nielsen, F Blaabjerg, N Mohan, Control Strategies for DynamicVoltage Restorer Compensating Voltage Sags With Phase Jump, APEC, 2001, vol. 2, pp. 1267–1273

[144] D. M. Vilathgamuwa and R. Perera, Voltage sag compensation with energy optimized dynamic voltage restorer, *IEEE Trans. Power Del.*, vol. 18, no. 3, pp. 928–936, Jul. 2003

[145] S Choi, J Li, D Vilathgamuwa, A generalized voltage compensation strategy for mitigating the impacts of voltage sags/swells, IEEE Trans. PD, vol. 20(3), pp. 2289–2297, 2005.

[146] M Banaei, S Mohammadi, G Gharean, Verification of a new control strategy for dynamic voltage restorer by simulation, *Sim Model. Prac Theory*, vol. 14(2), pp. 112–125, 2006.

[147] Moradlou, M Karshenas, Design Strategy for Optimum Rating Selection of Interline DVR, IEEE Trans PD, vol.26, no.1, pp.242-249, Jan. 2011

[148] J M Guerrero, J Vasquez, J Matas, M Castilla, Hierarchical Control of Droop-Controlled AC and DC Microgrids—A General Approach Toward Standardization, IEEE Trans *Industrial Electronics,* vol.58, no.1, pp.158-172, Jan. 2011

[149] R Teodorescu, M Liserre, P Rodríguez, Grid Converters for Photovoltaic and Wind Power Systems, 1st Ed, Wiley IEEE, 2011

[150] D. Velasco, C.L. Trujillo, G. Garcerá, E. Figueres, Review of anti-islanding techniques in distributed generators, Renewable and Sustainable Energy Reviews, Volume 14, Issue 6, August 2010, Pages 1608-1614

[151] Bahrani, B.; Karimi, H.; Iravani, R.; , "Nondetection Zone Assessment of an Active Islanding Detection Method and its Experimental Evaluation," *Power Delivery, IEEE Transactions on* , vol.26, no.2, pp.517-525, April 2011

[152] J Rocabert, G Azevedo, J M Guerrero, P Rodríguez, Intelligent Connection Agent for Three-Phase Grid-Connected Microgrids, IEEE Trans PE , vol.26 (10), pp.2993-3005, 2011

[153] I Balaguer, Q Lei, S Yang; F Z Peng, Control for Grid-Connected and Intentional Islanding Operations of Distributed Power Generation,*Industrial Electronics, IEEE Transactions on* , vol.58, no.1, pp.147-157, Jan. 2011

[154] Bloemink, J.; Iravani, M.R.; , "Control of a Multiple Source Microgrid With Built-in Islanding Detection and Current Limiting," *Power Delivery, IEEE Transactions on* , vol.27, no.4, pp.2122-2132, Oct. 2012

[155] D Dong, T Thacker, R Burgos, F Wang, G Skutt, Modes of Operation and System-Level Control of Single-Phase Bidirectional PWM Converter for Microgrid Systems, IEEE Trans *Smart Grid,* vol.3, no.1, pp.93-104, March 2012

[156] T. Thacker, F. Wang, R. Burgos, and D. Boroyevich, Islanding detection using a coordinate transformation based phase-locked loop, *IEEE PESC*, 2007, pp. 1151–1156.

[157] S.-K. Kim, J.-H. Jeon, J.-B. Ahn, B. Lee, and S.-H. Kwon, Frequency shift acceleration control for anti-islanding of a distributed-generation inverter, *IEEE Trans. Ind. Electron.*, vol. 57, no. 2, pp. 494–504, Feb. 2010.

[158] P. Rodriguez, A. Luna, M. Ciobotaru, R. Teodorescu, and F. Blaabjerg, Advanced grid synchronization system for power converters under unbalanced and distorted operating conditions, *IEEE Ind. Electron.*, Nov. 2006, pp. 5173–5178.

[159] P. Rodr´ıguez, A. Luna, I. Candela, R. Mujal, R. Teodorescu, and F. Blaabjerg, "Multiresonant frequency-locked loop for grid synchronization of power converters under distorted grid conditions," *IEEE Trans. Ind. Electron.*, vol. 58, no. 1, pp. 127–138, Jan. 2011.

[160] P Rodríguez, A Luna, I E Otadui, R Teodorescu, F Blaabjerg, A Stationary Reference Frame Grid Synchronization System for Three-Phase Grid-Connected Power Converters Under Adverse Grid Conditions, IEEE Trans PE, vol.27, no.1, pp.99-112, Jan. 2012

[161] M Brenna, R Faranda, A New Proposal for Power Quality and Custom Power Improvement: OPEN UPQC, IEEE Trans Power Delivery, Vol. 24(4), 2009, pp. 2107-2116

[162] T Assis, G Taranto, Automatic Reconnection From Intentional Islanding Based on Remote Sensing of Voltage and Frequency Signals, *Smart Grid, IEEE Trans,* article in press

[163] Karegar, H.K.; Nateghi, A. New method for reconnection of islanded wind turbines to grid, PECon*,* pp.617-621, 2010

[164] Redfern, M A; Shang, W T; O'Gorman, R; Auto-reclose for remote breakers in networks containing distributed generators, DSPS, pp.1-5, 2010

[165] G. Iwanski and W. Koczara, "DFIG-based power generation system with UPS function for variable-speed applications," *IEEE Trans. Ind. Elect.*, vol. 55, no. 8, pp. 3047–3054, 2008.

[166] D. N. Gaonkar, G. N. Pillai, and R. N. Patel, "Seamless transfer of microturbine generation system operation between grid-connected and islanding modes," *Electr. Power Compon. Syst.*, vol. 37, no. 2, pp. 174–188, Feb. 2009.

[167] S. Chung, "A phase tracking system for three phase utility interface inverters," *IEEE Trans. Power Electron.*, vol. 15, no. 3, pp. 431–438, May 2000.

[168] P Rodriguez, J Pou, R Burgos, D Boroyevich, Decoupled double synchronous reference frame PLL for power converters control, IEEE Trans PE, vol. 22(2), pp. 584– 592, Mar. 2007

[169] M Karimi, R Iravani, A method for synchronization of power electronic converters in polluted and variable-frequency environments, IEEE Trans PS, vol.19(3), pp. 1263–1270, 2004.

[170] H. Geng, D. Xu, B. Wu, A novel hardware based all digital phaselocked- loop applied to grid-connected power converters, IEEE Trans. IE., vol. 58, no. 5, pp. 1737–1745, 2010

[171] S Golestan, F Freijedo, J Guerrero, Design and tuning of a modified power-based PLL for single-phase grid-connected power conditioning systems, IEEE Trans PE, vol.27(8), pp.3639-3650, 2012

[172] H. Kim, T. Yu, S. Choi, Indirect current control algorithm for utility interactive inverters in distributed generation systems, IEEE Trans. PE, vol. 23(3), pp. 1342–1347, May 2008.

[173] Z Yao, L Xiao, Y Yan, Seamless transfer of single-phase grid interactive inverters between grid connected and stand-alone modes, IEEE Trans. PE,vol.25(6), pp.1597–1603, 2010

[174] F Gao, R Iravani, A control strategy for a distributed generation unit in grid-connected and autonomous modes of operation, IEEE Trans. PD, vol. 23, no. 2, pp. 850–859, Apr. 2008.

[175] Y Mohamed, A Radwan, Hierarchical control system for robust micro-grid operation and seamless mode-transfer in distribution systems, IEEE Trans. SG, vol. 2(2), pp. 352–362, 2011

[176] F Z Peng, J W McKeever and D J Adams, A Power Line Conditioner Using Cascade Multilevel Inverters for Distribution Systems, IEEE Trans IA, Vol 34(6), 1998, pp. 1293 – 1298

[177] B. Han, B. Bae, S. Baek and G. Jang, New Configuration of UPQC for Medium-Voltage Application, IEEE Trans Power Delivery, Vol. 21(3), 2006, pp. 1438 – 1444

[178] B. Han, S. Baek, H. Kim, and G. Karady, Dynamic characteristic analysis of SSSC based on multibridge inverter, IEEE Trans. Power Del. Vol. 17(2), 2002, pp. 623–629

[179] B.M. Han and P. Mattavelli, Operation analysis of novel UPFC based on 3-level half-bridge modules, IEEE Power Tech Conf., Jun. 2003, vol. 4, pp. 307–312.

[180] J A Munoz, J R Espinoza, Design of a Modular UPQC Configuration Integrating a Components Economical Analysis, IEEE Trans PD, Vol. 24(4), 2009, pp. 1763-1772.

[181] J Muñoz, J Espinoza, C Morán, E Espinosa, D Sbárbaro, Design of a Discrete-Time Linear Control Strategy for a Multi-Cell UPQC, IEEE Trans IE, 2011

[182] L Asiminoaei, E Aeloiza, P Enjeti, F Blaabjerg, Shunt Active-Power-Filter Topology Based on Parallel Interleaved Inverters, IEEE Trans IE, vol.55(3), pp.1175-1189, 2008

[183] T P Chen , Zero-Sequence Circulating Current Reduction Method for Parallel HEPWM Inverters Between AC Bus and DC Bus, IEEE Trans IE, vol.59(1), pp.290-300, 2012

Appendix 1

Instantaneous Reactive Power Theory

The current and voltage of a three phase four wire system can be converted into the $\alpha\beta0$ system (Clarke transformation) using the following equations:

$$\begin{bmatrix} \overline{v_0} \\ v_\alpha \\ v_\beta \end{bmatrix} = \sqrt{\frac{2}{3}} \begin{bmatrix} \dfrac{1}{\sqrt{2}} & \dfrac{1}{\sqrt{2}} & \dfrac{1}{\sqrt{2}} \\ 1 & -\dfrac{1}{2} & -\dfrac{1}{2} \\ 0 & \dfrac{\sqrt{3}}{2} & -\dfrac{\sqrt{3}}{2} \end{bmatrix} \begin{bmatrix} v_a \\ v_b \\ v_c \end{bmatrix} \tag{A1.1}$$

$$\begin{bmatrix} \overline{i_0} \\ i_\alpha \\ i_\beta \end{bmatrix} = \sqrt{\frac{2}{3}} \begin{bmatrix} \dfrac{1}{\sqrt{2}} & \dfrac{1}{\sqrt{2}} & \dfrac{1}{\sqrt{2}} \\ 1 & -\dfrac{1}{2} & -\dfrac{1}{2} \\ 0 & \dfrac{\sqrt{3}}{2} & -\dfrac{\sqrt{3}}{2} \end{bmatrix} \begin{bmatrix} i_a \\ i_b \\ i_c \end{bmatrix} \tag{A1.2}$$

Therefore, $\begin{bmatrix} p_0 \\ p \\ q \end{bmatrix} = \begin{bmatrix} v_0 & 0 & 0 \\ 0 & v_\alpha & v_\beta \\ 0 & v_\beta & -v_\alpha \end{bmatrix} \begin{bmatrix} i_0 \\ i_\alpha \\ i_\beta \end{bmatrix}$ $\tag{A1.3}$

where p_0 is the instantaneous zero-sequence power, p is the instantaneous real power, and q is the instantaneous imaginary power - are defined from the instantaneous phase voltages and line currents on the $\alpha\beta0$ axes.

The advantage of applying the $\alpha\beta0$ transformation is to separate zero-sequence components from the *abc* phase components. i_0 can be eliminated as the zero-sequence current does not exist in a three phase three-wire system.. Again, v_0 can be eliminated if

the three-phase voltages are balanced in a four-wire system, where no zero-sequence voltage is present.

The active and reactive power can be decomposed into two parts - AC and DC. The DC part ($\bar{p}, \bar{q}$) resulted from the fundamental current and voltage and the AC part ($\tilde{p}, \tilde{q}$) resulted from the harmonics.

$$p = \bar{p} + \tilde{p} \tag{A1.4}$$

$$q = \bar{q} + \tilde{q} \tag{A1.5}$$

The supply reference currents for harmonic power cancellation then can be determined by the DC values of p and q. If harmonic and reactive both current compensation is required, the reference current should be based on the DC value active power only. Therefore, in the latter case;

$$\begin{bmatrix} i_\alpha^* \\ i_\beta^* \end{bmatrix} = \frac{1}{v_\alpha^2 + v_\beta^2} \begin{bmatrix} v_\alpha & -v_\beta \\ v_\beta & v_\alpha \end{bmatrix} \begin{bmatrix} \bar{p} \\ 0 \end{bmatrix} \tag{A1.6}$$

where * denotes the reference value. Therefore, the reference values for the active filter will be:

$$i_{\alpha AF}^* = i_\alpha^* - i_{L,\alpha} \tag{A1.7}$$

$$i_{\beta AF}^* = i_\beta^* - i_{L,\beta} \tag{A1.8}$$

and the *abc* reference values for the active filter can be determined by the inverse transform of αβ0−abc;

$$\begin{bmatrix} i_{aAF}^* \\ i_{bAF}^* \\ i_{cAF}^* \end{bmatrix} = \sqrt{\frac{2}{3}} \begin{bmatrix} 1 & 0 \\ -\frac{1}{\sqrt{2}} & \frac{\sqrt{3}}{2} \\ -\frac{1}{\sqrt{2}} & -\frac{\sqrt{3}}{2} \end{bmatrix} \begin{bmatrix} i_{\alpha AF}^* \\ i_{\beta AF}^* \end{bmatrix} \tag{A1.9}$$

Appendix 2
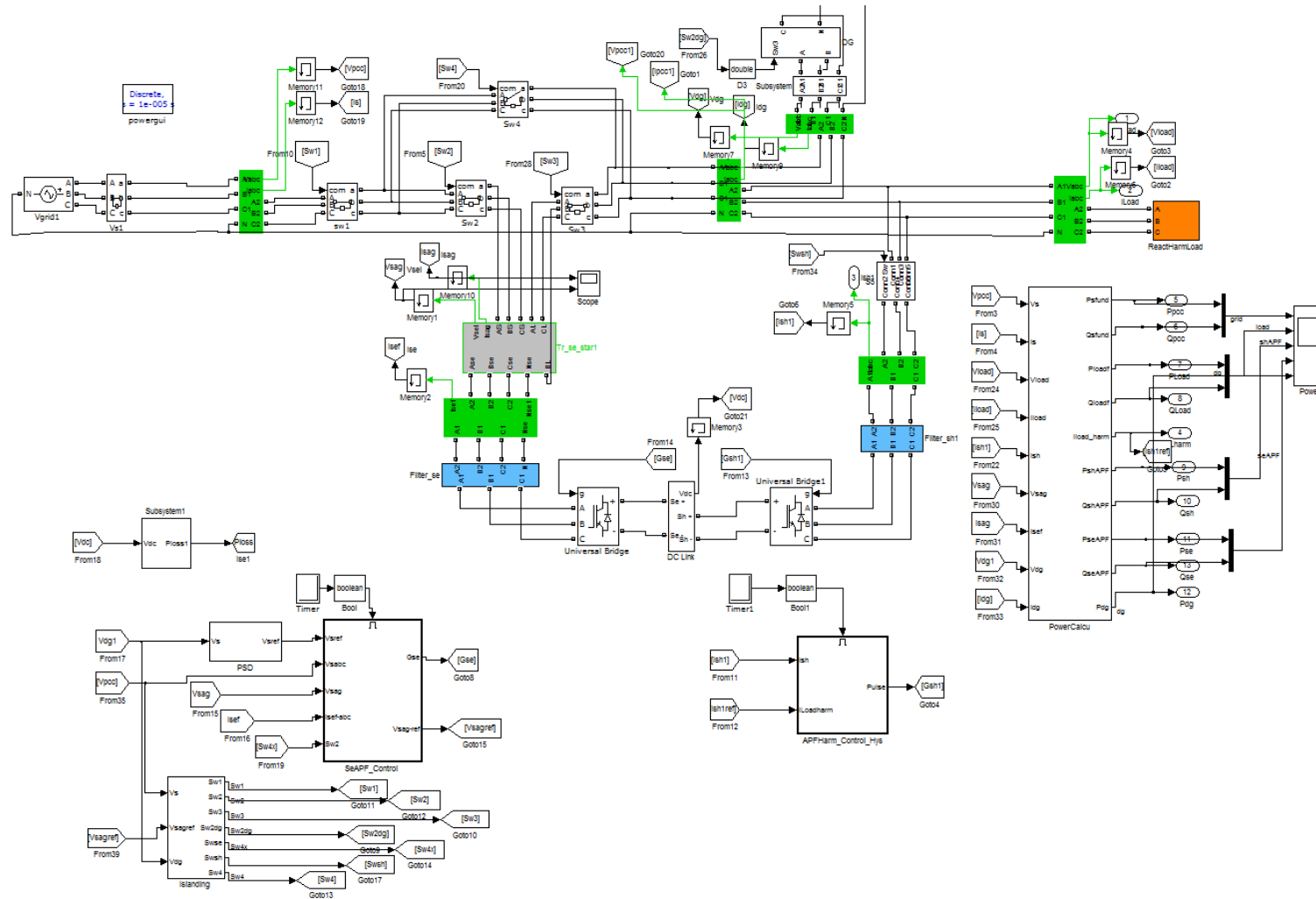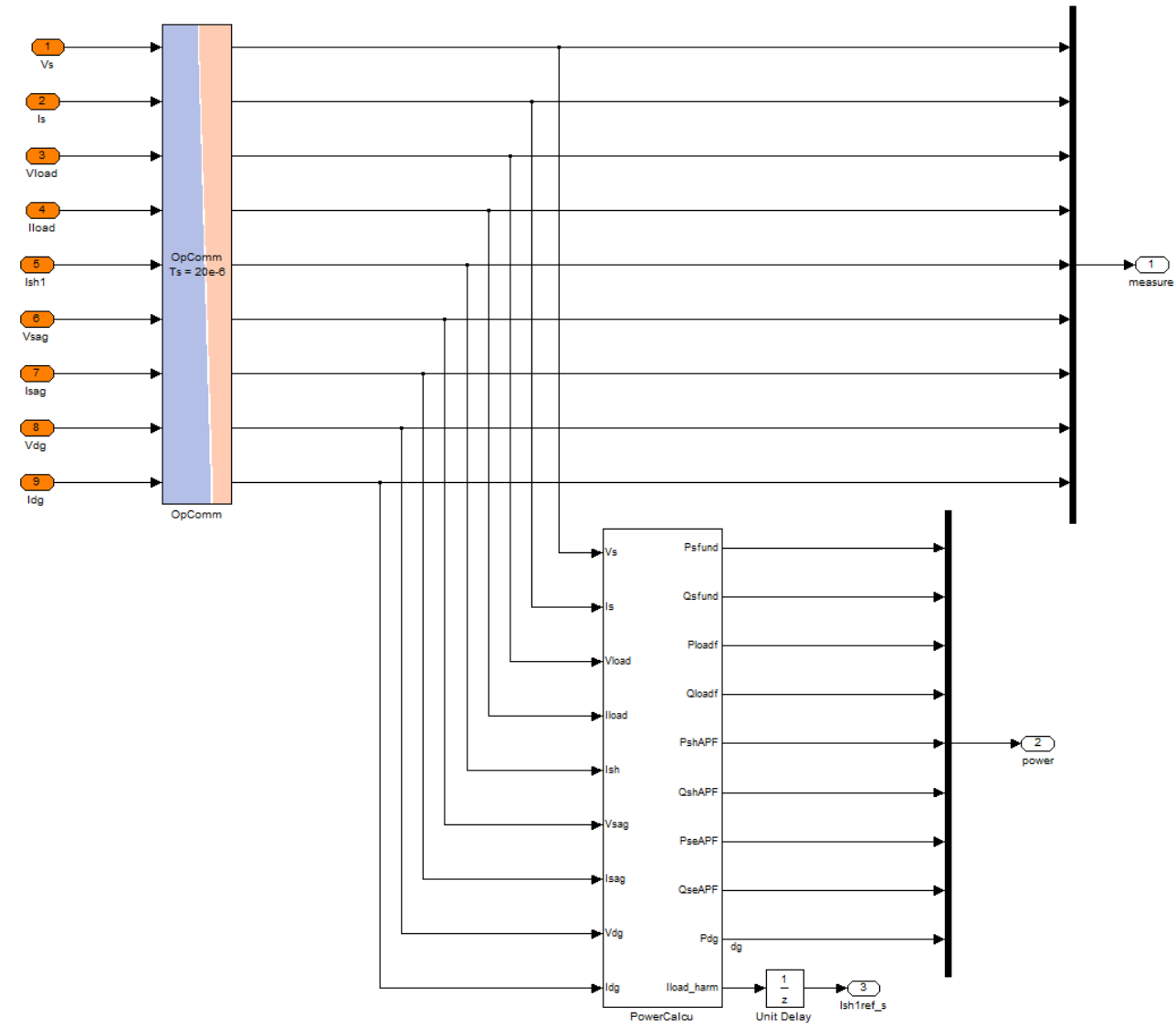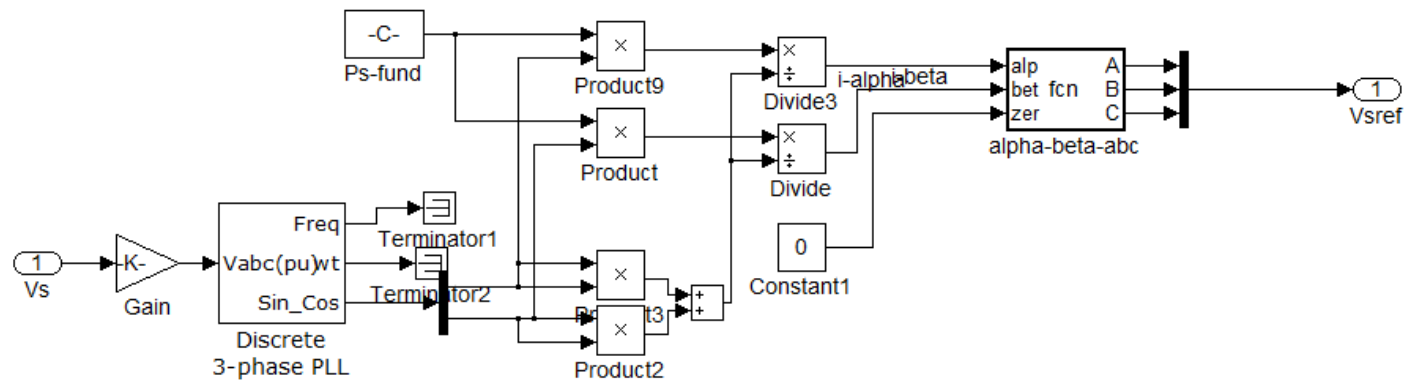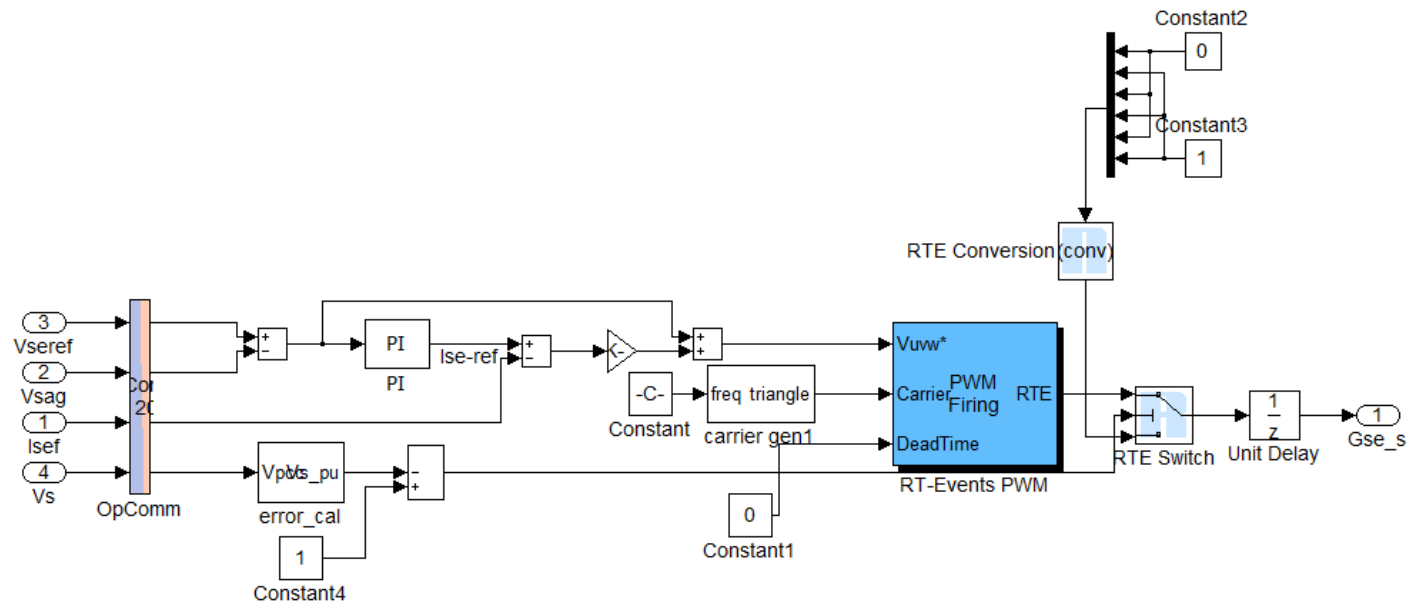

A2.1 MATLAB simulation of UPQC$_{\mu G}$

A2.2 Islanding and Reconnection method in MATLAB for UPQC$_{\mu G}$

A2.3 RT simulation of UPQC$_{\mu G}$
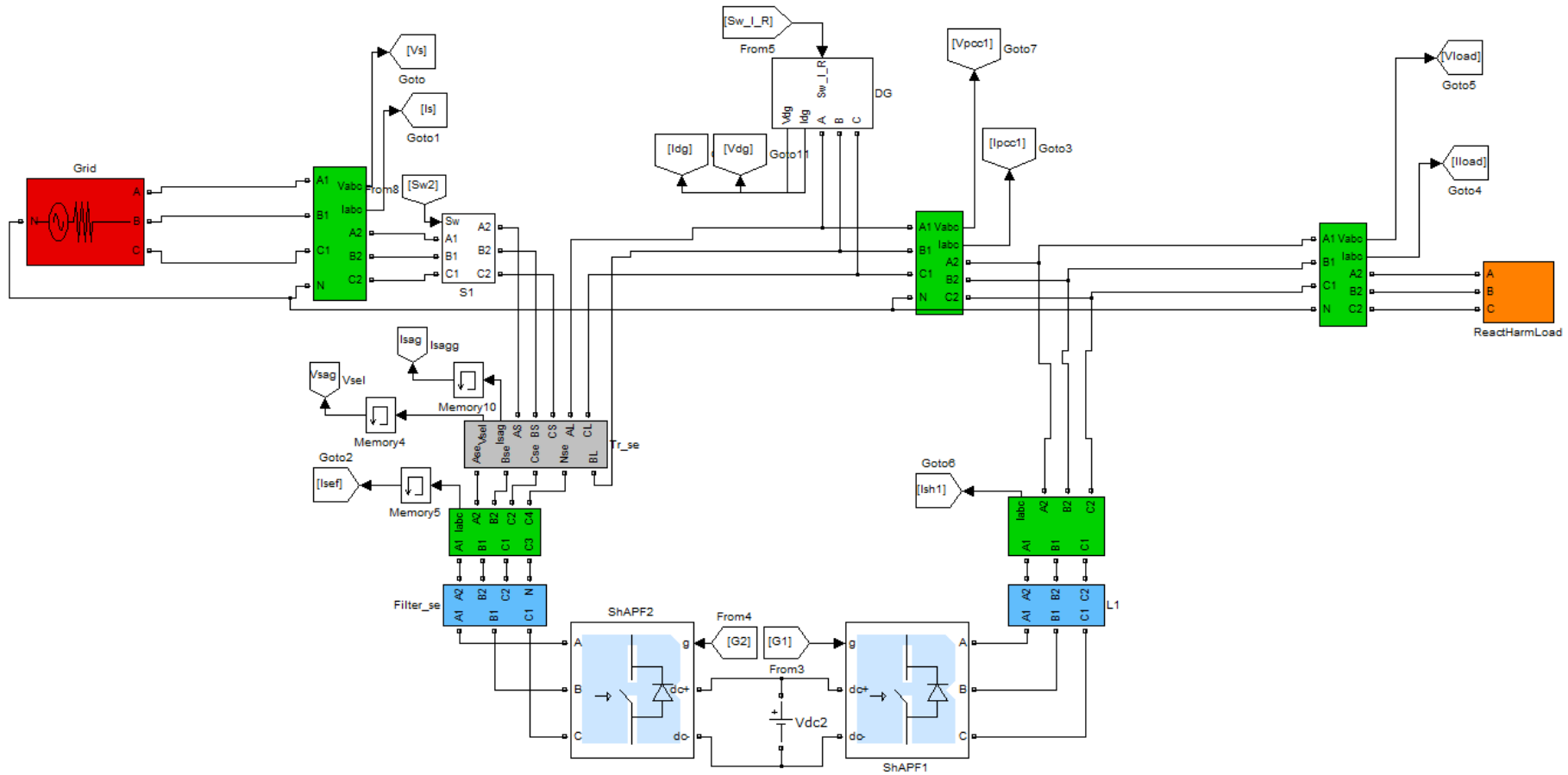
A2.4 sm_PowerSystem (Power System Network) of UPQC$_{\mu G}$ for RT simulation

A2.5 ss_measure of UPQC$_{\mu G}$ for RT simulation

219

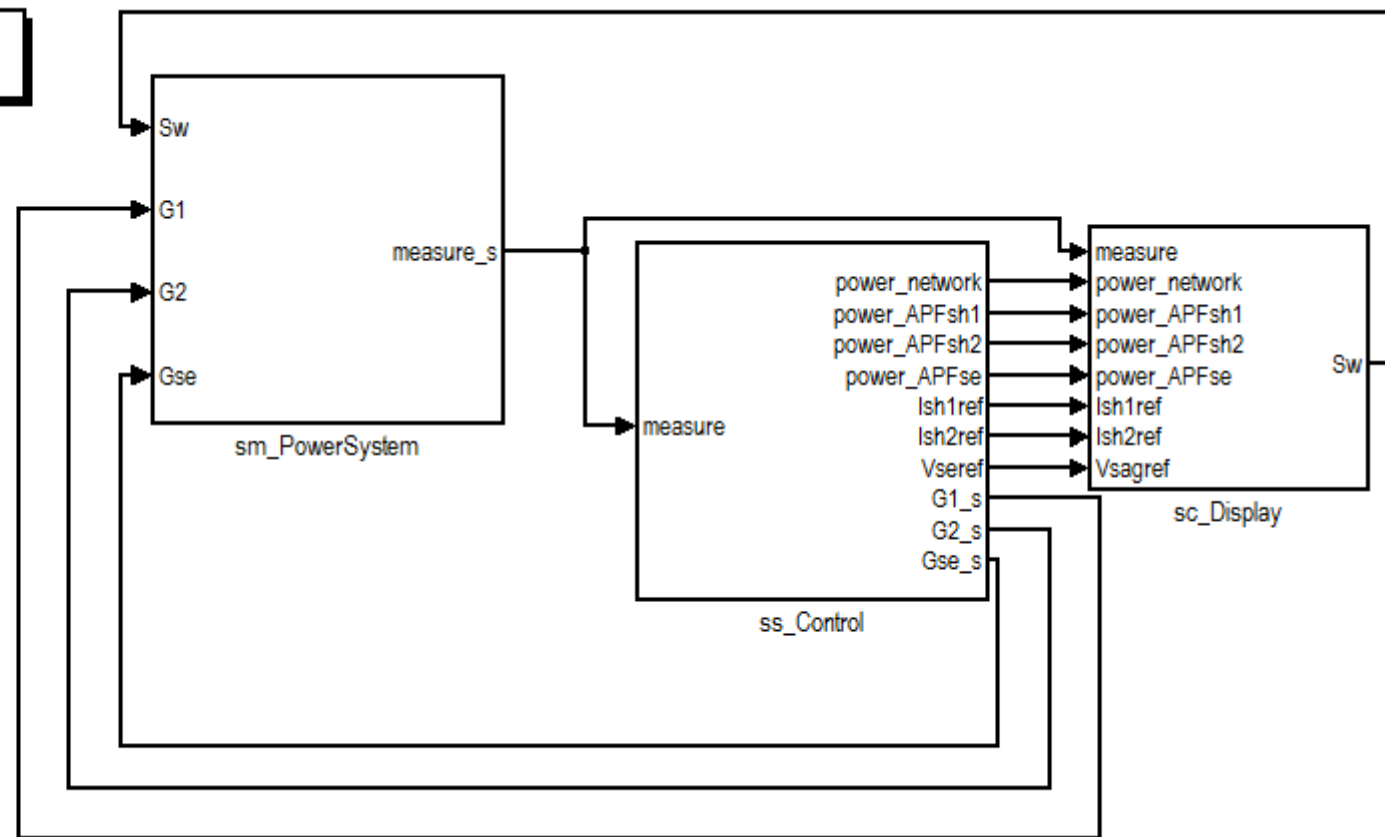A 2.6 ss_PSD of UPQC$_{\mu G}$ for RT simulation

A2.7 ss_seAPF block of UPQC$_{\mu G}$ for RT simulation
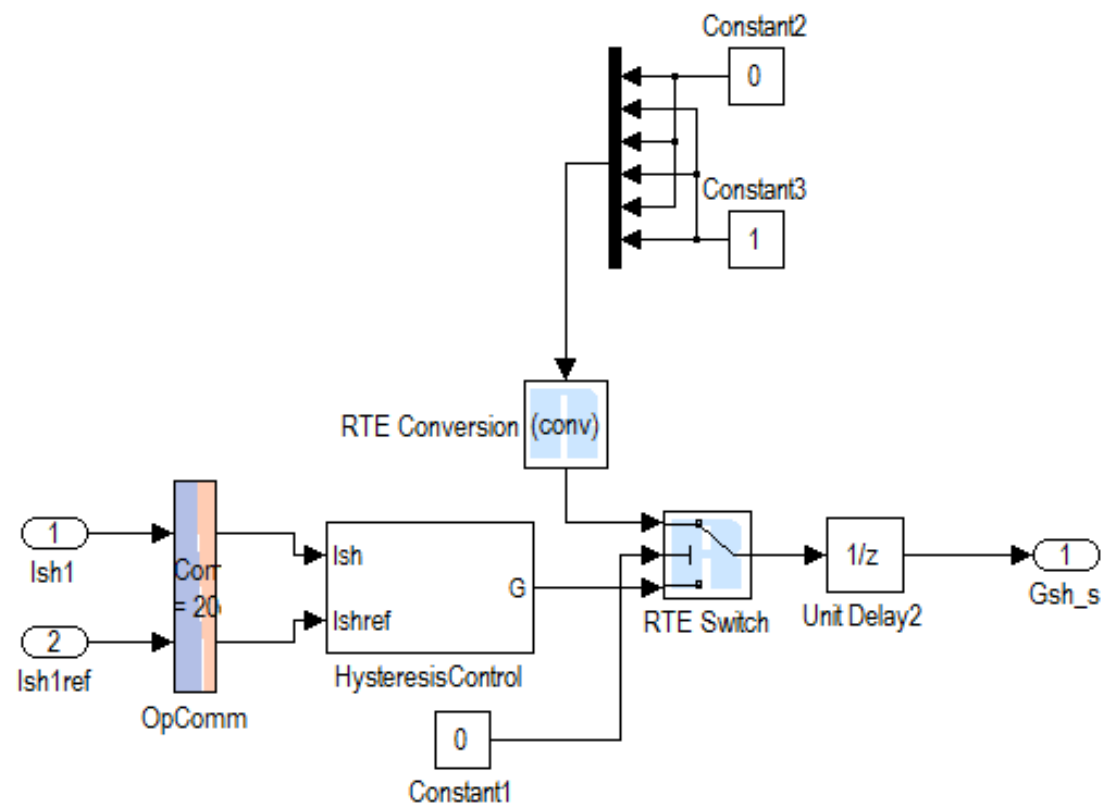
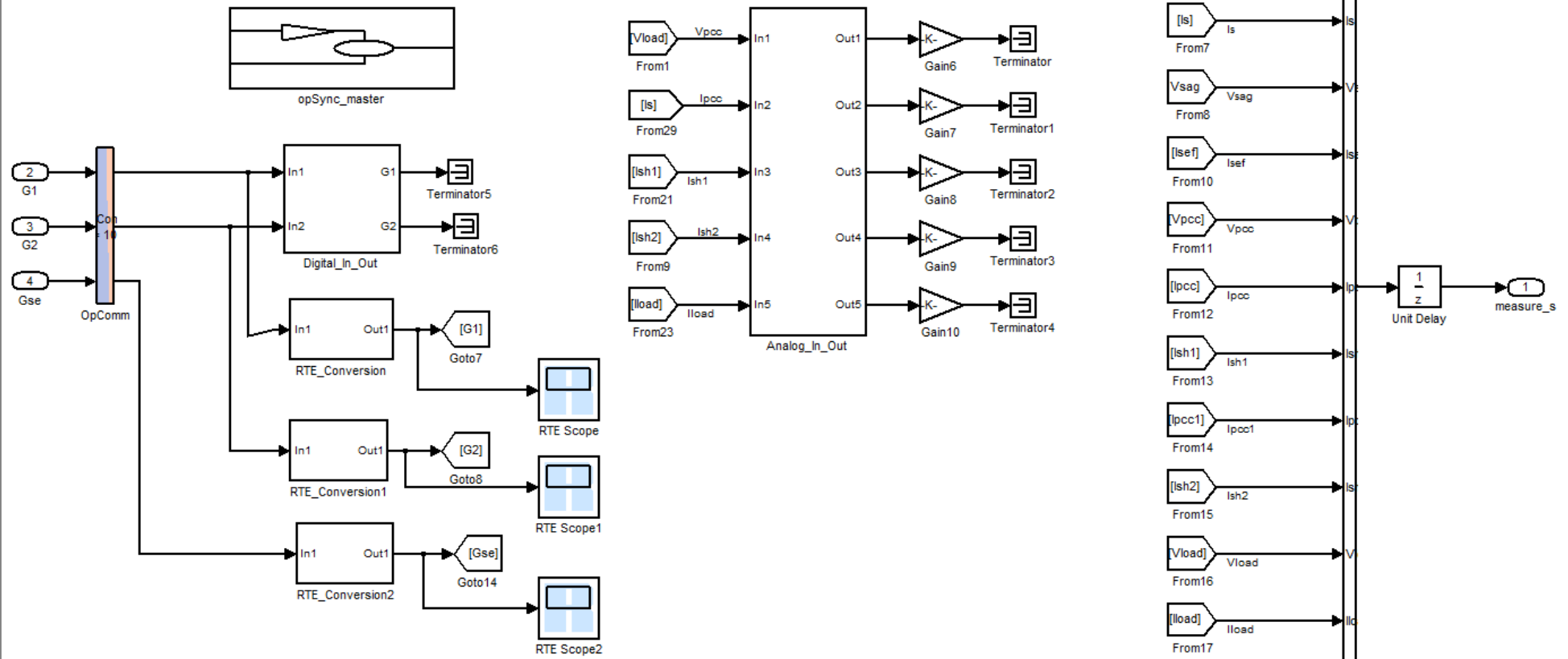A2.8 ss_shAPF of of UPQC$_{\mu G}$ for RT simulation

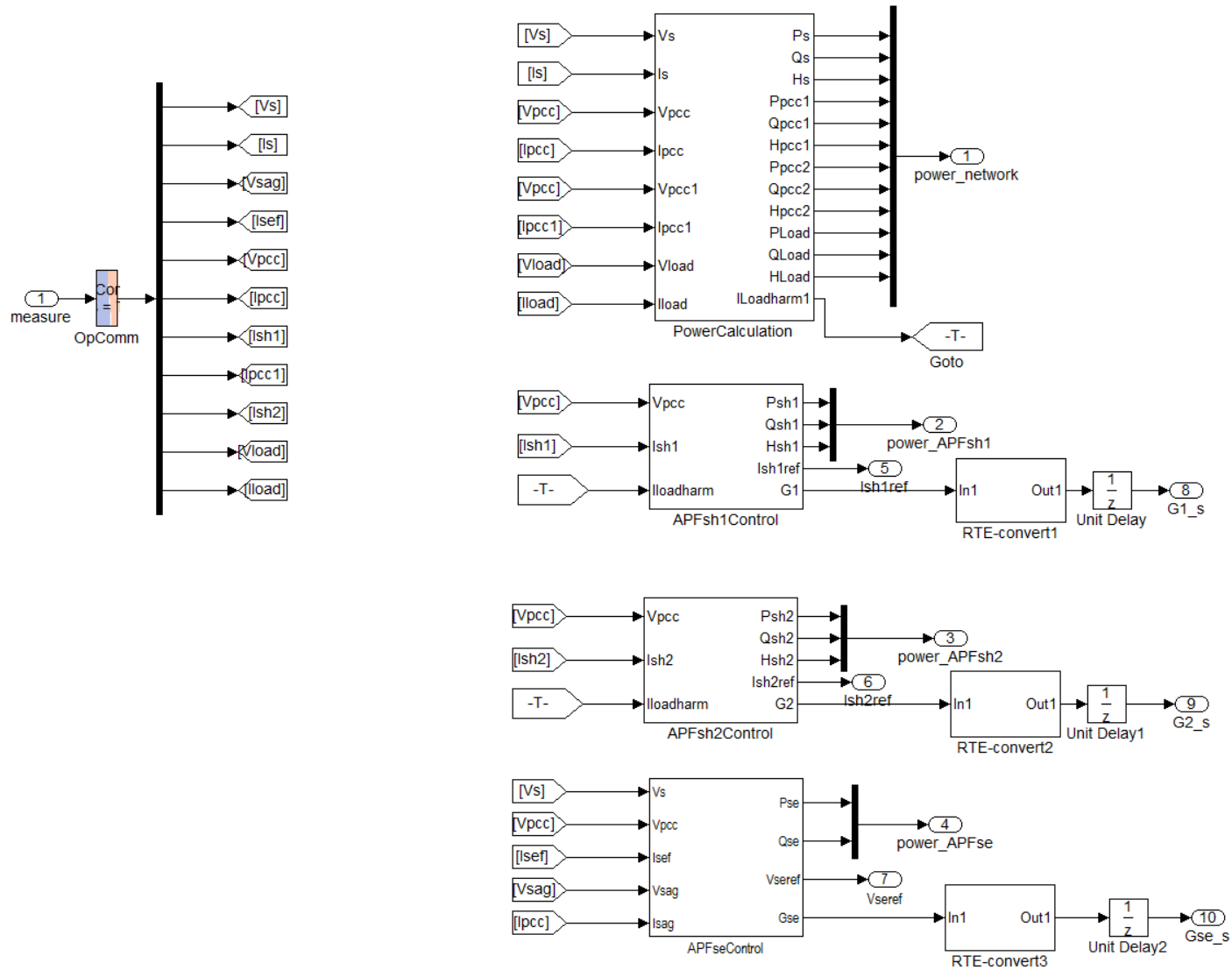A2.9 D-UPQC simulation blocks in RT LAB
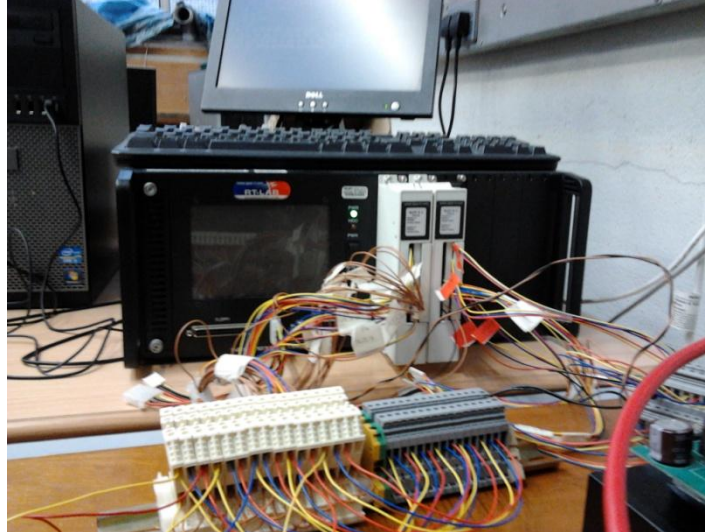
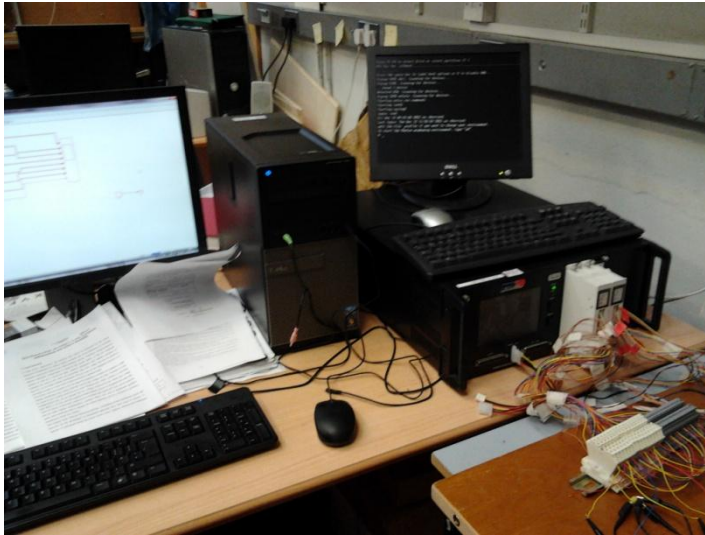**Grid --- D-UPQC --- Load**
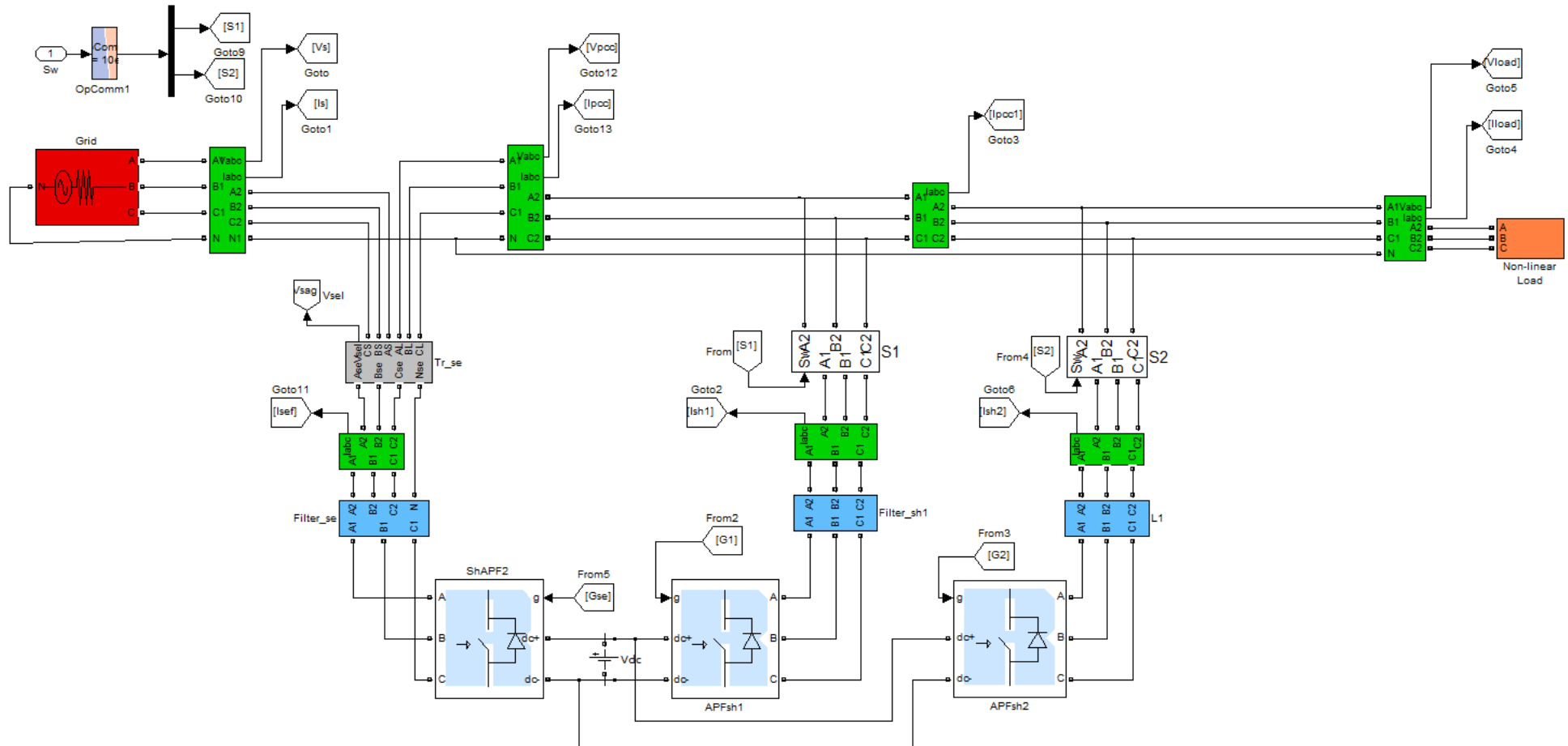
A2.10 sm_PowerSystem of D-UPQC

A2.11 Data acquisition system for D-UPQC

A2.12 Control block of D-UPQC

225

A2.13 Real-time simulator (OPAL-RT) setup for SIL configuration

Publication

(1) S K Khadem, M Basu and M F Conlon, UPQC for Power Quality Improvement in DG Integrated Smart Grid Network – A Review, International Journal of Emerging Electric Power Systems, Vol. 13(1), 2012, Article 3

(2) S K Khadem, M Basu and M F Conlon, Parallel Operation of Inverters and Active Power Filters in Distributed Generation System - a Review, Renewable and Sustainable Energy Reviews, Vol. 15(9), 2011, pp. 5155– 5168

(3) S K Khadem, M Basu and M F Conlon, Integration of UPQC for Power Quality Improvement in Distributed Generation Network – A Review, ISGT Europe 2011, Manchester UK, Dec 2011

(4) S K Khadem, M. Basu and M F Conlon, A review of parallel operation of active power filters in the distributed generation system, EPE 2011, Vol. 1, pp.1-10, Aug 2011

(5) S K Khadem, M Basu and M Conlon, Power Quality in Grid connected Renewable Energy Systems: Role of Custom Power Devices, ICREPQ, Spain, Mar 2010

In Progress:

(6) S K Khadem, M Basu and M Conlon, Harmonic Power Compensation Capacity of Shunt APF and its relationship to Design Parameters.

 (7) S K Khadem, M Basu and M Conlon, Critical Issues on Placement of UPQC in DG integrated Network

(8) S K Khadem, M Basu and M Conlon, UPQC$_{\mu G}$ - A new proposal for integration of UPQC in DG connected Micro-grid or Micro-generation network

(9) S K Khadem, M Basu and M Conlon, D-UPQC - A new proposal for capacity enhancement of UPQC in DG connected Micro-grid network